Modelling and Control of Wind Turbines with Aeroelastically Tailoring Blades

PhD Thesis

Rohaida binti Hussain

Wind & Marine Energy System
Electronic and Electrical Engineering Department
University of Strathclyde, Glasgow

December 19, 2023

This thesis is the result of the author's original research. It has been composed by the author and has not been previously submitted for examination which has led to the award of a degree.

Acknowledgements

First and foremost, I would like to express my ultimate gratitude to Allah The Almighty, The Most Gracious, The Most Merciful. Secondly, I would like to express my greatest appreciation to my supervisor Dr Hong Yue for her endless support and motivation. This thesis would not be completed without her tremendous help. Also, I would like to thank Dr Hong Yue again together with Professor Bill Leithead and Dr Luis Recaldo Camacho for giving me guidance throughout the whole process to complete my PHD journey. They helped a lot in nurturing me to become a true researcher with passion and courage. The unconditional love and support from my family especially my husband for being my backbone, Shaharudin Yub, the prayers from my mom Fadzilah Mat Taib and also the love from my children Nurmaisarah, Nurmasturah and Muhammad Muizzuddin. Also my siblings, in-laws, nephews and nieces, 'kopibin', 'datinciwi' you know who are. Thank you so much for believing in me. A big thank you to Drew Smith for coordinating my studies in the first 4 years of my time at Wind Energy and Control Centre and also to my fellow CDT friends for the academic support. Not to forget my main sponsor, MARA and University Kuala Lumpur from Malaysia and the Engineering and Physical Science Research Council (EPSRC) from the UK for the funding for the first 4 years of my studies. Finally, thank you to my fellow Malaysians in Glasgow whom I called family who were always there whenever needed. Your love and support will always be remembered.

Abstract

The increased size of wind turbines (WTs) improves power generation efficiency but also imposes larger loading effects on the turbine system. A wind turbine with an aeroelastic tailoring blade (ATB) is proposed to alleviate the loading effect in wind turbine blades. A turbine with ATB is designed to respond to the incoming wind forces by deforming the shape of the blade and then reforming to its initial formation. The blade is manufactured with composite materials, incorporated with pre-twist angle and bend twist coupling (BTC) characteristics. Wind turbines with ATB are a new development that needs a better understanding of their operational performance and their potential when properly controlled. This PhD project aims to investigate the modelling and control of industrial-scale ATB WTs and assess the control performance with systematic studies.

The thesis work includes two connected parts, model development, and control system design. A set of models has been developed for system analysis and controller design. To start with, a baseline model is revisited that covers key modelling elements of a 5MW standard HAWT wind turbine. This model is indexed as Model 0 in this thesis, it is the basis for other ATB WTs. To characterise ATB features, firstly the static BTC distribution is added to the turbine aerodynamics to account for the blade's pre-bend-twist design. This static ATB model is integrated to the baseline model giving the full nonlinear turbine model, called Model 1, which will be used for the gain-scheduling baseline controller. Next, the ATB dynamics is approximated by a spring damper model to describe the blade structural dynamic response to wind speed variations. The developed turbine model combining the static ATB and dynamic ATB is called Model 2, based on which a linearised and discretised state-space model is developed

for adaptive model predictive control (MPC). Additionally, a composite ATB model is established, in which the power coefficient values are generated from physical laboratory experiments for a composite materials blade. This model is referred to as Model 3, will also be used for adaptive MPC.

Two controllers are investigated for the above-rated ATB WT operational control. The first controller is the gain scheduling baseline controller developed by the Wind Energy and Control Centre, initially for full envelope WT control of a standard machine without ATB. This baseline controller is redeveloped for the ATB WT using Model 1. The second controller is the adaptive MPC proposed and developed in this thesis work, which includes a general predictive controller enhanced by the use of a Kalman filter and online model update. This adaptive MPC is applied to Model 2 and Model 3 to examine the control performance.

Several tools are used to support model development and controller design. Model 0 (including the baseline controller) is a nonlinear full-envelope model developed in Simulink (Chapter 3). Model 1 is developed by introducing the pre-twist angle and BTC in GL Bladed software, the generated power coefficients are then imported to the Simulink model. The simulation of Model 1 and the adapted baseline controller is made in Simulink (Chapter 3). Model 2 is developed by combining the data generated for static ATB in Model 1 and the dynamic ATB model. The full model for baseline control (Chapter 4) and the simplified state-space model for adaptive MPC (Chapter 5) are implemented in Matlab and Simulink. Model 3 is used for adaptive MPC, also realised in Matlab and Simulink (Chapter 6).

Based on the comprehensive investigation, it is concluded that the ATB WT models developed in this work are suitable for controller design. Both the adapted gain scheduling baseline controller and the proposed adaptive MPC can be applied to achieve satisfactory control performance, that is, to mitigate fatigue load without compromising the power generation of the turbine system. With adaptive MPC, the system demonstrates improvement in reducing pitch activity, tower acceleration and blade root bending moment.

Contents

List of Figures

List of Tables

Nomenclature

Normal Letters

C_D	Drag coefficient
C_L	Lift coefficient
C_p	Power coefficient
$C_{L\beta}$	Pitch lift coefficient
$C_{m\beta}$	Pitching moment coefficient
C_{xy}	Flap edge stiffness (N/m)
C_{xz}	Torsion edge stiffness (N/m)
C_{yz}	Torsion edge stiffness (N/m)
EI_y	Elastic second moment area in y direction
EI_z	Elastic second moment area in z direction
$F_X(r)$	The curve fitting expression
F_x	Blade force in x direction (N)
F_y	Blade force in y direction (N)
F_z	Blade force in z direction (N)
GA_y	Shear modulus area in y direction (Pa)

GA_z	Shear modulus area in z direction (Pa)
GI_x^*	Torsional stiffness around the shear (torsional) axis (N/m)
I_a	Moment of inertia about the elastic axis (kgm^2)
M_x	Blade moment in x direction (Nm/m)
M_y	Blade moment in y direction (Nm/m)
M_z	Blade moment in z direction (Nm/m)
P	Wind power (W)
T_0	Transformation matrix
T_r	Transformation matrix
U	Mean wind speed (m/s)
U_∞	True wind speed (m/s)
W	Apparent wind speed (m/s)
L	Aerodynamic lift (N/m)
M	Aerodynamic moment (Nm/m)
$\overline{\overline{C}}$	Stiffness matrix
a	Axial induction factor
b_s	Semi chord length (m)
c	Chord length (m)
c_h	Plunge damping coefficient
c_s	Nonlinear parameter coefficient

Nomenclature

c_β	Pitch damping coefficient
dF_D	Sectional drag force (N)
dF_L	Sectional lift force (N)
dF_T	Sectional thrust force (N)
dL	Section lift force (N)
dr	Sectional blade length (m)
e	Elongation of the elastic axis
h	Plunge spring displacement (m)
$i_{\xi\eta\zeta}$	The deformed blade coordinate
$i_{X'Y'Z'}$	The initial tower coordinate fixed on the ground
i_{XYZ}	Orthogonal vector of the top of the tower
i_{xyz}	Orthogonal vector of the blade pitch angle located on the top of the tower
k_h	Spring stiffness (N/m)
$k_\beta(\beta)$	Pitch stiffness (N/m)
m	Mass (kg)
r	Length parameter from root to the considered section of the blade (m)
u	Longitudinal deflection in i_x direction (rad)
v	Longitudinal deflection in i_y direction (rad)
w	Longitudinal deflection in i_z direction (rad)
x_a	Elastic position (m)
$\dot{h}$	Plunge velocity (m/s)

$\ddot{h}$	Plunge acceleration (m/s^2)

Greek Letters

α	Angle of attack (rad)
β	Pitch angle (rad)
β_0	Pitch angle at operating point (rad)
β_p	Coning angle between the vertical plane and the elastic axis of the blade (rad)
β_{eff}	Efficient pitch angle (rad)
$\ddot{\beta}$	Pitch acceleration (m/s^2)
$\dot{\beta}$	Pitch rate of change (rad/s)
γ_x	Blade displacement in x direction (m)
γ_y	Blade displacement in y direction (m)
γ_z	Blade displacement in z direction (m)
κ_x	Blade orientation in x direction (rad)
κ_y	Blade orientation in y direction (rad)
κ_z	Blade orientation in z direction (rad)
λ	Tip speed ratio
Ω	Rotor speed (rad/s)
ϕ	Local torsional deformation at each section of the blade (rad)
ϕ_p	Pitch angle of the blade section (rad)
$\phi_T(r)$	Total geometric twist angle of the section (rad)
ϕ_{p0}	Blade pitch at the tip (rad)

ψ	Angle of relative wind (rad)
ρ	Air density (kg/m^3)
σ	Flap deflection angle (rad)
θ	Phase angle of the blade (rad)
θ_p	Section pitch angle (rad)

Abbreviations

AEP	Annual Energy Production
ARX	utoRegressive eXogenous
ATB	Aeroelastic Tailoring Blade
BEM	Blade Element Momentum
$BEMT$	Blade Element Momentum Theory
$BRBM$	Blade root bending moment
BTC	Bend twist coupling
CAR	Above-rated control
CBR	Below-rated control
EA	Elastic area
$EBRBM$	Edgewise blade root bending moment
$FBRBM$	Flapwise blade root bending moment
$GEBT$	Geometrically Exact Beam Theory
$HAWT$	Horizontal Axis Wind Turbine
IP	Inplane

Nomenclature

$LCOE$	Levelised Cost of Energy
OOP	Out of plane
QP	Quadratic programming
$RPME$	Recursive polynomial model estimator

Chapter 1

Introduction

This chapter presents an overview of the thesis work. It introduces the research motivation, the aims and objectives of the PhD project, highlights the contribution to knowledge and gives the outline of the full thesis.

1.1 Overview

Renewable energy is described as clean energy and comes from natural resources such as the sun, wind, waves and biomass. Energy from wind resources is one type of renewable energy that is widely explored in the United Kingdom (UK). The geographical location of the UK is the factor of wind resources with sufficient annual mean wind speed available throughout the year.

Globally, renewable energy system technology specifically wind energy is progressing well led by China, followed by the United States, Germany, India, Spain and the UK (Dwyer & Teske 2018). These are the top six countries with wind power capacity, and the UK is in fifth place with 0.7 GW additional capacity in 2017. Murdock et al. (2021) reported that an amount of 93 GW of wind power capacity was installed globally in 2020, and in 2022, the offshore wind farm is expanding in a progressive manner with an increase of 20% compared to the year 2021. In a report for the year 2021 on wind energy focusing on Europe (Ivan Komusanac et al. 2022), it is reported that the UK has the highest new wind turbine installation of 2,317 MW offshore and 328 onshore followed by Sweden, Germany, Turkey and the Netherlands. It is 15% of overall wind

turbine installations in Europe. It indicates that the UK is taking serious measures in moving towards the use of renewable energy. By 2030, 95% of British electricity could be low-carbon and by 2035, the electricity system will be decarbonised, subject to security of supply (Service 2022). The UK government is also planning to provide cheaper wind energy supplies and looking forward to generating energy 100% from solar and wind by 2050 (Service 2022).

The scenario motivates industrial players in the wind energy sector to progress further, improving the performance of wind turbine systems. The size of wind turbines has been increased from small-scale wind turbines with blade lengths of less than 10 meters in the 1980s to industrial-scale wind turbines with blade lengths greater than 100 meters by 2050. Although longer blade results in larger wind turbine power production, the shortcoming is that it also increases blade loading effect.

1.1.1 Aeroelastically tailoring blade (ATB) wind turbines

The structure of wind turbine blades consists of properties such as the spar, layups, aerodynamic shapes, and bend and twist coupling (BTC) characteristics. The spar provides structural integrity and stiffness. It involves composite materials like fibreglass or carbon fibre to balance strength and weight. The blades have several layups where the outer skin covers the structure and contributes to the aerodynamic profile. It is also typically made of composite materials. The cross-sectional shape of the blade is an airfoil, which generates lift as wind flows over it, driving the rotation of the turbine. Furthermore, the blades are designed with intentional twists along their length. This means the angle of attack changes from the root to the tip of the blade.

Aeroelastically tailoring blade (ATB) wind turbine is proposed as one of the alternatives to support the efforts in alleviating the loading effect in the wind turbine blades as the blade size increases. The physical bending and twisting of wind turbine blades are influenced by their structural design, aerodynamic shape, and the dynamic forces exerted by the wind. ATB represents an advanced design approach where the aeroelastic properties of the blades are intentionally tailored to enhance the aerodynamic performance.

BTC is designed to couple bend and twist characteristics for the purpose of optimising the aerodynamic performance. BTC can be measured by BTC coefficients, which quantify the relationship between the bending and twisting deformations. The coefficients are dimensionless and the values indicate the magnitude or strength of this coupling effect, meaning how much bending deformation is accompanied by twisting and vice versa. Smaller values of BTC coefficients would suggest a relatively weaker coupling between bending and twisting deformations, while larger coefficient numbers show stronger coupling effect.

For an ATB, the aeroelastic properties are deliberately adjusted for designed aerodynamic performance through use of composite materials, twist and tailored structural design. ATBs may incorporate materials that can adapt to changing conditions. These materials can change their shape or properties in response to variations in wind speed, allowing for real-time adjustments. Some ATBs feature variable twists along the blade length. This adaptability allows the blade to adjust its twist dynamically based on wind conditions, optimising aerodynamic efficiency. The structural design of ATBs is tailored to achieve specific aeroelastic properties. This may involve optimising the stiffness distribution along the blade length to enhance performance and load distribution. ATBs are designed to reduce loads on the turbine components, enhancing the overall reliability and lifespan of the system. Load reduction is achieved by adjusting the blade's response to varying wind conditions.

As such, the physical BTC of wind turbine blades are inherent to the design and response to aerodynamic forces. ATB takes this a step further by intentionally adjusting the aeroelastic properties, incorporating composite materials, and optimising the structural design for enhanced performance and load reduction. These advancements contribute to the efficiency and sustainability of wind energy systems.

The aeroelastic behaviour study on a horizontal axis wind turbine (HAWT) with ATB was initiated by Veers et al. (1998) focusing on the wind turbine structure. Fast forward to the year 2014, Capuzzi et al. (2014*b*) experimented with wind turbine blades made of composite materials on the idea that ATB is designed to deform and reform its shape to its initial formation whenever it interacts with the incoming wind forces. This

ability can alleviate the loading effect on the wind turbine system. In the year 2020, simulation results in (Scott et al. 2020) summarised that the load of a 122 metre-long ATB blade is reduced by 2.66% during operation.

The key objectives of using ATB wind turbines are often related to improving energy capture efficiency, reducing loads on the turbine components, and enhancing the adaptability of the blades to varying wind conditions. The load alleviation is the primary goal of wind turbines with ATB. It includes the load reduction on the turbine components such as the blades, tower, and other structural elements. By optimising the aerodynamic design and aeroelastic characteristics, ATB aims to distribute loads more evenly along the length of the blades. This can contribute to a reduction in fatigue load and increase the lifespan of the turbine.

ATB wind turbines are also designed to optimise energy capture efficiency. The more efficient aerodynamic profiles, the adaptable features, and the upgraded materials all contribute to improved performance in a range of wind conditions. ATB wind turbines incorporate features that enhance adaptability to varying wind conditions. This adaptability can result in more stable operation under turbulent conditions, reducing the impact of gusts and variations in wind speed. As a result, the turbine may experience fewer extreme loading events.

1.1.2 Controllers for ATB wind turbines

Industrial-scale wind turbines with standard blades operate with an established gain-scheduling controller. Gain-scheduling is a control strategy that involves adjusting the controller gains based on the operating conditions of the system. In above-rated operations, when wind speed changes, the control system adjusts gain to compensate nonlinearity for rated power generation, while avoiding excessive loads. The pitching of the blades affects the angle of attack, the latter influences the lift and drag forces on the blade element. The lift coefficient, C_L, and drag coefficient, C_D, are determined by the airfoil characteristics. C_L is related to the lift force, and C_D is related to the drag force. The total forces on the blade are a combination of the lift and drag forces from each blade element. The control adjustments, blade element forces, and angle of attack

jointly make an impact on the wind turbine's ability to capture wind energy efficiently.

Based on the fundamental design of an ATB, a gain-scheduling controller developed for a baseline wind turbine may require specific tuning to maintain its performance and produce the desired outputs for ATB wind turbines. The baseline controller is taken as an indicator by which to measure the control performance of an ATB wind turbine system.

ATB wind turbines may enable the use of advanced control strategies, such as individual pitch control or MPC, to optimise operation performance based on real-time conditions. These strategies can contribute to load reduction, improved energy capture, and enhanced overall stability. However, the actual impact on energy production depends on various factors, including the specific design of the ATBs, the wind resource at the site, and the effectiveness of the control strategies implemented. It should be noted that advancements in ATB are an ongoing area of research and development, and the specific outcomes can vary based on the design choices and the intended operational conditions of the wind turbine.

Model predictive control (MPC) is an advanced control strategy used in various engineering applications, including wind turbine control. Unlike conventional control methods, MPC considers a predictive model of the system and optimises control actions over a future time horizon. It repeatedly solves an optimisation problem to determine the best control input sequence based on the predicted system behaviour. MPC requires a dynamic model of the system. This model represents the relationships between inputs, outputs, and internal states of the system over time. MPC predicts the future behaviour of the system over a specified prediction horizon. This can involve estimating how the system will evolve over time given the current state and inputs. MPC solves an optimisation problem at each time step to find the optimal control inputs over the prediction horizon. The optimisation considers system constraints and performance objectives. At the next time step, the process repeats. MPC continuously updates the prediction based on new measurements and re-optimises the control inputs.

In comparison, the conventional controller uses a fixed control law based on current system states, whereas, MPC considers predictions over a future horizon and adapts

its control actions accordingly. Additionally, MPC naturally handles constraints by incorporating them into the optimisation problem. This allows for effective control in the presence of constraints on inputs, outputs, or other system variables. MPC relies on dynamic models of the system, which are more complex than the simplified models often used in conventional control approaches. MPC predicts future states by simulating the system forward in time using the dynamic model. It considers the effects of various control inputs over the prediction horizon, accounting for disturbances and uncertainties.

Applying MPC to wind turbines is not a trivial task because of its computational intensity required for optimisation, the modelling challenges due to the highly nonlinear characteristics of a wind turbine, and perhaps the complexity in implementation related to real-time optimisation. Even so, MPC is considered as having good potential for wind turbines with ATBs mainly because of its adaptability to varying wind conditions, its capability to handle complex dynamics that may lead to load mitigation advantage with optimisation techniques and its unique feature in handling constraints by using an optimisation approach. The decision to use MPC depends on the specific requirements of the application and the trade-offs between computational complexity and control performance.

1.2 Motivation of Research

Wind energy systems have been growing rapidly since 1980s. The size of wind turbines is also escalating in the 1980s, the blade length is from 8 metres to 9 metres. It is projected to rise reaching more than 100m radius by the year 2050 as reported in (Dwyer & Teske 2018). For example, in 2020, Renewables 2021-Global Status Report reported that 93GW wind power capacity was installed globally in 2020 and it is predicted to increase in the years after (Dwyer & Teske 2018). According to the report, the UK has the highest new wind turbine installation and it is 15% of overall wind turbine installations in Europe. The size of wind turbines increases from small scale to blade with a length greater than 120 meters. Although a longer blade results in larger wind turbine power production, the shortcoming is that it also increases blade loading effect.

The length of the wind turbine blade has significant impact on power generation and load performance for the reason that it determines the swept area of the wind turbine. In essence, the blades characterise the output performance of wind turbine systems. Besides the length of the blade, the blade structure, which includes the materials selection, the blade shape options and the spar cap designs, also contribute to the loading effects of turbine. The blade loading effect is one factor in the operation and maintenance cost of wind turbine systems.

There are several studies looking into this matter, for example (Liu et al. 2015, 2017, Zhang et al. 2016). This existing problem is advancing together with the increase in blade length throughout the years. By 2022, researchers are looking into a 20MW wind turbine with 120 meters of blade length. Generally, longer blades are exposed to more loading effects that require better maintenance preparation. Thus, ATB is proposed to alleviate the loading effect of the blade. ATB is built up with the combination of more than two materials which is also described as composite materials. The materials applied in the blade structure result in the wind turbine system's new power coefficient, C_p. The stochastic nature of wind causes a loading effect problem to the blade and tower of a wind turbine, let alone the extreme wind can damage the structure (Xie & Aly 2020). An investigation on wind turbine blades built with composite materials concluded that the blade has structural integrity over various load and fatigue tests (Kong et al. 2005).

Wind industries always look into increasing power production which can be achieved by increasing the length of the blade. However, as discussed earlier, the increase in the blade size will cause an increase in the blade loading effect. As such the goals are to alleviate the loading effect of the wind turbine specifically in the wind turbine blades and to maintain the power production of the wind turbine system. Both goals will lead to a positive impact in cutting down the maintenance and operational costs of the wind turbine system.

There is a huge knowledge gap in the context of ATB wind turbines related to their modelling and control procedures. The lack of complete understanding of the aeroelastic characteristics and optimal control methods for an ATB wind turbine raises

challenges to its effective application. Addressing this knowledge gap is critical for the development of the wind energy industry, and allows for the development of specific models and advanced control approaches. Furthermore, the goal of this research is to deliver important information that not only elevates our understanding of blade loading effects in larger wind turbines but also allows for the informed design and implementation of ATB wind turbines for a more sustainable and efficient renewable energy landscape.

1.3 Research Questions

The following research questions are set to provide a clear direction for investigation and analysis.

1. How to develop effective models to include the aeroelastic properties and structural dynamics of ATB wind turbines suitable for simulation study and controller design?

2. How does the baseline controller address the key performance characteristics and challenges associated with operating ATB wind turbines in the above-rated region?

3. How can the customization of MPC harness the specific advantages of ATB wind turbines and result in performance improvements compared to the existing baseline controller?

4. How do variations in design parameters impact the effectiveness of the advanced controller across different models of ATB wind turbines?

1.4 Research Aims and Objectives

The aims of this research are to improve understanding on ATB wind turbines from a modelling and control point of view and explore control methods to improve the above-rated operation performance.

This study will establish a clear framework for the investigations by specifying certain assumptions, such as uniform material properties throughout the blade, the implementation of steady-state wind conditions for the analysis of baseline wind turbine performance, the availability of data for implementing MPC, and assuming structural similarities between alternative models and the original ATB wind turbine model. These assumptions serve as a basis for the research and give a framework for analysing the aeroelastic behaviour and control strategies of ATB wind turbines.

By outlining the assumptions, the research objectives are written as follows.

1. To develop working ATB wind turbine model(s) for simulation study, controller design and performance assessment.

2. To analyse ATB wind turbine performance in the above-rated region with the baseline gain-scheduling controller.

3. To develop an advanced controller (MPC) for ATB wind turbine, and compare its performance with the baseline controller.

4. To test the advanced controller with an alternative ATB wind turbine model.

The thesis will cover the aeroelastic properties and dynamic behaviour of ATB wind turbines, performance analysis in the above-rated region with the baseline controller, tailoring MPC for ATB wind turbines and comparing it with the baseline, and comparative responses of the advanced controller on alternative ATB wind turbine models.

For ATB wind turbine modelling, the models serve as the foundation for designing and optimising blades in wind turbine systems. The models are expected to be as simplified as possible with relevant accuracy. The balance between simplicity and accuracy ensures that the results are both reliable and manageable. The model is reliable enough to closely match real-world performance to enable engineers to make informed design decisions and optimise blade performance. Moreover, the ATB wind turbine models should be adaptable to various operating conditions. This adaptability ensures that the design can meet specific performance requirements under diverse conditions. The models also should provide results promptly to expedite the design and optimisation phases where Time-efficient models are often favoured for practicality.

Furthermore, the model's calculation time is critical and it must be both accurate and efficient. In addition, the selection of a good ATB wind turbine model is dependent on careful examination of a number of characteristics, including simplicity, accuracy, efficiency, and resilience. However, the detailed analysis of specific manufacturing processes for ATB, the site-specific considerations and variations in wind farm layout and the microscale turbulence effects on blade performance will not be covered in the thesis.

1.5 Thesis Contributions

The thesis contributions can be divided into two large parts, model development and controller development. The contributions to each part are summarised in the following.

Model Development

1. Development of an industrial-scale static ATB wind turbine model (Model 1). This model is developed to represent the fundamental static properties of an industrial-scale ATB wind turbine. The development procedure includes taking into account the aeroelastic properties and structural dynamics, as well as parameters such as blade geometry, BTC coefficients, and aerodynamics information. The goal of developing a static model of an ATB wind turbine is to provide a representation to assist in the investigation of the wind turbine's behaviour under operational conditions. The development of this model helps to reach a better understanding of the ATB turbine characteristics in a static condition, providing a fundamental for further dynamic studies and control system design. Overall, Model 1 represents a significant understanding in representing the physical characteristics of ATB wind turbines on an industrial-scale.

2. Development of dynamic ATB wind turbine model using an analytical method (Model 2). This dynamic model aims to capture the aeroelastic behaviours and reactions of an ATB wind turbine. During the development phase, analytical approaches are used to simulate the dynamic interactions between the wind, the blades, and the supporting structure. Model 2 is the combination of Model 1 with a spring damper model to approximate the ATB wind turbine dynamic

characteristics.

3. Development of combined materials model of ATB wind turbine (Model 3). This model is an advanced approach to addressing the complex material properties associated with ATB construction. Model 3 incorporates the different properties of multiple materials utilized in ATBs, such as composite laminates, structural cores, and any extra layers that contribute to the blade's composition, as opposed to simpler models that may treat materials uniformly.

Controller Development

4. Development of a baseline gain-scheduling controller for ATB wind turbine (Controller 1). The development of Controller 1 is an essential step towards establishing the fundamental control strategy for ATB wind turbines. The controller serves as the basis for controlling the performance of ATB wind turbines, covering critical factors like pitch control and generator torque control, to provide consistent and efficient performance under varying wind conditions.

5. Development of MPC for ATB wind turbine (Controller 2). Controller 2, offers an advanced development in controller design by integrating predictive models to optimise control inputs over a specified future time horizon. This controller seeks to improve on the baseline controller in terms of adaptability, load mitigation, and energy capture efficiency. Its establishment represents a step towards more advanced and adaptive control approaches, ensuring ATB wind turbines work optimally in varied wind conditions.

To help understanding the main work in this thesis, two diagrams are produced to show the models and controllers, as presented in Figure 1.1 and 1.2.

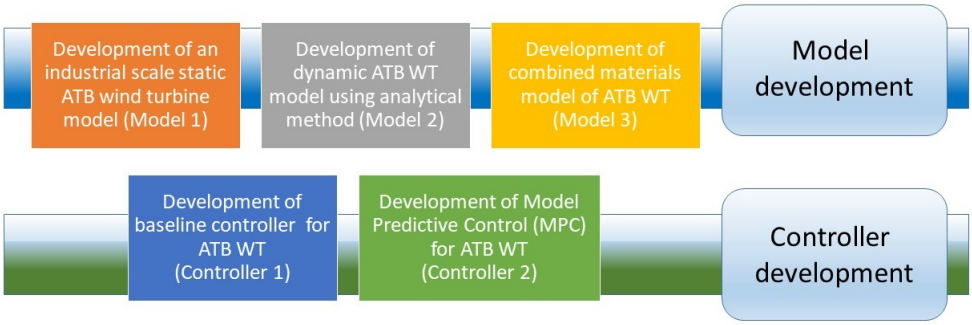

Figure 1.1: Thesis contributions

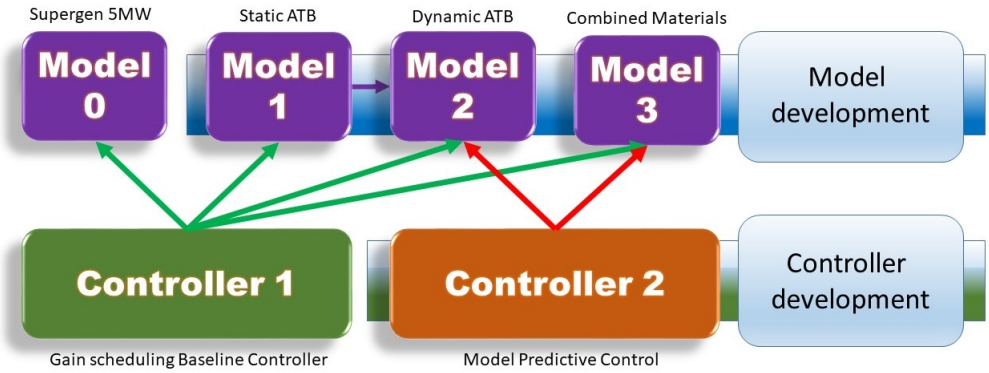

Figure 1.2: Developed models and controllers

Figure 1.1 shows there are three models developed. The first one is the static model (Model 1). The second one is the dynamic model (Model 2), which is a combination of the static model and a spring damper model. The third model is the combined materials model (Model 3) which is developed and analysed with the baseline controller and MPC. For controller development, the gain-scheduling baseline controller is called Controller 1 and the developed MPC is called Controller 2.

Figure 1.2 simplifies Figure 1.1 where the three developed ATB wind turbine models, Models 1, 2, and 3, are included. Model 0 is the baseline wind turbine model without ATB. It is a 5MW Supergen WT model. Controller 1 is applied to all 4 models, Controller 2 is applied to the two dynamic ATB wind turbine models with ATB.

1.6 Thesis Organisation

Chapter 1, provides an introduction and an overview of the research subject, and it is distributed into 7 sections starting from the research overview, followed by the research motivation, research questions, aims and objectives, novelty contribution, thesis organisation and list of publications.

Chapter 2 explains the state of the art of ATB for wind turbine systems. It provides relevant background information concerning the fundamental understanding on modelling of ATB wind turbines. There are limited research publications concerning the ATB model development. Due to this shortage of modelling, the controller development with regards to ATB wind turbines is also limited. It comes to the conclusion that the ATB model can be developed by applying the analytical method. This chapter also reviews wind turbine controllers. A wind turbine is a highly nonlinear system, which makes challenges in developing full envelop controllers. The well-established and successful wind turbine controller is discussed in this chapter. This chapter also explores the advanced modern controller, MPC and its applications in wind turbine control.

Chapter 3 describes the development of Model 1, the static model of an ATB integrated to the dynamic wind turbine model using data provided by GL Bladed. The ATB model in Model 1 is developed using smaller-scale wind turbine data, which is upscaled based on the assumptions made in publications. This model is evaluated using a baseline gain-scheduling controller and compared to a baseline wind turbine model with standard blades – Model 0. It comes to the conclusion that Model 1 does not fully represent the wind turbine operation over a wide wind speed. Further work is expanded in which a dynamic model is developed to fill in the gap in Model 1. The main results in this chapter is published at IFAC-PapersOnline (2017).

Chapter 4 explains the development of Model 2, the wind turbine model with a dynamic ATB characterisation included. The model takes the second-order transfer function for a spring mass damper model to approximate the ATB dynamics in the 5MW Simulink model. The baseline gain-scheduling control is applied to Model 2. Comparisons are made between Model 0 with baseline gain-scheduling and Model 2

with baseline gain-scheduling.

Chapter 5 extends the controller development for Model 2. The full model is linearised in Simulink as a single-input-single-output (SISO) plant. MPC is selected as the controller for Model 2. The results of MPC of Model 2 are compared with the baseline gain-scheduling control of Model 0.

The works and key findings from Chapter 4 and Chapter 5 are presented at TORQUE (2022) and published at Journal of Physics: Conference Series (2022).

Chapter 6 presents an alternative model on ATB wind turbine – Model 3, which is developed based on GL Bladed data. The model refers to the blade that is designed with combined or composite materials and is compared to the baseline blade as an individual blade structure. From the laboratory results, the combined materials blade produced a new power coefficient, C_p, and thrust coefficient, C_Q. These new C_p and C_Q are applied in the baseline wind turbine model as an alternative ATB wind turbine model. MPC is applied to Model 3 and is compared with Model 2 with MPC. The performance of both models is evaluated and presented in this chapter.

Chapter 7 summarises the results of the thesis, draws conclusions and discusses the future work on model development and controller design for ATB wind turbines.

Thesis conceptual flow

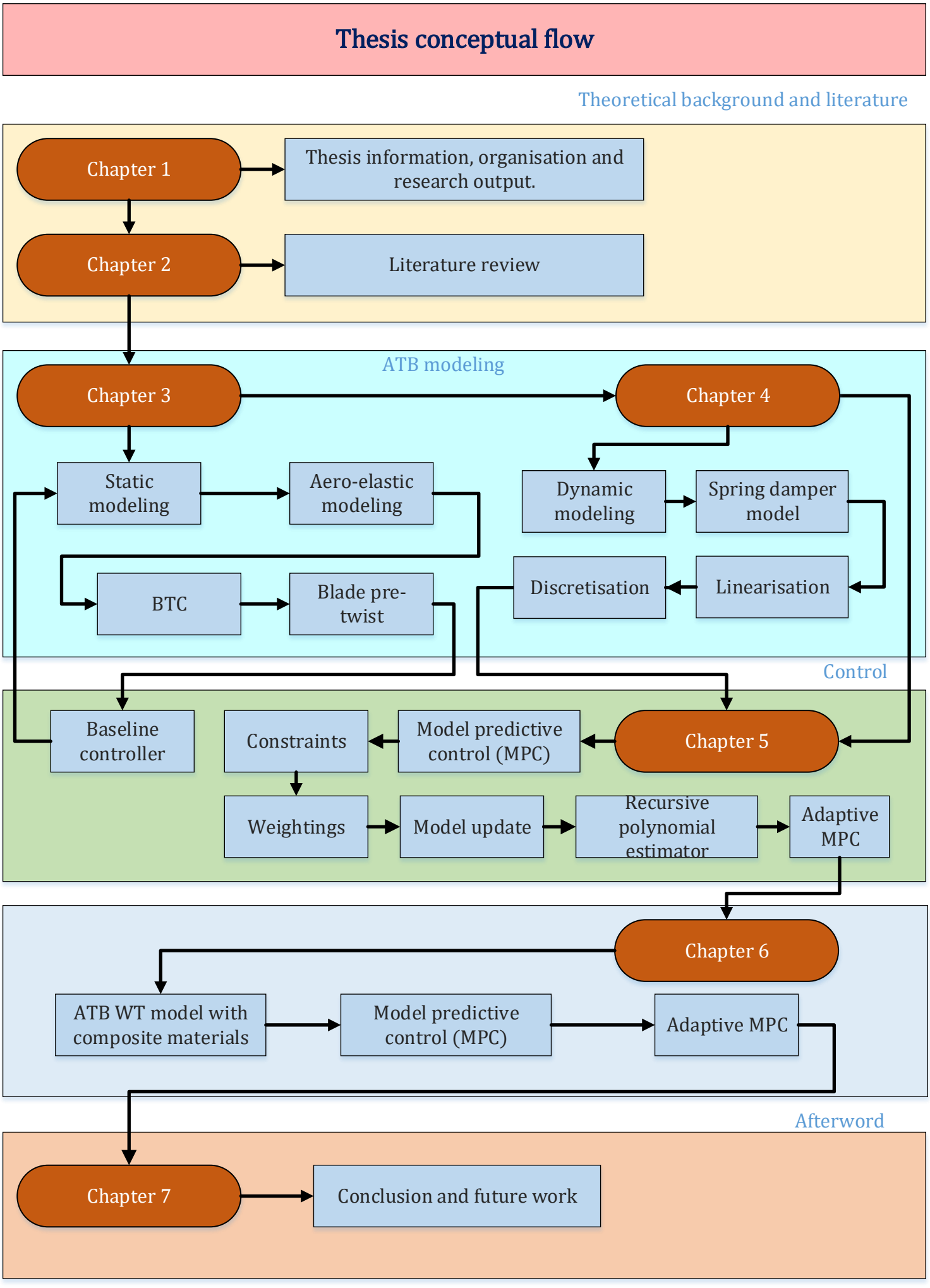

1.7 List of Publications and Disseminations

Publications

1. Hussain, R., H. Yue, W.E. Leithead and Q. Xiao (2017). Modelling and analysis of controlled aeroelastic tailoring blade wind turbine, IFAC-PapersOnLine, 50(1): 9926–9931.

2. Hussain, R., H. Yue and L. Recalde-Camacho (2022). Application of model predictive control on a wind turbine with aero-elastically tailored blades, Torque 2022, 1-3 June, 2022, Delft, The Netherlands,

3. Hussain, R, H. Yue and L. Recalde-Camacho (2022). Model predictive control of wind turbine with aero-elastically tailored blades. Journal of Physics: Conference Series, 2265, 032084: 1-12.

4. Hussain, R., H. Yue and L. Recalde-Camacho (2024). Aeroelastically tailored blades wind turbine – development of a combined adaptive model for control. In: The Science of Making Torque from Wind TORQUE 2024, 29-31 May, 2024, Florence, Italy.

5. Hussain, R, H. Yue and L. Recalde Camacho. Aeroelastically tailored blades wind turbine – development of a combined adaptive model for control. Journal of Physics: Conference Series (to be submitted by 15 January 2024).

Presentations

1. Poster presentation, Title: 'State Feedback Disturbance Rejection for Pitch Regulated Variable Speed Wind Turbine', European Academic of Wind Energy (EAWE) PhD Seminar, Stuttgart, Germany, 22 to 25 September 2015.

2. Poster presentation, Title: 'Control of Wind Turbines with Aeroelastic Tailoring Blades', Futurewind 2015 Event, University of Strathclyde, Glasgow, UK, 13 January 2016.

3. Poster presentation, Title: 'Control of Wind Turbines with Aeroelastic Tailoring Blades', Energy Showcase 2016, University of Strathclyde, Glasgow, UK, 3 May 2016.

4. Poster presentation, Title: 'Control of Wind Turbines with Aeroelastic Tailoring Blades', Research Presentation Day, University of Strathclyde, Glasgow, UK, 22 June 2016.

5. Poster presentation, Title: 'Control of Wind Turbines with Aeroelastic Tailoring Blades', Supergen General Assembly, Manchester, UK, 16 November 2017.

Others

Photography presentation (Finalist), Title: 'The Turbulent Life of Turbines', Image of Research Competition, University of Strathclyde, Glasgow, UK, 2 May 2017.

Chapter 2

Aeroelastically Tailoring Blade (ATB) Wind Turbine Model and Controller - A Review Perspective

This chapter presents the literature review on the wind turbine model with the state-of-the-art of aeroelastically tailoring blade (ATB) and the controller in the wind turbine system environment. It discusses the ATB concept on wind turbine systems with the description of fundamental knowledge of aeroelasticity and its relevance, the background of research history on the modelling of aeroelasticity for a wind turbine system. The chapter also explores the main control approaches including the advanced modern control particularly model predictive control (MPC) in wind turbine systems.

The chapter is outlined as follows. An overview is given in Section 2.1. Section 2.2 presents fundamentals for ATB wind turbines. Section 2.3 describes the modelling approaches of ATB for wind turbines. The control background is presented in Section 2.4, the baseline controller and MPC are discussed in Section 2.4.1 and Section 2.4.2, respectively. The conclusion is given in Section 2.5.

2.1 Overview

In a wind turbine system, the fatigue loading effect is a way to measure the lifespan of the system. The increase in the fatigue loading effect reduces the lifespan of a wind turbine system. It will also increase the operation and maintenance costs of the system. A wind turbine with ATBs is proposed as one of the solutions to alleviate the loading effect in the system. ATB is designed based on the natural aeroelasticity behaviour that occurs in many structures specifically in wind turbine systems. It is a blade structure designed and built from composite materials. ATB is still immature in the wind energy development, causing limited resources on modelling and control.

Note that, the main objectives of this project are to establish an ATB wind turbine model and to examine the ATB wind turbine model with an advanced control approach, to compare and analyse its performance to the baseline wind turbine model. The analysis is based on the motivation of this project; to alleviate the loading effect in the wind turbine system with the ATB design.

This chapter will walk through the state-of-the-art ATB for wind turbine systems, covering fundamentals of aeroelasticity, aeroelastic tailoring and bend-twist coupling (BTC). The understanding of these are important to a proper development of ATB wind turbine models in the following chapters.

This chapter also explores the control approaches in wind turbine systems. The controller development is challenging due to the stochastic nature of wind and the complexity of the turbine structure. One successful controller is a gain-scheduling strategy with PID control. This controller is referred to as the baseline controller in this thesis. Apart from the gain-scheduling baseline controller, other control techniques are also explored in wind turbine control applications. For example, MPC, sliding mode control, artificial intelligent control and many more. This thesis investigates MPC applications to ATB wind turbine models.

2.2 ATB Fundamentals for Wind Turbines

The exploration of aeroelastic tailoring for wind turbine blade application was initiated in the 1990s. Veers et al. (1998) published a paper reviewing the benefits of ATB for wind turbines as it is cost-effective and capable of load reduction. It also reviewed the aeroelastic tailoring for helicopter blades. In 2003, Veers et al. (2003) reviewed the trends in the design, manufacture and evaluation of wind turbine blades. Since then, no ATB prototypes have ever been manufactured to validate the theory for a while. On a positive note, Capuzzi et al. (2014*a*), Capuzzi et al. (2014*b*) studied and built an adaptive blade to review the aeroelastic behaviour of wind turbine applications.

In 2016, the state-of-the-art aeroelastic modelling for wind turbine blades was well presented in Wang et al. (2016). It discussed three model approaches; the aerodynamic model, the structural model and the cross-sectional analysis model. Each of the models was divided into its own model types, for example aerodynamic model has four models, the structural model has two models and the cross-sectional analysis model has three model types. The review of the three modelling approaches is helpful to understand a reliable modelling approach for ATB wind turbines.

ATB for wind turbines is proposed to improve the performance of wind turbine systems by alleviating the loading effect and maintaining the power production performance. The design of the blade cross-sectional structure in ATB is the type of airfoil selection with the combined materials that will change the centre of gravity of the airfoil compared to a standard wind turbine blade. The spar cap of the airfoil is also changed in the ATB design. A wind turbine with ATB requires a control system to achieve the desired output performance. The controller development needs a reliable model to run and test the method. However, based on the literature study, there are no feasible models of ATB wind turbines that can be used for controller design. The available models mainly focus on CFD applications and structural models.

2.2.1 Aeroelasticity in wind turbine system

Aeroelasticity is a natural behaviour that can be found in structures. It is the interaction between inertial forces, aerodynamic forces and elastic forces. The build-up of the structure such as the materials selection and the geometry of the structure would influence its aeroelasticity. The main structure of a wind turbine comprises a tower, a hub and a rotor also known as blades. Each of these components is subjected to its own structural aeroelasticity and all those three components are designed to their optimum capability. If any of them is designed beyond its capability, major instability problems can occur.

Aeroelastic tailoring is essentially the design with the exploitation of aeroelasticity characteristics. The structure is purposely designed to embed aeroelastic properties and must operate within its stability region. Since aeroelastic tailoring applies the aeroelastic properties in the structural design, the structure must comply to operate in its stability region. This means that the structure is always firm and steady, in another word, the aeroelastically tailored structure should not have instability problem.

In theory, aeroelasticity can be defined as the combination of three forces which are aerodynamics forces, inertial forces and structural forces (Hodges & Pierce 2011). It is also known as dynamic aeroelasticity as illustrated in Figure 2.1. The study on aeroelasticity is widely used in aeronautical applications, particularly in helicopter systems. In a wind turbine system, aeroelastic is the changes in the behaviour of the wind turbine structure caused by either internal or external forces (Holierhoek 2013b, Tingrui & Yongsheng 2008). Practically, even though the design has ensured that the structures must only operate within their stability region, there is still a risk that the structures could initiate instability problems in the system. The instability potentials are caused by the stochastic behaviour of the wind especially at high altitudes and also the materials and layups applied to the structural design.

Aeroelastic is the changes of behaviour by nature while aeroelastic tailoring applies the idea of aeroelastic and tailors it in a way that it can satisfy some expected performances. The aeroelastic tailoring in turbine blades was adapted from aerodynamics principles in helicopters. The similarity of airfoil geometry in both helicopters and wind

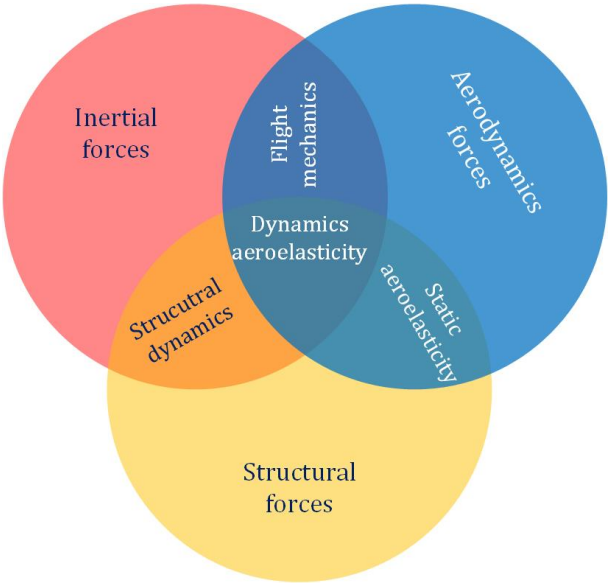

Figure 2.1: Simplified description of dynamic aeroelasticicity

turbines suggests that the principle theory in helicopter rotor systems is suitable to be adopted into wind turbine applications.

A study in (Cornette et al. 2015) focused on aeroelastic tailoring in helicopter blades. The concept is relevant to ATBs for wind turbine research. A brief comparison of an aeroelastic point between helicopters and wind turbines is explained in (Holierhoek 2013b). The main differences between these two are the angle of attack during operation and the direction of the aerodynamic force. Other dissimilarities include the following: wind turbines have larger blades twists, the wind turbine blade mass axis in chordwise view is usually behind the aerodynamic centre, and the wind turbine torque is changing continuously during operation compared to helicopters.

There are several features that differentiate the two systems. An obvious one is that the blade is in horizontal position for a wind turbine and in vertical position for a helicopter. This requires further analysis in aerodynamics principle. Another dissimilarity is the direction of the aerodynamic forces applied to blades. Despite these differences, a main problem in a helicopter is the flutter instability. Failure to control the flutter problem means the helicopter becomes unstable and will cause fatal damage to the whole helicopter system. The same goes for the wind turbine system where

flutter instability may occur in blades, and if it is not properly controlled, the turbine will face similar consequences as the helicopter system.

Flutter is a common instability exhibited by a machine with rotating aerodynamics. Flutter happens in rotating blades when the external force frequency is higher than the natural frequency, which causes the natural damping to decrease. The system will be in catastrophic disaster when the damping reaches a negative value. For a wind turbine, the aeroelasticity forces on the blade have the knock-on effect of aeroelasticity forces on the drive train and the tower. Another common instability is known as flap-lag instability. Both instabilities are relevant to wind turbine systems, but flutter creates a higher barrier in wind turbine design (Politakis et al. 2008). Thus, it is important to avoid flutter in wind turbine blade design notably when designing a flexible blade as ATB.

It is known that wind turbine is a nonlinear system. The nonlinearity of a structure will have a direct impact on the aeroelasticity. There are publications on structure nonlinearity of wind turbines. For example, in (Nezamolmolki & Shooshtari 2016), the nonlinearity effects are classified into three descriptions; geometric nonlinearities, material nonlinearities and joint slip effects. It shows the effect of the structure nonlinearity on system performance. Their work focused on a 100kW wind turbine, which is too small compared with industrial-scale wind turbines. The state-of-the-art aeroelastic modelling is explained in (Wang et al. 2016). Aeroelasticity was also studied in (Asareh et al. 2016), but focused on aeroelasticity in the tower only, not the blade.

2.2.2 Blade with aeroelastic tailoring design

The idea of aeroelastic tailoring is hypothetically different from aeroelasticity. Generally, it is applying the aeroelasticity nature of the beam to the benefits of a new system. Aeroelastic tailoring in helicopter blades employs the same principle of BTC. The materials, the size and the way the structure is designed influence the aeroelastic behaviour of the structure. In blade design, either for helicopters or wind turbines, the composite materials and the design of the spar cap are crucial in the design. In wind turbine systems, the objectives are to alleviate the loading effects on the blades and to

maintain the power generation performance.

Advancing on to the manufacturing phase, a common design method is often used to manufacture a baseline blade. A baseline blade is manufactured with a standard design process where there are certain parameters such as the number of layups, the spar cap position along the blade and other parameters that need to be designed to satisfy the required performance. The wind turbine tower is designed to be as high as 97 meters because the wind speed is greater at higher altitudes. The design has taken into account the blade's ability to withstand aeroelasticity in high altitudes and also during high wind speeds.

The ATB in a wind turbine has the ability to deform and reform whenever forces are applied to it. The challenge for ATB design is to ensure that the blade is able to return to its initial formation after the deformation caused by wind speed variations, especially when the blade tip is at the highest position. Composite materials are applied to the blade structure to design a flexible blade like an ATB.

The ATB is generally an improved version of the baseline blade. It is designed based on the idea of adopting the natural behaviour of plants that have bending leaves where the leaves are flexible to the incoming forces. That capability is also known as adaptive behaviour. A blade with adaptive behaviour towards wind forces has lower loading effects compared to a rigid blade. Although the baseline blade is referred to as a rigid blade, in practice it is not strictly rigid as in theory. The baseline blade has its own aeroelasticity characteristics. When the blade size is increased, the loads on the blade are also increased. At this point, it is essential to design a blade that is more flexible than the baseline blade. ATB wind turbines can reduce the blade loads by employing the adaptive blade made with composite materials.

An adaptive blade means that it is capable of adapting to wider forces applied to it. One example is the smart rotor blade, and another one is the ATB. The differences between these two are that the smart rotor operates with active mechanical gesture while ATB reacts with passive responses. It requires more studies on the development of ATB structure, the strength and limitations of the blade performance.

Figure 2.2 shows an airfoil section of the structurally optimised adaptive spar cap in

comparison with the corresponding conventional layout (Capuzzi et al. 2014*b*, Pirrera et al. 2012). With this design, the stiffness in Figure 2.2a is reduced by moving the spar cap position towards the leading edge in Figure 2.2b, where the airfoil is thicker, therefore the trailing edge becomes more flexible. A larger surface area towards the trailing edge will provide a better response to the wind forces.

(a) Conventional design (b) Adaptive design

Figure 2.2: Spar cap position for conventional and adaptive design

2.2.3 ATB development in wind turbines

ATB is a relatively new design concept in wind turbine systems. Since the early year of 2000s, several studies related to this subject field have been explored.

In 2003, aeroelastic blade analysis was modelled as equivalent beams. The aeroelastic modelling was simplified by including information such as the elastic axes' location and warping effects in the beam stiffness matrices of the structural information (n.d.).

In 2008, the bi-stable laminated composite structures for morphing an aerofoil section are reported (Diaconu et al. 2008). Bi-stable structures were introduced because they are able to sustain in natural equilibrium after changes of shapes occur in the structures. Bi-stability is driven by the temperature change where it is good for colder temperatures and will be lost when the temperature exceeds 80^oC. This characteristic is suitable for wind energy systems since the temperature is low at higher altitudes.

In 2013, the morphing concept was suggested in wind turbine blades where it is able to change shape with actuation forces but still able to maintain structural integrity (Lachenal et al. 2013). While most of the wind turbine research are focused on the trailing edge flaps, this work suggests that it is possible to reduce fatigue loading with span-wise or chord-wise expansions and also the morphing twist. The span-wise

expansion blade of 18m diameter was tested at a low wind speed of 7–9m/s, and the expansion was in the range of 8–12m. The power production increased 20-50% for below-rated region. However, the power captured was not very good at the rated wind speed and above-rated wind speed. The span-wise expansion was also not practical for large-size wind turbines.

In 2014, the distribution target of an elastic twist was defined as the difference between the target curve of a single blade and the blade root structural constraint. The importance of the distribution target is to obtain the passive structural behaviour which is not available for a standard blade. Bending and twisting deformation is coupled to the spar cap with unbalanced laminates (Capuzzi et al. 2014*b*).

In 2015, an adaptive spar cap was designed to satisfy the adaptive behaviour of the blade structure (Capuzzi et al. 2015). The tests were made for one blade, not the complete rotor structure. Also, load reduction due to aeroelastic tailoring was not included in this work. Their studies were conducted based on the conventional blade structure and the adaptive capability does not compromise structural integrity such as strength, stability and stiffness. However, the results showed that the final design was not optimised (Capuzzi et al. 2015).

A study was published in 2016 on a 10MW wind turbine with ATB, conducted by the Technical University of Denmark (DTU), where the blade is altered by simulation and their results show that power production is increased by 11% at below-rated wind speed. This 10MW DTU model is currently used as the baseline for further investigation of other 10MW machines. Since a 10MW wind turbine was not physically available at that time, this model was developed by upscaling data of a 5MW wind turbine.

In 2018, the University of Strathclyde started a joint project with University of Bristol, on a 10MW wind turbine considering the blade aeroelastic characteristics from the control point of view.

2.3 Modelling Approaches for ATB Wind Turbines

Modelling of ATB wind turbines were mainly conducted by the computational fluid dynamics (CFD) simulation method; (Li et al. 2019) and (Ding et al. 2019). Mathematical models of ATB wind turbines are not found in any publications. A number of issues need to be considered in modelling an ATB wind turbine such as the aerodynamics, structures, mathematical representations and the simulation tools.

The main difficulty on modelling of ATB wind turbine in an aerodynamics context is to describe the bend-twist coupling, also, the unknown elastic centre at each section and the changes of the centre position when the wind speed changes. After looking into various aspects in the related area, several assumptions can be made to develop a mathematical model of an ATB wind turbine.

There are two approaches to model a wind turbine blade, the chord-wise approach and the span-wise approach. The chord-wise approach is widely discussed in helicopter blade research publications (Barbarino et al. 2010, Lim & Chopra 1990, Pirrera et al. 2012), while the span-wise approach is new in this research area. The two approaches are explained in the following sections.

2.3.1 Chord-wise approach

In the chord-wise approach, the analysis is made of the cross-sectional area of the blade section, which has the airfoil shape, and the aeroelastic model of the airfoil is combined with the blade element momentum (BEM) theory. The total forces and blade moments of one single blade can be formulated by a mathematical expression.

A wind turbine blade can be built in different airfoil profiles. The aeroelasticity in an airfoil of a blade section is illustrated in Figure 2.3 (Shams & Esbati Lavasani 2019). The spring with k_h as the spring stiffness represents the plunge, and h is the up and down movement of the spring. The pitch angle is represented by β, and σ is the flap deflection. When a force is applied to the airfoil, pitch and plunge are apparently moving simultaneously and give a new output response. The movement also affects the flap deflection σ at the trailing edge. This aeroelasticity model of the airfoil is modified

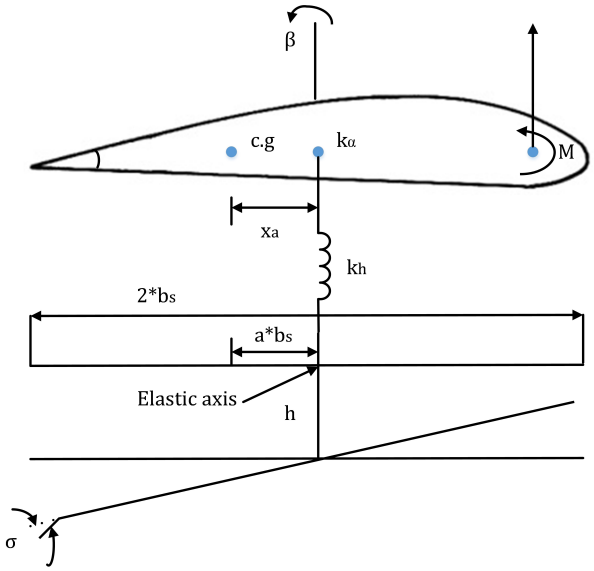

Figure 2.3: Aeroelastic model of a blade cross-sectional area

to comply with the aerodynamic properties of the wind turbine blade. However, in practice, this model is inapplicable for large-scale wind turbines due to the large blade size.

The range of the elastic centre of each airfoil section is estimated based on the design of the blade. The elastic centre varies in a small range between the aerodynamic centre and the chord centre. Also, the twist angle and the vertical displacement of the blade are extracted from the test results. These two known parameters will help to derive the velocity and acceleration of the twist angle and the airfoil position.

Composite materials are applied in designing an aeroelastic tailoring blade structure. Technically the spar cap position contributes to aeroelastic tailored features because the elastic centre is determined by the position of the spar cap. Composite materials also enable the blade to deform and return to its initial formation.

The power production by the ATB wind turbine can be designed to be higher than the baseline wind turbine. The major design factor that is extremely important is the C_p - λ curve. The C_p input into the power equation is basically similar to the baseline machine (Capuzzi et al. 2014*a*). Commonly the linear beam theory is combined with the BEM theory to model the turbine. Other methods have been studied as well, for example, Riziotis & Voutsinas (2006) opted 3D free-wake vortex method instead of

the BEM theory. Wang et al. (2014) and Lago et al. (2013) analyse the BEM theory model and Ahlström (2005) later proposed Geometrically Exact Beam Theory as an alternative method Wang et al. (2014).

In BEM theory, the lift force and drag force on a span-wise length of dr of each blade, normal to the direction of wind speed, W, is given by

$$dF_L = \frac{1}{2}\rho W^2 c C_L dr \tag{2.1}$$

$$dF_D = \frac{1}{2}\rho W^2 c C_D dr \tag{2.2}$$

where dF_L is the section lift force, dF_D is the section drag force, c is the chord length, C_L is the lift coefficient, C_D is the drag coefficient and dr is the span wise length. The following assumptions are considered in BEM.

- Force of a blade element solely affects the change of momentum of the air which passes through the annulus swept by the element.
- There is no radial interaction between the flows passing through adjacent annuli.

The BEM theory is strictly only applicable if the blades have uniform circulation. For a non-uniform circulation, there is a radial interaction and exchange of momentum between flows through adjacent elemental annular rings. It cannot be stated that the only axial force acting on the flow through a given annular ring is due to the pressure drop across the disc. However, in practice, it appears that the error involved in relaxing the above constraint is small for tip speed ratios greater than 3 Burton et al. (2001).

The component of the aerodynamic force on a blade element, resolved in the axial direction is

$$dL = dF_L \sin(\psi) - dF_D \cos(\psi), \tag{2.3}$$

where dL is the lifting force applied to a blade section. However, take note that for the blade elements, each element has its own span-wise length, dr, all elements make the aerofoil profile. In ATB, the additional elastic axis will contribute to an altered value of torque and thrust value. The aeroelastic model of a blade is modelled from the BEM model. Technically, this is the same model with additional parameters (Librescu

& Marzocca 2005, Tingrui & Yongsheng 2008, Xing & Singh 2000). Figure 2.3 shows a typical aeroelastic wing section. The equations of motion are given by

$$\begin{bmatrix} m & mx_ab_s \\ mx_ab_s & I_a \end{bmatrix} \begin{bmatrix} \ddot{h} \\ \ddot{\beta} \end{bmatrix} + \begin{bmatrix} c_h & 0 \\ 0 & c_\alpha \end{bmatrix} \begin{bmatrix} \dot{h} \\ \dot{\beta} \end{bmatrix} + \begin{bmatrix} k_h & 0 \\ 0 & k_a(\beta) \end{bmatrix} \begin{bmatrix} h \\ \beta \end{bmatrix} = \begin{bmatrix} -\mathbf{L} \\ \mathbf{M} \end{bmatrix} \tag{2.4}$$

$\mathbf{L}$ is the aerodynamic lift, $\mathbf{M}$ is the aerodynamic moment, m is the blade section mass, x_a is the distance between the center of elasticity to the center of gravity b_s is the chord length, I_a h is the plunge distance, β is the pitch angle, c_h is the damping coefficient, c_α is the damping coefficient with elasticity, k_h is the spring coefficient, and k_α is the spring coefficient with elasticity. The assumptions for quasi-steady aerodynamic force and moment are given in (2.5) and (2.6) (Bichiou et al. 2014).

$$dL = \rho W^2 b_s C_{L\beta}(\beta_{eff} - c_s\beta_{eff}^3)dr \tag{2.5}$$

$$M = \rho W^2 {b_s}^2 C_{m\beta}(\beta_{eff} - c_s\beta_{eff}^3) \tag{2.6}$$

$$\beta_{eff} = \beta + \frac{\dot{h}}{W} + (\frac{1}{2} - a)\frac{b}{W}\dot{\beta} \tag{2.7}$$

$$dF_D = \rho W^2 b_s C_{ld} dr \tag{2.8}$$

Equation (2.5) is substituted into Equation (2.3), giving the output of new aerodynamic force on the blade element.

$$dL = \rho W^2 b_s C_{L\beta}(\beta_{eff} - c_s\beta_{eff}^3)drsin(\psi) - \rho W^2 b_s C_{ld} drcos(\psi) \tag{2.9}$$

Although the total aerodynamic force of the blade element can be calculated mathematically, this approach is not popular for a large-scale blade. The sectional lift force will be ignored due to the large forces coming from the wind.

2.3.2 Span-wise approach

The span-wise modelling is able to determine the blade deflection at different wind speeds. The wind turbine blade is modelled using the finite element model, with which

the deflection of cracked wind turbine blades is analysed (Hassena et al. 2013). This study shows the model can indicate the change in natural frequencies due to a change in wind turbine blade structure. The BEM theory is applied in the modelling process, and then a curve fitting technique is applied to deduce the polynomial expression of the force of the cracked blade. The curve fitting expression for the out-of-plane force is,

$$F_X(r) = 34.544 + 15.816r + 2.469r^2 \tag{2.10}$$

where $F_X(r)$ is the out of plane force, and r is the rotor radius. $F_X(r)$ is affected by the rotor radius of the blade length in a quadratic function. The blade deformation curve can be seen in the wind turbine when it is in operation.

Large deformation modelling of a wind turbine blade is translated in mathematical expression (Rezaei et al. 2015). The blade tip deformation in its x, y and z axes are called ξ, η and ζ. These three deformations depend on the blade root deformation, and the initial axis is taken from the tower base axis. The initial coordinate system is the reference coordinate that is fixed to the ground and its orthogonal vector is i_{XYZ}. The blade is placed at the top of the tower and the pitch angle of the blade section is located along the longitudinal axis. The deformed local coordinate system is fixed to the unwrapped blade structural deformation and is expressed by $i_{\xi\eta\zeta}$.

$$i_{XYZ} = \mathbf{T_r}(i_{X'Y'Z'}) \tag{2.11}$$

$i_{X'Y'Z'}$ is the orthogonal unit vector with regards to reference coordinate that is fixed to the ground.

$$\mathbf{T_r} = \begin{bmatrix} \cos(\beta_p) & 0 & \sin(\beta_p) \\ 0 & 1 & 0 \\ -\sin(\beta_p) & 0 & \cos(\beta_p) \end{bmatrix} \begin{bmatrix} \cos(\theta) & -\sin(\theta) & 0 \\ \sin(\theta) & \cos(\theta) & 0 \\ 0 & 0 & 1 \end{bmatrix} \tag{2.12}$$

where β_p is the coning angle between the vertical plane and the elastic axis of the blade.

$$\mathbf{T_0} = \begin{bmatrix} 1 & 0 & 1 \\ 0 & \cos(\phi_p) & \sin(\phi_p) \\ 0 & -\sin(\phi_p) & \cos(\phi_p) \end{bmatrix} \tag{2.13}$$

where ϕ_p is the pitch angle of the blade section.

$$i_{xyz} = \mathbf{T_0}(i_{XYZ}) \tag{2.14}$$

$$\mathbf{T_0} = \begin{bmatrix} 1 & 0 & 0 \\ 0 & \cos(\phi_p) & \sin(\phi_p) \\ 0 & -\sin(\phi_p) & \cos(\phi_p) \end{bmatrix} \tag{2.15}$$

where ϕ_p is the pitch angle of the blade section.

$$i_{\xi\eta\zeta} = \mathbf{T}(i_{xyz}) \tag{2.16}$$

$$\mathbf{T} = \begin{bmatrix} 1 & 0 & 0 \\ 0 & \cos(\phi) & \sin(\phi) \\ 0 & -\sin(\phi) & \cos(\phi) \end{bmatrix} \begin{bmatrix} B_{11} & B_{12} & B_{13} \\ -B_{12} & B_{11} + B_{13}^2/(1+B_{11}) & B_{12}B_{13}/(1+B_{11}) \\ -B_{13} & B_{23} & B_{11} + B_{12}^2/(1+B_{11}) \end{bmatrix} \tag{2.17}$$

where, ϕ is the local torsional deformation at each section of the blade.

$$B_{11} = \frac{1+u}{1+e} \tag{2.18}$$

$$B_{12} = \frac{v}{1+e} \tag{2.19}$$

$$B_{13} = \frac{w}{1+e} \tag{2.20}$$

$$e = \sqrt{(1+u)^2 + v^2 + w^2} - 1 \tag{2.21}$$

where u is the longitudinal deflection in i_x direction, v is the longitudinal deflection in i_y direction, w is the longitudinal deflection in i_z direction, e is the elongation of the elastic axis. This study neglected e.

The deflection that is shown in Figure 2.4 is relevant to the ATB design where

the elastic twist from the composite materials is causing extra deflection in the blade spanwise. The simulation tool GL Bladed has the blade deflection feature in the simulations. The Bladed simulation model and the mathematical model as explained in this section can be integrated together to develop an ATB model.

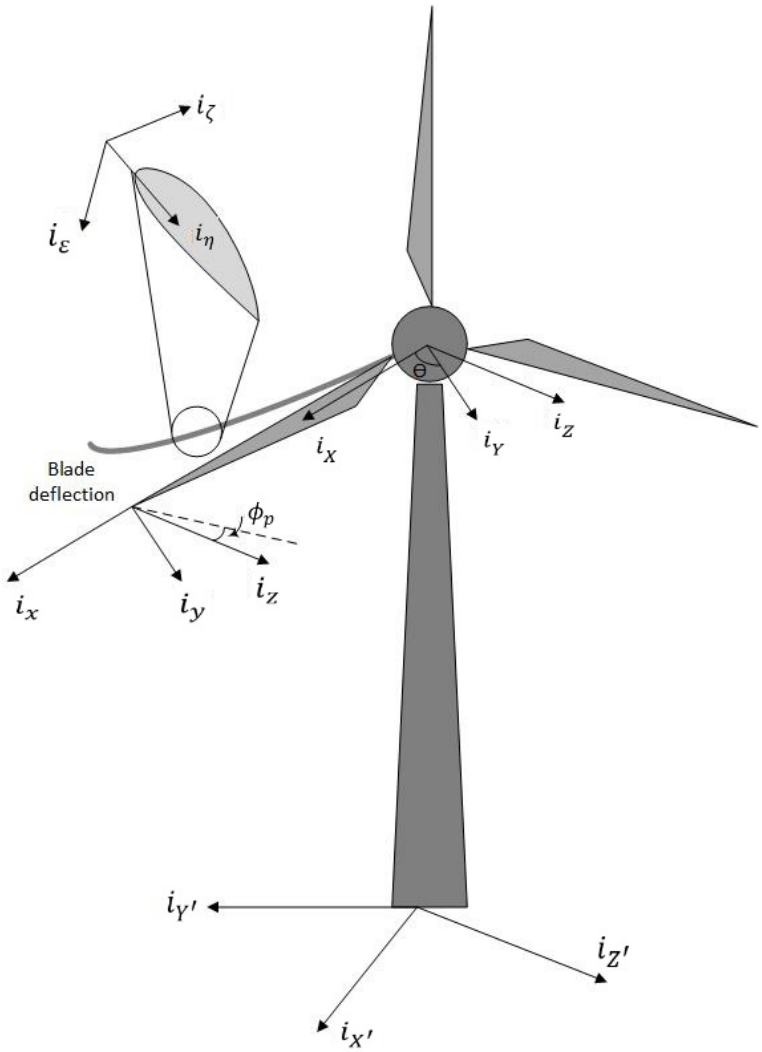

Figure 2.4: Blade transformation coordinate

2.3.3 Bend and twist coupling (BTC) in ATB wind turbine model

BTC is the coupling between the bending and torsional deflection of a wind turbine blade. It is also known as aeroelastic tailoring. BTC has an effect on the angle of attack (AoA), α of a wind turbine blade. It also contributes to reducing the loads in

wind turbine blades provided that the blade design has a torsional deflection towards feather. Feather is when the blade turns to the angle where the wind is parallel to the blade. As such, BTC towards feather lowers the AoA.

BTC arises from aerodynamic loads which alters with AoA, (Fedorov et al. 2012). GL Bladed investigates the effects of BTC on aeroelastic modal properties where BTC is represented in the stiffness matrix of the structural blade section model. Typically, for models that have zero diagonal values mean, BTC is not included in the equation. A matrix with non-zero values suggests that the structure contains BTC. Some publications explore BTC for wind turbine blades (R. Stäblein 2016, R. Stäblein et al. 2016, Vesel Jr & McNamara 2014). BTC is the mean to alleviate turbine blade load and it affects the blade frequency, damping and stability (R. Stäblein 2016, R. Stäblein et al. 2016). The impact of having forces on the torsional area will alleviate the loading on a surface such as the wind turbine blade.

A blade also has its mode frequencies due to the materials used in the structure. An experimental study to identify cracks in wind turbine blades was carried out to identify cracks by running the modal test on the blade. The cracks were indicated by determining the mode frequencies (Ganeriwala et al. 2011).

A further modal analysis estimated the total damping of an offshore wind turbine (Shirzadeh et al. 2013). The estimation process took aerodynamic effects into account to identify how the blade mode frequency affects the fundamental fore-aft (FA) tower mode. Their results show that one of the peaks that contributes to the FA peak comes from the blade modes.

A study on the effect of BTC and flutter on a large-scale 5MW wind turbine blade was done by Hayat et al. (2016). Three types of unbalanced laminates were analysed: the ply angle, the material and the thickness. Their findings showed that using lighter and stiffer carbon fibres ensures higher structural BTC of the blade.

For a large-scale wind turbine blade, the deformation is mainly affected by composite materials. BTC is one way to introduce significant blade deformation (Stäblein 2016). BTC is proven to be able to reduce the fatigue loading effects on wind turbine blades. When designing BTC blades, the angle pre-twisting can be designed to compensate the

power generation loss due to the coupling.

The modelling of BTC is outlined in the GL Bladed manual for a beam structure and it is represented in a 6×6 cross-sectional stiffness matrix form as shown in (2.22).

$$\begin{bmatrix} F_x \\ F_y \\ F_z \\ M_x \\ M_y \\ M_z \end{bmatrix} = \left[\begin{array}{ccc:ccc} EA & & & & & \\ 0 & GA_y & & & Symm & \\ 0 & 0 & GA_z & & & \\ \hdashline & & & GI_x^* & & \\ & 0 & & C_{xy} & EI_y & \\ & & & C_{xz} & C_{yz} & EI_z \end{array}\right] \begin{bmatrix} \gamma_x \\ \gamma_y \\ \gamma_z \\ \kappa_x \\ \kappa_y \\ \kappa_z \end{bmatrix} = \overline{\overline{C}} \begin{bmatrix} \gamma_x \\ \gamma_y \\ \gamma_z \\ \kappa_x \\ \kappa_y \\ \kappa_z \end{bmatrix} \tag{2.22}$$

where, F_x, F_y, F_z and M_x, M_y, M_z are the forces and the moments of inertia for three directions x, y, z. EA, GA_y, GA_z, GI_x^*, EI_y^*, EI_z^* are the constant coefficients of the materials in the blade given that E and G are elastic and shear modulus of the material, A is the area, I_y, I_z are the second moments of the area, I_x^* is the torsion constant of the cross section and $\gamma_x, \gamma_y, \gamma_z, \kappa_x, \kappa_y$ and κ_z are vectors of the beam strain.

$$\overline{\overline{C}} = \left[\begin{array}{c:c} \mathbf{P} & \mathbf{Q} \\ \hdashline \mathbf{R} & \mathbf{S} \end{array}\right] \tag{2.23}$$

where, $\mathbf{P}$, $\mathbf{Q}$, $\mathbf{R}$ and $\mathbf{S}$ are defined in (2.22). BTC is defined in $\mathbf{S}$ where C_{xy} and C_{yz} are the flap edge stiffness and C_{xz} is the torsion edge stiffness, i.e.,

$$\mathbf{S} = \begin{bmatrix} GI_x^* & & \\ C_{xy} & EI_y & \\ C_{xx} & C_{yz} & EI_z \end{bmatrix} \tag{2.24}$$

The blade moment is factorised by the stiffness terms, as the diagonal terms in $\mathbf{S}$ and all such values can be defined in GL Bladed for further investigation. The latest version of GL Bladed allows users to simulate the flexibility of the blade model incorporating the finite element model in the tools.

BTC is effective for mitigating loads in wind turbine blades. A better load reduction

system requires higher structural aspects of BTC compared to underlying structures. However, care must be taken in the selection of BTC because it may increase dynamic instabilities (Hayat et al. 2016). In ATB wind turbines, the ATB is designed with composite materials, and it includes unique parameters such as BTC coefficients, types of materials and numbers of blade layups.

BTC exists in the blade structure with interactions between two or more structural modes. Theoretically, BTC arises from aerodynamic interaction with forces such as wind, and it varies the shape of the blade structure. There are three modes in wind turbine blades, but typically only two are considered and they are the flapwise and edgewise modes. An additional mode is the torsional mode but it is not found in the baseline model.

Based on the stiffness matrix as shown in (2.22), C_{xy}, C_{xz} and C_{yz} are defined as zero for the baseline blade. This means that BTC's existence in the baseline wind turbine can be ignored.

No dynamic models for ATB wind turbines are found in literature. The available approaches are mostly based on CFD modelling. A CFD model cannot be used for controller development. A static model of ATB is developed for a small-scale wind turbine with composite materials blade based on the steady-state condition (Capuzzi et al. 2015). Further discussions on the static ATB model is explained in Chapter 3.

The spring damper model is well known for modelling various types of structures such as a cable structure in (Shan et al. 2020). Shan et al. (2020) explained that the modelling flexibility with the mass-spring model is based on the number of the mass points. The flexibility of a beam, cable, etc. can be described by discretising the subject into several segments. There are several geometrical approaches to model an ATB wind turbine such as the GEMT (Wang et al. 2014) and the blade model (Baumgart 2002, Li et al. 2014). Most aeroelastic blade models are based on the aerodynamics principle of the structure, limited to smaller-scale wind turbines. Results for an industrial-scale 5MW wind turbine are reported in (Capuzzi et al. 2014*a*). Their research focused on aerodynamic performance using CFD, but a model for power performance analysis is not included.

2.3.4 Modelling computational tools

A important support in this study is the simulation tools. There are numerous simulation softwares in wind energy systems, for example, the industrial-scale software by Garrad Hassan, GL Bladed, National Renewable Energy Laboratory (NREL) open source FAST software, educational level of QBlade software, ANSYS, COMSOL and some more (Kumar et al. 2016). One advantage GL Bladed is that it is capable of interfacing with Matlab and Simulink software. The parameters in GL Bladed are very close to the industrial-scale wind turbine parameters. The capability of this software to integrate into Matlab helps a lot in testing the machine in various conditions. GL Bladed is a licensed software not an open source as FAST or QBlade. A comparison is made between the baseline wind turbine and higher scale wind turbine using GL Bladed (Beardsell et al. 2016, Collier & Sanz 2016). The comparisons are made for the normal and flexible blades. With GL Bladed, the nonlinear blade deflection was defined by splitting the blade into several linear bodies. This method could be one of the possible techniques in modelling ATB.

FAST is an open source software developed by NREL, which is also widely used in wind energy studies. Compared to GL Bladed, FAST would require more programming skills. However, both GL Bladed and FAST are popular among wind energy researchers (Wright & Fingersh 2008).

QBlade, on the other hand, is not an industrial-scale software. It does not have industrial data verification (Marten et al. 2013). But, it is indeed a very convenient software for a beginner to design a wind turbine starting from blade design, drive train, tower and also the wind profile.

Since GL Bladed has the architecture of an industrial-scale wind turbine model, in this thesis work, it is used together with Matlab and Simulink to develop the ATB models for simulation and controller design.

2.4 Wind Turbine Control

Control plays important roles in wind turbine systems. Generally, the control objectives are to ensure the stability of the controlled system, minimise the steady state error and minimise the cost of operation and maintenance of the system. Wind turbine control strategies are developed for the full envelop of turbine operations. In below-rated operation, the control objective is to maximise energy capture as wind speed varies. While the rated power is practically unattainable in this region, the control technique offers that the power generated is optimum by adjusting the rotor speed through torque control. In above-rated operation, the control system works to maintain the power generation at the rated level by pitch control.

Wind turbine control approaches can be categorised into four groups: fixed speed stall regulated control, fixed speed pitch regulated control, variable speed stall regulated control and variable speed pitch regulated control, among them the variable speed pitch-regulated control is mostly used for modern turbines.

In a separate context, there is a passive control strategy for a wind turbine system. The passive control in wind turbine is applied in stall control where the geometry of the rotor blade is aerodynamically designed to ensure that the blade is stalled and it prevents the lifting force of the rotor blade from acting on the rotor (Branner et al. 2012). However, there is a disadvantage of this design – the power capture is not at its optimum value. Nonetheless, some results show that the passive control performance for an ATB wind turbine is better than the baseline wind turbine at below-rated wind speed (Capuzzi et al. 2014*a*). Note that their results are from experiments on a small-scale wind turbine.

It is critical to develop a working model for ATB wind turbine control. A turbine with ATBs has special characteristics in aerodynamics, rotor dynamics and other factors. No dynamic models are available for control purposes. Due to this gap, a baseline wind turbine controller can be firstly adopted to the ATB wind turbine model. A baseline controller may not fully work for an ATB turbine, but it will provide useful insights for further exploration.

2.4.1 Gain-scheduling baseline controller

A brief review of wind turbine modelling and control can be found in (Leithead et al. 1991). The gain-scheduling wind turbine controller is established for the full envelope wind turbine control with a switching mechanism between the below below-rated controller and the above above-rated controller. At above-rated, the controller is successful in achieving the rated power and without increasing the loading effect on the turbine. Control engineers investigate other controllers such as linear quadratic control, sliding mode control, MPC and many more for wind turbines.

There are computational tools developed for controller design such as GL Bladed and FAST. GL Bladed is a licensed software that is mainly applied for commercial wind turbines and is also used by academics. FAST is an open source software widely in wind turbine control studies.

2.4.2 Model predictive control (MPC) for wind turbines

MPC was initially known as receding horizon control in the 1960s and has been widely applied to various industries such as chemical engineering, robotics, steel manufacturing, and many others. The study on MPC for wind turbine systems was initiated around 2010s (Li et al. 2021). There are several types of MPCs applied in wind turbine systems such as the linear MPC, nonlinear MPC, economic MPC and robust variation, as summarised in (Mirzaei et al. 2012, Sinner et al. 2021). For wind farm control, there are also adaptive MPCs which are also applied on a wind turbine system, centralised MPCs and random MPCs. Munters & Meyers (2018) experimented with MPC on a wind farm to investigate dynamic induction and yaw control strategy on individual turbines and the effect on the wind farm power generation.

MPC uses a predictive model to estimate the future event based on the current event. It solves an optimal control problem in every time step for a finite horizon to determine a control input by conforming to the constraints. MPC is computationally demanding since the optimisation problem must be solved at every time step of the control process. The findings of MPC applied to a standard wind turbine system can be used as the benchmark for its application to an ATB wind turbine.

There are a group of works looking into MPC in wind turbine systems equipped with LIDAR measurement since LIDAR measurement can provide preview of wind speed before it reaches the turbine. A comparison is made on nonlinear MPC and feedforward controller to a baseline controller with wind speed data simulated by LIDAR, and the results show that LIDAR-based MPC has the benefit of reducing the fatigue loads as MPC is capable of limiting the blade pitch rates (Schlipf et al. 2012). The significance of LIDAR-based MPC control for wind turbines is discussed in (Koerber & King 2013). In 2015, Jain et al. (2015) studied linear MPC for wind turbines for all regions with multi-objective cost functions.

Another popular MPC application in wind turbines is economic MPC (EMPC). It is designed to optimise the control actions to satisfy common economic and operation performance cost functions. EMPC applies to most nonlinear MPC, for example, Loew et al. (2022) studied on nonlinear EMPC of fatigue formulation for wind turbine control, Dyrska et al. (2021) studied nonlinear EMPC application to wind turbine control. An economic nonlinear MPC is analysed by examining the closed-loop performance under different control parameters (Gros & Schild 2017).

MPC was also integrated with fatigue-based prognosis to limit the damage to wind turbine components. The basic control parameters were similar to the standard MPC and the fatigue is modelled by rain flow cycle (Sanchez et al. 2015). More recent works include nonlinear MPC to offshore floating wind turbines (Pustina et al. 2022), MPC for individual pitch control and load alleviation (Pamososuryo et al. 2022, Petrović et al. 2021), just to mention a few.

Besides its application in wind turbine aerodynamic control, MPC is also well established in wind power generation control. For example, the switching performance is improved with MPC for wind turbines over the full wind speed range (Xing et al. 2018); a full range wind turbine control is developed by integrating simulations in FAST and Simulink (Dittmer et al. 2021); MPC is applied on a variable speed controller of a wind generation system (Jawad et al. 2022).

2.5 Summary

This chapter gives a fundamental understanding of aeroelasticity, aeroelastic tailoring, ATB development and their applications in wind turbine technology. The chapter also discusses the aeroelastic modelling for a wind turbine system. Two approaches, chordwise and spanwise are explained. The chordwise approach is not applicable to a large-scale wind turbine blade. But, a fundamental understanding is still required. Theoretically, the spanwise approach is more relevant to ATB modelling, but it has never been applied to a flexible blade model. Finally, a brief theory of BTC is explained for basic understanding of ATB.

In ATB wind turbines, the blade design is inspired to follow nature's concept of leaves and in a technical context, the physical design involves composite materials and a design twisting profile. For a large-scale wind turbine, the fundamental concept of the elastic blade axis can be ignored. A basic understanding, however, of wind turbine principles such as BEMT is required. The dynamics of the ATB wind turbine are different from the dynamics of the baseline wind turbine. The ATB wind turbine design results in new dynamics of the blade and causes new dynamics in the whole turbine as well. Thus, new controller development is required to achieve the main objectives, to reduce the fatigue loading without compromising the power production.

This chapter also briefly presents wind turbine control and its significance for ATB wind turbine systems. Some existing control strategies can be re-developed for ATB wind turbines provided that the ATB wind turbine model is developed.

The baseline gain-scheduling wind turbine controller is well established and widely applied in existing wind turbine control. This baseline controller will be re-tuned for the new ATB wind turbine system. Furthermore, MPC is considered to be a good potential for ATB wind turbine control since it provides real-time optimisation design subject to constraints, as evidenced in many successful applications.

Chapter 3

Wind Turbine with Static ATB Model and Baseline Control

This chapter presents the static model of ATB wind turbine development in GL Bladed and discusses the application of baseline controller in the ATB wind turbine model referring to the basic controller application in the baseline wind turbine model. ATB wind turbine model is a new approach in the wind turbine research environment. The model development presented in this chapter will give an idea of the ATB wind turbine performance and its performance with the existing standard baseline controller.

This chapter comprises 6 sections. Section 3.1 starts with wind model, Section 3.2 explores the 5MW Supergen wind turbine model which covers the aerodynamics, rotor dynamics, drive-train dynamics and tower dynamics. Section 3.3 discusses the fundamental theory of wind turbine control and Section 3.4 describes the modelling of a static model of an ATB wind turbine. Section 3.5 discusses the simulation set up of the ATB static model and the chapter is summarised in 3.6.

3.1 Wind Model

The power generation of a wind turbine system is given as, The power production for a wind turbine system is given by,

$$P = \frac{1}{2}\rho\pi R^2 C_p(\lambda, \beta)U^3 \tag{3.1}$$

where P is the power, ρ is the air density, R is the blade length, C_p is the power coefficient and U is the wind speed, λ is the tip speed ratio and β is the pitch angle. Note that the power coefficient, C_p is dependent on pitch angle,β and tip speed ratio, λ.

3.1.1 Wind spectra

Wind has stochastic behaviour in nature. However, the predictability of the wind is important for integrating wind power into the electricity network and organising the system properly. One of the useful methods is using the Van der Hoven spectrum. The Van der Hoven spectrum effects were recorded in New York in 1957 and is still significant in wind analysis. Figure 3.1 shows the Van der Hoven spectrum with 3 clear peaks, the sypnotic, diurnal and turbulent. The synoptic peak is the highest peak with 4 days of wind fluctuation recorded. The second highest peak is the turbulent peak. For the turbulent peak, the Van der Hoven spectrum suggests there are substantial amount of energy in 1 minute periodic fluctuation of the wind. The valley between diurnal peak and turbulent peak or between 10 hours and 3 minutes is also known as the spectral gap means very little energy is recorded between 2 hours and 10 minutes. Diurnal peak is the third highest peak where it shows the amount of energy recorded in approximately 12 hours.

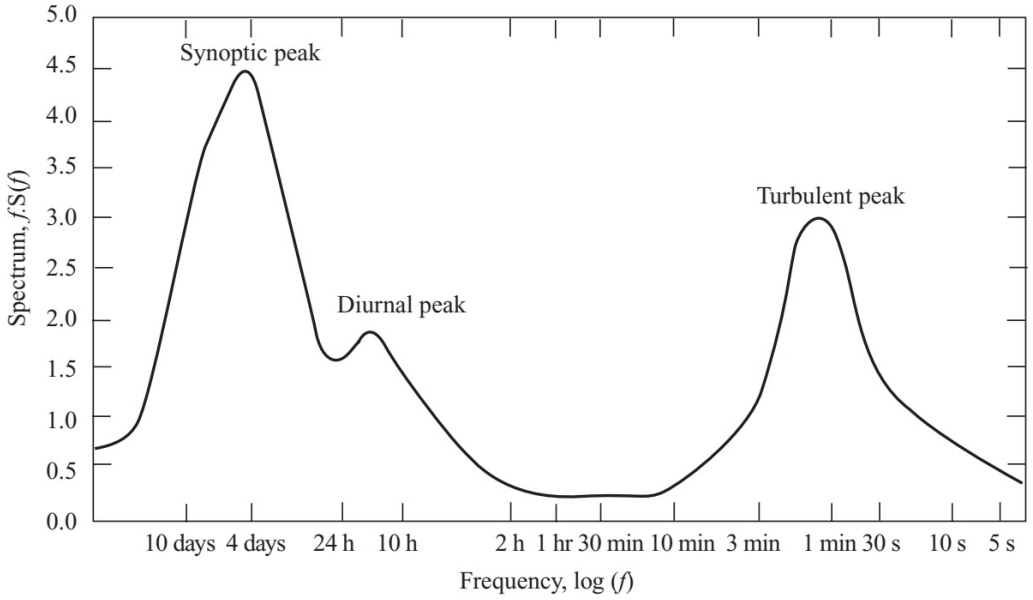

Figure 3.1: Van der Hoven wind spectra (Burton et al. (2001))

3.1.2 Annual and seasonal variations

The wind speed variations over a year-long can be interpreted using a probability distribution. The Weibull distribution in Equation (3.2) represents the variation in the hourly mean wind speed over a year at various common sites.

$$F(U) = \exp\left(-\left(\frac{U}{c}\right)\right)^{k} \tag{3.2}$$

where, U is the mean wind speed, $F(U)$ is the fraction of time for which the hourly mean wind speed exceeds U, c is the scale parameter, and k is the shape parameter that describes the variability of the mean.

Higher k shows a higher median of wind speed. For example, $k < 2$ refers to a location with lots of low wind speeds and some very strong winds and $k = 3$ refers to consistent wind speed around the median. For $k = 2$, the Weibull distribution is known as a special case which is also called the Rayleigh distribution. Figure 3.2 shows the example of Weibull distribution with $c = 9$ and k is varied from $k = 1.25$ to $k = 3.0$.

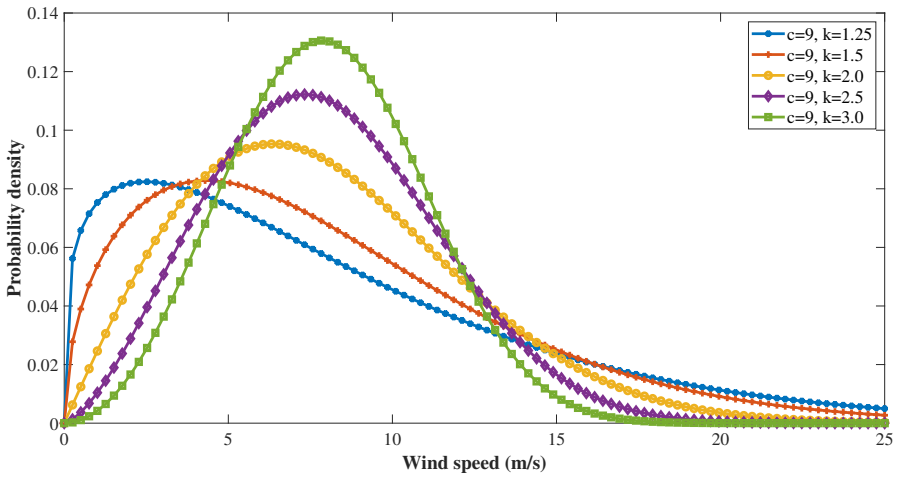

Figure 3.2: Examplar Windbull distributions

The Weibull distribution of hourly mean wind speed over a year is well documented and true at many locations. However, there are factors that cause the Weibull probability to differ from the expectation such as the seasonal effects where there is a time when the earth tilts the rotation axis. There is also a time in winter or summer when the atmosphere is windier than the usual seasons. Regardless of those effects, Weibull distribution is the most significant tool to predict wind characteristics.

3.1.3 Turbulence intensity

Turbulence is the wind speed fluctuations on a time scale of less than 10 minutes. It refers to the turbulent peak area in Figure 3.1. Turbulence is generated from two causes, friction with the earth's surface and the thermal effects that cause the change in temperature which results in the vertical movement of the air masses. Turbulence is complex but it can be measured by the turbulent intensity. The turbulence intensity is the ratio of the root means squared of the turbulent wind over the standard deviation of the mean wind speed U that is usually defined as 10 minutes or 1 hour. In the atmosphere, this turbulent intensity could reach quite large values. Typical values of 20 or 30% could be reached for low winds, and relative turbulence intensity decays

when the mean speed increases. The turbulence intensity is represented by

$$I = \frac{\sigma}{U} \tag{3.3}$$

where σ is the standard deviation of the wind speed, and U is the mean wind speed.

The turbulence intensity, I, depends on the roughness of the ground surface, z_0, and the height, h above the surface. Apart from these two variables, it also depends on the terrain such as buildings, trees, and hills or mountains. Table 3.1 presents the typical surface roughness for different types of terrains. It shows that cities and forests have the highest surface roughness, z_0, compared to other terrains. Also, indicate the reasons wind farms are commercially built over the hills and offshore.

Table 3.1: Typical Surface Roughness Lengths (Burton et al. 2001)

Types of terrain	**Roughness length, z_0 (m)**
Cities, forests	0.7
Suburbs, wooded countryside	0.3
Villages, countryside with trees and hedges	0.1
Open farmland, few trees, and buildings	0.03
Flat grassy plains	0.01
Flat desert, rough sea	0.001

For simulation works, turbulent intensity is defaulted at 10% or 0.1 and is varied depending on the work demand. According to the Normal Turbulence Model (NTM), the representative value of the turbulence standard deviation, σ, shall be given by the 90% quantile for the given hub height wind speed (Leu et al. 2014).

3.1.4 Wind modelling for wind turbine technology

Wind speed can be modelled using several types of approaches. Gala Santos (2018) explored the point wind speed approach for wind turbine technology. The approach has been in the wind turbine field since 1980. Based on the Van der Hoven spectrum, the point wind speed is described as the combination of two components; a low-frequency component and a high frequency component. The low frequency component defines long term and slow variation and the high frequency defines fast variations or turbulence.

The low frequency component can be used for site assessment and can be described by a Weibull distribution for selected $k = 2$. At time t, the point wind speed is expressed as,

$$v(t) = v_m(t) + v_t(t) \tag{3.4}$$

where $v(t)$ is the wind speed, $v_m(t)$ is the low frequency component and $v_t(t)$ is the high frequency component.

Figure 3.3 shows the wind speed model configuration. $v_m(t)$ is the low frequency component generated in the time series. From $v_m(t)$, T_F, K_F and the standard deviation, σ_v, are extracted, where T_F and K_F are filtered by H_t. The white noise, $w(t)$, is also filtered with the same filter. The output from the filter is multiplied by standard deviation, σ_v, results in the output high frequency wind speed, $v_t(t)$. The final wind speed is the summation of the low frequency and high frequency components. T_F and K_F depend on the mean of the low frequency wind speed $v_m(t)$ where K_F can be defined as

$$K_F \approx \sqrt{\frac{2\pi}{\beta(1/2, 1/3)} . \frac{T_F}{T_s}} \tag{3.5}$$

where

$$T_F = \frac{L_t}{v_m} \tag{3.6}$$

L_t is the turbulent length scale, β is the beta function, and T_s is the sampling time of the turbulent component.

From the figure, $v_t(t)$ is the high frequency wind speed with turbulent components, $w(t)$ is the white noise, H_t is the shaping filter, $\times$ is a multiply operation, σ_v is the standard deviation.

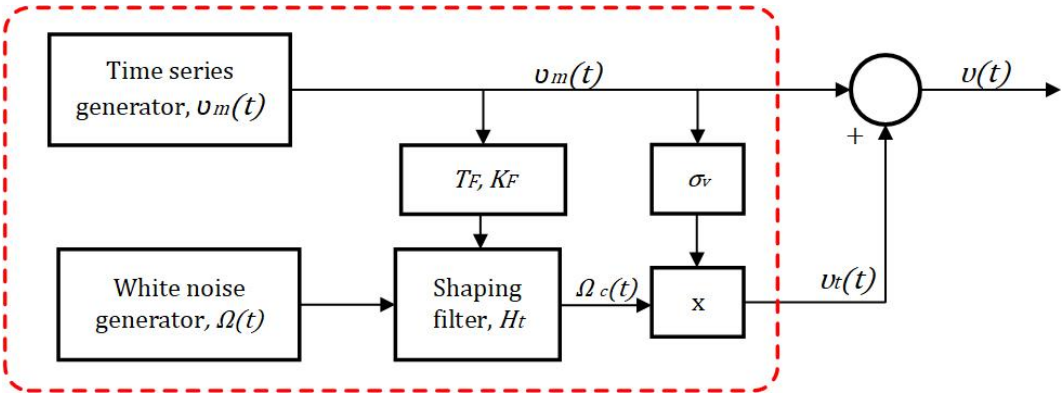

Figure 3.3: Wind speed model (Gala Santos 2018)

3.2 5MW Supergen Wind Turbine Model

In basic energy conversion, wind turbine harnesses the kinetic energy from the wind through the swept area of the blades. The wind that passes through the blade will experience different velocities and pressures that are caused by the rotor disc. This is also called stream tube energy extraction. The wind that passes through the rotor disc is extracted and converted into electrical energy through several processes. To simplify the understanding of the wind turbine system, it is modelled into separated parts that represent the aerodynamic model, rotor dynamics and drive-train dynamics.

3.2.1 Aerodynamics of wind turbines

The aerodynamics of wind turbines can be effectively analysed using the stream tube concept, which simplifies the flow of air through the rotor into a series of cylindrical stream tubes. This approach allows for a streamlined examination of changes in air velocity and pressure as it interacts with the rotating blades. The continuity equation,

$$A_1 U_1 = A_2 U_2 \tag{3.7}$$

expresses the conservation of mass, where A_1, U_1 are the cross-sectional area and the velocity of the incoming wind, and A_2, U_2 are for the downstream of the rotor. Additionally, the conservation of energy is addressed through Bernoulli's equation, given

by,

$$\frac{1}{2}\rho U_1^2 + P_1 = \frac{1}{2}\rho U_2^2 + P_2 + \frac{1}{2}\rho \Omega^2 R^2 \tag{3.8}$$

where, ρ is the air density, P_1 and P_2 are the pressures, Ω is the angular velocity of the rotor, and R is the rotor radius. While the stream tube model provides valuable insights into velocity distribution and power extraction, more advanced analyses often incorporate BEM theory, which considers detailed aerodynamic forces on individual blade elements for a comprehensive understanding of wind turbine aerodynamics.

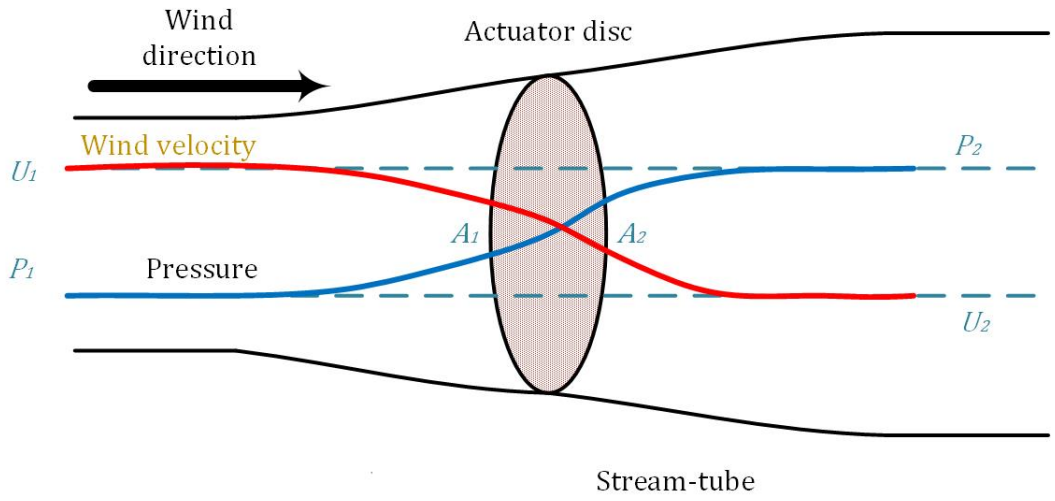

Figure 3.4: An energy extracting actuator disk and stream tube

3.2.2 Rotor dynamics

Rotor plays an important role in wind turbine systems. The wind that passes wind turbines actually passes the rotor disc, where the concept of the stream-tube model is analysed. Thus, the theories of blade element theory and BEM theory will be detailed in this section. Figure 3.5 shows 2 points of view of a 3 bladed wind turbine rotor, the front view and the side view. The parameters shown in the figure are basically the angular displacement of the rotor edgewise and flapwise. The front view shows the edgewise angle displacement and the side view shows the flapwise angle displacement. θ_R is the rotor blade edgewise or side-to-side angle displacement, θ_H is the hub side-to-side angle displacement, θ_T is the tower side-to-side angle displacement, ϕ_R is the rotor

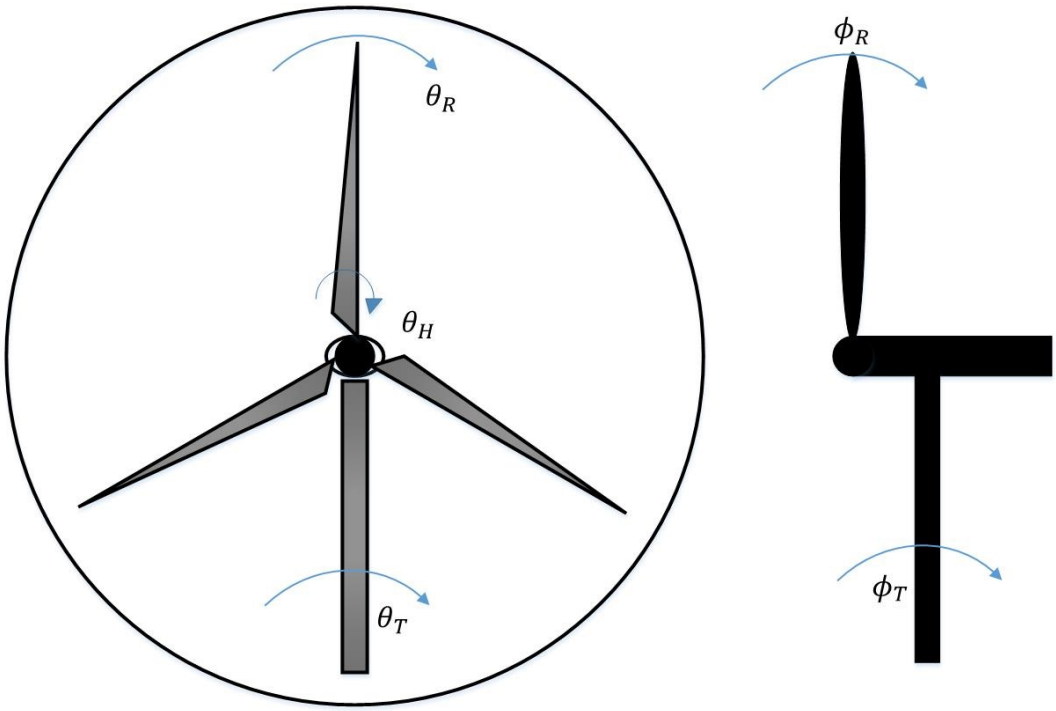

Figure 3.5: Wind turbine parameter representation

blade flapwise angle displacement and ϕ_T is the tower's fore-aft angle displacement. These parameters are important to represent the rotor dynamics formulation.

Wind turbine blades are one of the main parts of a wind turbine system, as it determines the output power produced by the system. The stream tube model shows that wind energy passes the rotor blade, and there are changes in pressure and velocity that are determined by the size and number of blades. The blade properties are also important in determining the output of the system. It is translated in Equation (3.12) where, for example, K_E and K_F are the stiffness coefficients for the edgewise and flapwise of a single blade. The stiffness is determined by the structural properties of the blade.

The blade element theory assumes that the forces on a blade element can be calculated using the angle of attack of an airfoil. The airfoil has drag coefficients, C_d that vary with the angle of attack for values a and a' can be determined. From Burton et al.

(2001), the resultant relative velocity at the blade is shown in Equation (3.9),

$$W = \sqrt{U_\infty^2(1-a)^2 + \Omega^2 R^2(1+a')^2} \tag{3.9}$$

where W is the apparent wind speed, U_∞ is the true wind speed, a is the axial induction factor, a' is the tangential flow induction factor, Ω is the rotor speed, and R is the rotor radius which W acts at an angle of rotation, as shown in Figure 3.6 and Figure 3.7. Figure 3.6 shows a blade element sweeps out of an annular ring. It is cut out of the blade of the wind turbine. When rotating, the wind speed that touches each blade element is not the same. The idea is to take out one section of the blade and analyse the section only. Assumptions were made based on the section and taken as a representation of the whole turbine.

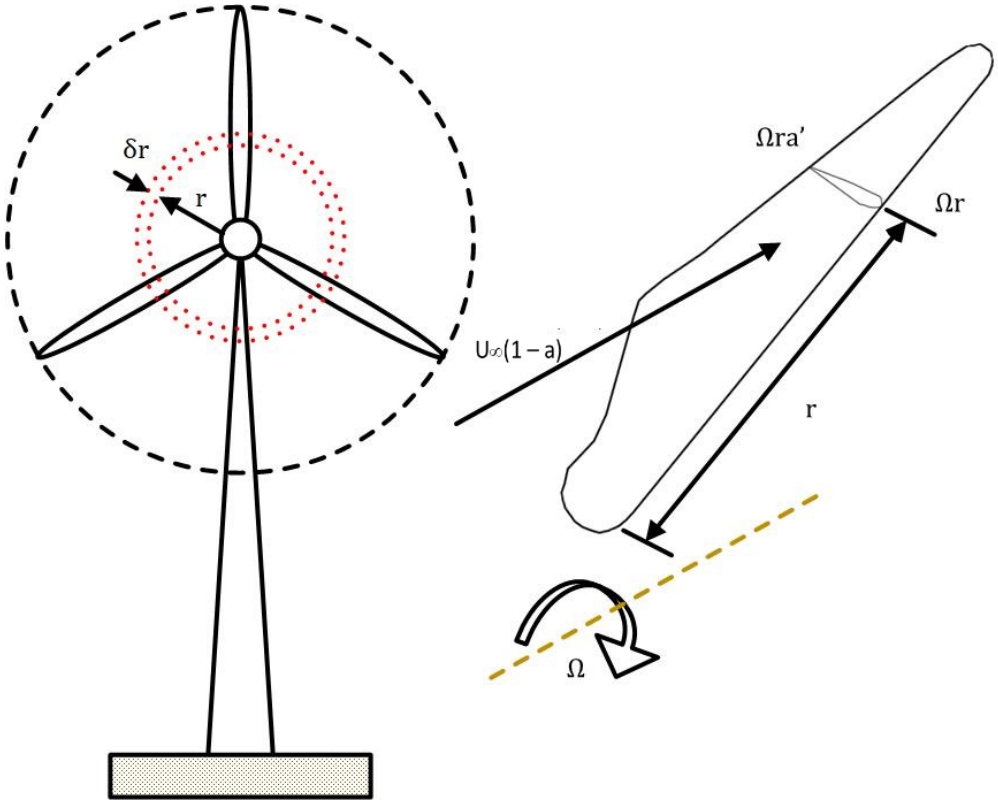

Figure 3.6: A blade element sweeps out an annular ring
Burton et al. (2001)

In Figure 3.7, dF_D is the drag force, dF_L is the lift force, dF_N is the total force,

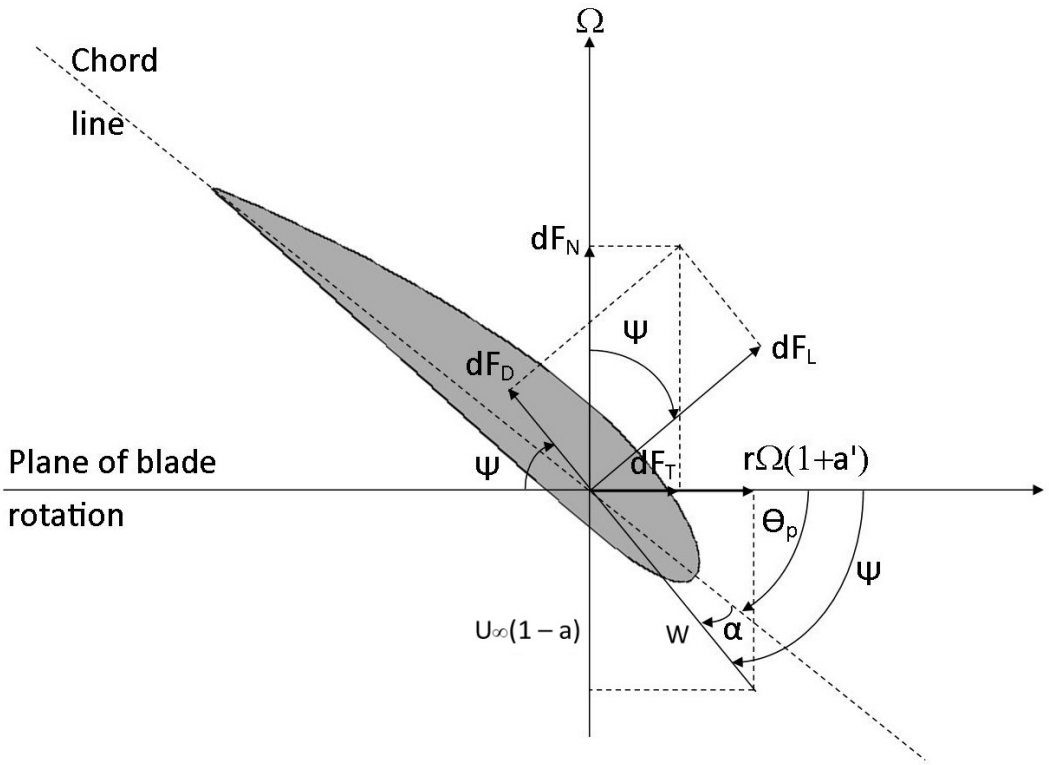

Figure 3.7: Blade element velocities and forces
Burton et al. (2001)

dF_T is the thrust force, Ψ is the total angle, α is the angle of attack, θ_p is the pitch angle, R is the rotor radius, Ω is the rotor speed, a is the axial induction factor.

The BEM model is largely used to model a baseline wind turbine rotor. The blade is analysed individually by dividing it into sections, and each section has different airfoil profiles. The force that was caused by the wind will generally create the torque which is proportional to the power production by the factor of the blade length. The power production of the wind turbine depends on its power coefficient, C_p.

Basically, the actuator disc model has proven that the maximum C_p is 0.59 only Burton et al. (2001). The performance of ATB wind turbine is basically adopting the similar power curves as the baseline machine, where technically the C_p-λ curve for a three-bladed wind turbine is referred to. The aerodynamic modelling as explained and proved by simulation in Capuzzi et al. (2014*a*) referred to the standard BEM.

BEM assumed that the force of a blade is accountable for the change of air momen-

tum that passes through the swept element. The component of the aerodynamic force on N blade elements resolves the axial direction as below,

$$\delta L cos\phi + \delta D sin\phi = \frac{1}{2}\rho W^2 N_c (C_L cos\phi + C_d sin\phi)\delta r \tag{3.10}$$

The rate of change of axial momentum of the air passing through the swept annulus is

$$\rho U_\infty (1-a) 2\pi r \delta r 2 a U_\infty = 4\pi \rho U_\infty^2 a(1-a) r \delta r \tag{3.11}$$

where, δL is δD is ϕ is the total angle of angle of attack and the twist angle, W is the apparent wind speed, U_∞ is the wind speed, δr is the cut-out blade, r is the blade length from the hub to the cut-out blade and a is the axial induction factor.

The wind turbine model for simulation is developed from the 4 main components that contribute to the dynamics of the system; aerodynamics, rotor dynamics, drive-train dynamics, and tower dynamics.

The summarised equations derived by Leithead & Rogers (1996a) and further discussed in Chatzopoulos (2011) are the ones used to develop the 5MW Supergen wind turbine model.

Aerodynamics:

$$\begin{aligned} J\ddot{\theta}_R = &- (K_E + J\dot{\theta}_R^2)[(\theta_R - cos\beta) - (\phi_R - \phi_T) sin\beta] cos\beta \\ &- (K_F + J\dot{\theta}_R^2)[(\theta_R - \theta_H) sin\beta + (\phi_R - \phi_T) cos\beta] sin\beta + F_1 \end{aligned} \tag{3.12}$$

where J is the inertia of the rotor, K_E and K_F are the edgewise stiffness and the flapwise stiffness of a single blade, θ_R is the rotor in-plane angular displacement, ϕ_R is the rotor out of plane displacement, θ_H is the hub angular displacement, ϕ_T is the hub fore-aft angular displacement, α is the twist angle of the blade, β is the angle between the blade edgewise mode plane and the plane of the rotor. F_1 and F_2 are the inplane and out-of-plane aerodynamic torques on the blade, Ω_0 is the nominal angular velocity of the rotor, J_C is the cross-coupling inertia of the tower and rotor. The in-plane and out-of-plane angle of the rotor, hub and tower is shown in Figure 3.5.

Rotor dynamics

$$\begin{aligned}\frac{1-\frac{J_C^2}{JJ_T}}{1+\frac{J_C}{J_T}}J\ddot{\phi}_R =&(K_E+J\dot{\theta}_R^2)[(\theta_R-\theta_H)cos\beta-(\phi_R-\phi_T)sin\beta]sin\beta\\ &-(K_F+J\dot{\theta}_R^2)[(\theta_R-\theta_H)sin\beta+(\phi_R-\phi_T)cos\beta]cos\beta\\ &+[F_2+\frac{J_C}{J_T}B_T\dot{\phi_T}+\frac{J_C}{J_T}K_T\phi_T]/(1+\frac{J_C}{J_T})\end{aligned} \tag{3.13}$$

$$J_C = MhR_C, \tag{3.14}$$

where, M is the mass of the rotor, h is the hub height of the rotor, R_C is the distance from the hub to the center mass of a blade, K_T is the tower stiffness, D_T is the fore-aft damping force with,

$$D_T = -B_T\dot{\phi}_T \tag{3.15}$$

The aerodynamic model represents the aerodynamics of the wind turbine model. The edgewise and the flapwise rotor stiffness with the angle displacement are the main components in the aerodynamic model. The rotor dynamics model consists of the angle displacement and velocity of the rotor and the hub. Other components such as the inertia of the hub and rotor and the stiffness also contribute to the model.

For the rotor dynamics, each blade of the rotor has two dominant structural modes; the flapwise mode and the edgewise mode in the direction of the principal axes of the blade. These two modes can contribute to the drive-train dynamics. There are 3 modes of the rotor 1 blade is stationary and two other blades are oscillating at the same frequency but out of phase. The total motion of these 3 blades is zero. Therefore, they constitute only 2 independent modes of the rotor. The third model is all 3 blades are oscillating at the same frequency, in phase.

In the Simulink model, the output from the rotor dynamics is the hub torque. The rotor dynamics model is combined with the aerodynamics model and is called aero-rotor block. The hub torque is the input to the drive-train block.

3.2.3 Drive-train dynamics

The drive-train model is the most significant part of the wind turbine to develop the controller. The performance of the wind turbine model is measured from the drive-train model such as the generator speed and power production. Regardless, these 3 main models are necessary to represent a complete industrial-scale wind turbine system. The dynamics of the drive train comprise the hub, low-speed shaft, gearbox, high speed shaft, generator, and the tower side-to-side movement, caused by the generator reaction torque.

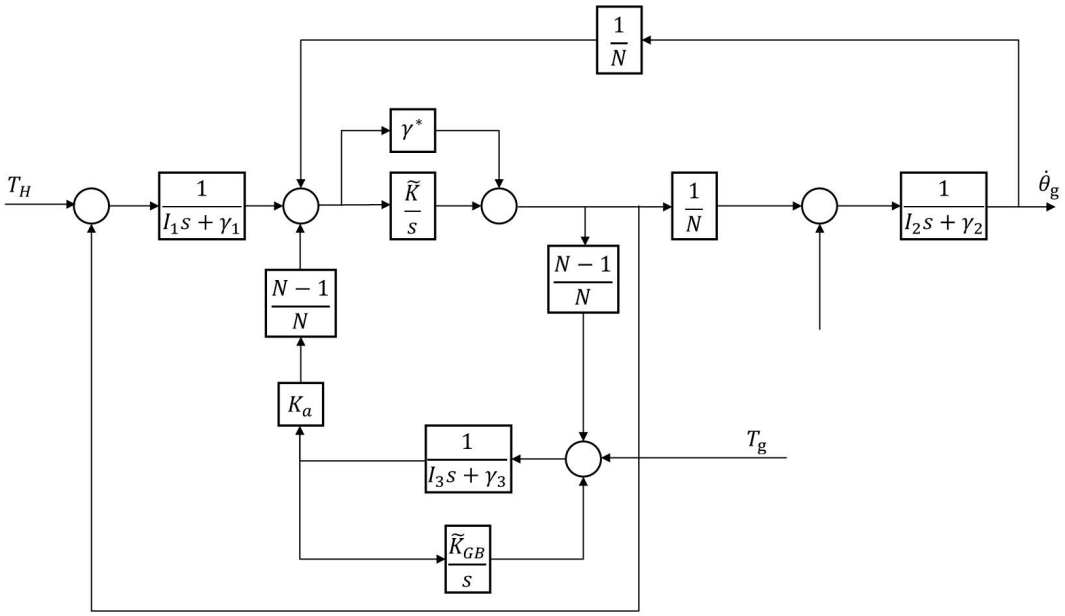

Figure 3.8: Simplified block diagram for drive-train model

Figure 3.8 shows the drive-train block diagram model. The input of the block diagram is the torque hub, T_H and generator torque, T_g and the output is the generator speed, $\dot{\theta}_g$. N is the gearbox ratio, γ_1, γ_2 and γ_3 are the damping factors for low-speed shaft, high-speed shaft and gearbox respectively, I_1, I_2 and I_3 are the inertia for low-speed shaft, high-speed shaft and gearbox respectively, $\widetilde{K} = N^2 K_1 K_2/(K_1 + N^2 K_2)$ where K_1 is the low speed shaft stiffness and K_2 is the high speed shaft stiffness, $\widetilde{K}_{GB}$ is the stiffness for gearbox and K_a is the multiplier. The block diagram model is applied in the 5MW wind turbine Simulink model.

3.3 Baseline Controller

The modern wind turbine control has 2 main tasks to establish a convenient operational state as conditions change and to enhance its dynamic properties. It has 2 categories; supervisory control and operational control. Supervisory control is a passive control where it supervises the plant's behaviour to deliver the given specifications as required. Operational control is the focus of the project. It is an active control to make sure the wind turbine system operation fulfils the objectives. In general, the operation is divided into 3 regions; below-rated, above-rated, and rated region. The regions are depicted in Figure 3.9. Below-rated region is determined within the range of approximately 4 m/s to 11 m/s. In this region, the control objective is to capture as much power as possible by tracking the maximum power coefficient, C_{p_max} by varying the rotor speed, Ω.

In general, the baseline controller has 2 types; below-rated controller and above-rated controller. The variable speed pitch regulated wind turbine control refers to the above-rated control. In the ATB wind turbine context, theoretically, the blade for an ATB wind turbine model is a flexible blade that is designed to react in a minimum movement when the blade is pitching in above-rated region. Not that, in below-rated region, the blade is not pitched. It controls the generator torque speed to track the maximum Cp. Thus, the blade behaviour is more reasonable to be analysed in the above-rated region compared to the below-rated region.

3.3.1 Below-rated control

Wind turbine operation is divided into 3 regions, below-rated region, the rated region and the above-rated region. The regions are depicted in Figure 3.9. Basically, the regions are measured in wind speeds. The range of wind speed distributed from 4 m/s to 24 m/s where below-rated region is commonly starts from 4 m/s to approximately 11 m/s, the rated region is around 11 to 12 m/s and above-rated region is from approximately 12 m/s to 24 m/s. In the control strategy, below below-rated region and above-rated region are controlled with 2 separate controllers. The controllers are below-rated controllers and above-rated controllers. These controllers will determine

the performance of the wind turbine system with a good control strategy.

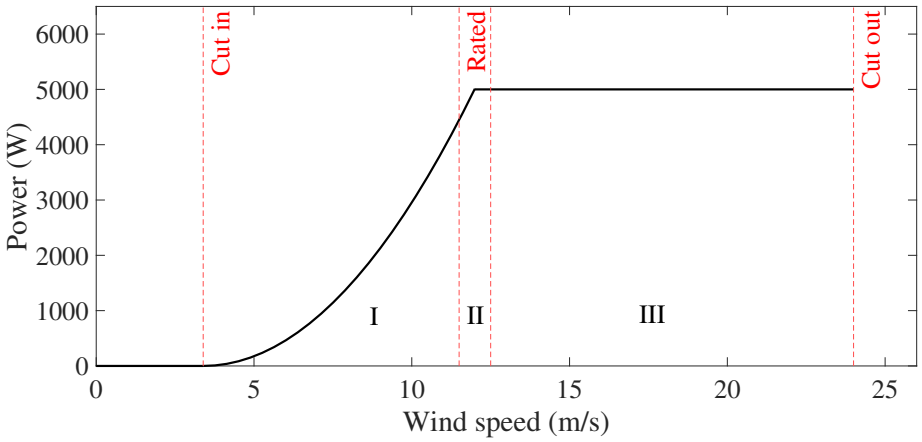

Figure 3.9: Power curve region

Below-rated controller is also known as the torque controller, where the main objective is to track the maximum power coefficient, C_p by varying the generator speed. In this region, the pitch angle is fixed at fine pitch.

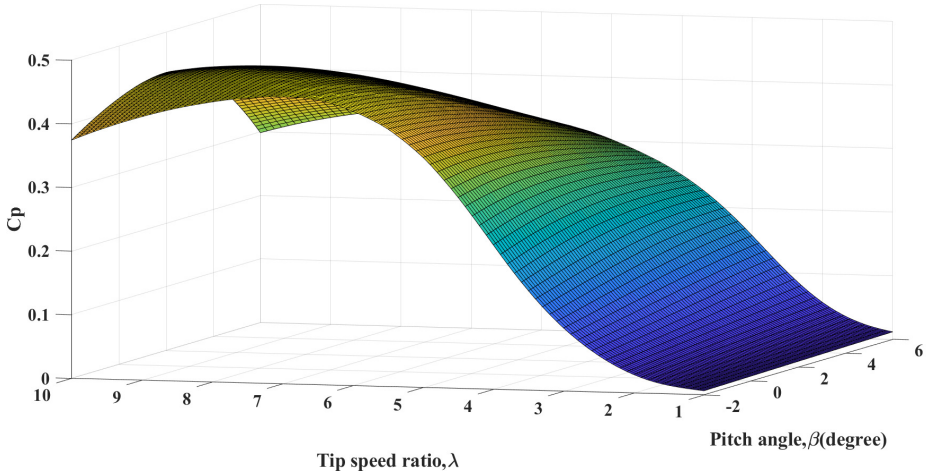

Figure 3.10: Power coefficient, $C_p(\lambda, \beta)$

Figure 3.10 shows power coefficient, C_p dependency to pitch angle, β and tip speed ratio, λ. Equation (3.1) mathematically presents that the power is generated by the

factor of C_p. C_p varies with the range of tip speed ratio, λ. Note that,

$$\lambda = \frac{\Omega R}{U} \tag{3.16}$$

In the below-rated region, generator torque is given as,

$$T_g = k\Omega_g^2 \tag{3.17}$$

where, k is the coefficient of,

$$k = \frac{\rho \pi R^5 C_p}{2\lambda^3} \tag{3.18}$$

In this region, the generator torque is varied to control the generator speed. When C_p is at its maximum, the aerodynamic efficiency is also at a maximum. This maximum value is achieved at the optimum value of the tip speed ratio, λ. The rotor speed is proportional to the wind speed and the generator torque demand T_g is calculated to be proportional to the measured generator speed, Ω_g as shown in Equation (3.17) and (3.18). The relationship between generator torque and generator speed is quadratic. The mechanical losses may vary with speed. As such, it is ignored in Equation (3.18) to maintain the quadratic relationship between rotor aerodynamic torque and rotor speed. The quadratic relationship is the tracking of the maximum power coefficient, C_p curve in the system.

3.3.2 Above-rated control

The strategy applied in the above-rated region is more interesting to explore. The above-rated region begins at approximately 11 m/s up to 24 m/s wind speed. The maximum wind speed is limited to 24 m/s. In theory, power production increases as the wind speed increases. However, when the wind speed is too high, the produced power will be a waste to the system. For example, a 5MW wind turbine will limit its power production to 5MW only even when the wind speed exceeds 24 m/s. The power is limited to 5MW by controlling the pitch angle with the pitch actuator whenever the

wind is changing. The strategy takes the wind speeds as the disturbance where the wind speeds are pre-calculated and represented with pitch angles respectively. The control system operates based on the input of the pitch angles measures the instant pitch angle and responds to instruct the pitch actuator to pitch to the expected pitch angle. The established strategy reflecting the method is known as gain-scheduling. The objective of an above-rated control or pitch control strategy is to maintain the power production at the rated value by varying the pitch angle. The strategy is difficult to handle due to the rapidly changing behaviour of the wind speed. The gain-scheduling technique is proposed to handle the situation. Wind speed is taken as the disturbance. However, the pitch angle is pinned to the wind speed based on the torque-speed diagram. The relationship between the wind speed, pitch angle and torque is formulated where the pitch angle is dependent on the wind speed and the linear relationship between pitch angle and torque is established with the partial differential of both.

In the pitch control region, the generator torque is held constant, while the pitch angle is varied. The pitch angle responds to the wind speed to achieve the rated power Zhang et al. (2008). The cutout wind speed is limited to 24 m/s. Mathematically, the power production is proportional to the wind speed which means that at a higher wind speed, more power can be produced. Traditionally, the wind cut-out wind speed is 24 m/s for wind speeds more than the cut-out wind speed, the power generated will be wasted. However, in recent years, there have been wind turbines that operate with cut-out wind speeds greater than 24 m/s. For example, Siemens Gamesa SG 14-222 DD has a cut-out wind speed of 25 m/s.

Figure 3.11 shows the basic control strategy approach for a wind turbine system. The plot is also known as a torque speed diagram with a control strategy where it consists of information such as the wind speed, power coefficient, C_p peak distribution, and rated power. The blue line is the control strategy for a 5MW wind turbine. The rotor speed, Ω_r varies from the minimum at 6 m/s and starts tracking the maximum power coefficient, C_{p_max} as the wind speeds change. The rotor speed, Ω_r will remain at constant speed when it reaches the rated region, approximately at 11 m/s. At this region the controller is switched to pitch control where the pitch actuator will pitch the

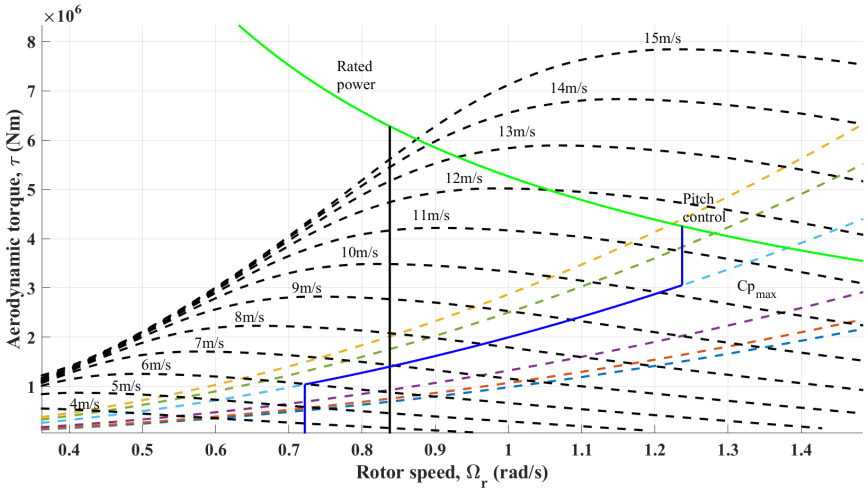

Figure 3.11: Control strategy of a standard wind turbine system

blade based on the pitch angle demand to maintain the power production is limited at a rated power of 5MW Burton et al. (2001).

3.3.3 Gain-scheduling technique in above-rated pitch control

For the pitch control strategy in the wind turbine system, the blade is pitched to achieve the rated power when the wind speed reaches the rated value. At this moment, generator torque, T_g is held constant, indicating that the controller is switched to pitch control from torque control. During this operation, a small change in pitch can result in a large effect on torque. In Bossanyi (2003), it mentioned that frequently the torque sensitivity changes almost linearly with pitch angle and it can be compensated for by varying the overall gain of the controller linearly with pitch angle. This is where the gain-schedule term is significant in wind turbine control. Thus, it is important to have a system linear model corresponding to selected values of operating points between the rated region (region II) and the above-rated region (region III). Then, choose a gain-schedule to satisfy the system performance for the entire range.

Equation (3.19) is aerodynamic torque, T in a baseline wind turbine. It is nonlinearly dependant on the pitch angle, β, the rotor speed, Ω, and the effective wind speed, v,

$$T = T(\beta, \Omega, v) \tag{3.19}$$

Figure 3.12 shows the dynamic relationship of aerodynamic torque. The pitch angle is determined from the pitch demand to the pitch actuator and the pitch angle to the torque. Torque, T, is the input of the drive-train and wind turbine power generation part.

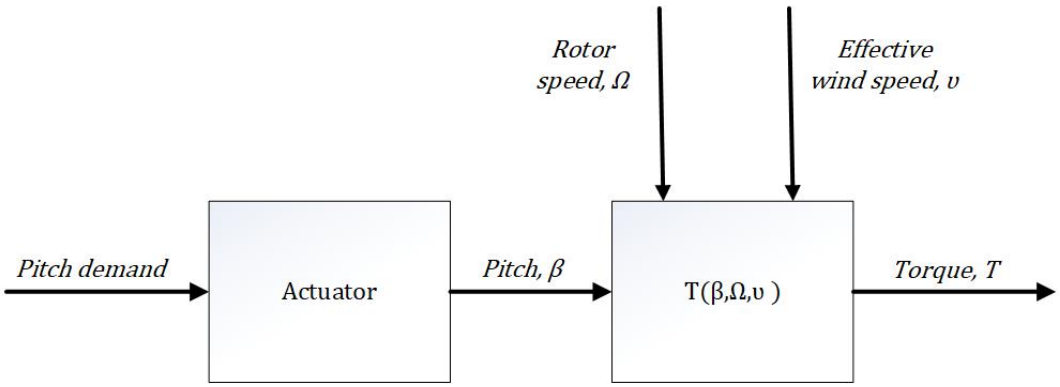

Figure 3.12: Dynamic relationship of aerodynamic torque

The aerodynamic torque has a dynamic relationship where it is nonlinearly dependent on the pitch angle, rotor speed and the wind turbine. It also shows that for each wind speed above-rated, the aerodynamic torque is attained at a unique pitch angle. This suggests that all wind speeds there correspond to their subjected pitch angle. These sets of wind speeds define the locus of equilibrium operating points of the wind turbine system.

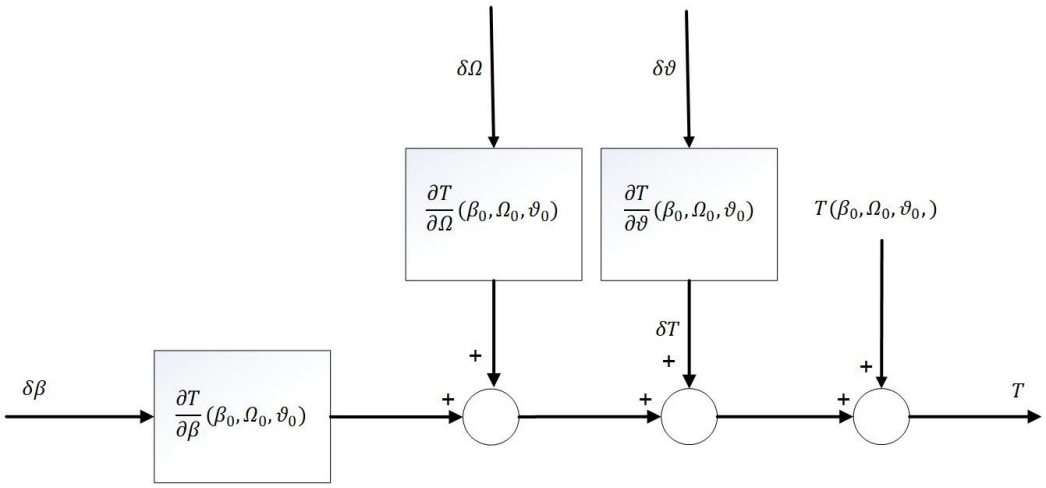

Figure 3.13: Local linearisation of aerodynamic nonlinearity

At a specific equilibrium operating point, the nonlinearity is linearised as shown in Figure 3.13, which shows perturbation of partial derivatives of torque, pitch and wind speed of a variable speed wind turbine system. The partial derivatives at equilibrium points are collected in a partial derivative table. The pitch control strategy is challenging due to the stochastic behaviour of the wind speed. From Equation 3.1, power coefficient, C_p is calculated depending on the pitch angle, β and the tip speed ratio, λ. Also, the maximum value of C_p according to the BEM theorem, is 0.59 in theory where it is applied in the torque control strategy. In pitch control strategy, C_p is not a fixed number. It is a set of matrices that depend on the pitch angle, β and tip speed ratio, λ that reflects the changes in wind speed too. For example, at rated wind speed, the rotor speed is constant, and the blade is pitched at the fixed pitch angle with respect to the wind speed taken from the lookup table of C_p.

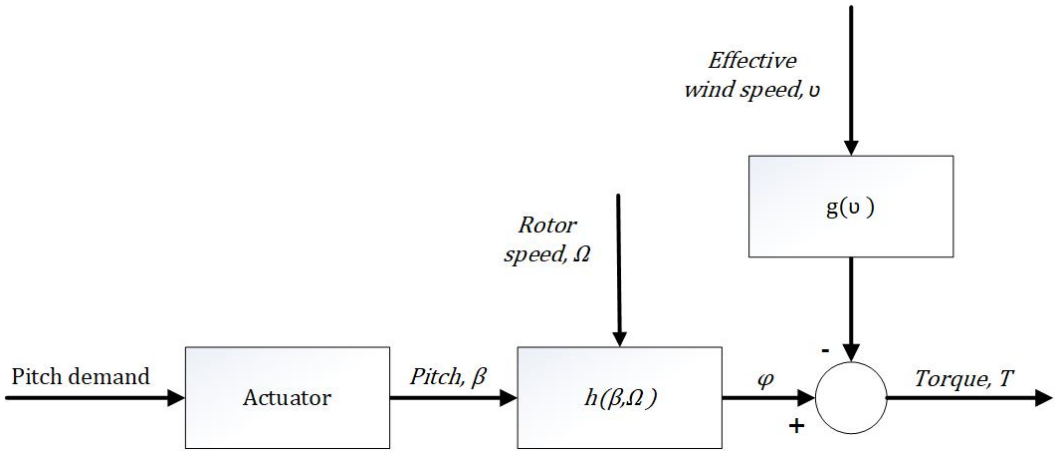

Figure 3.14: Aerodynamic nonlinearity decomposition block diagram

Figure 3.14 shows the block diagram of aerodynamic nonlinearity decomposition. The structure is applied to the Simulink for simulation purposes. The figure shows the decomposition of pitch angle, rotor speed and wind speed which is given by,

$$T = h(\beta, \Omega) - g(v) \tag{3.20}$$

where Ω is the rotor speed and $h(\beta, \Omega)$ is the function composition of pitch angle, β, Ω and a separate function of wind speed, $g(v)$. It is proven that the variation of torque

over pitch angle and rotor speed varies substantially with changes in wind speed. The theory of separability states that the dynamics of the wind turbine can be separated into 2 parts, $h(\beta, \Omega)$ and $g(v)$. Separability in wind turbine control was also actively discussed in the 1990s such as in Leithead et al. (1992), Leithead et al. (1995), Leith & Leithead (1997), Jamieson et al. (2011).

Separability investigated the aerodynamic torque of a variable speed wind turbine. The aerodynamic torque is given by,

$$T = \frac{1}{2}\rho A R U^2 C_Q(\lambda, \beta) \tag{3.21}$$

C_Q is the torque coefficient.

For pitch regulated wind turbines the rotor speed, Ω is held to setpoint value and results in the function h only dependent on pitch angle, β. As such, for the implementation, the inverse of $h(\beta)$ is incorporated in the controller to cancel out the dynamics. This technique is developed by Gala Santos (2018).

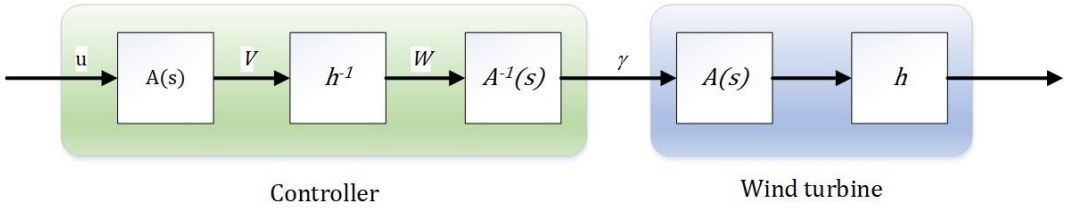

Figure 3.15: Gain-scheduling implementation

Figure 3.15 shows the gain-scheduling implementation with separability theory embedded in the block diagram. $A(s)$ in the diagram refers to the actuator and the inverse of h, h^{-1} is the inverse of nonlinear wind turbine dynamics taken from $h(\beta)$. This approach is implemented in the simulation where analytically the actuator and the h function are inverse to cancel out the dynamics in the wind turbine system. In essence, the standard PID control for a wind turbine system with a gain-scheduling technique is by far the most acknowledged in its range.

Besides the baseline controller which applies a PID controller, another method of control system for a wind turbine system is explored. This thesis particularly selects

MPC as an alternative controller for a wind turbine system.

3.3.4 Switching design

The control laws between below-rated control and above-rated control have different objectives and approaches. During the operation, the changing of the control operation between region I and region III is known as the switching dynamics. In control systems, the switching theory has been developed since the 1990s. The main focus of the study is the stability Liberzon & Morse (1999). Another issue is the switching transient Leithead & Connor (2000). Figure 3.16 shows basic multicontroller switching architecture where a high level decision maker decides which controller is chosen to be connected to the plant as a closed loop system. The stability of the switching system can be achieved by keeping each controller in the loop for a limit of time, long enough to allow transient dissipation.

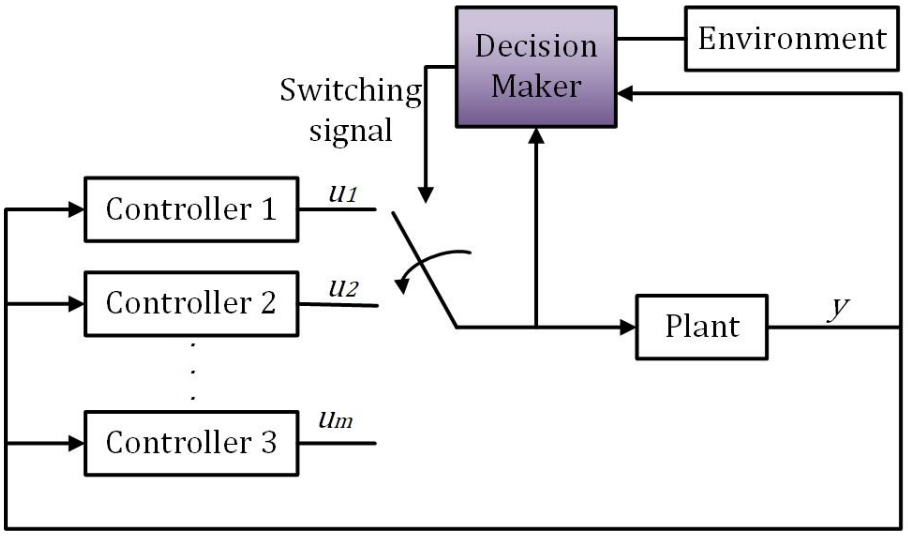

Figure 3.16: Basic architecture for multi controller switching

However, during operation, the sudden transient can cause the risk of having undesirable situations such as vibrations in the main components of the system such as the drivetrain, tower and blades that will lead to fatigue loading problems. A study by Palejiya & Chen (2015) worked to address the concern and the simulation results demonstrated the method has a positive outcome. The paper applied a new control

technique with the objective of attenuating the steep and large unstable dynamics during turbine switching while without compromising the original system structure and maintaining the system's stability.

Theoretically, during torque control, as the wind speed increases the generator torque is varied to capture the optimum power by tracking the C_{p_max}. Once the rated power of torque is reached, pitch control will held to torque speed constant at its rated value. In order to prevent the torque and pitch controllers from interfering with each other, the speed set point for the pitch controller is set a little higher at point **D**. The torque-speed trajectory **A-B-C-D** as shown in Figure 3.17 can influence to stay close to optimum C_p over a wide range of wind speed. **A-B** and **C-D** can be achieved by using a PI controller for the torque demand, in response to the generator speed error with the set point at **A** or **C**. Transitions between constant speed and C_{p_max} curve are handled by using the C_{p_max} curve as the PI controller limits the upper torque when operating at **A**, or the lower limit when at **C**. The set point flips between **A** and **C** when the measured speed crosses the midpoint between **A** and **C**. The transition is completely smooth because the controller will be saturated on the C_{p_max} limit curve both before and after the transition.Burton et al. (2001).

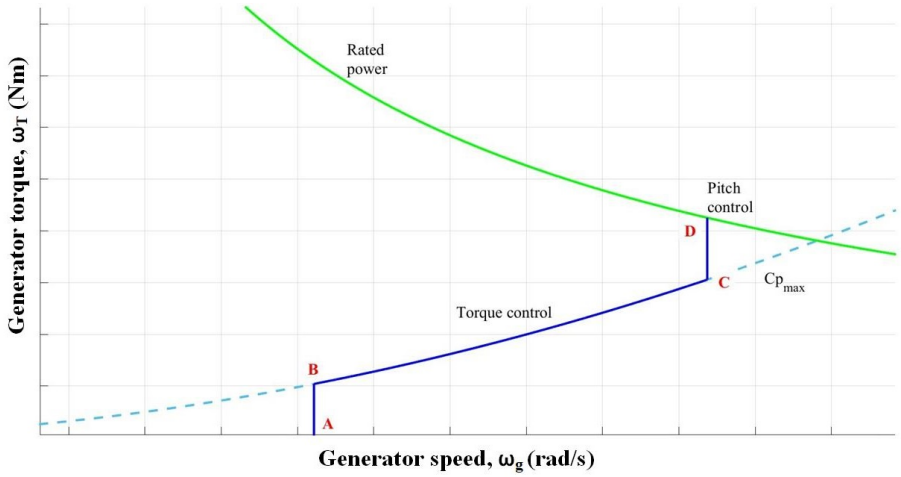

Figure 3.17: Basic control switching strategy for a wind turbine system

3.4 Static ATB Modelling

The increase in wind turbine size depends on the length of the blade. A longer blade carries extra load due to the additional space on the blade. The purpose of exploring wind turbine blades with ATB characteristics is to alleviate the loading effect in a wind turbine system. The blade design contributes to the loading effect of a wind turbine system, such as the increase in blade mass due to the materials used for the blade. As such, with the new design of the ATB application for a wind turbine, it is expected that the blade loading effect can be alleviated and will have a positive impact on the operational and maintenance costs of the wind system. This is because the loading effect will increase the operation and maintenance costs of the system. For instance, the innovation of an adaptive blade can adapt to the wind and be able to deform subject to the incoming wind force independently. The action can help to reduce the blade loading effect, which affects the tower loading effect and reduces the loading effect of the system.

From the literature, there are limited resources for an ATB modelling approach in research publications. There are ATB modelling development approaches using CFD techniques. Since the objectives of the thesis are to model an ATB wind turbine, develop a controller for the model, and analyze the performance of the ATB wind turbine system, the CFD modelling technique is not relevant for controller development studies. With regard to that, a static model of an ATB is developed based on a small-scale wind turbine model. The model modified the pre-twist data in GL Bladed based on the small-scale wind turbine data.

GL Bladed provides a steady calculation for the ATB wind turbine model, therefore the dynamic does not show in the simulation. The ATB wind turbine comprises flexible blades that behave differently from the baseline blade. The main difference between the baseline wind turbine and the ATB wind turbine is the dynamic behaviour of the ATB. The steady calculation in GL Bladed is used to describe the approximate dynamic behaviour of the ATB wind turbine model. The outcomes show differences such as the power coefficient and the transfer functions for below-rated and above-rated wind

speeds.

The static model of the ATB wind turbine is developed based on the understanding that the BTC is incorporated in the baseline blade. The study requires a model to represent the ATB with the static model of the ATB wind turbine developed in GL Bladed by upscaling a small-scale wind turbine model of 3MW into a 5MW industrial-scale wind turbine model.

In 2015, Capuzzi et al. (2015) tested a 45 meter blade of a 3MW wind turbine with the blades built up with 2 materials. The blades were physically experimented with in the laboratory and the results were analysed and discussed in detail as it was the earliest attempt at developing an ATB model. The blade was compared to a baseline blade. Although the experiment was performed to study the blade structure only, a similar method was adopted to study a 5MW wind turbine system by tailoring the blade design with a pre-twist angle as presented in Capuzzi et al. (2015). The angles are tuned in GL Bladed.

The 5MW wind turbine model in GL Bladed has a 63 meter length blade. It is displayed in the blade structure feature. Figure 3.18 shows the pre-twist angle distribution over 19 blade sections for a 5MW wind turbine with a 63 meter blade. The blade is segmented into different types of airfoils. The first section of the blade is the closest to the blade root and the airfoil shape is round. The airfoil segment is shown in Table 3.2. The airfoil shapes are varied for different sections with sizes and shapes. The blade is divided into 19 sections as listed in Table 3.2. Table 3.2 shows 8 types of airfoils along the blade. Airfoil sections 1 and 2 are cylindrical sections 1 and 2 which are for sections 1 to 4 of the blade section. A cylindrical airfoil has a cylindrical shape due to the blade section position that is close to the blade root. Airfoil sections from 3 to 8 are the airfoil shapes with the codes. These airfoils consist of dedicated leading edge and trailing edge specifications and also different spar cap position structures.

The simulation applies existing data in GL Bladed Bossanyi (2009) where the blade geometry is altered to mimic the behaviour of the ATB. The twist angle in the blade geometry section is modified based on Figure 3.18 by interpolating the angle to readjust it into the sections. The figure shows 3 models, Model A, Model B and Model C. Model

Table 3.2: 19 sections of airfoil distribution along the blade

Blade section	**Airfoil section**	**Airfoil name**
1	1	Cylindrical 1
2	1	Cylindrical 1
3	1	Cylindrical 1
4	2	Cylindrical 2
5	3	DU40
6	4	DU35
7	4	DU35
8	5	DU30
9	6	DU25
10	6	DU25
11	7	DU21
12	7	DU21
13	8	NACA64
14	8	NACA64
15	8	NACA64
16	8	NACA64
17	8	NACA64
18	8	NACA64
19	8	NACA64

A is the targeted twist model which describes the maximum angle expected that can be achieved by the blade. It is the targeted twist angle distribution expected from the blade theoretically. Model B is the linear finite element (FE) where the blade applies a linear FE approach. The blade is tailored with linear FE twist angles and the values are constant. Model C is tailored with the nonlinear FE where the blade is designed with nonlinear FE twist angles. The values correspond to the mathematical functions where the values will change accordingly under different circumstances, Hughes (2012), Reddy (2004). The details of the models are presented in Table 3.3.

3.5 ATB Modelling set-up

The simulation is set up based on the Capuzzi et al. (2014*a*), Capuzzi et al. (2015) where this approach is adapted from a 3MW wind turbine model to an industrial-scale wind turbine with 5MW power production. In the previous work, 3 models,

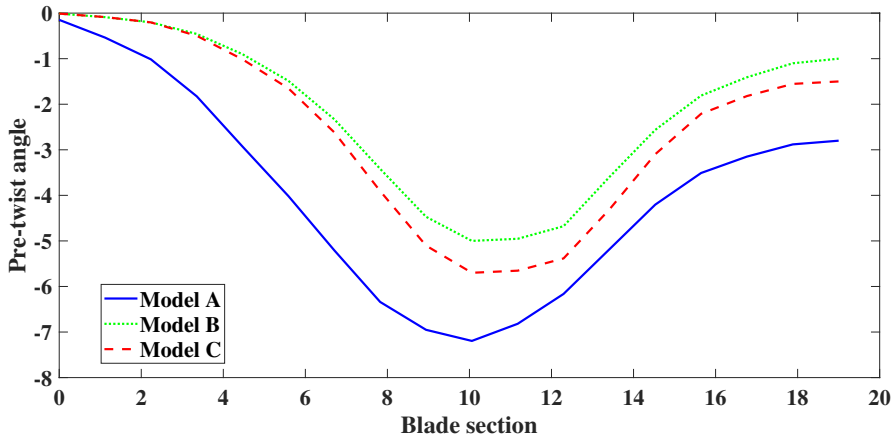

Figure 3.18: Pre-twist angle distribution

model A, B and C were developed, tested and analysed where model A is the linear FE model, model B is the nonlinear FE model and model C is the combination of materials model for a 3MW wind turbine system. The blade data from Capuzzi et al. (2014*a*), Capuzzi et al. (2015) is interpolated in Matlab and the results are compared in Table 3.3. The 3 models are simulated to produce their steady operation outputs. Model C is selected as the working model based on the blade characteristic of the composite materials structure. However, there is a limitation of the model development, where the evaluation of the models is only for 1 selected steady wind speed operation. Based on the limitation, the model is referred to as the static ATB model (Model 1). The system dynamic is not presented in this chapter. The baseline controller is applied to the static ATB model (Model 1) in GL Bladed to observe the steady operation outputs and the results are true for a single wind speed at a single point of observation only. Another variable is the power coefficient. The power coefficient for the ATB model (Model 1) is generated in GL Bladed which is different from the baseline wind turbine model due to the incorporation of BTC coefficient data in it.

Table 3.3 shows the aerodynamic twist distributions for 19 sections of a 63 meter blade. It also compares the twist angle between the baseline blade and the three targeted twist distributions. The angles were interpolated from data produced by Capuzzi et al. (2015) using Matlab. Figure 3.19 is the snapshot of GL Bladed and this provides an example of the twist angle distributions along the blade. Figure 3.19

Table 3.3: 19 sections of aerodynamic twist distribution along the blade

Blade Section	Baseline	Model A	Model B	Model C
1	13.31	0.00	0.00	0.00
2	13.31	-0.15	-0.01	-0.01
3	13.31	-0.54	-0.09	-0.09
4	13.31	-1.01	-0.20	-0.20
5	13.31	-1.83	-0.46	-0.50
6	11.48	-2.93	-0.90	-1.02
7	10.16	-4.02	-1.49	-1.65
8	9.01	-5.21	-2.33	-2.62
9	7.80	-6.34	-3.42	-3.91
10	6.54	-6.95	-4.47	-5.10
11	5.36	-7.20	-5.00	-5.70
12	4.19	-6.82	-4.95	-5.65
13	3.13	-6.16	-4.68	-5.38
14	2.32	-5.18	-3.60	-4.31
15	1.53	-4.20	-2.56	-3.10
16	0.86	-3.51	-1.81	-2.21
17	0.37	-3.15	-1.41	-1.82
18	0.11	-2.88	-1.10	-1.55
19	0.00	-2.80	-1.00	-1.50

also shows the blade information for 19 sections such as the distance along the blade, distance along the pitch axis, the chord length, aerodynamic twist, all the relevant axes and the foil section. The data of the blade distribution is Figure 3.19 is tabulated in Table 3.4

The distance along the blade is measured from the blade root to the sections. For example, the distance along the blade for section 1 is 0, and the distance for section 2 is the measurement from section 1 to section 2 which is 1.37 meter in length. The distance from section 2 to section 3 is 4.12 meter. The chord length is the width of the blade and it is also related to the foil section. The foil section for sections 1, 2 and 3 refers to the circle shape of the airfoil with different diameters. Details are shown in Table 3.2.

Table 3.4: 19 sections of blade distribution information

Blade section	Distance along blade (m)	Distance along pitch axis (m)	Chord (m)
1	0	0	3.50
2	1.37	1.37	3.54
3	4.12	4.10	3.85
4	6.86	6.83	4.17
5	10.31	10.25	4.56
6	14.45	14.35	4.65
7	18.56	18.45	4.46
8	22.66	22.55	4.25
9	26.77	26.65	4.00
10	30.87	30.75	3.75
11	34.97	34.85	3.50
12	39.07	38.95	3.26
13	43.18	43.05	3.01
14	47.28	47.15	2.76
15	51.38	51.25	2.52
16	54.79	54.67	2.31
17	57.54	57.40	2.09
18	60.27	60.13	2.88
19	61.64	61.50	2.80

3.5.1 ATB Modelling with BTC

Bend twist coupling (BTC) is discussed in Chapter 2 where the coefficient C_{xy} and C_{xz} are introduced in Section 2.3.3. C_{xy} is the flap edge stiffness and C_{xz} is the torsion edge stiffness. From the referred work, the blade is developed with a combination of materials and tested. The results from the test provided BTC data and the data is applied in GL Bladed. The BTC data such as C_{xy},C_{xz} coefficients are assigned and simulated in GL Bladed. As a result of the BTC coefficients incorporated in GL Bladed, a new power coefficient, C_p of the wind turbine system is generated. The power coefficient, C_p has changed some values when compared to the baseline C_p. BTC coefficients affect the overall performance of the ATB wind turbine model. The pitch angle is also affected by the BTC coefficients.

Figure 3.20 shows the results produced by GL Bladed of the blade structure with new BTC coefficient without changing other parameters. The new parameters intro-

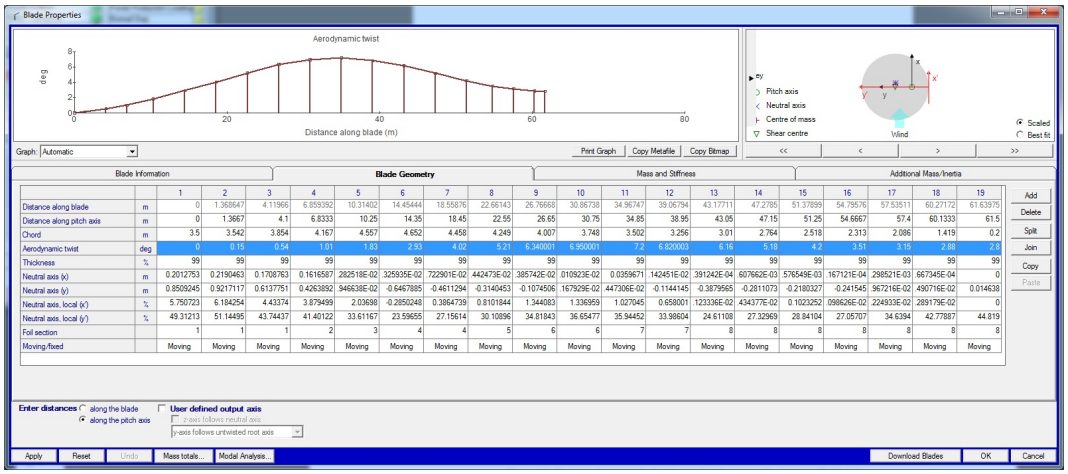

Figure 3.19: Example of twist angle distribution for 19 sections 63m blade in GL Bladed

duced in the simulation are the BTC coefficients. Figure 3.20 shows the power coefficient, C_p is compared between ATB with BTC also referred to as Model 1 and the baseline blade. The ATB model (Model 1) has a lower peak, C_{pmax} value compared to the baseline model. The range tip speed ratio for C_{pmax} is wider for Model 1 than the baseline model from approximately $7 \leq \lambda \leq 12$ and $8 \leq \lambda \leq 10$ respectively.

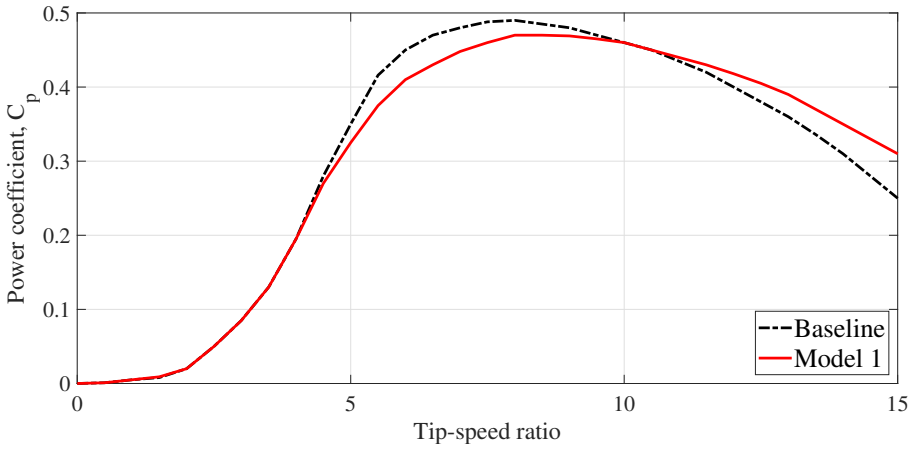

Figure 3.20: Power coefficient comparison

Based on the results, it conferred that there is insufficient data to investigate the model. Thus, a more reliable model of an ATB is required. Apart from adjusting the BTC coefficient in the simulation, GL Bladed has a feature that can represent the BTC element in the wind turbine system.

Another feature of GL Bladed is the Flexibility Modeller (FM). FM feature in GL Bladed is used to analyse wind turbine blades by selecting the number of modes. Typically, only two modes are considered when examining a wind turbine's behaviour. The two modes are the flapwise mode and the edgewise mode. The modes have a range of frequency distributions from low frequencies to high frequencies generated by GL Bladed. Though, the study examines only the first two frequencies which are the first and the second frequencies of each mode. A flexible blade such as an ATB has an additional mode to consider which is the torsional mode. This 3^{rd} mode also takes on two modes, the 1^{st} and 2^{nd} torsional modes. In GL Bladed, the torsional mode only occurs at the 13^{th} and 14^{th} frequency range. Table 3.5 shows the selected blade modes and the frequencies. The frequencies of the six modes show six different modes; two flapwise modes, two edgewise modes, and two torsional modes with their respective frequencies. However, the study focuses on the first mode flapwise and the first mode edgewise only. The modes are normally visible in a bode diagram of a wind turbine system.

Table 3.5: Blade modes and frequencies

No.	Modes	Modal Frequency (Hz)	Frequency (rad/s)
1	1st flapwise mode	0.7242741	4.55
2	1st edgewise mode	1.1409829	7.17
3	2nd flapwise mode	2.0333853	12.78
4	2nd edgewise mode	4.481252	28.16
5	1st torsional mode	57.61903	362.03
6	2nd torsional mode	86.59619	544.10

3.5.2 Blade twist angle and angle of attack (AoA)

GL Bladed is a simulation software that can evaluate wind turbine performance very similar to the industrial-scale wind turbine data. However, this approach has a limitation, which it can only produce steady operation calculations for a single operation point at a time. Due to that, the simulation was run at 5 operation points of selected wind speeds to analyse the blade angles at each section of the blade. The wind speeds cover the 3 regions of the wind turbine system which represent low wind speed at below-

rated region, rated wind speed and high wind speed at the rated region. Below-rated wind speeds are represented by 5 m/s and 8 m/s, rated wind speed is 12 m/s and above-rated wind speeds are 16 m/s and 18 m/s. 5 separate simulations are conducted and the results are recorded and presented in Figure 3.22 and Figure 3.23.

Figure 3.21 shows the results of the blade aerodynamic pre-twist angle, θ_p produced by GL Bladed. and then applies this to Equation 3.22 as the pre-twist angle, θ_p. The aerodynamic twist in GL Bladed is the blade twist that is designed to encounter the aerodynamic input. This blade was considered constant for a baseline wind turbine. In ATB models the blade twist is no longer constant as it changes according to the varying wind speeds. The blade twist changes as the prediction using FE analysis in Section 3.4 is only valid for one particular time, t only. In this section, the blade twist changes dynamically as the wind and time vary.

Referring to BEM theory in Figure 3.7, AoA is a fundamental parameter that wind turbine controllers use to optimise the performance of the turbine blades and enhance overall energy capture while ensuring the system operates within safe operational limits. It refers to the angle between the chord line of the blade and the oncoming wind. The chord line is an imaginary straight line connecting the leading edge to the trailing edge of the blade. The AoA influences the lift forces, C_L and drag forces, C_D experienced by the blades. Pre-twist is an intentional rotation of the blade along its length and it is important in optimising AoA across the rotor span by aligning the blade with the expected wind speed distribution. The pitch angle is the angle between the chord line and a plane perpendicular to the rotor's axis. It is adjusted to regulate the AoA, influencing the wind turbines' rotational speed and output power. The twist coupling ensures adaptability to varying wind conditions along the blade. The AoA directly impacts aerodynamic efficiency, load control, and operational safety. Efficient AoA ensures optimal energy conversion, with a pitch control approach. As such, AoA is very important in the design and operation of wind turbine systems. From Figure 3.7, the AoA, α is determined by the total angle of the twist, Φ provided that the pitch angle, θ_p is known. In this study, the pitch angle, θ_p is called the pre-twist angle. The

relationship between all angles is given by Equation (3.22).

$$\Phi = \theta_p + \alpha \tag{3.22}$$

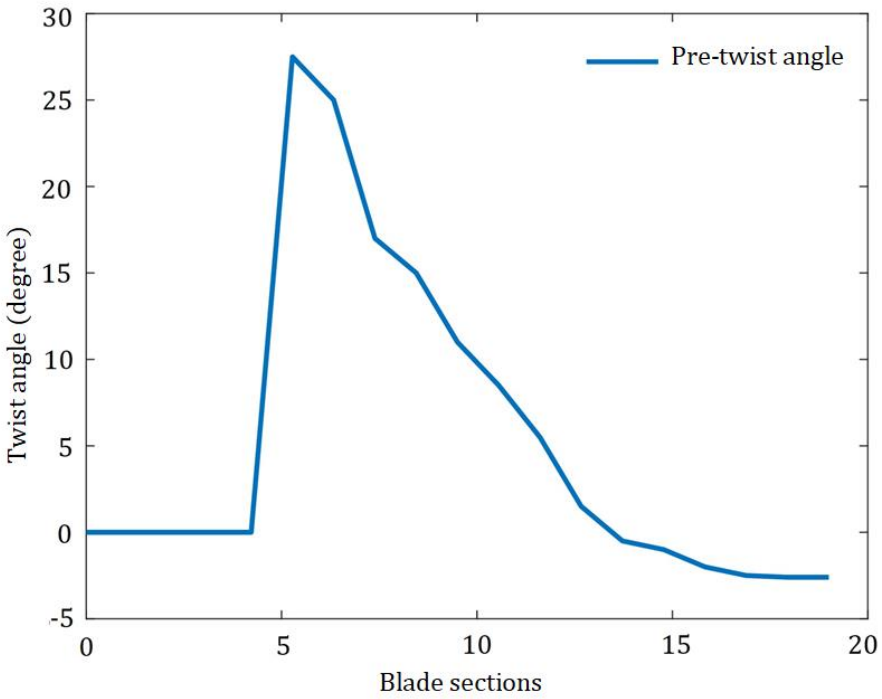

Figure 3.21: Blade pre-twist angle for Model 1

Figure 3.22 illustrates the AoA, α in power production loading in GL Bladed. 5 wind speeds are selected to represent below-rated and above-rated regions. The AoA, α is the result of the BTC coefficient effect that is predefined in GL Bladed. Theoretically, from Section 2.3.3, BTC arises with the aerodynamic changes in the AoA, α of the blade. Based on Figure 3.22, the AoA, α at the first section of the blade runs from 65 to 80 degrees, and then it drops to around 0 degrees at the 5th section of the blade. The angle decline is due to the airfoil shape of the blade section. From sections 1 to 5 of the blade, the airfoil is cylindrical which accounts for the 0 degrees shown in Figure 3.21. The AoA, α from sections 5 to 19 varies from around -5 to 10 degrees. This is also a result of the blade's pre-twist angle. The angle variations are in a narrow range because ATB is a flexible blade.

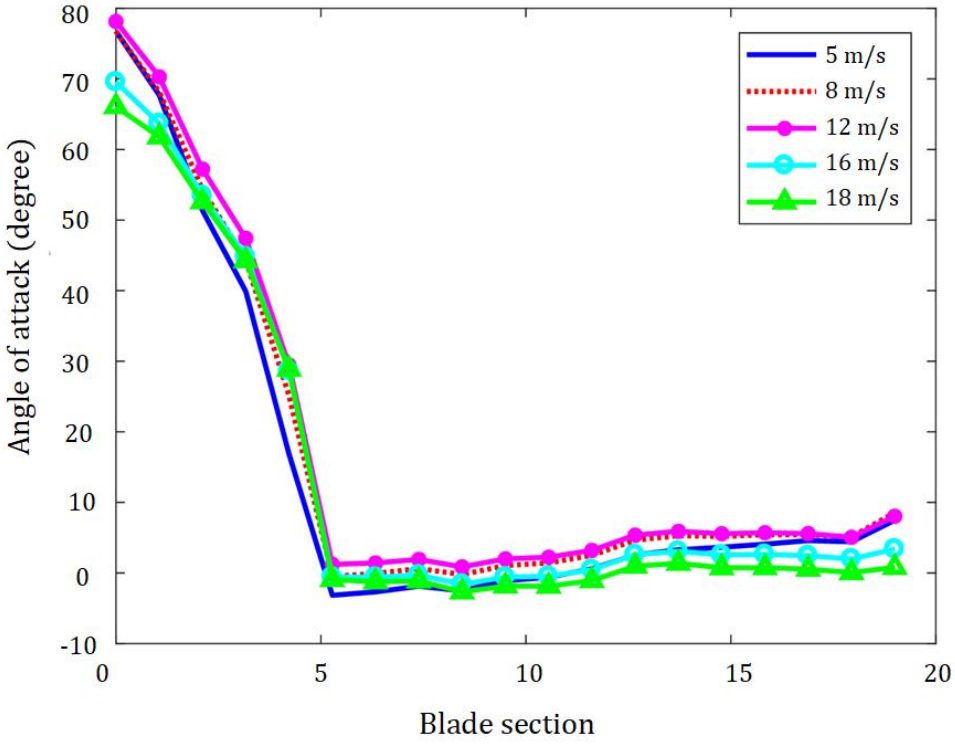

Figure 3.22: Model 1 blade dynamic effect over AoA

Figure 3.23 shows the dynamic output of the total blade twist angle in the ATB wind turbine model. The obvious change is the angle at the 4th section for 5m/s wind speed and it also shows at a wind speed of 8 m/s wind speed with a smaller change of angle. The AoA, α for 12 m/s, 16 m/s, and 18 m/s show similar output response compared to the 5 m/s and 8 m/s. The angle change could be because of accounted for the pitching activity in the above-rated region in which for the below-rated region the angle changed for 5 m/s and 8 m/s at the fourth section of the blade due to no active pitching activity.

The static model of an ATB wind turbine requires a controller to analyse its performance. It is to examine whether the model is responding to the controller. The gain-scheduling baseline controller (Controller 1) is applied to the model. Generally, Controller 1 adopts a similar control strategy for a baseline wind turbine to the ATB wind turbine model.

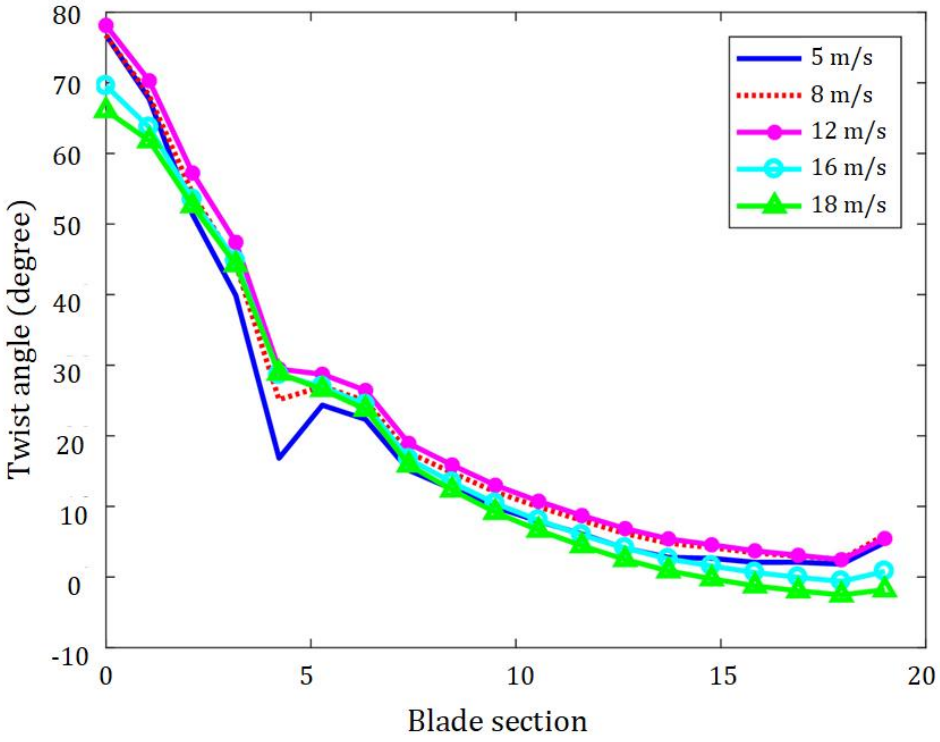

Figure 3.23: Total twist angle of Model 1 along the blade

3.5.3 Above-rated control for ATB wind turbine model

In wind turbine control, the control regions are divided into 3 parts; below-rated region, rated region and above-rated region as shown in Figure 3.9. As seen from the figure, the below-rated is ranges from 4 m/s to approximately 11 m/s, the rated region is approximately from 11 m/s to 12 m/s and the above-rated region is from 12 m/s to 24 m/s. The works in the thesis focus on the above-rated region. In the context of an ATB wind turbine, the blade's reaction towards above-rated wind speeds is challenging as it faces a strong force that can break the structure of the blade. For that reason, the ATB wind turbine is designed to be able to respond to the incoming wind forces, and to examine the performance, an above-rated controller is required.

The static ATB WT model was developed based on Capuzzi et al. (2015). The model with the combination of materials model is selected to be further developed for the 5MW application. Based on that, the power coefficient for the 5MW baseline wind turbine model is compared to the static ATB model. The results were shown in Figure

3.20 and Figure 3.24.

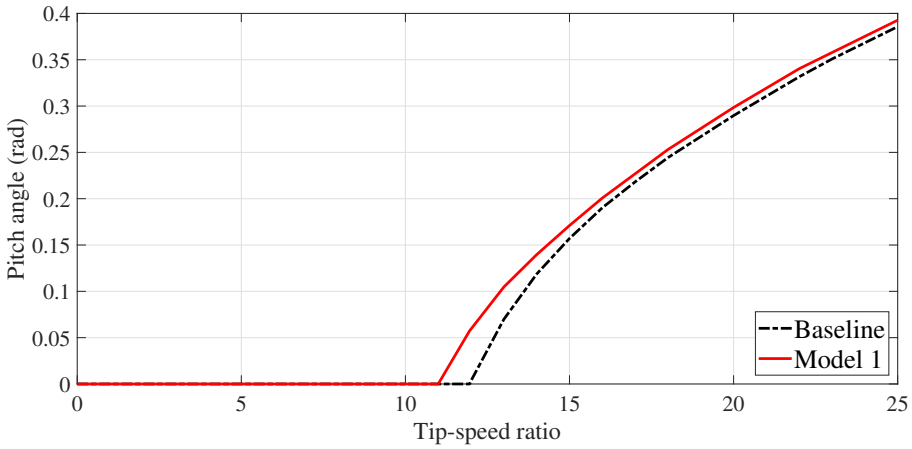

Figure 3.24: Pitch angle comparison

The maximum C_p for a horizontal axis wind turbine is 0.59 while C_p for a 5MW wind turbine is given as 0.5.

Below-rated control is also known as the C_p tracking region where the rotor speed varies in region I and always ensures that C_p is at its maximum value. The C_{pmax} curve is represented by,

$$C_{pmax} = k_{opt}\Omega^2 \tag{3.23}$$

where k_{opt} is the optimum coefficient for the rotor speed, Ω.

Once the wind speed reaches the rated region, the rotor speed reaches the rated speed and is kept constant at the rated speed value. In this region and as the wind speed increases to region III, the operation is switched to above-rated control. Above-rated control is also called pitch control. In region III, the torque is constant and the pitch actuator varies the pitch angle as the wind speed changes.

A total of 3 important diagrams were produced to represent the ATB model presented in Chapter 3, the torque-speed diagram, the power curve diagram and the $C_p - \lambda$ diagram.

The operation strategy of the baseline wind turbine is adapted to the ATB wind turbine model. From the torque vs speed diagram, it is shown that the maximum C_p tracking varies from 95% to 100%. It shows that the C_p track fluctuates to capture the

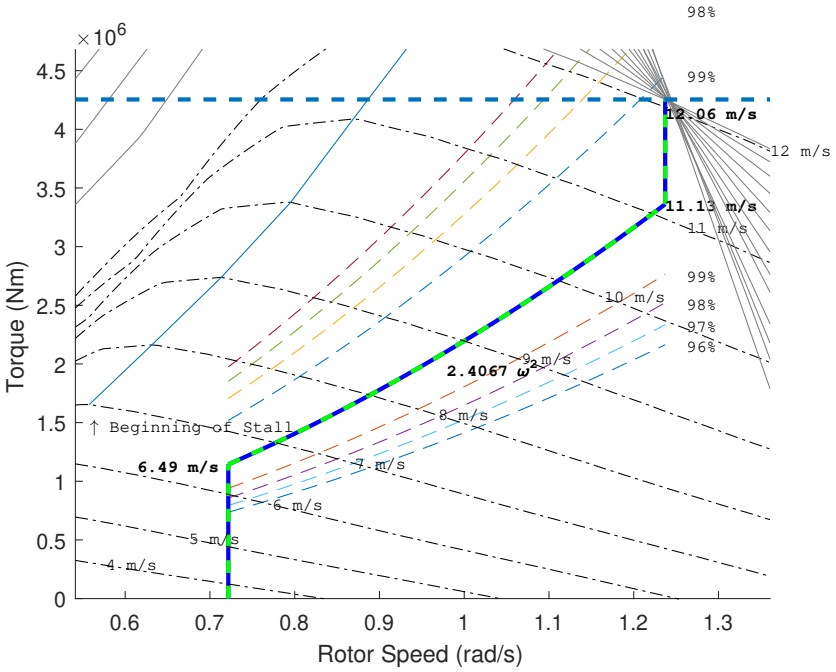

Figure 3.25: Model 1 with new C_p operation strategy

maximum power by varying the rotor speed.

The ATB wind turbine has its Cp-λ curves. It represents the unique characteristics of the wind turbine. This information is crucial in wind turbine control development because the controller is designed based on the turbine's characteristics.

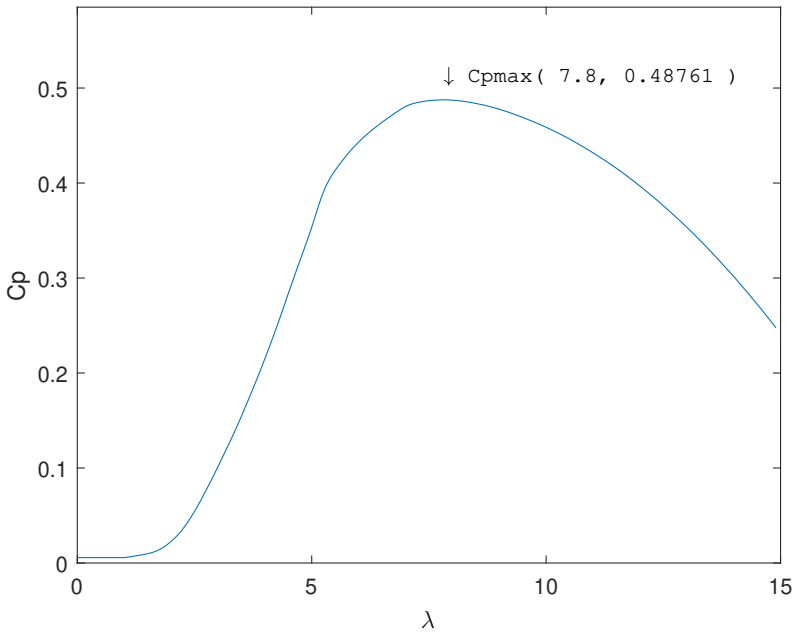

Figure 3.26: Cp - λ max curves for Model 1

The above-rated control for baseline wind turbines applies gain-scheduling as the method to deal with random changes in wind speeds. This technique is well-established and widely applied in wind turbine control. The relationship of the partial derivative of torque and pitch angle determines the gain for the wind speed.

The power coefficient determines the power production of a wind turbine system as stated in Equation (3.1). In BEM theory, the maximum C_p for a horizontal axis wind turbine is 0.59. The C_p for 5MW wind turbine is 0.5 at tip speed ratio, λ at 7.8. The C_p for an ATB with Capuzzi et al. (2015) compares with the baseline C_p is shown in Figure 3.20.

The plots show that the maximum C_p is slightly lower than the baseline C_p. The blade design for the composite material has lower $C_{p_{max}}$ due to the manufacturing design of the blade. The blade design has changed the spar cap position and altered the blade character. Note that, in this chapter, the ATB static model has an estimated value of power coefficient, C_p that is different from the baseline power coefficient. Based on the new C_p value, the performance of the static ATB model is observed using the

5MW Simulink model.

The effect of power coefficient, C_p is shown in pitch angle comparison as shown in Figure 3.24. The ATB wind turbine starts pitching at 11 m/s and the baseline wind turbine starts at 12 m/s.

3.6 Summary

This chapter outlines the model development of Model 1 which is the static ATB wind turbine system to evaluate its performance in comparison to Model 0 which is the baseline wind turbine model. The initial method is to incorporate the BTC coefficients into Model 0 and adjust the pre-twist angle of the wind turbine blade inspired by the preliminary work done by Capuzzi et al. (2014*a*). The work is conducted within the GL Bladed environment.

The blade is designed with a pre-twist angle where the angle of the blade is adjusted based on the work by Capuzzi et al. (2014*a*). The rationale for designing the blade with pre-twist angle is based on the outcome by Capuzzi et al. (2014*a*) where the angle of attack of the blade is expected to reduce the blade pitch angle. BTC coefficient is incorporated in GL Bladed to introduce BTC characteristics in the wind turbine model. For Model 0, the BTC coefficient is not included in GL Bladed, indicating that the blade is rigid. Based on the results from the initial inputs provided to GL Bladed for Model 1 blade design, a new power coefficient, C_p, is generated. This new C_p for Model 1 exhibits a slight difference compared to C_p for Model 0.

This chapter explores the experimentation with Model 1 using a gain-scheduling baseline controller (Controller 1) and compares its performance to Model 0 with a similar controller. The results show that Model 1 with Controller 1 pitched at 11 m/s and Model 0 with Controller 1 pitched at 12 m/s. Generally, Model 1 is expected to pitch after 12 m/s based on the blade design, which incorporates the pre-twist angle and the BTC coefficient. GL Bladed may have influenced the results due to its limitation of simulating the model only under steady-state conditions.

The ATB wind turbine static model is a steady-state model that suggests the possibility of analytical modelling. However, as wind turbines are highly nonlinear systems

heavily influenced by stochastic wind speeds, the static model is inadequate for representing the ATB wind turbine system. Nevertheless, this model demonstrates the effects of pre-twist angle in blade design and illustrates steady-state performance. This chapter delves into the steady-state modelling and dynamics of an ATB wind turbine in GL Bladed. The ATB wind turbine model modifies the 5MW Supergen baseline model in GL Bladed and incorporates BTC coefficients into the baseline model. GL Bladed also provides linearisation tools that simplify the analysis of the ATB wind turbine model. The linearised ATB wind turbine model is further simplified to lower states for in-depth exploration in ATB control system development.

In conclusion, Model 1 represents a well-developed and functional steady-state model of an ATB wind turbine. The performance of Model 1 is evaluated using Controller 1, which requires fine-tuning to achieve the anticipated outcomes. This work is further explored in Chapter 4, where the dynamic ATB wind turbine model is developed.

Chapter 4

Wind Turbine with Dynamic ATB Modelling and Baseline Control

In this chapter, a dynamic ATB wind turbine model is developed and later examined with the gain-scheduling baseline controller (Controller 1). In Chapter 3, a static ATB wind turbine model is developed in GL Bladed environment and tested using Controller 1. The findings showed that the model performs effectively under steady-state conditions. The model is further developed in this chapter by introducing the dynamic characteristics of the wind turbine system.

The preliminary model of an ATB wind turbine is modelled by incorporating a rotational spring damper model into the baseline blade. It is represented by a second order transfer function connected between the pitch mechanism and the aerodynamic part of the blade model in Simulink. The motivation for experimenting with dynamic modelling is based on the limited resources of the ATB wind turbine model that can be applied for controller development. While there are existing studies on flexible blade models, there is a gap in comprehensive wind turbine models integrating these flexible blades. Many studies have applied the second order model to represent various physical interactions of wind turbine systems (Sarkar & Fitzgerald 2020),(Bhattacharya & Adhikari 2011). In this chapter, the model is examined with a baseline controller.

This chapter is structured in the following sequences; Section 4.1 provides the introduction, Section 4.2 details the methodology, Section 4.3 outlines the model development and Section 4.4 presents the implementation of model development. The discussion of results and analysis is covered in Section 4.5 and the chapter concludes in Section 4.6.

4.1 Wind Turbine Model with Dynamic ATB

In Chapter 3, the static model of the ATB wind turbine is presented using steady-state data from GL Bladed. GL Bladed is reliable software that represents an industrial-scale wind turbine system. It provides data that is very similar to the industrial-scale wind turbine. This chapter extends the model development of an ATB from a static model to a dynamic ATB wind turbine model. The dynamic ATB wind turbine model is developed using the 5MW wind turbine Simulink model and the model is taken as the baseline wind turbine. At the end of the chapter, the dynamic ATB model can be analysed using the baseline controller to evaluate its performance and compare it to the baseline wind turbine performance. The ATB characteristic is incorporated in the Simulink model and is named the ATB wind turbine model. The objectives of this chapter are to model an ATB wind turbine by introducing the flexible characteristic to the blade with a rotational spring damper model, to examine the existing controller for the ATB wind turbine model and to evaluate the results of the controller in Simulink.

In Chapter 3, a static ATB wind turbine model is developed based on the results presented in Capuzzi et al. (2014*a*) where it is up-scaled from a 3MW wind turbine to a 5MW wind turbine. The data is modified in the existing 5MW wind turbine model in GL Bladed. Then, it is simulated to produce a new performance coefficient for the updated wind turbine system which is later called the ATB wind turbine system. The difference in the performance coefficient between the ATB wind turbine and the baseline wind turbine is too small. But note that it does affect the blade flexibility characteristic whereas fundamentally, baseline wind turbine blades do not have the flexible characteristic since the blade is built as a standard blade structure. An observation from the results provided by GL Bladed suggests that the flexibility of the

blade can be modelled using the software. However, this approach only allows for a single assessment at a time. The static ATB wind turbine model can be assessed for 1 selected wind speed at 1 instant. Therefore, a more reliable model that can represent the blade dynamics is required to mimic the ATB wind turbine behaviour.

The major obstacle in the ATB wind turbine research area is to model an ATB wind turbine system that can be used for simulation and analysis purposes. There are papers and publications about ATB modelling but most of it apply the CFD technique to model the system. CFD modelling approach is not relevant for the purpose of developing and investigating a controller for the system. Hence, an analytical model is a better preference for developing a significant controller for a wind turbine system. Again, it is a setback to develop and investigate the ATB wind turbine performance due to inadequate literature on the analytical modelling of the ATB wind turbine. Nonetheless, the ATB wind turbine is modelled using the aerodynamic information provided by GL Bladed and the controller performance analyzed in Simulink.

The ATB behaviour is introduced into a baseline wind turbine model as an additional aerodynamic effect on the system. The baseline model is available in Simulink which is the 5MW Supergen industrial-scale wind turbine model.

4.2 Methodology

A dynamic ATB wind turbine model is developed based on the baseline model embedded with a spring damper model analytically as a representation of the dynamic behaviour of the blade.

4.2.1 Overall control system configuration

The aerodynamics of a baseline wind turbine are affected by the ATB characteristic introduced in the model. A baseline wind turbine model is represented by an aerodynamics block connected to rotor dynamics, drive-train dynamics and generator dynamics that have effects on each other and the wind turbine system. Figure 4.1 shows the ATB wind turbine configuration with Ω is the rotor speed, Ω_g is the generator speed,

T_g is the generator torque demand, β_d and β are the pitch demand and pitch angle applied to the wind turbine, θ_{ATB} is the rotor in-plane displacement due to ATB, T is the aerodynamic torque.

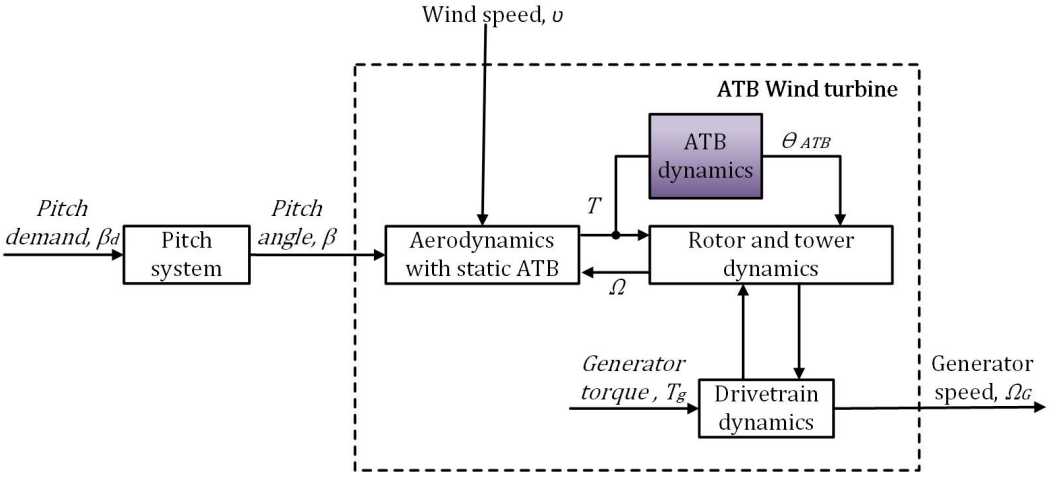

Figure 4.1: ATB wind turbine model configuration

It adopts the baseline wind turbine configuration with an additional block of ATB dynamics. The basic block diagram consists of 3 blocks that represent the dynamic components of the wind turbine system. The blocks in the main wind turbine block are aerodynamics, rotor and tower dynamics and drive-train dynamics. A generator is part of the drive-train component. It does not show in the diagram since it separates the generator dynamics from the drive-train dynamics as The generator dynamics are not covered in this project. The focus of the project includes the 3 main components as shown in Figure 4.1. The pitch angle system has a pitch actuator model and a pitch delay. The input to the pitch angle system is the pitch demand, β_d and the output is the pitch angle, β. The pitching mechanism pitches the blade that is physically moved by the pitch actuator. The output from the pitch system is the input to the aerodynamics. Aerodynamics varies based on the wind speed, v. The aerodynamics of a wind turbine system were explained in Chapter 3. The aerodynamics block interacts with the rotor dynamics block with torque input and rotor speed output. The rotor dynamics react to drive-train dynamics and experience effects from the generator dynamics too. There are 2 inputs for the baseline wind turbine, the pitch angle demand and the torque demand.

Based on this fundamental block diagram of a baseline wind turbine, an analytical ATB block is placed at the rotor dynamics block. The rotor dynamics consists of the rotor angle displacement; in-plane and out-of-plane, and the tower out-of-plane displacement that has the knock-on effect to the drive-train dynamics.

In a wind turbine system, aerodynamic torque, T can be calculated from,

$$T = \frac{P}{T_g} \tag{4.1}$$

where, P is the power generated by the wind turbine, and T_g is the generator torque. From power derivation, aerodynamic torque is,

$$T = \frac{1}{2}\rho A \pi R^2 V^2 C_Q(\lambda, \beta) \tag{4.2}$$

$$C_Q(\lambda, \beta) = \frac{Cp((\lambda, \beta)}{\lambda} \tag{4.3}$$

where the torque coefficient, C_Q is proportional to the power coefficient, C_p.

The generator torque is assumed to be similar to torque demand since the power converter is relatively fast and is defined to be equal to the rated generator torque as the controller is only tested at above-rated wind speed values.

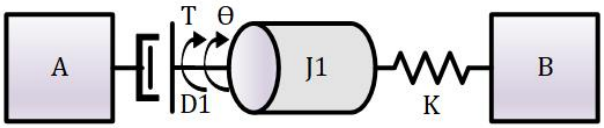

Figure 4.2: Mass spring damper model

4.2.2 Model configuration

The ATB is modelled with a spring damper rotational mechanical system. Figure 4.2 shows the basic model of the spring damper model. The mass spring damper transfer function gives additional rotational spring in between the 2 blocks interaction, the aerodynamics block and the rotor dynamics block. In ATB flexibility modelling, there is only one segment with 2 mass points positioned at both ends, included in the existing

Simulink model. If more mass points are added in between the two mass points the subject will become more flexible but the degree of freedom will increase. Due to this, only 1 segment is added which will introduce flexibility in the existing model. Note that the blade model structure is not compromised here. The transfer function of the mass spring damper model is

$$G(s) = \frac{1}{J_1 s^2 + D_1 s + K} \tag{4.4}$$

where K is the spring stiffness, J_1 are the moment of inertia, D_1 is the damper, T is the torque, θ is the rotation angle.

The input for the transfer function is the torque and the output is the phase angle. The spring damper model is considered a part of the blade in which the blade is physically manufactured with composite materials which changes the properties of the blade. The parameters in Equation (4.12) are determined as follows:

The stiffness of the segment, K can be expressed as,

$$K = \frac{EA}{\Delta l} \tag{4.5}$$

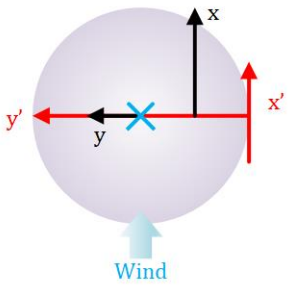

Figure 4.3: Cross-sectional area of the first section of the blade

Where E is the elastic Young's modulus of the blade root, A is the area of the cross-section of the blade root and Δl is the length of the segment. The selection of the stiffness is based on the estimation data of the blade structure. The Young's modulus for composite material is $72N/m^2$, the cross-section area at blade root is taken from

Table 4.1: Blade information for 1st and 2nd section

Blade section	**Units**	**1st**	**2nd**
Neutral axis (x)	m	0.20	0.22
Neutral axis (y)	m	0.85	0.92
Neutral axis, local (x')	%	5.75	6.18
Neutral axis, local (y')	%	49.31	51.14

Figure 4.3 and the details are tabulated in Table 4.1

$$A = \pi R^2 \tag{4.6}$$

The value for R is selected by referring to Figure 4.3 where y is the diameter of the first section of the blade. Thus, the radius R,

$$R = \frac{0.86}{2} m = 0.41m \tag{4.7}$$

gives,

$$A = \pi(0.41)^2 m = 0.528m^2 \tag{4.8}$$

thus,

$$K = \frac{EA}{\Delta l} = 27.75 \tag{4.9}$$

Specifically, a single blade mass for the 5MW wind turbine is $17,741$ kg. Thus, the values that are selected for the spring damper model should be relative to the blade mass and torque for the wind turbine system. The blade mass is $17,741$ kg and it is divided into 19 sections. To determine J_1 ,

$$J_1 = \frac{17,741kg}{19} = 933kg \tag{4.10}$$

In general, the new transfer function creates a new dynamic to the blade as shown in Fig 4.2.

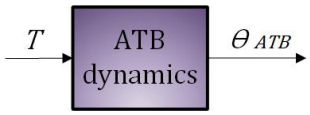

Figure 4.4: General block diagram for ATB

The transfer function is,

$$\frac{\theta_{ATB}}{T} = \frac{1}{J1s^2 + Ds + K} \tag{4.11}$$

This spring damper model introduces a flexible behaviour of the blade aerodynamic. The model is presented in the transfer function in Simulink. An independent block of the model is analysed in Simulink before it is adapted to the baseline Simulink model. A simple step input feeds in the block transfer function and the output is observed in the scope and plotted in Matlab. This simulation is simple and the purpose is to observe whether the spring damper model is feasible for the ATB model with the chosen parameters.

The ATB is modelled by introducing the blade adaptive behaviour with a spring damper rotational mechanical model. Figure 4.2 shows the basic model of the mass spring damper model. The mass spring damper transfer function gives additional rotational spring in between the pitch actuator and the root of the blade. The spring gives a flexible characteristic to the baseline blade. It will behave like the ATB where the blade moves in free form to make it more flexible compared to the baseline blade. Note that, the spring model does not represent the adaptive blade's behaviour. It models only the flexible characteristic of the blade (Sun & Chen 2017).

The modelling applies the fundamental modelling method, which is based on assumptions and rationales of the ATB wind turbine model. Then, the initial coordinate system that is located at the hub is established. The system elements and the variables are identified and the free body diagram for the elements is illustrated and represents the model with its equation.

$$J_1\ddot{\theta_1} + D_1\dot{\theta_1} + K = T \tag{4.12}$$

Referring to Figure 4.2, it shows that the chosen elements are the moment of inertia, J_1, the dampers, D_1, and the spring stiffness, K. The spring damper model is introduced at the root of the blade. J_1 a represents the mass that is connected to the first section of the blade. Block A represents the aerodynamics block and Block B represents the rotor dynamics. Both blocks interact with each other which means the changes will affect the outputs of the blocks and the operation of the wind turbine system. The purpose of including the dynamics in the model is to introduce flexibility to the blade. The spring is proportional to the mass of the blade to make sure it is unbreakable. The damper theoretically has a smaller mass compared to the blade mass to allow the blade to experience flexible characteristics. The spring is built with high stiffness to accommodate the baseline blade stability and is required to hold the mass of the whole blade. In general, the new transfer function creates a new dynamic for the blade, as shown in Figure 4.4 where the output is the angle displacement of the rotor. The changes in angle displacement in rotor dynamics affect the operation of the wind turbine system, and its performance is evaluated with the baseline controller.

4.3 Model development

There are several simulation methods, such as model linearisation and model reduction. This section explains the variation methods available in the system.

4.3.1 Model linearisation

Generally, a dynamic system can be written as continuous-time nonlinear differential equations,

$$\dot{x} = f(x(t), u(t), t) \tag{4.13}$$

$$y(t) = g(x(t), U(t), t) \tag{4.14}$$

where $x(t)$ represents the system states, $u(t)$ represents the inputs to the system, and $y(t)$ represents the outputs of the system.

A linearised model of this system is valid in a small region around the operating point $t = t_0$, $x(t_0) = x_0$, $u(t_0) = u_0$, and $y(t_0) = g(x_0, u_0, t_0) = y_0$.

To represent the linearised model, the new variables are defined centered very close around the operating point:

$$\delta_x(t) = x(t)x_0 \tag{4.15}$$

$$\delta_u(t) = u(t)u_0 \tag{4.16}$$

$$\delta_y(t) = y(t)y_0 \tag{4.17}$$

The linearised model in terms of $\delta x(t)$, $\delta u(t)$, and $\delta y(t)$ is valid when the values of these variables are small:

$$\delta\dot{x}(t) = A\delta x(t) + B\delta u(t) \tag{4.18}$$

$$\delta y(t) = C\delta x(t) + D\delta u(t) \tag{4.19}$$

The wind turbine system is a highly nonlinear system. Model linearisation is an approach to obtain a simplified model at one operating point. The baseline model linearised in GL Bladed is represented in the standard state space equation,

$$\begin{aligned} x(k+1) &= Ax(k) + Bu(k) \\ y(k) &= Cx(k) \end{aligned} \tag{4.20}$$

where k is the time index, $A \in \mathbb{R}^{13\times13}$ and $B \in \mathbb{R}^{13\times1}$ are the parameter matrices for the state transition equation. The output parameter matrix is $C = [0_{13\times1}1]$.

Another useful feature of GL Bladed is the linearisation tool. This feature can translate the relationship between generator speeds and generator torque for below-rated and generator speeds, pitch angles, fore-aft acceleration and pitch for above-rated.

In the GL Bladed linearisation tool, there are 5 selected inputs and 2 selected outputs. The inputs and outputs as shown in Table 4.2 are;

Table 4.2: GL Bladed input and output linearisation

Input	**Output**
Collective wind speed	Generator speed
Horizontal wind shear	Tower acceleration
Vertical wind shear	
Collective pitch angle demand	
Collective generator torque demand	

The linearised output from GL Bladed is expressed in the state space model in Equation (4.20) and then is transformed into transfer functions representing the outputs and inputs associated with the system.

The linearisation produces 241 states for the wind turbine system. It gives an output for all ranges of wind speeds from 4m/s to 25m/s.

Although the selection of the input is listed as 5 inputs, the state space representation can select a single input and single output (SISO) representation that can clearly represent the wind turbine system.

From the linearisation, the system can be divided into 2 parts, the below-rated system and the above-rated system. The controller for a wind turbine system has 2 interests, below-rated control and above-rated control. Below-rated control is a torque controller where the generator torque is varied to track the maximum C_p curve and the above-rated system is a pitch control system where the torque is held constant and the pitch angle is varied. Thus, the state space equation for the below-rated system is taken from generator torque to generator speed and the state space equation for the above-rated system is taken from pitch angle to generator speed.

The state space model for a baseline wind turbine from GL Bladed gives the output in the state space equation in Equation (4.20), where $A \in 241 \times 241$ matrix, $B \in 241 \times 1$ matrix, $C \in 1 \times 241$ matrix, $D \in 0$ matrix, $\mathbf{x}$ is a vector with 241 states and u is the input. The dimension of the state space equation is very large because the nature of wind turbines is highly nonlinear and this makes it difficult to solve. The model is used as the GL Bladed baseline model in comparison with the Simulink linearised model.

The Simulink model is linearised and compared to the full-state wind turbine model

using the linearisation tools. The model is linearised at the same input and output measurement. The model is translated in state space representation from pitch angle to generator speed and both are linearised at 16 m/s. In Simulink, the pitch angle is identified as the input perturbation and the generator speed is the output measurement.

The simulation is set up as the following: The transfer function of the system is taken from the pitch angle to the generator speed. In the Simulink editor, the linearisation steps are as follows; *Analysis* > *Control Design* > *Linear Analysis*. In the linear analysis tool, the specified input/output (IO) is linearised and the result is generated in the Bode diagram. The information of the linearised model can be analysed from the Bode plot. It has the state space equation of the linearised model named *linsys1* by default. The *linsys1* represents the linearised system at the selected operating point.

A similar technique is applied to the ATB wind turbine Simulink model. The results are compared in a Bode plot as shown in Figure 4.5. The figure shows the responses of 2 models, baseline with reduced order and ATB wind turbine with reduced order. The reduced order yields a simpler response which allows a manageable and efficient analysis. This simplification is beneficial for controller design. The reduced-order Bode diagram captures the main system dynamics. The 2 models shown in the figure are comparable at low frequencies. Low frequencies translate how the system responds to slow wind speeds. The wind turbine's ability to adapt to slow changes in wind speed is represented by low-frequency gain, which has an effect on the efficiency of the energy. While low frequency phase shifts are an indication of any response time delays in the system. This affects how fast the wind turbine can change direction or speed in response to variations in wind speed. The figure shows that the baseline model responds similarly to the ATB wind turbine up to 5 rad/s and after 5 rad/s it adapts to the change of wind speed faster than the ATB wind turbine with reduced order. The phase shift shows that the baseline model with reduced order responses changes direction faster than the ATB wind turbine model. These results are expected since the baseline wind turbine model is an established model while the ATB wind turbine model has yet to be established. However, the results are sufficient and are comparable

in the low frequency gains.

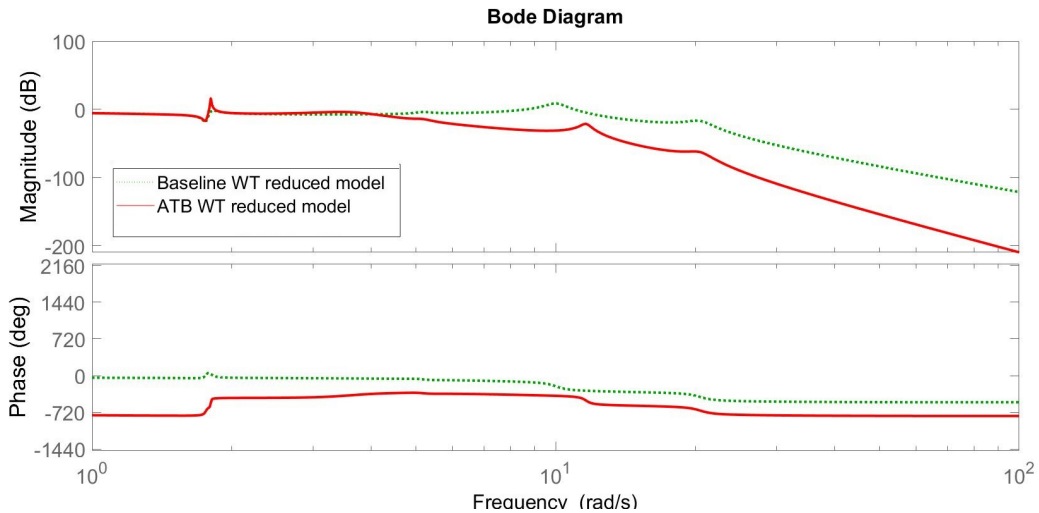

Figure 4.5: Linearised model comparison

The modelling concerns above-rated control taken at 16 m/s as the operating point. The performance of the linearised model is evaluated with the baseline controller.

The ATB wind turbine model is linearised at a single operating point. The linearised model is represented in a state space model with A, B, C and D matrices. The model recognises 13 states which will be discussed later in Chapter 5. The model is discretised in a sample time of 0.2 seconds. The ATB wind turbine has a highly nonlinear characteristic that, ideally can be discretised in a smaller sampling time. However, it is not ideal for simulation purposes. The model is discretised using the $c2d$ function in Matlab. The discretisation gives new A, B, C and D matrices. The size of matrix A is 13×13.

The state vector x consists of 13 states, i.e.

$$x = \left[\theta_R, \Omega, \Omega_H, \theta_T, \dot{\theta}_T, \phi_R, \dot{\phi}_R, \phi_T, \dot{\phi}_T, \beta, \dot{\beta}, \theta_{ATB}, \dot{\theta}_{ATB}, \dot{\theta}_s, \Omega_g\right]^T.$$

These states represent key variables in the turbine model, which are listed in Table 4.3.

The control input is the pitch angle $u(k) = \beta(k)$, the output is the generator speed $y(k) = \Omega_g(k)$. This is a single-input single-output model that is used for the controller design in Chapter 5.

Table 4.3: States and descriptions

States	Description	Symbol
x_1	rotor displacement	θ_R
x_2	rotor speed	Ω
x_3	hub speed	Ω_H
x_4	tower displacement ss	θ_T
x_5	tower speed ss	$\dot{\theta}_T$
x_6	rotor displacement oop	ϕ_R
x_7	rotor speed oop	$\dot{\phi}_R$
x_8	tower displacement oop	ϕ_T
x_9	tower speed oop	$\dot{\phi}_T$
x_{10}	ATB displacement	θ_{ATB}
x_{11}	ATB speed	$\dot{\theta}_{ATB}$
x_{12}	equivalent LSS and HSS displacement	θ_s
x_{13}	generator speed	Ω_g

4.3.2 Model reduction

Model reduction is a method of reducing the states in linearised system by selecting the significant states only. The states that are considered as not significant are removed from the system. In the ATB wind turbine system, the linearised model from GL Bladed has 241 states. The large number of states will cause difficulty in designing MPC controllers. It will take much more simulation time to solve the optimisation problem. Thus, model reduction is used to produce a model that is sufficient for MPC. It is not as precise as the actual wind system but it will not jeopardise the system performance.

Hankel singular value decomposition (HSVD) is a measurement method of energy for each state in a system. It is normally applied in model reduction in which the high energy states are retained and the low energy states are removed. The reduced model keeps the important features of the original model.

There are 241 states associated with the ATB wind turbine model generated by GL Bladed. However, the system does not require all states to analyse the system. The system is simplified by applying state reduction to streamline the process of analysing the results without compromising the entire system.

The system applies HSVD methods for system reduction in the linearised model

produced by BLADED. The size of the state space model is reduced by obtaining the controllability and observability gramian and then inserting this into the Lyapunov function in Equation (4.21) and (4.22). Then the new state space model is known as $\hat{A}$, $\hat{B}$, $\hat{C}$ and $\hat{D}$. Next eigenvalue and eigenvectors, Σ^2 , U and U^T are calculated. By solving the transformation matrix, T the reduced model can be calculated.

$$AP + PA^2 + BB^T = 0 \tag{4.21}$$

$$A^T Q + QA + C^T C = 0 \tag{4.22}$$

The controllability equation is given by:

$$P = S_{\tau=0}^{\infty} e^{A\tau} BB^T eA^T d\tau \tag{4.23}$$

The observability equation is given by:

$$Q = S_{\tau=0}^{\infty} A^{T_\tau} C^T Ce^{A\tau} d\tau \tag{4.24}$$

Since P and Q are unbalanced, HSVD is the method to overcome the situation, where it will make,

$$\hat{P} = \hat{Q} = \begin{bmatrix} \sigma_1 & ... & ... & 0 \\ 0 & \sigma_2 & ... & ... \\ ... & ... & \sigma_{n-1} & ... \\ ... & ... & ... & \sigma_n \end{bmatrix} \tag{4.25}$$

$$\hat{A}(TPT^T) + (TPT^T)\hat{A}^T + \hat{B}\hat{B}^T \tag{4.26}$$

and gives a new balanced controllability gramian, $\hat{P}$, where $\hat{P} = TPT^T$.

and the second Lyapunov equation is solved to,

solving,

$$\hat{A}\hat{Q} + \hat{Q}\hat{A} + \hat{C}^T\hat{C} = 0 \tag{4.27}$$

and gives new balanced observability gramian, $\hat{Q}$, where $\hat{Q} = TQT^T$.

For a balanced system, $\hat{P}$ must equal to $\hat{Q}$.

$$\hat{P} = \hat{Q} = \Sigma \tag{4.28}$$

$$\hat{P}\hat{Q} = \Sigma^2 \tag{4.29}$$

where,

Σ^2 is the eigenvalue, λ with a diagonal matrix as shown in Equation (4.25).

Then the eigenvalues are plotted as below,

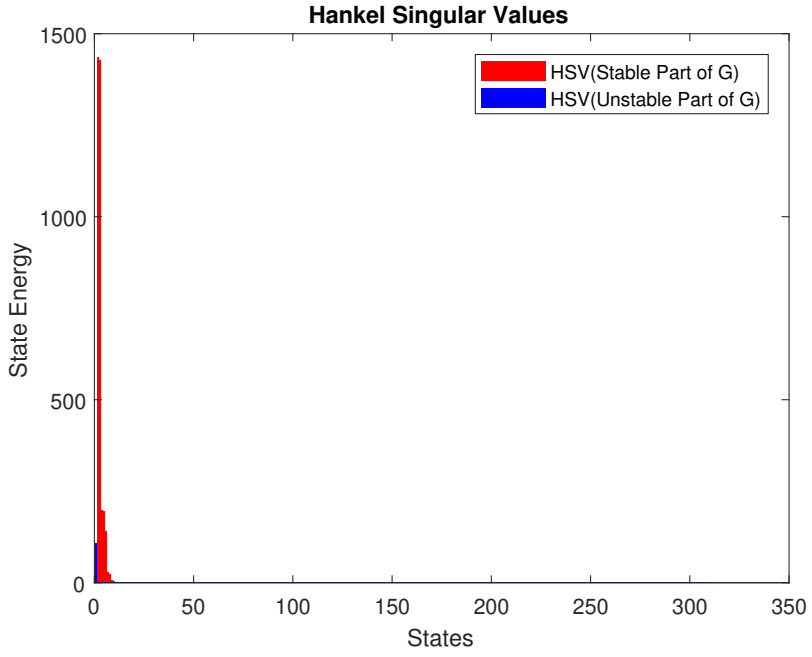

Figure 4.6: Overview of State Energy for 241 States

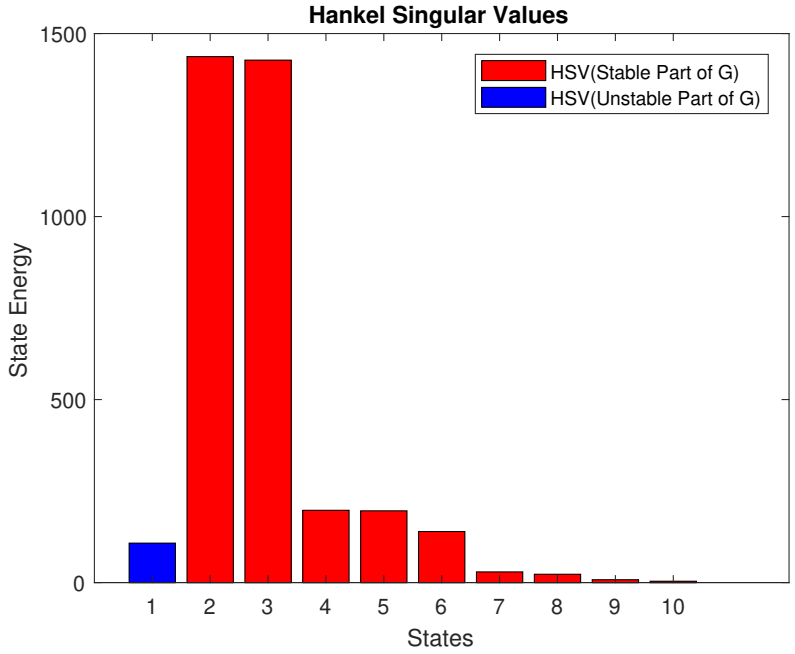

Figure 4.7: Zoomed State Energy for 10 States

The results showed that insignificant states have zero power. That is how the reduction of the linearised system is arrived at theoretically, and the results shown are from Matlab, where the power of the dominant states shows the majority of the power.

The results in Figure 4.6 and 4.7 are plotted using Matlab. Dominant state energy appears from states 2 to 6. State 1 is unstable and is not considered in the system reduction. The system is reduced to 10 states by Matlab.

This thesis applies the model developed from Leithead & Rogers (1996a),Leithead & Rogers (1996b) and translated into Simulink blocks. From the equations, the derived model consists of 13 states for the ATB wind turbine model as shown in Table 4.3. Since the number of states derived from the Simulink model is already low, all states are considered as important to the system, this state space model is the one chosen for baseline controller evaluation.

4.4 Implementation of Dynamic ATB Model (Model 2) with Baseline Controller (Controller 1)

The implementation of the ATB wind turbine dynamic model applies a 5MW Supergen wind turbine model with a gain-scheduling baseline controller (Controller 1). The model development is explained in Chapter 3. The mathematical model is applied in Simulink and is taken as the model for the ATB dynamic model implementation.

4.4.1 Baseline controller with gain-scheduling for ATB wind turbine model

The transfer function of the spring damper model is embedded into the Simulink 5MW wind turbine model in between the aerodynamic block and the rotor block. It introduces the flexible characteristic that gives effect to the rotor angle displacement and the tower displacement as well. Ideally, the ATB in the Simulink will present a fluctuating characteristic of a 5MW wind turbine blade. The baseline wind turbine is built with a conventional blade which does not have adaptive behaviour. This section will analyse the ATB model with the existing baseline controller.

4.4.2 Supergen 5MW wind turbine model and Controller 1

The simulation work applies the baseline model of the Supergen 5MW wind turbine model in Simulink. The dynamic of the ATB is adapted to the model as explained in Section 4.1. The model is a nonlinear model where the mathematical expressions to describe a wind turbine model is translated into Simulink blocks.

The wind turbine block in Simulink consists of 4 main blocks, the aerodynamics, rotor, drive-train and generator torque block. Referring to Figure 4.1, there are 2 inputs to the ATB wind turbine model. The inputs are coming from the baseline controller in which 1 input is from above-rated controller and 1 input is from the below-rated controller. The baseline wind turbine control scheme has these 2 techniques to control the baseline wind turbine.

The first block is the pitch mechanism block. It consists of the pitch actuator that

supplies pitch angle output to the aero-rotor block. The second block is the aero-rotor block. This block is formed with two inner blocks; the aerodynamics block and the rotor dynamics block and the third block is the drive-train block. The block consists of information on the components in the drive train such as the gearbox, the high-speed shaft and the low-speed shaft.

The interest block in the model is the aero-rotor block where the ATB is located. The ATB wind turbine will have similar aerodynamic information as what is applied in the baseline model. The rotor dynamic block consists of the wind turbine rotor with an individual blade model. Physically, the blade for the ATB fluctuates more than the baseline blade. The characteristics of the ATB will affect the drive train block and will have an impact on the entire wind turbine system.

In theory, the dynamics of the flexible blade influence the performance of the wind turbine system. For example, the rotor dynamics affect the tower acceleration for fore-aft and side-to-side directions. This is also proportional to the effects of the tower fatigue. The objective of developing ATB for wind turbine systems is to alleviate the loading effects without compromising the power production of the system. In the simulation set-up, the dynamics model of an ATB Wind turbine is tested with the standard baseline controller with a gain-scheduling approach. Note that, the baseline controller is uniquely designed for a 5MW wind turbine model without ATB characteristics embedded into it.

The gain-scheduling technique is adopted for ATB wind turbine model. However, it is not responding to the baseline with the gain-schedule controller due to the ATB wind turbine model is not the same as the baseline wind turbine model. The baseline gain-schedule controller was carefully designed to match the baseline wind turbine model.

4.5 Results and analysis

The dynamic model of an ATB wind turbine is analysed by applying the baseline controller to the system. A set of simulation results is presented and discussed in this section. The simulation takes part in above-rated control only and the wind speed selection is 16 m/s. 16 m/s wind speed is chosen as the simulation parameter due to

the fact that at this wind speed, the tendency of the blade to brake is high without a good control system. Higher wind speeds are considered too high and are not suitable for simulation purposes. The system output response is taken from the pitch angle input to the generator speed output. The comparison between the output responses of baseline wind turbine with a gain-scheduling controller and ATB wind turbine model with gain-scheduling controller are plotted in the bode diagram as shown in Figure 4.8 - 4.12.

The baseline wind turbine model is compared to the dynamic ATB wind turbine model in Simulink. The simulations were executed in a Matlab environment. The ATB wind turbine model is simulated with the baseline controller gain-scheduling and plotted to compare to the baseline wind turbine model with a similar controller. The results are to observe the performance of the baseline wind turbine model and the dynamic ATB wind turbine model with the same controller. Fundamentally, it is known that the baseline gain-schedule controller is designed specifically for the baseline wind turbine model. Thus, the results of the same controller adapted to the ATB wind turbine model are expected to be as perfect as the baseline wind turbine model. The ATB wind turbine performance with controller and without controller is summarised in 2 segments; the power generation which consists of power production, generator speed and pitch angle and the fatigue loading effect with tower acceleration and root bending moment.

4.5.1 Power generation

Figure 4.8 shows the comparison of the results between the baseline wind turbine and ATB wind turbine the gain-schedule controller. The ATB wind turbine model (Model 2) represented by the blue line indicates large fluctuations compared to the black line that represents Model 0 which is the baseline wind turbine model. Both models (Model 0 and Model 2) apply a gain-scheduling controller to the system. The results show that Model 2 depicts its dynamics but does not respond to the controller. This is because the controller is tailored to meet the characteristics of Model 0. The results show that Model 2 cannot use the controller for Model 0. This can be a result of performance

limitations, or a lack of resilience in the system. Figure 4.9 shows the generator speed comparison. The figure also shows similar output behaviour as 4.8. The results also compare the output pitch angle in Figure 4.10. The results show that the pitch angle is out of the range when compared to Model 0. These 3 figures show coherent outputs as expected.

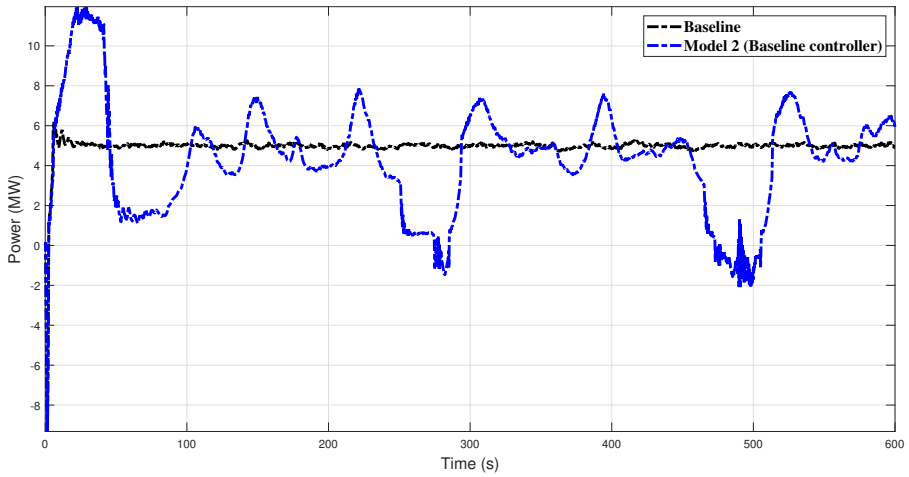

Figure 4.8: Power generation comparison for Model 0 and Model 2

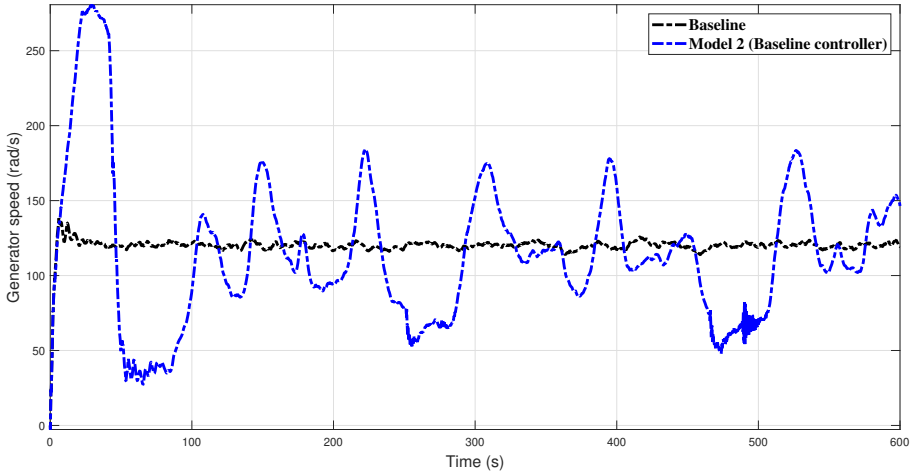

Figure 4.9: Generator speed comparison for Model 0 and Model 2

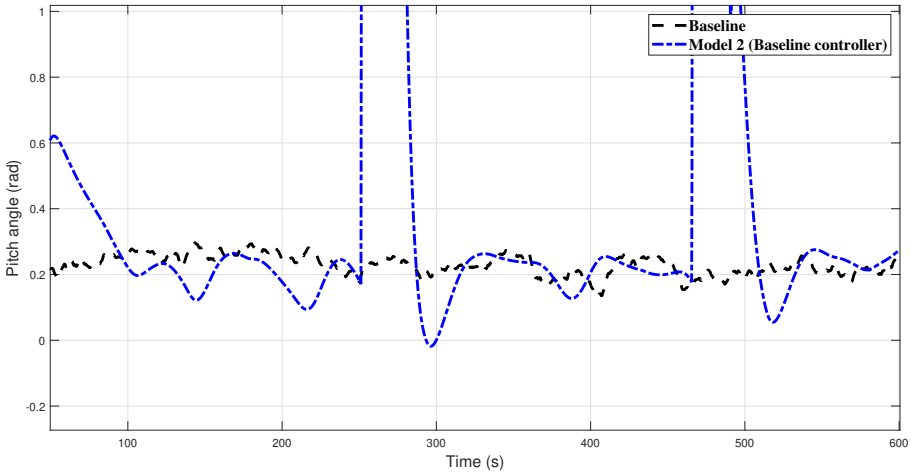

Figure 4.10: Pitch angle comparison for Model 0 and Model 2

4.5.2 Loading effect

The results for tower acceleration and root bending moment are as shown in Figure 4.11 and 4.12 respectively. With a baseline controller, the fatigue loading occurs in a nasty manner for the system due to the flexible behaviour of the blade. All of the responses show the ATB wind turbine model is not responding to the baseline gain-schedule controller. This is due to the new characteristic introduced to the wind turbine model. The dynamics behaviour is embedded in the baseline wind turbine model and it is clearly shown in the results.

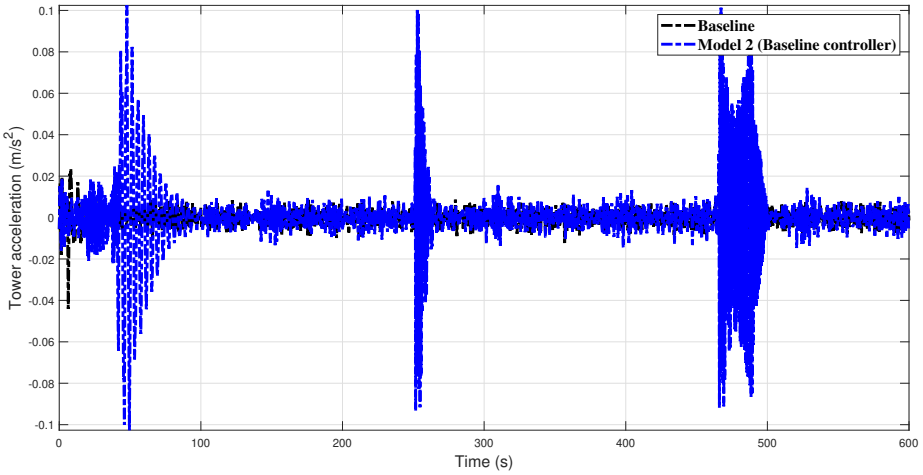

Figure 4.11: Tower acceleration comparison for Model 0 and Model 2

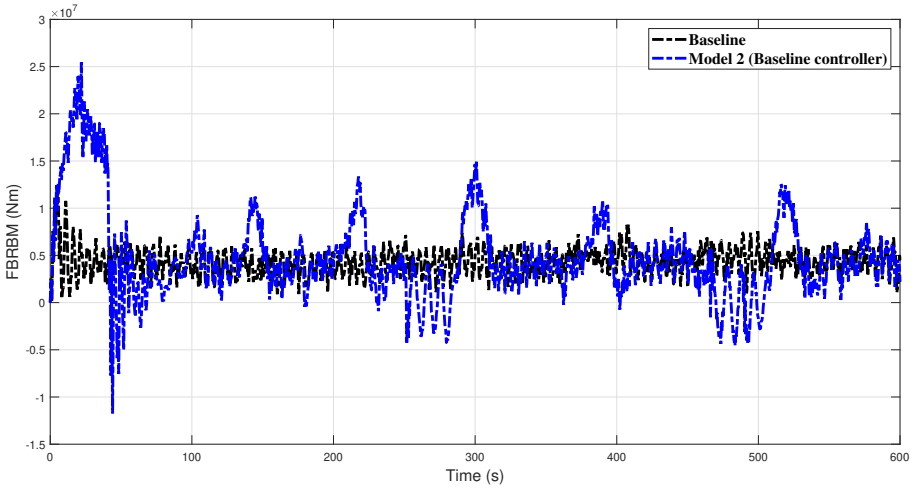

Figure 4.12: Root bending moment comparison for Model 0 and Model 2

In this chapter, the first part discusses the dynamic ATB wind turbine model (Model 2) where the dynamics of the wind turbine blade are represented by a spring damper model. The second part is to examine the model with the standard baseline gain-scheduling baseline controller (Controller 1). The objective is to validate that Model 2 is a feasible model of a dynamic ATB wind turbine. Controller 1 is developed specifically for the baseline wind turbine model (Model 0) and it is simulated as a controller for

Model 2 to observe its performance in response to the controller. The results show the dynamic behaviour of Model 2 and it is not responding to Controller 1. The controller needs to be redesigned, tuned, or otherwise altered to better suit Model 2. To address performance gaps and optimise the controller for dependable and efficient functioning in a particular situation, this iterative process may involve updating parameters, and algorithms, or adding new features.

4.6 Summary

The chapter explores the performance of the ATB wind turbine by applying the gain-scheduling baseline controller (Controller 1). It develops a model of an ATB wind turbine based on the ATB's aerodynamic behaviour. This section delves into the discussion and analysis of Controller 1 application in the ATB wind turbine (Model 2) model, mirroring the application of the basic controller in the baseline wind turbine model (Model 0).

A wind speed of 16 m/s was selected for the performance analysis, representing an above-rated wind speed scenario. Above-rated control is also known as the pitch control strategy. The results demonstrate that Model 2 is a feasible model that can be effectively analyzed by applying the Controller 1 technique. The dynamic behaviour introduced in Model 2 influences the output performance in maintaining the generated power at 5 MW.

The ATB wind turbine model is an analytical approach that enhances the baseline wind turbine model by incorporating an additional system to introduce flexible characteristics to the baseline blade. The model takes into account the baseline blade parameters such as the blade length, blade width, blade mass and the blade twist angle. The inclusion of these parameters allows for a more accurate representation of the ATB wind turbine's behaviour.

Model 2 is developed using an analytical model by applying the spring damper model to introduce the dynamic characteristics of the model. It is pre-analysed with the static model based on Capuzzi et al. (2015). The model with FE nonlinear model is selected to be further developed for the 5 MW wind turbine application. Based on

that, the power coefficient for the 5MW baseline wind turbine model is compared to the static ATB model. A feasibility study is conducted on the proposed model by embedding it into the 5MW Supergen Simulink model using the baseline controller. The results show that the spring damper model is feasible for the wind turbine system.

The aim of this chapter is to develop a Simulink model of an ATB wind turbine specifically for control applications for ATB wind turbines. To accomplish this, a dynamic model that can capture the behaviour of ATB wind turbines is developed using the Simulink environment. The model represents the response of the ATB wind turbine to the specific 16 m/s wind speeds over 600 seconds time. The Simulink model of an ATB wind turbine will be applied in developing the control approach for further investigation. Based on the new properties of Model 2 developed in this thesis, the controller shows that it needs further improvement for it to control the Model 2 system. It is feasible for further work on developing an alternative controller for the model. Thus, MPC is suggested to improve the performance of Model 2.

In conclusion, it is a challenge to model the ATB characteristics in wind turbines referring to the aerodynamic properties and stochastic wind behaviour. One of the approaches to model a reliable representation of an ATB wind turbine is by adding a spring damper model to the existing wind turbine blade model. Thus, MPC is proposed for the dynamic ATB wind turbine.

Chapter 5

Model Predictive Control (MPC) of ATB Wind Turbine

In Chapter 4, a dynamic model of the ATB wind turbine system (Model 2) is developed using spring damper model and it is examined with a gain-scheduling baseline controller (Controller 1) with the control parameter designed for a baseline wind turbine model. Controller 1 is connected to the Model 2 and its performance is analysed. The results show that Model 2 is not responding to the baseline controller. This is mainly because the control parameters are not designed for the ATB wind turbine. However, the results show the dynamic response of the system based on the existing baseline controller. This chapter introduces a modern controller to control the performance of Model 2 and to analyse the results. MPC is selected as the controller for the ATB wind turbine model (Model 2) developed in Chapter 4. MPC can predict the upcoming event by taking the current event as a reference. It is beneficial for a wind turbine system because it can predict incoming wind force which is stochastic in nature. This chapter investigates MPC in ATB for wind turbine systems. MPC is referred to as Controller 2 when discussing the results in this thesis. The chapter is divided into 7 sections; Section 5.1 is the MPC introduction, Section 5.2 reviews the MPC design and Section 5.3 explains the MPC development of a wind turbine system. Section 5.4 discusses MPC basic algorithm in wind turbine systems, Section 5.5 explains the MPC implementation, results are presented and analysed in Section 5.6 and the chapter is summarised in

5.1 Wind Turbine System Model Predictive Control (MPC)

MPC is a powerful control system that is widely used in various areas of applications such as in the chemical industries, financing and of course engineering. MPC predicts a set horizon by optimising the first term of the horizon and predicts the next set of horizons in a discrete function. MPC is an advanced version of linear quadratic regulator control (LQR) and it has more advantages compared to the LQR. For example, one advantage of MPC is it optimises the system in a receding time horizon while LQR optimises in a fixed time horizon. It means that the system is optimised along the time domain without having to introduce a new horizon every single time. Another advantage of MPC is, that it also solves the problem in a time horizon whereas LQR only solves problems in a single solution. Also, LQR is not capable of solving constraints, which gives the advantage to MPC where it is able to handle constraints and can give solutions for migration of a nonlinear system away from its linearised operating point. Constraint handling is the reason why MPC is commonly used in process control where it is designed to satisfy the set of constraints. Another advantage of MPC is, that it operates with a linear system which is easier to handle. In digital control, MPC is the most commonly applied in various areas due to its advanced technique as compared to the pole placement and the linear quadratic regulator (LQR) technique.

MPC is applied in various applications, one of which is in wind turbine system applications. Compared to the conventional gain-scheduling baseline controller (Controller 1) which controls the wind turbine system over the full range of operation, MPC will need to control the wind turbine independently for below-rated wind speed and above-rated wind speed, particularly for a linearised wind turbine system. For MPC, there are 2 type of controller that is used in wind turbine control; linear MPC and nonlinear MPC. Linear MPC is commonly used in wind turbine control due to its simplicity and straight forward solutions. However, this technique is also known as not accurate as Controller 1 because the system is simplified through linearisation method.

On the other hand, nonlinear MPC is theoretically more accurate compared to

linear MPC. The system is represented in nonlinear function and is controlled based on the cost function which determines the main objectives in wind turbine control such as minimising the loading error and pitch rate error. Even though in theory the nonlinear MPC looks very promising as it can control the wind turbine system performance equivalent to Controller 1, the research in this interest is very limited. There are publications about nonlinear MPC for wind turbines but the approach mostly focuses on economic nonlinear MPC.

In the MPC framework in this thesis, Model 2 is linearised at 16 m/s wind speed. The model is a collective pitch control where all blades are pitched at the same pitch angles. The linearised model has 13 states that are tabulated in Table 4.3. This model is the predictive model applied in MPC.

5.2 MPC Design for Wind Turbine System

A wind turbine is a highly nonlinear system. In this project, the wind turbine is modelled into a lower order system and linearised to test with MPC. Based on the standard equations, MPC requires computational solutions. A system with a higher number of matrices implies the complexity of the system. The complex system requires high speed calculation to reduce the solution time. MPC can be applied to linear systems and nonlinear systems. MPC also can be extended as an adaptive MPC. This project starts with standard MPC as the basic controller and then improves the controller to adaptive MPC configuration to control the system. The standard MPC configuration is shown in Figure 5.2. The figure shows a linearised single-input-single-output (SISO) system, the constraints, and the cost function to determine the system performance. Further explanation on implementing MPC in a wind turbine system is explained in the next section. MPC can be further developed as the adaptive MPC configuration where it applies the same standard MPC parameters and it consists of further developed block functions. Both standard MPC and adaptive MPC apply a linearised system. For instance, a linearised system is represented with a state space model. From the state space model, the number of inputs, outputs, and states can be identified. For an adaptive MPC, the linearised model requires a model update

connected to the controller. The updated model receives the predicted states, evaluates the performances and adapts to the current system to optimise the performance. The adaptive MPC for a linearised system works similarly to a nonlinear system except that for a nonlinear model, an extended Kalman filter is required. This is due to the nonlinear system will not give a Gaussian output if the standard Kalman filter is applied. The extended Kalman filter will select one point as the operating point and that point is multiplied with the Gaussian input given the output in the Gaussian form subjected to the y-axis. However, note that the extended Kalman filter may not work on a highly nonlinear system. The thesis focuses only on the linearized system with adaptive MPC and standard Kalman filter.

In linear MPC, the nonlinear system is linearised along the operating region. However, if the system is highly nonlinear, the MPC may not be responding to the controller as the changes from the operating point are too far. Nonlinear MPC requires a nonlinear Kalman filter or extended Kalman filter (EKF), a nonlinear cost function, and a non-quadratic solver.

The continuous nonlinear system is linearised at every sampling time. The linearised continuous system is discretised for the given controller sampling time. The discretised linear model generates the matrices to compute the prediction horizon and the control horizon. The prediction matrices are used to form a quadratic programming (QP) problem to find a solution to minimise the cost function. The details of the scheme are described below,

The system with N_x states, N_u inputs, N_y outputs from $\mathbf{x} \in \mathbb{R}^{N_x}$, input $\mathbf{u} \in \mathbb{R}^{N_u}$ and output $\mathbf{y} \in \mathbb{R}^{N_y}$ vectors. The nonlinear function of output y with x states is written as $y_i = z_i(\mathbf{x}, \mathbf{u})$, $i = 1, ..., N_y$, and $\dot{x} = f_i(\mathbf{x}, \mathbf{u})$, $i = 1, ..., N_x$, respectively. The system dynamics can be represented as,

$$\dot{\mathbf{x}} = F(\mathbf{x}, \mathbf{u}), \mathbf{y} = Z(\mathbf{x}, \mathbf{u}) \tag{5.1}$$

The constraint for the system in Equation (5.1) is specified by

$$\mathbf{x}_l \leq \mathbf{x} \leq \mathbf{x}_u \tag{5.2}$$

and

$$\mathbf{u}_l \leq \mathbf{u} \leq \mathbf{u}_u \tag{5.3}$$

where, $\mathbf{x}_l, \mathbf{x}_u, \mathbf{u}_l, \mathbf{u}_u$ are the lower and upper limit for the states and control input respectively.

The system in Equation (5.1) can be linearised by finding the gradient matrices at the specified operational point. Jacobian sub-matrix of the function F in derivatives of states vector is written as,

$$A_c = \begin{bmatrix} \frac{\partial f_1}{\partial x_1} & \frac{\partial f_1}{\partial x_2} & \cdots & \frac{\partial f_1}{\partial x_{N_x}} \\ \frac{\partial f_2}{\partial x_1} & \frac{\partial f_2}{\partial x_2} & \cdots & \frac{\partial f_2}{\partial x_{N_x}} \\ \vdots & \vdots & \ddots & \vdots \\ \frac{\partial f_{N_x}}{\partial x_1} & \frac{\partial f_{N_x}}{\partial x_2} & \cdots & \frac{\partial f_{N_x}}{\partial x_{N_x}} \end{bmatrix} \tag{5.4}$$

also can be written as,

$A_c(i,j) = \dfrac{\partial f_i}{\partial x_j}$, where the same notation can be applied to write $B_c(i,j) = \dfrac{\partial f_i}{\partial u_j}$, $C_c(i,j) = \dfrac{\partial z_i}{\partial x_j}$ and $D_c(i,j) = \dfrac{\partial z_i}{\partial u_j}$.

The specified states operational point is $\mathbf{x}_o$, the derivative is $\dot{\mathbf{x}}_o$ and the control input is $\mathbf{u}_o$.

The system evolution for the linearised system can be described as,

$$\dot{\mathbf{x}}_L = \dot{\mathbf{x}}_o + A_c(\mathbf{x}_L - \mathbf{x}_o) + B_c(\mathbf{u}_L - \mathbf{u}_o) \tag{5.5}$$

Taking the constant term from Equation (5.5) into $\kappa = \dot{\mathbf{x}}_o + A_c\mathbf{x}_o - B_c\mathbf{u}_o \in \mathbb{R}^{N_x}$, the state space representation of linearised system is.

$$\dot{\mathbf{x}}_L = A_c\mathbf{x}_L + B_c\mathbf{u}_L + \kappa \tag{5.6}$$

$$\mathbf{y}_L = C_c\mathbf{x}_L + D_c\mathbf{u}_L \tag{5.7}$$

where A_c, B_c, C_c and D_c are the matrices in the continuous function. X_L and u_L

are the linearised functions of the states and the input.

MPC requires a discrete system to operate. As such, the linearised equations in Equation (5.6) and (5.7) must be descretised. The general discretisation steps begin with the multiplication of the matrices by the matrix exponential $e^{-A_c t}$ to both sides of Equation (5.6)

$$e^{-A_c t}\dot{\mathbf{x}}_L(t) = e^{-A_c t}A_c\mathbf{x}_L(t) + e^{-A_c t}(B_c\mathbf{u}_L(t) + \kappa)e^{-A_c(t-\tau)}(B_c\mathbf{u}_L(\tau) + \kappa)d\tau \tag{5.8}$$

reorganised,

$$\frac{d}{dt}(e^{-A_c t}A_c\mathbf{x}_L(t)) = e^{-A_c t}(B_c\mathbf{u}_L(t) + \kappa) \tag{5.9}$$

solve for $\mathbf{x}_L$,

$$\mathbf{x}_L(t) = e^{-A_c t}\mathbf{x}_L(0) + \int_0^t e^{A_c(t-\tau)}((B_c\mathbf{u}_L(\tau) + \kappa)d\tau \tag{5.10}$$

Discrete time is denoted as $\mathbf{x}_L[k] = \mathbf{x}_L(kTs)$, where Ts is the sampling time and can be rewrite as,

$$\mathbf{x}_L[k+1] = e^{A_c Ts}\mathbf{x}_L[k] + \int_{kTs}^{kTs+Ts} e^{A_c(kTs+Ts-\tau)}((B_c\mathbf{u}_L(\tau) + \kappa)d\tau \tag{5.11}$$

Assuming $\mathbf{u}_L = \mathbf{u}_L[k]$,

$$\mathbf{x}_L[k+1] = e^{A_c Ts}\mathbf{x}_L[k] + A_c^{-1}(e^{A_c Ts} - I)(B_c\mathbf{u}_L[k] + \kappa) \tag{5.12}$$

$$\mathbf{y}_L[k] = Cc\mathbf{x}_L[k] + D_c\mathbf{u}_L[k] \tag{5.13}$$

The discrete state space matrices can be written as, $A_d = e^{A_c Ts}$, $B_d = A_c^{-1}(e^{A_c Ts} - I)B_c$, $\mathbb{K} = A_c^{-1}(e^{A_c Ts} - I)\kappa$, $C_d = C_c$ and $D_d = D_c$

The discrete time linearised space space equations can be written as,

$$\mathbf{x}_D(k+1) = A_d\mathbf{x}_D(k) + B_d\mathbf{u}_D(k) + \mathbb{K} \tag{5.14}$$

$$\mathbf{y}_D(k) = C_d\mathbf{x}_D(k) + D_d\mathbf{u}_D(k) \tag{5.15}$$

MPC is also known as receding horizon control, where the prediction horizon and control horizon are finite and are optimised upon past and future events. It is realised by minimising the predefined cost function for N steps ahead to build a controller. The obtained control is applied for the current time instant only. The step is repeated after a new value if x_t is obtained. The parameters of the model must be ready to be changed with a set of T at some time instant. In model parameters estimation, the purpose is to estimate and detect changes in the parameters of the model.

5.3 Wind Turbine Model Development for MPC

MPC development requires the wind turbine model to be represented in a state space equation. The model is developed in Chapter 4.

5.3.1 State space equation for wind turbine model

The state space equation was introduced in Equation (4.20), in which 2 linearised models were introduced in Chapter 4.2; the linearised model generated from GL Bladed and the linearised model generated from Supergen Simulink model with different numbers of states. In this chapter, the linearised model of a 5MW Supergen wind turbine from Simulink is applied where there are 13 states as listed in Table 4.3.

5.3.2 Model output prediction

The output prediction for MPC is given by,

$$x(k+1) = Ax(k) + Bu(k) \tag{5.16}$$

$$y(k+1) = Cx(k) + Du(k) \tag{5.17}$$

where k is the time in discrete and A, B, C, D, x, y and u are similar to Equation (4.20). The model output prediction is expressed in discrete time where $x(k+1)$ and $y(k+1)$ indicate the state and output equation at a future time when other parameters are measured at the current time.

5.3.3 Kalman filter algorithm overviews

Kalman filter is an efficient estimator that can estimate the state of discrete-data controlled processes from measurements that carry noises into providing an estimate computed from the random estimates. Kalman filter is a powerful method to determine state estimation with high accuracy over the uncertainty from input measurements.

MPC uses the Kalman Filter in identifying the state estimator and also to formulate the covariance and determine the Kalman gain. Kalman is computed based on the number of measurements taken out of uncertainty.

Figure 5.1 shows the standard Kalman filter architecture explaining how the Kalman filter operates in MPC (Busarello & Simões 2019). From the figure, $\hat{x}$ is the state variable, P is the state covariance matrix, z is the measurement, A is the state transition matrix, H is the state-to-measurement matrix, R is the measurement covariance matrix, Q is the process noise covariance matrix, and L is the Kalman Gain. The first step is initiating the system state estimate and system error covariance of $\hat{X}(0), P(0)$ and taking the measurement. The following step is predicting the system state and system state error covariance to measurement time giving $\hat{x}(k-1) = A\hat{x}(k-1)$ and $P(k-1) = AP(k-1)A^T + Q$. After that, Kalman gain, L can be calculated using the formula, $L(k) = P(k-1)H^T(HP(k-1)H^T + R)^{-1}$. Finally, estimating the state and state error covariance to the measurement time giving $\hat{x}(k) = \hat{x}(k-1) + L(k)(z(k)H\hat{x}(k-1))$ and $P(k) = P(k-1) - L(k)HP(k-1)$.

In Simulink, MPC and adaptive MPC are the ready-to-use MPC block that has the built-in function of the Kalman filter.

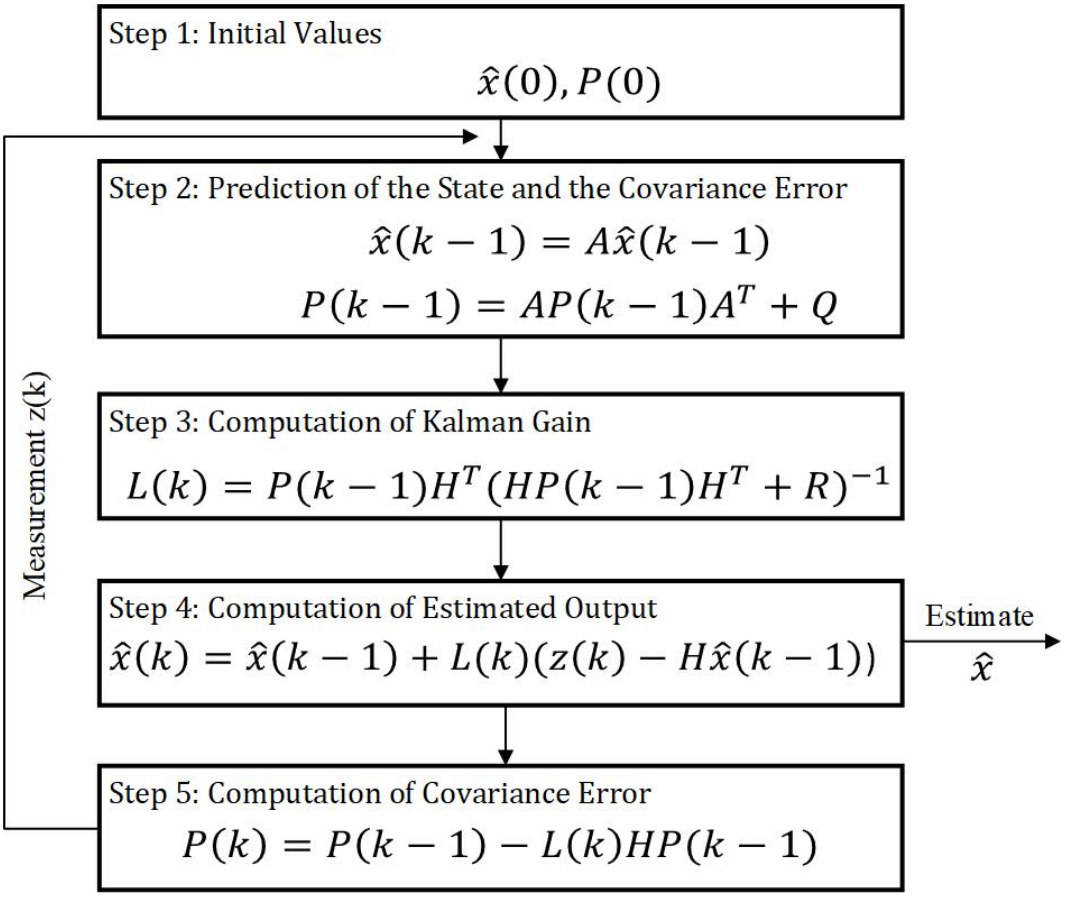

Figure 5.1: Kalman filter standard architecture

5.4 MPC basic algorithm

MPC is a powerful control method in modern control technology due to its capability to predict future events by evaluating the current state.

The control system block diagram with MPC is shown in Figure 5.2. The linearised MPC is designed based on the linearised state-space model and the control action is applied to the nonlinear wind turbine model. When the controller is used to regulate wind turbine generator speed across the full range of above-rated wind speeds, adaptive MPC is required to compensate for the mismatch between the linearised model in MPC and the nonlinear wind turbine model. Model update and Kalman filter are introduced for such purpose. The model update can be made by methods such as

recursive least square parameter estimation, neural-network-based tuning, normally conducted in a larger time scale than the sampling time for control. For simulations of turbulent wind speed, with a set mean value, the nonlinear dynamics are slowly varying and a combination of Kalman filter and MPC suffices. With this design scheme, the computational demand for real-time optimisation is reduced compared to using nonlinear MPC, while the control performance is not compromised by linear control.

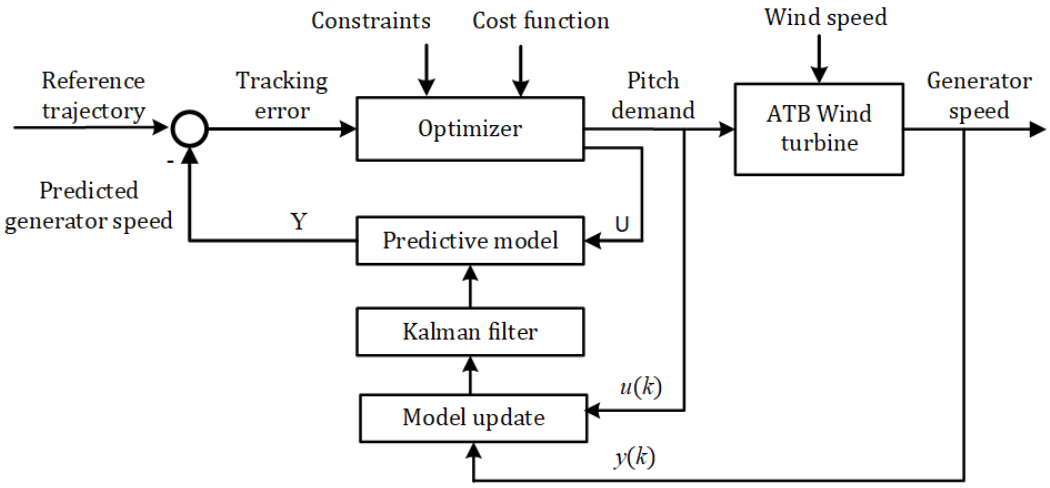

Figure 5.2: Block diagram for ATB wind turbine with MPC

The MPC solution requires the estimated states at each time k, for which a steady-state Kalman filter is designed. The Kalman filter equations are

$$\begin{aligned} \hat{x}(k) &= A\hat{x}(k-1) + Bu(k) + L\left(y(k) - \hat{y}(k)\right) \\ \hat{y}(k) &= C\hat{x}(k-1) \end{aligned} \tag{5.18}$$

where $\hat{x}(k)$ is the model estimated states, $\hat{y}(k)$ is the linearised model output and $y(k)$ is the nonlinear model output. The Kalman gain L is derived by solving a discrete Riccati equation.

The optimiser in Figure 5.2 is developed upon 2 unique parameters for MPC which are the cost function and the constraints. MPC is measured by minimising the cost function of a system by tuning the weightings of the inputs or the states or errors. The

cost function is given by

$$\underset{\mathbf{\Delta u(k)}}{\mathbf{minJ}} = \mathbf{\hat{e}(k+1)^T Q\hat{e}(k+1) + \Delta u(k)^T R\Delta u(k)} \tag{5.19}$$

where, J is the cost function or the objective function, $e(k)$ is the error, $u(k)$ is the input, Q is the weighting coefficient reflecting the importance of the states, $x(k)$ and R is the weighting coefficient penalising relative big changes in input, $u(k)$.

Linear MPC (LMPC) is a straight forward MPC optimisation technique. The non-linear model is linearised over an operating point assuming that the system is in good operation even it is outside the operating region. Linear MPC uses Kalman filter (KF), linear cost function and linear constraints in optimising the linearised system. The linearised system is taken as the predictive model in developing the MPC. Kalman filter is the filter to check the linearised system when noises are applied to it. Typically, the Kalman filter determines the covariance with respect to the noise of the state prediction, x_k and the updated state estimation, $\hat{x}_k$.

Assume that $\{\mathbf{y}_r(k+j|k) : j = 1, 2, ...p\}$ denotes future desired setpoint trajectory at sampling time, k. MPC at k is defined as a constraint optimisation problem where the future manipulated input moves $\mathbf{u}(k|k), \mathbf{u}(k+1|k).....\mathbf{u}(k+q-1|k)$ are determined by minimizing the objective function, J.

Based on a state space system equation, the optimal constrained control problem of linear MPC reference tracking is,

$$\underset{\Delta u}{min} \sum_{k=0}^{N-1} (\mathbf{y}(k+1) - r(t))^T \mathbf{Q}(\mathbf{y}(k+1) - \mathbf{r}(t)) + (\mathbf{u}(k) - \mathbf{u}(k-1))^T \mathbf{R}(\mathbf{u}(k) - \mathbf{u}(k-1)) \tag{5.20}$$

$$s.t. : \mathbf{u}_{min} \leq \mathbf{u}(k), k = 0, ..., N-1$$

$$\Delta\mathbf{u}_{min} \leq \mathbf{u}(k) - \mathbf{u}(k-1) \leq \Delta\mathbf{u}_{max}, k = 0, ..., N-1$$

$$\mathbf{y}_{min} \leq \mathbf{y}(k) \leq \mathbf{y}_{max}, k = 0, ..., N-1$$

where, N is the number of steps, and the quadratic program (QP) can be re-

rewritten in,

$$\min_{\Delta \mathbf{U}} J(\Delta \mathbf{U}, \mathbf{x}(t)) = \frac{1}{2}\Delta \mathbf{U}^T \mathbf{H} \Delta \mathbf{U} + [\mathbf{x}^T(t)\ \mathbf{r}^T(t)\ \mathbf{u}^T(t-1)]\mathbf{F}\Delta \mathbf{U}$$
$$s.t. \quad \mathbf{G}\Delta \mathbf{U} \leq \mathbf{W} + \mathbf{S}\begin{bmatrix} \mathbf{x}(t) \\ \mathbf{r}(t) \\ \mathbf{u}(t-1) \end{bmatrix} \tag{5.21}$$

Based on the receding horizon concept, the optimal sequence is derived over N_c steps but only the first element is taken as the optimal control movement $u(k)$. At time $k+1$, a new measurement or state is calculated and the optimisation repeats. Essentially, the feedback information is exploited to update the optimisation over the control horizon N_c to predict the future events of the system outputs. The prediction model describes how the system output is expected to operate. The system constraint is the limit subjected to the pitch actuator. The set point is the desired generator speed. The cost function is the goal of minimum output error. The receding horizon control strategy would re-plan the optimum pitch angle at the wind speed at time instant, k, find the overall set of actions over a time horizon, apply the first control input Δu into the system and re-plan for the next step.

The optimisation problem is represented in the following form:

$$\begin{aligned} \text{minimise} \quad & \frac{1}{2} z^T H_z + h^T z \\ s.t \quad & F(z) = f \\ & G_z \leq g \end{aligned} \tag{5.22}$$

where,

$$z = [x^T(k), x^T(k+1), ..., x^T(k+N), u^T(k), u^T(k+1), ..., u^T(k+N-1)]^T \tag{5.23}$$

$$H = \begin{bmatrix} Q & 0 & \cdots & & & S & 0 & \cdots & 0 \\ 0 & Q & & & & 0 & S & & \vdots \\ \vdots & & \ddots & & & \vdots & & \ddots & \\ & & & Q & & & & & S \\ & & & & Q_f & 0 & \cdots & & 0 \\ S^T & 0 & \cdots & & 0 & R & 0 & \cdots & 0 \\ 0 & S^T & & & \vdots & 0 & R & & \vdots \\ \vdots & & \ddots & & & \vdots & & \ddots & \\ 0 & \cdots & & S^T & 0 & 0 & \cdots & & R \end{bmatrix} \tag{5.24}$$

$$h = \begin{bmatrix} Td(k)) \\ Td(k+1) \\ \vdots \\ Td(k+N-1) \\ 0 \\ Ud(k) \\ Ud(k+1) \\ \vdots \\ Ud(k+N-1) \end{bmatrix} \tag{5.25}$$

At each sampling time, the future behaviour is predicted over a finite length of prediction horizon using the Kalman predictor. The manipulated input at any instant k, and p is the future manipulated input moves can be denoted as,

$$\Delta u(k_i), \Delta u(ki+1), ..., \Delta u(ki+N_c-1), \tag{5.26}$$

where N_c is the control horizon controlling the number of parameters used to get the future control trajectory.

In a wind turbine environment, the parameters of MPC are roaming around certain specific values. In Anand et al. (2022), Pamososuryo et al. (2022) the parameters such as the sampling time, the prediction horizon, and the control horizon are almost similar.

Note that the papers are on economic MPC.

Based on previous research and publications, MPC was initially widely applied in the below-rated region to control the generator torque to track the maximum power coefficient, C_p. The control parameters in this region are easier to determine and tune. On the other hand, the control tuning parameters for the above-rated region are more complex. A variable speed wind turbine has active pitching activity at above-rated region. During this region, the generator torque is kept constant at $37450Nm$ for a 5MW wind turbine and the pitch demand varies to achieve rated power. This is more complex due to the pitch angle changing rapidly corresponding to the effective wind speed which changes stochastically. As compared to the baseline wind turbine controller with gain-scheduling, MPC can be improved by applying a gain-schedule to control the pitch angle in a more effective manner.

Other than the sampling time, constraints are the most important control parameters for MPC. Constraints represent the bounded limits corresponding to the system. An example, a constraint can be a state constraint or/and input constraint. Constraints also are determined by the controller. A larger number of control parameters will require more optimisation time, The constraints for a wind turbine system are the torque constraints for below-rated and the pitch angle constraints for above-rated wind speed.

A linear MPC is designed to control the wind turbine generator speed at a selected above-rated wind speed. The optimisation design problem at time k is formulated as

$$\min_{\Delta u(k)} J(k) = \sum_{i=1}^{N_P} e(k+i)^T Q e(k+i) + \sum_{i=0}^{N_C-1} \Delta u(k+i)^T R \Delta u(k+i) \tag{5.27}$$

s.t.

$$x(k+1) = Ax(k) + Bu(k)$$

$$u_{\min} \leq u(k) \leq u_{\max}$$

$$\Delta u_{\min} \leq \Delta u(k) \leq \Delta u_{\max}$$

where N_P is the output prediction horizon, N_C is the control horizon, and $N_C < N_P$.

In Equation (5.27), the first term penalizes the tracking error between the reference and the output,

$$e(k) = y(k) - r(k) \tag{5.28}$$

and the second term penalizes the incremental changes in the control input,

$$\Delta u(k) = u(k) - u(k-1) \tag{5.29}$$

Weights Q and R are used to compromise the trade-off between the tracking error and the control cost. The constraints are applied to the control input, $u(k)$, which is the pitch angle, and its changing rate in $\Delta u(k)$. At each time k, the constrained optimisation problem is solved with the quadratic programming (QP) method to give the control sequence over the control horizon N_C, and the first control signal in this sequence is applied to the system (Buijs et al. 2002).

5.5 MPC Simulink Set-up

In Simulink, MPC is designed using the MPC designer and the system input, pitch angle is defined as manipulated variable, MV and the output measurement, generator speed is named measured output, MO. The system is a single input single output (SISO) plant. The sampled time is determined at $0.2s$. The Simulink MPC designer begins to run the default simulation and generates the plots for input response and output response. The closed loop system tracks the desired measured output, however, for a wind turbine system, the output response does not achieve the desired measured output.

Next is the selection of attributes for input and output. The input $u(1)$ is the pitch angle and the output $y(1)$ is the generator speed. The prediction horizon, N_p is specified at 20 and the control horizon, N_C is 2. The configuration of N_p and N_c has effects on the response plots. The next important configuration setting is the constraints. Physically, the control inputs, u, and Δu cannot violate the limits of the pitch actuator. With these concerns, the constraints are bounded subject to the limits

of the pitch actuator and the rate of change limit too.

Then, the MPC can be tuned by determining the weights. The input rate weight, Δu is increased to 0.3 from the default value of 1. Increasing Δu penalises large u changes in the controller optimisation function. The set-up for y is kept at 1.

Simulink has a linearisation feature to linearise a system that generally has a standard input and output. The feature produces the linearisation results in the bode diagram and time response. The output is given in the form of state space representation. The Simulink linearisation tool is applied to a nonlinear model by identifying the desired input and output. In the ATB wind turbine Simulink model, the result is selected to be a single-input-single-output (SISO). The model is linearised at 16 m/s representing the above-rated wind speed where the input is the pitch angle and the output is the generator speed.

5.5.1 MPC design approach for ATB wind turbine

In this project, adaptive MPC is developed for the ATB wind turbine model (Model 2) that was developed in Chapter 4 and it is linearised into state space form. The work starts with MPC and is further advanced with adaptive MPC in 2 steps.

The first step is to apply MPC to the linearized predictive model. The outputs show that the pitch angle is tuned at the range of constraint between -0.3 to 0.3 rad. The generator speed produces significant output to compare with the baseline model. The MPC is tuned using the linearized model and then tested with the nonlinear system. The nonlinear system shows several outputs such as the power production, pitch angle and pitch angle rate.

The second step is to apply adaptive MPC to the system to observe the performance when the input is varied. The results showed that the output is stable for time less than 300 seconds and then it is approaching instability. This shows that the adaptive MPC is sufficient only for a limited time due to the wind turbine model itself. The wind turbine model is a highly nonlinear system and it is linearised to a single input single output system. The linearisation ignores a number of significant parameters from the nonlinear system that affect the actual dynamic of the ATB wind turbine system. In

future work, nonlinear MPC can be proposed to control the nonlinear ATB model.

5.5.2 ATB wind turbine MPC Simulink parameter set-up

The cost function is Simulink is calculated within the MPC toolbox and shows 3 main measurements which are the reference, manipulated variables and measured output. Reference is the model output reference. It can be chosen as the reference value across the prediction horizon by determining each element specifies the reference of the output variable. To preview the references from time $k + 1$ to $k + p$ the references must be connected to a matrix signal with N_y columns and Np rows. Each row contains the references for the 1 N_p step.

The pitch angle reacting to the constant torque is in between -0.3 to 0.3 radian which is equivalent to -17.2 to 17.2 degree. The value is taken from the relationship between partial derivative torque to pitch angle. The value is not far from the pitch angle for the baseline wind turbine.

5.5.3 Adaptive MPC implementation

Adaptive MPC is an enhanced MPC method that can adapt to the changes in input which will affect changes in output. The configuration of adaptive MPC is similar to the linear MPC where the Kalman filter is the standard Kalman filter and the MPC configuration is the same. However, it requires an additional input to the adaptive MPC that represents the important parameters of the controlled model. There are a few methods to apply the adaptive MPC to a linearised system such as by using codes in Matlab or a combination of codes and blocks in Simulink. This thesis opted for the latter. Since the configuration of adaptive MPC is similar to the LMPC, the model is basically tested with LMPC and later uses similar control parameters with additional parameters such as the states and the input from the model.

The model requires inputs as the feedback to the system which has similar parameters only with updated states model. The states updated from the linearised model is connected to the updated model to update and adapt the states to the current event and send the input control to the adaptive MPC controller. In Simulink, an adaptive

controller block is available in the MPC application. However, it also requires the Matlab function to represent the additional updated model.

In wind turbine control, the MPC control approach mostly focuses on torque control. The control input is torque and the output measurement is the generator speed. The weightings only penalized the output measurement, not the input control. Managing the input control for pitch control poses a considerable challenge and adds complexity when dealing with the ATB wind turbine model.

Adaptive MPC is an extended version of the standard MPC. It applies a similar control parameter as MPC with additional features to adapt the system to the controller. The additional feature is the model update feature, which means that the model in the form of state space variables is updated.

The control action u is the pitch angle, β also called the manipulative variable in Simulink. The optimum u is calculated using quadratic programming (QP) over the control horizon, N_c. The output produces a set of u at every N_c and at each N_c, the first control action $u(1)$ is selected as the control action for the round. The next round produces a new set of u and the process continues until the cost function, J is satisfied.

The measured output in the implementation is the generator speed, Ω_g which is also called MO in Simulink. The output, Ω_g is also the feedback to the ATB wind turbine closed loop system. The feedback is compared to the reference speed or the setpoint, Ω_{SET} to result in the error, e which later becomes the parameter formulating the cost function, J. The error, e however, is not weighted since the control action for the system is the input only.

The control input, u is penalised with the weight, R value of 50. The weight for the error is Q and it is defaulted at the value of 1 since the main objective is to control the pitch angle, β. The N_p and N_c are also determined before tuning the other control parameters of the controller. Note that, changing the values of N_p and N_c will affect the performance of the ATB wind turbine system such as the rise time and the overshoot.

Another important parameter in MPC is the constraints. The constraints, subject to the control input, u or pitch angle, β have a lower limit and upper limit. The u and Δu are subject to the limit of the pitch actuator. It is crucial to understand the limits

of the physical control action otherwise, it will not work as planned. The maximum pitch angle for a wind turbine system is 30° of 0.5 rad and the choice of Δu must be lower than u. Since the constraints for the control inputs, u and Δu are subjected to the pitch actuator limits, it is a hard constraint.

The ATB wind turbine system is represented in the state space equation and the state space model is linearised. The system is a single-input-single-output (SISO) with the input of pitch angle and output generator speed. With all the parameters defined, the MPC controller is simulated with the linearised state space model to analyse the output. The parameters are tuned again until the results show the desired output. Then, a properly tuned controller is applied to the nonlinear system and analysed how the nonlinear system reacted to the MPC controller. The results are presented in the following section.

5.5.4 Recursive polynomial model estimator

For online model estimation, the recursive polynomial model estimator (RPME) is used to estimate the discrete time input-output polynomial and time-series model.

The model structure is represented as,

$$A(q)y(t) = B(q)u(t - n_k) + e(k) \tag{5.30}$$

where, q is the time-shift operator, n_k is the input delay, $u(t)$ is the input, $y(t)$ is the output and $e(t)$ is the error. $B(q)$ indicates the number of inputs. This study examines SISO which means $B(q)$ refers to 1 polynomial only. The order of the models represented by the exponent of q as the example below,

$$1 + a_1 q^{-1} + a_2 q^{-2} + ... + a_{na} q^{-na} \tag{5.31}$$

where na is the maximum number of time-shift referring to $A(q)$.

The $B(q)$ polynomial operates on the input and the order nb is the order of the polynomial $B(q) + 1$ as,

$$b_1 + b_2 q^{-1} + b_3 q^{-2} + ... + b_{nb} q^{-(nb-1)} \tag{5.32}$$

The structure is called ARX in Simulink.

The orders na, nb, nc, nd, nf and input delay nk are known ahead of time. In Simulink, the block estimates $A(q), B(q), C(q), D(q), and F(q)$ coefficients

$$\begin{aligned} A(q) =& 1 - 5.1929q^{-1} + 11.6907q^{-2} - 13.7831q^{-3} + 5.3284q^{-4} + 10.4417q^{-5} - 21.5087q^{-6} \\ &+ 18.6811q^{-7} - 5.4271q^{-8} - 6.5529q^{-9} + 9.7678q^{-10} - 6.3698q^{-11} + 2.4005q^{-12} \\ &- 0.5444q^{-13} + 0.0692q^{-14} \end{aligned} \tag{5.33}$$

$$B(q) = 1 \tag{5.34}$$

5.5.5 Adaptive MPC simulation steps

The simulation steps were done in both Matlab and Simulink environments. The first is to build the nonlinear ATB wind turbine model. The model is adopted from the 5MW Supergen model as explained in Chapter 4. The region of interest is the above-rated region where the torque is kept constant at its setpoint of $TQSET = 47350Nm$. The model is simplified into a subsystem with a single input single output. The input is the pitch angle and the output is the generator speed. This Simulink subsystem block is imported to the Matlab workspace for the next step.

Next, the nonlinear model is called in Matlab workspace to create the operating point with *operspec* algorithm. The operating point has the states, input and output information. From this information, the simulation determines the desired states, input and output using *findop* algorithm. Once the desired operating point is satisfied, the model is linearised using *linearise* command. The linearised model is important for the next step which is to discretise the model with selected sampling time. The process flow is depicted in Figure 5.3a.

The linearisation and discretisation process is crucial in developing an MPC con-

troller. Figure 5.3b illustrates the MPC designing process. After the model is linearised and discretised, the plant is converted into a state space model in the standard matrix form of A, B, C and D. The size of the matrices is subjected to the number of states, input and output. For this project, 13 states are selected as shown in Table 4.3 and the system is a SISO system with pitch angle input and generator speed output.

From the state space model, the MPC is designed using the *mpc(plant)* algorithm in Matlab. The MPC design is done simultaneously in Matlab and Simulink. The MPC function in Simulink is available in the MPC apps. For this work, the initial process applied MPC apps and later imported to the Matlab workspace for tuning purposes. The MPC tuning in the Matlab workspace is more reliable compared to the MPC apps. The MPC parameters are imported from Simulink and are tuned in the Matlab workspace until the design is satisfied. This process is applicable for the standard MPC only.

To proceed with the adaptive MPC, RPME is added to the simulation. The RPME takes both input and output from the linearised plant model to convert it into a polynomial automatically in Simulink. The polynomials, Aq and Bq are imported to Matlab. The polynomial Aq and Bq are converted to state space matrices in Simulink using a model type converter block. It converts ARX to SS. ARX is AutoRegressive eXogenous. ARX model assumes that the current system output is a function of the previous system outputs and inputs. The output from ARX to SS gives a set of models that consists of matrix A, B, C, D; input U and output Y; states X and DX. These are the updated models connected with a bus and input to the adaptive MPC with similar control parameters as the standard MPC. The satisfied results are published and plotted in the results section.

The MPC parameters tuning are outlined in Table 5.1.

5.6 MPC Results Validation

The results are presented with a comparison between baseline and adaptive MPC. The results are presented in time series and frequency series. The wind speeds are generated at 16 m/s with 10% turbulent intensity for 6 seeds.

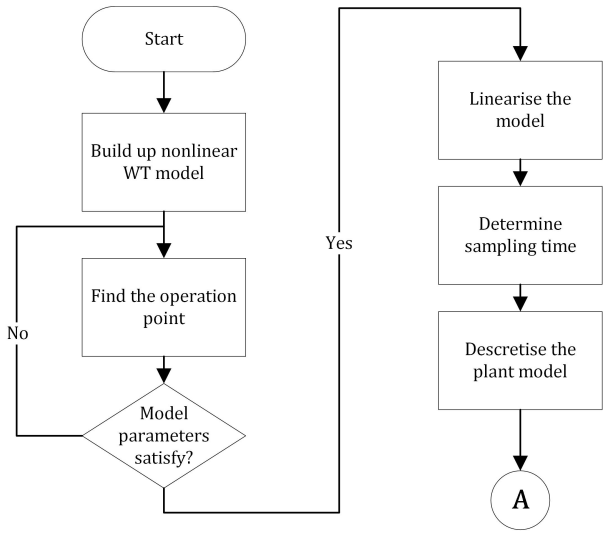

(a) Linearisation and discretisation

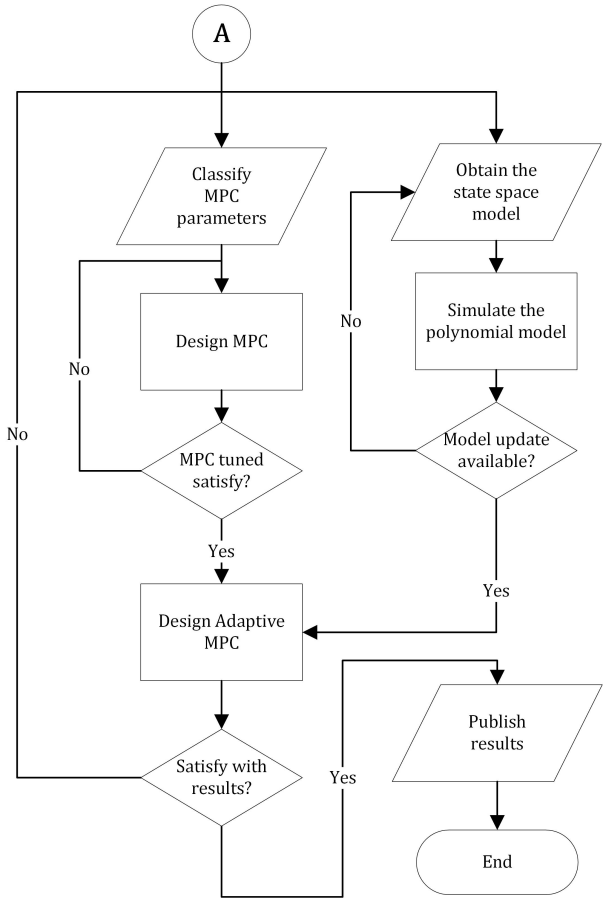

(b) MPC parameterisation

Figure 5.3: Simulation step flowchart

Table 5.1: MPC parameters tuning

Variable Name	Value
Prediction horizon, N_p	20
Control horizon, N_c	2
Sample time, Ts	0.2 s
Constraints	-0.3 $\leq \beta \leq$ 0.3 -0.01 $\leq \dot{\beta} \leq$ 0.01
Weighting	1.8

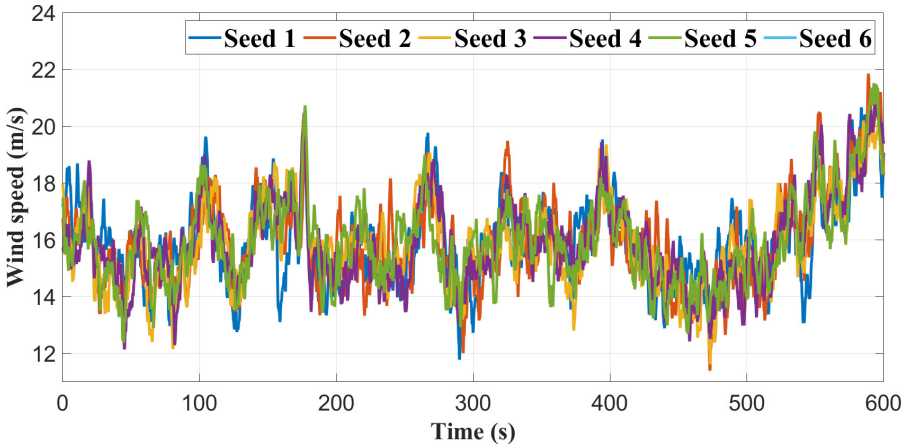

Figure 5.4: 6 seeds wind speed variations

5.6.1 ATB wind turbine performance with MPC

The main objectives of the project are to develop an analytical model of an ATB wind turbine and establish a controller for the model. The model is then analysed to alleviate the loading effect without compromising the power production of the ATB wind turbine system. The simulation applies a 5MW wind turbine system. As shown in Chapter 4, the ATB wind turbine model is not responding to the baseline controller due to the characteristic of ATB that was introduced to the baseline wind turbine model. In order p develop a controller for the ATB wind turbine model, MPC is chosen as the controller for the ATB wind turbine model. One of the advantages is its capability to predict future events by analysing the current event at the sampled time. 5 outputs are presented in this section, pitch angle, output power, measured generator speed, root bending moment and tower acceleration. The results are presented in time series with

a comparison to the baseline model (see Figure 5.5 - 5.9. The outputs are presented according to IEC standards, to perform the results in 10 minute time series.

Figure 5.5 shows the pitch angle output variation of the ATB dynamic model and the baseline model. The pitch angle is the input constraint to the MPC parameter tuning. Based on the baseline pitch angle variations, the constraints for pitch angle are bounded in between -0.3 rad and 0.3 rad. The results show that the pitch angle output follows the constraints as tuned in the MPC. The baseline pitch angle varies from 0.1 rad to 0.32 rad. This is consistent with the pitch angle and wind speed relationship where at 16 m/s the baseline pitch angle is within the range above. Thus, the input constraint is limited in between -0.3 rad and 0.3 rad. The pitch angle response is taking a slower time to reach the upper limit. It increases 0.24 rad within the transient time and falls back to 0.17 rad at $t = 120sec$. The pitch angle rises to the upper limit after $120sec$ and fluctuates within the 0.12 to 0.3 rad range.

The output power results in Figure 5.6 show the comparison of the dynamic ATB wind turbine model with adaptive MPC to the baseline wind turbine model with the baseline controller. The adaptive MPC outputs are aimed to be close to the baseline model output. The output from the adaptive MPC shows stable output but at a much lower power production after $t = 300sec$ compared baseline wind turbine model. Figure 5.7 shows the output of generator speed. The set point of the generator speed is approximately 120 rad/s, and the output from the ATB dynamic model with MPC is much lower than 120 rad/s where it is obviously depicted after a 300-second time series similar to the power. The generator speed outputs are one of the important analyses for the study. In standard equation, the generator speed, Ω_g is proportional to the power production, P with the factor of torque, T,

$$\Omega_g = \frac{P}{T} \tag{5.35}$$

which means, the increase in generator speed is the increase of the power production. However, the analysis of a generator speed is still significant to the work because it represents the characteristics of the wind turbine performance directly.

Figure 5.8 shows the out-of-plane root bending moment (RBM) comparisons. It shows that the RBM variation is lower as compared to the baseline model. A similar trend is shown in Figure 5.9 for tower acceleration fore-aft variation where the ATB dynamic model shows the reduction in acceleration as compared to the baseline model. The tower acceleration measures the tower acceleration at the top of the tower that is connected to the nacelle and the rotor. The tower head is basically holding the load of the system. The proposed blade design of an ATB suggests the load can be alleviated which can reduce the tower acceleration. The results are shown in Figure 5.9 for the time series.

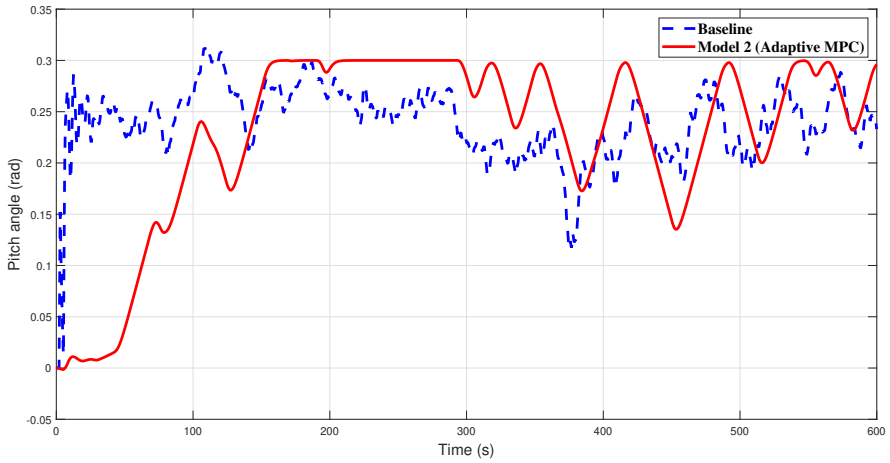

Figure 5.5: Pitch angle comparison between Model 0 and Model 2

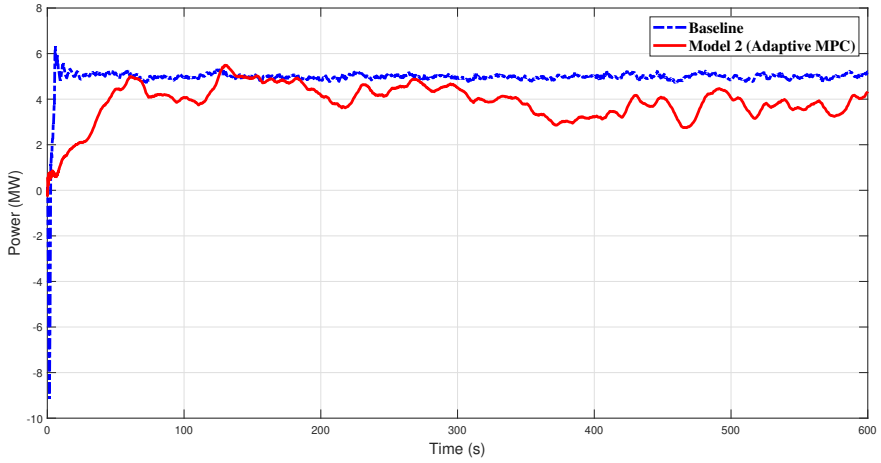

Figure 5.6: Power comparison between Model 0 and Model 2

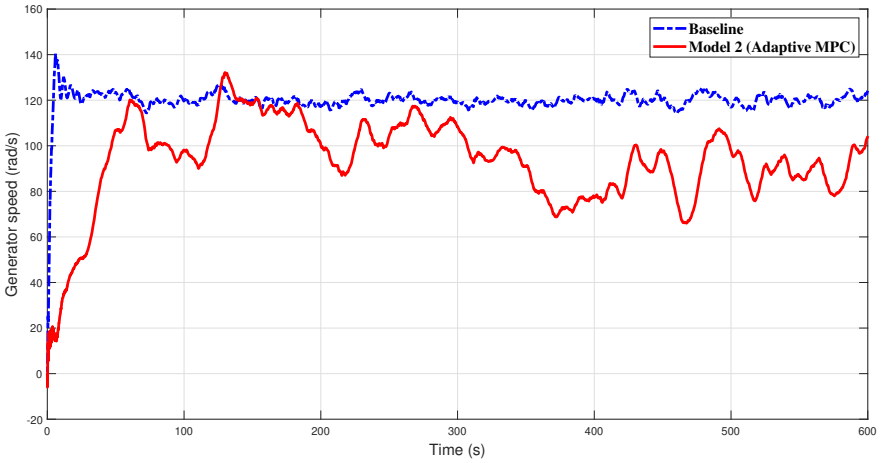

Figure 5.7: Generator speed comparison between Model 0 and Model 2

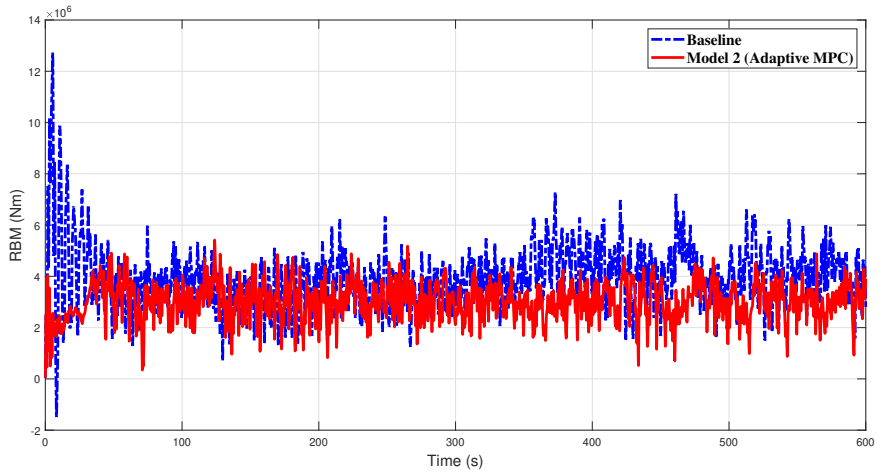

Figure 5.8: Root bending moment comparison between Model 0 and Model 2

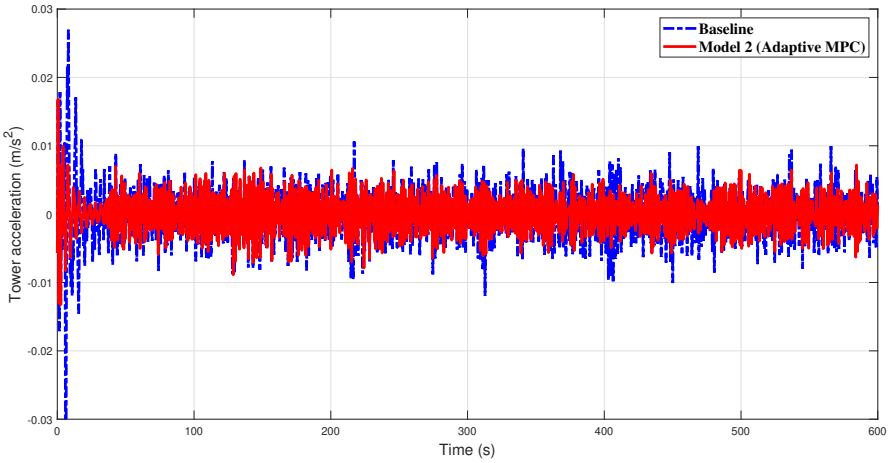

Figure 5.9: Tower acceleration comparison between Model 0 and Model 2

5.6.2 Performance analysis with power spectral density (PSD) and cumulative power spectral density (CPSD)

PSD is a fundamental concept in signal processing and engineering that provides a valuable representation of how the power or energy in a signal is distributed across different frequencies. It is a frequency-domain analysis tool used to analyse the frequency content of a signal. PSD quantifies the distribution of power across various frequency

components. CPSD is a fundamental concept in signal processing and data analysis. It provides valuable insights into the distribution of power across specific frequency bands within a signal or data stream. It offers insightful information about how power is distributed among a signal's or data stream's various frequency ranges. PSD is integrated over a certain frequency range to produce the CPSD, effectively accumulating the energy present in that band.

The PSD and CPSD results for ATB wind adaptive MPC are presented in Figure 5.10 to Figure 5.14. The blue line indicates PSD and the red line indicates CPSD. Figure 5.10 presents PSD and cumulative PSD for pitch angle. No spike is visible in the PSD plot. The results show good outputs where the distributions of PSD over frequencies are smooth. While the CPSD output shows the energy accumulated for the frequency range, it is very low.

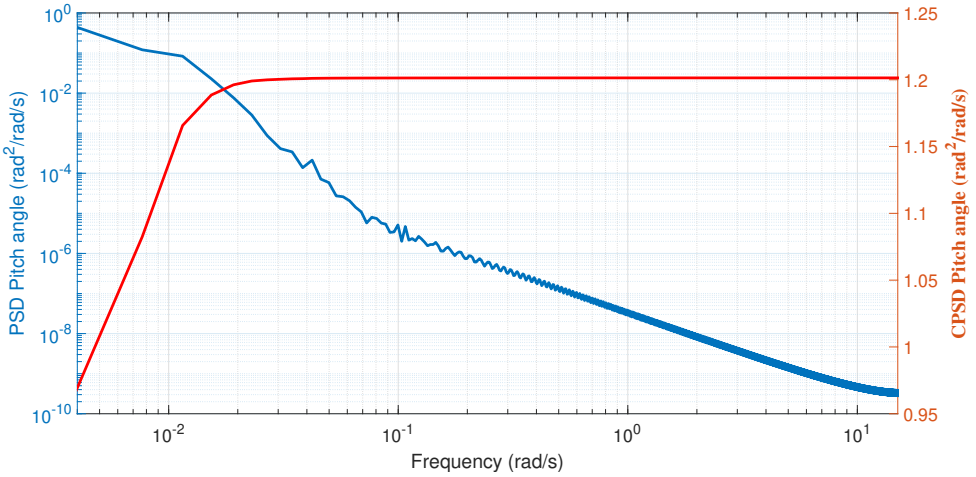

Figure 5.10: PSD (blue) and CPSD (red) plot for Pitch angle

Figure 5.11 shows PSD and cumulative PSD for output power. A spike at approximately 1 rad/s is clearly visible in the plot and it is consistent with the measured generator speed as plotted in Figure 5.12 due to the proportional relationship between output power and measured generator speed. The occurrence of a prominent peak at 1 rad/s PSD in Figure 5.11 and Figure 5.12 is closely tied to the fundamental frequency of the wind turbine's rotor rotation. As wind turbines operate, the rotor blades rotate in response to the wind, and the angular frequency corresponds to the rate of this

rotation. Consequently, this fundamental frequency, often near 1 rad/s, is inherently present in the PSD analysis of the power generation output. This peak represents the primary harmonic component of the turbine's mechanical operation, which provides crucial information about the rotational speed of the turbine. Moreover, harmonics of this fundamental frequency may also appear in the PSD, providing information about the condition and performance of the rotor.

The values on the y-axis represent the power density. It is a measure of the amount of power per unit frequency interval. In essence, it signifies how the power generated by a wind turbine is distributed across different frequency components. The height of the plot at a specific point along the y-axis indicates the concentration of power within a particular frequency band. Higher values on the y-axis denote greater power density, revealing where the wind turbine generates more power within the spectrum of frequencies. The peak around 1 rad/s shows at this frequency the wind turbine is efficient in harnessing wind energy. In contrast, flatter regions on the y-axis indicate lower power density. It can be due to the presence of interference or noise in the wind power signal obviously at higher frequencies.

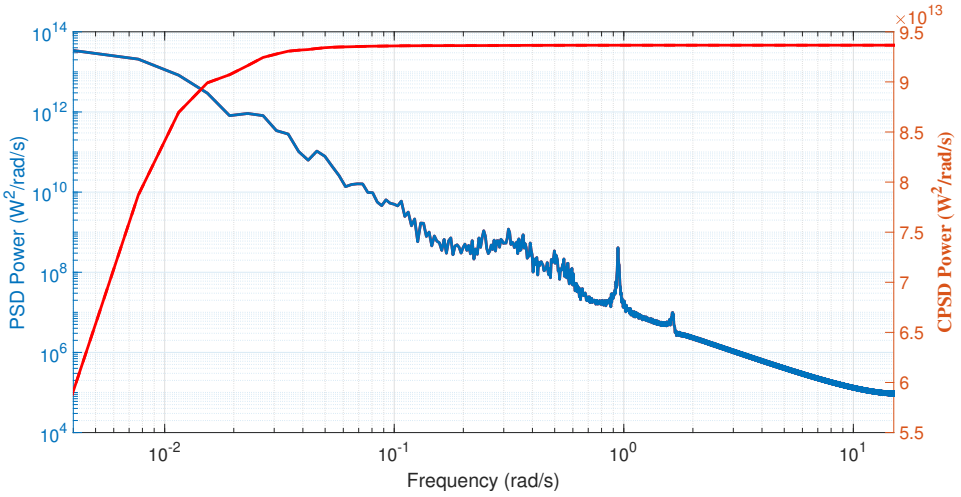

Figure 5.11: PSD (blue) and CPSD (red) plot for power generation

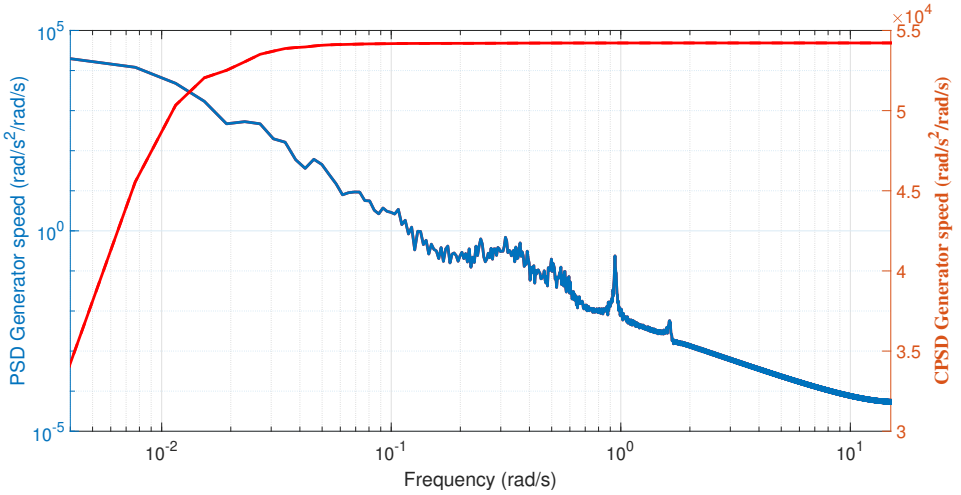

Figure 5.12: PSD (blue) and CPSD (red) plot for generator speed

Figure 5.13 and Figure 5.14 show PSD and cumulative PSD diagram from root bending moment (RBM) and tower acceleration respectively. For Figure 5.13, the PSD distribution is high at low frequencies and from approximately 0.5 rad/s to 1 rad/s shows a decreasing pattern towards high frequencies. It reflects the dynamics of the wind turbine's structural response to varying wind conditions. The high RBM at low frequencies indicates that the blade experiences significant bending moments when subjected to slow and varying wind conditions, such as gusts and turbulence. The low-frequency load can have an impact on the blade's structural integrity. However, the drop in RBM around 1 rad/s is associated with the wind turbine's natural frequency, where the blade's reaction might be less obvious. This behaviour is an indication of frequency control systems or damping effects intended to reduce excessive structural stresses close to the natural frequency, maximizing the performance of the turbine while reducing stress on the blade and the overall turbine structure. The initial low CPSD at low frequencies refers to a limited power contribution at times of low wind speed or reduced wind turbulence. The CPSD rises with frequency, showing an increased power concentration, likely in response to higher wind speeds or gustier conditions. The CPSD levels at high frequencies indicate a constant power distribution across a wide range of frequency components, which is the most interesting observation, nevertheless. This behaviour suggests the wind turbine performs effectively in a range of wind speeds,

capturing energy without being constrained by any particular frequency components. The wind turbine's ability to adapt and be effective in capturing wind energy under a variety of circumstances is highlighted by the flat region in the high-frequency band, making it an important component.

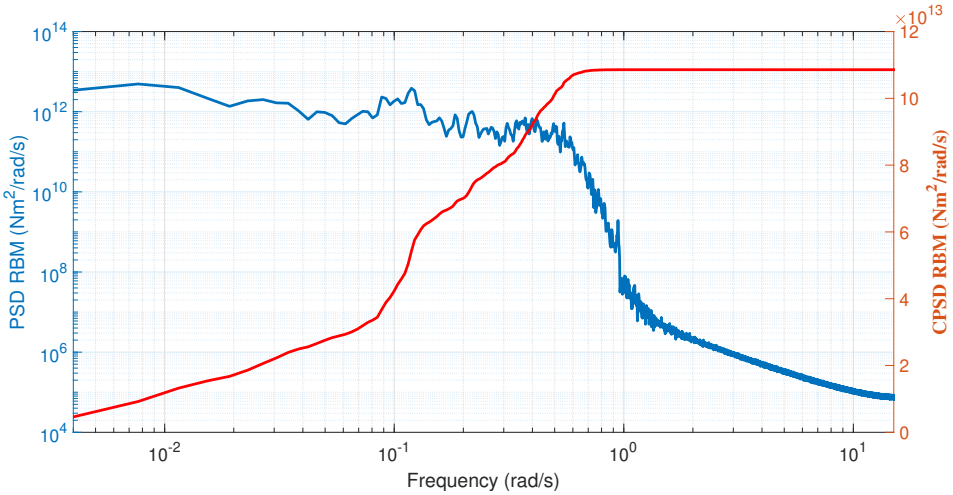

Figure 5.13: PSD (blue) and CPSD (red) plot for root bending moment

The CPSD shows a similar response as RBM except this response is steeper compared to Figure 5.13. The steeper CPSD of about 1 rad/s indicates a significant concentration of power or energy within this frequency range. The trend indicates the signal's dominance of the frequency component around 1 rad/s, which is very important in the context of wind energy. It frequently corresponds to the fundamental rotational frequency of the rotor blades of a wind turbine. The steeper slope indicates that the wind turbine captures and converts wind energy efficiently at or near this frequency, indicating optimal operational circumstances. This resonance at 1 rad/s may also represent the wind turbine's structural dynamics, with its components responding to wind forces most aggressively at this frequency.

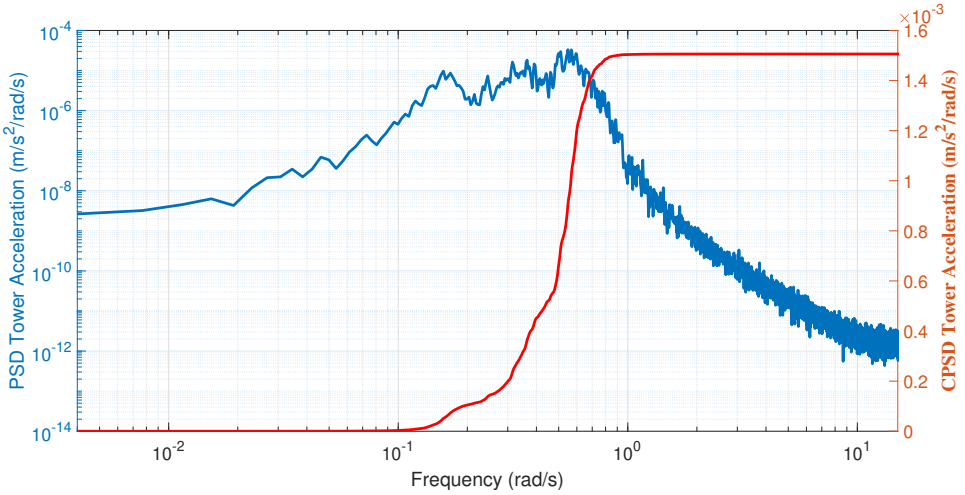

Figure 5.14: PSD (blue) and CPSD (red) plot for tower acceleration

5.6.3 MPC performance with different turbulent intensity

The ATB wind turbine performance over 3 different turbulent intensities of 5%, 10% and 15% is presented in Figure 5.15. The plot follows the IEC standard to run the simulation for 600 seconds for each turbulent intensity. All 3 turbulent intensities for a 16 m/s wind speed apply similar MPC tuning parameters. Figure 5.15 shows the time series results for ATB wind turbine output power. The results show that for 16 m/s to 18 m/s, TI is 5%, TI = 10% and TI = 15%.

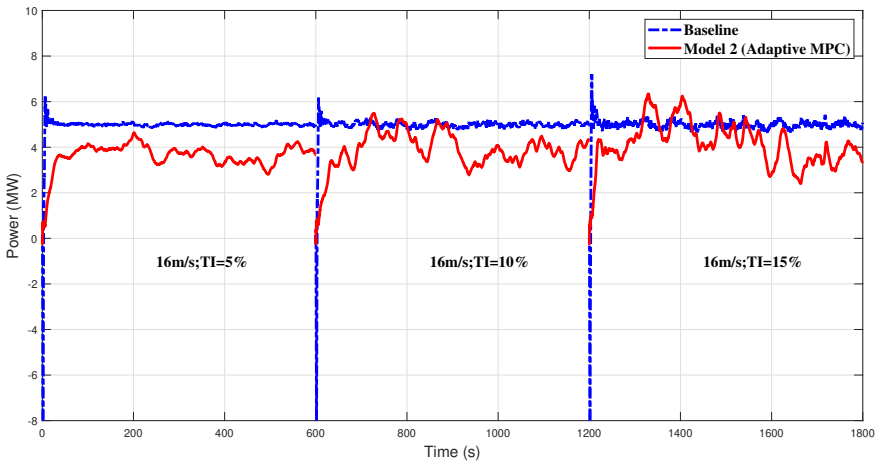

Figure 5.15: Power generation comparison at 16 m/s with TI variations

5.6.4 ATB wind turbine performance in wide range

The performance of an ATB wind turbine with MPC is also analysed for a wide range of wind speeds. Figure 5.16 shows the power production in comparison to the baseline wind turbine with a baseline controller from 16 m/s to 18 m/s. It is understandable that the outputs are not exactly close to the baseline outputs due to the nature of the ATB wind turbine. The outputs, however show significant results and the mean outputs are about the range of the rated power of 5 MW.

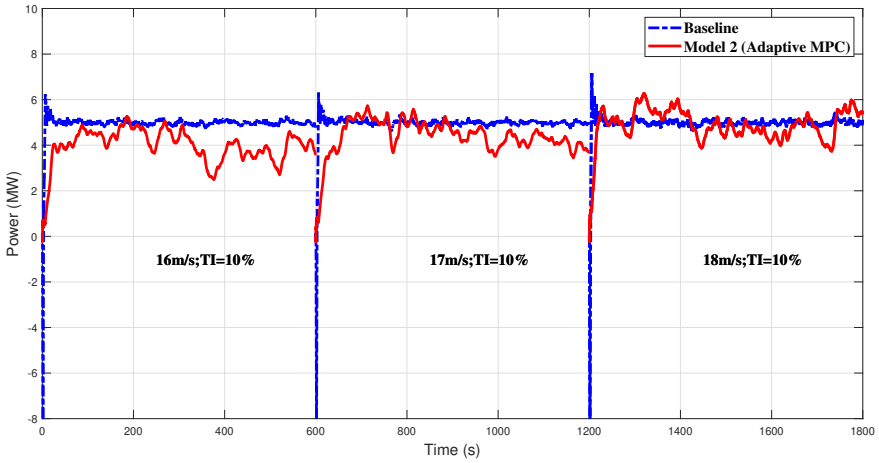

Figure 5.16: Power generation comparison at 10% TI with wind speed variations

5.7 Summary

This chapter details the key parameters for applying adaptive MPC to the ATB wind turbine model. The simulation steps are also presented with the aid of a flow diagram for easy visual understanding. Adaptive MPC is applied to the ATB wind turbine model to validate that the standard MPC tuning parameters are applicable at different wind speeds. The results show 5 outputs of the ATB wind turbine, power, generator speed, pitch angle, tower acceleration and root bending moment, presented in both time series, and PSD plots. Overall, the results for the ATB wind turbine with adaptive MPC are almost close to the baseline wind turbine-baseline controller. The power production is able to reach almost 5MW as compared to the baseline wind turbine-baseline controller.

The ATB wind turbine model employed in this study differs from the baseline wind turbine model. Given the distinct analytical modelling technique used for the ATB wind turbine, evaluating MPC performance within this framework holds significant value. The results indicate satisfactory performance in terms of output power and generator speed, aligning with the benchmark established by the baseline wind turbine equipped with the gain-schedule controller. While these initial outcomes are encouraging, further refinement of the adaptive MPC strategy is warranted to optimize performance in the future.

Chapter 6

ATB Wind Turbine Predictive Control based on Combined Materials Model

This chapter discusses the significance of the aerodynamic effect on a wind turbine blade with composite material design and the performance of the wind turbine system with the gain-scheduling baseline controller (Controller 1) and MPC. The model's performance is evaluated using Controller 1 following similar tuning parameters to verify the feasibility of the design. It is further examined using MPC with a similar control parameter applied in Chapter 5. The results from Chapter 5 (Model 2) and the results from Chapter 6 (Model 3) are compared and assessed to analyse ATB wind turbine models performance. The chapter is outlined as the following; the introduction to the wind turbine model is in Section 6.1, Model 3 simulation with Controller 1 in Section 6.2, MPC simulation implementation including the parameter set-up and adaptive MPC for Model 3, the application of MPC to the model in Section 6.3, results are presented in Section 6.4 and the chapter is summarised in Section 6.5

6.1 5MW wind turbine model with combined materials blade (Model 3)

The ATB models in Chapter 3 and 4 (Model 1 and Model 2) are developed using the analytical modelling approach by introducing the ATB characteristic using BTC theory and embedding spring damper model in it. Chapter 6 discussed another ATB wind turbine model, which is the 5MW wind turbine with blades that are specifically designed with a physical adaptive blade shape and the blade composition layup is built from combined materials. The blade design has an impact on the aerodynamic response of the wind turbine system. The model is developed and validated by a group of researchers from the University of Bristol. This model (Model 3) is a high-fidelity model of an ATB wind turbine model where it is developed and simulated using real value data. Theoretically, the dynamic response of a complete wind turbine structure is experimented with Scott et al. (2020) in which it is a work using simulation tools to demonstrate a 122-meter blade with aeroelastically tailored structure. The blade is optimised and designed with blade twist distribution for maximum annual energy production (AEP) and summarised that the swept blade load is reduced by 2.66% compared to a non-swept mass. It suggests that the ATB load is smaller during operation. A project collaboration by the University of Strathclyde and the University of Bristol reported the reduction of wind turbine fatigue load on a wind turbine with passive adaptive strategies which has a similar interest to a dynamic ATB wind turbine (Recalde-Camacho et al. 2020).

In theory, the changes in the blade structure have an aerodynamic impact on the wind turbine system's performance. The ATB wind turbine with combined materials (Model 3) is developed by the University of Bristol team and the data is shared with the University of Strathclyde control team in GL Bladed for control system development. GL Bladed generated a new power coefficient, C_p value, and the value is applied to the wind turbine Simulink model.

The aeroelastic behaviour is explained in Chapter 2; where a blade structure with the combination of more than 2 materials will change the center of gravity and the

center of axis in the blade chord. However, the theory is valid for a small scale wind turbine with small scale blade. Other factors for an industrial-scale wind turbine are the blade planform size and the blade shape for example the blade design for Model 2 has pre-twist angle to optimise the blade performance.

6.1.1 Power coefficient, C_p analysis on Model 3

Model 3 is simulated using real value data in GL Bladed and new power coefficient, C_p is generated. The power coefficient, C_p for Model 3 has a very minimal difference when it is compared to the baseline wind turbine model (Model 0).

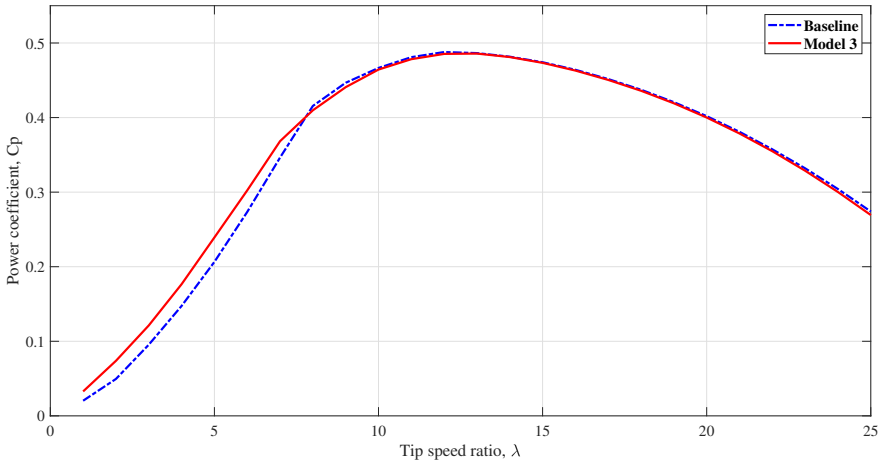

Figure 6.1: Power coefficient, C_p

Figure 6.1 shows the comparison of power coefficient, C_p for a baseline wind turbine model (Model 1) and Model 3 respectively. The power coefficients, C_p for both the baseline wind turbine model and ATB wind turbine model are very close to each other. It also shows the power coefficient, C_p for the baseline wind turbine model (Model 0) is lower than Model 3 for the tip speed ratio, λ range between approximately 1 to 8. For tip speed ratio, λ range between 8 to 20, the power coefficient, C_p for Model 0 is slightly higher than Model 3. The maximum power coefficient, $C_{p_{max}}$ for the Model 0 is 0.4888 and 0.4858 for the Model 3 at the optimum tip speed ratio, λ approximately 11.5. Even though the differences between Model 0 and Model 3 are very small, the

aerodynamic impact on the system is significant and is shown in the results in Section 6.4.

6.1.2 Above-rated analysis for Model 3

The power coefficient, C_p of Model 3 has an immediate impact on the pitch activity of the system. Fundamentally, wind turbine system is divided into 3 regions, below-rated region, the rated region and above-rated region. The relationship between the power coefficient, C_p, tip speed ratio, λ and wind speed, v is given by, wind speed, v.

$$\lambda = \frac{R\Omega}{v} \tag{6.1}$$

where, as wind speed, v increases, λ goes to zero by the factor of radius, R.

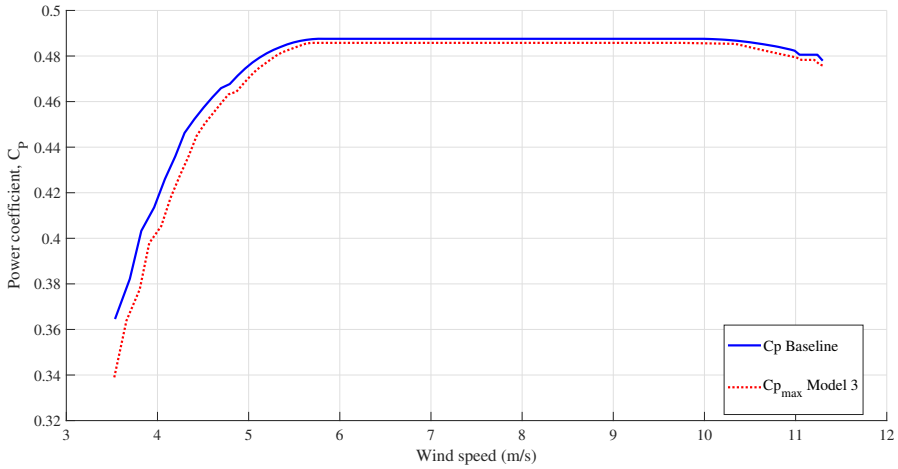

Figure 6.2: Below-rated pitch comparison

Figure 6.2 shows the power coefficient, C_p across the full operating envelope for a given pitch angle, β. As depicted in Figure 6.2, the power coefficient, C_p from 3.5 m/s to approximately 6 m/s for Model 3 is clearly lower than the baseline model (Model 0) for roughly 0.1 difference. At this range, the controller is tracking the power coefficient, C_p and after 6 m/s to 10 m/s, the tracking has reached the maximum power coefficient, C_p. It is also recorded that the maximum power coefficient, Cp for Model 3 is still lower than the baseline model but in much smaller differences. In the below-rated region

where the wind speed is from 4 m/s to 11 m/s, the power coefficient, Cp increases as the wind speed increases and it is limited at the maximum power coefficient, Cp_{max}. At this point, the rotor speed, Ω is varied. The power coefficient, C_p increases from 0.3 to 0.4 from approximately 3.5 m/s to 5 m/s respectively and keeps increasing to the maximum power coefficient, C_p and constant from 5.5 m/s to approximately 11 m/s. It is consistent with the $C_{p_{max}}$ tracking for the below-rated control strategy.

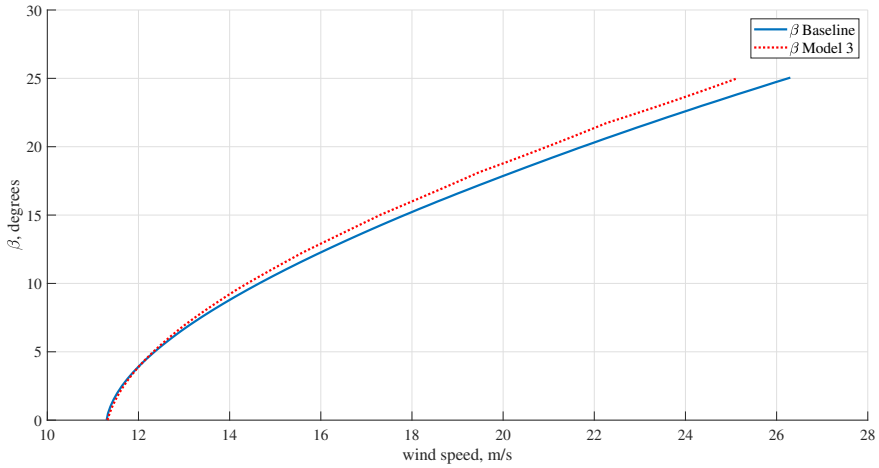

Figure 6.3: Steady pitch comparison

At the above-rated region, the model is evaluated with the similar controller as the baseline model. Above-rated controller applies gain-scheduling to select a single operating point for pitch activity. Figure 6.3 presents the pitch angle at steady state. It shows both models pitch at almost similar wind speeds, at approximately 11.5 m/s but the pitch angle for Model 3 is higher than the baseline model starting from 14 m/s to 25 m/s. At 16 m/s, the pitch angle, β difference is roughly 0.5 degrees. Although the difference is likely insignificant, the impact of less pitching activity is huge on the tower acceleration results.

The pitch angle, β selection for gain-scheduling is at 1. The partial derivative of torque and β is directly proportional to β. Compared to the baseline model, the gradient for the baseline model is larger than the gradient for Model 3.

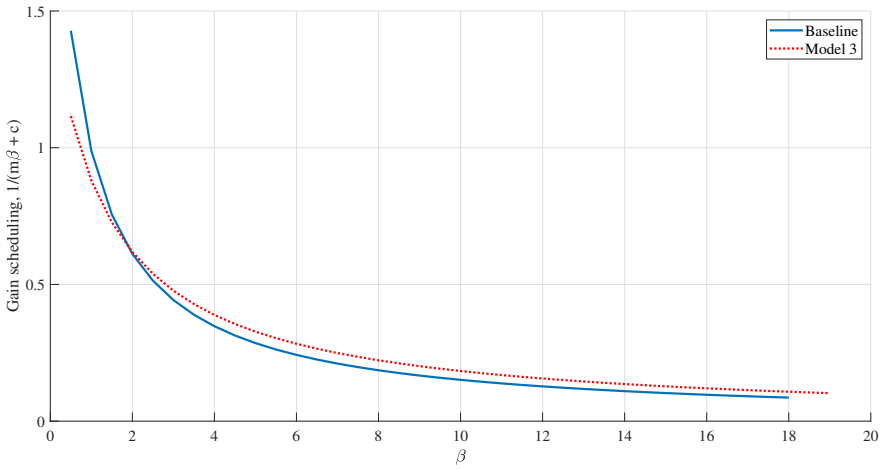

Figure 6.4: Approximation of the partial derivative of torque to pitch

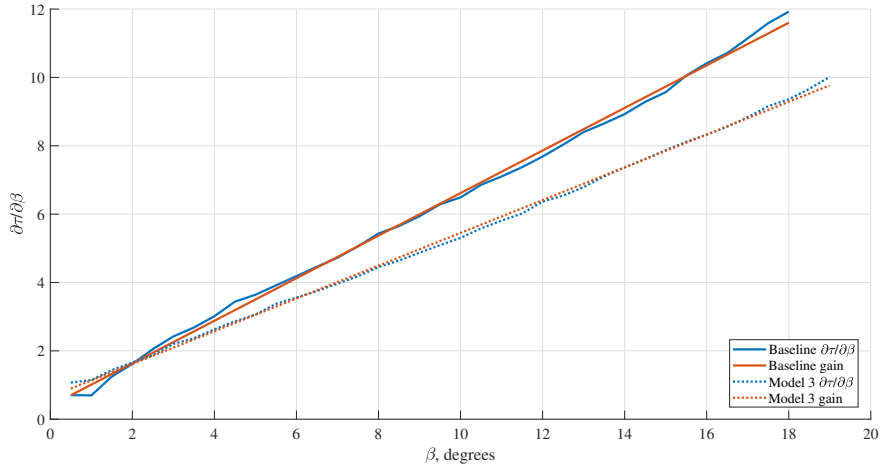

Figure 6.5: $\partial\tau/\partial\beta$ for different β

Figure 6.4 presents the approximation of the partial derivative of torque to pitch angle and Figure 6.5 shows the partial derivatives of torque to pitch angle over the range of pitch angle, β from 0.5 degree to 18 degree for Model 0 and 19 degree for Model 3. The plot of Figure 6.5 is calculated from Figure 6.4 and is approximated to produce a line of $y = mx + c$, where m is the gradient from the fitted line. The models are compared where the obvious difference is Model 3 has a lower gradient as compared to Model 0.

6.2 Model 3 Performance Evaluation with Gain-scheduling Baseline Controller (Controller 1)

Model 3 is initially evaluated by the gain-scheduling baseline controller (Controller 1) where it applies the control strategy adapted from the baseline wind turbine model (Model 0) and Controller 1. Figure 6.6 shows the torque-speed diagram for Model 3. It presents the wind speeds range from 4 m/s to 15 m/s, the rotor speed, Ω from 0.4 rad/s to 1.5 rad/s and the aerodynamic torque from 0 Nm to 9 $\times 10^5$ Nm. The rated power is 5MW and it is described in the green line in Figure 6.6. The power coefficients are plot plotted in the diagram from 96% to Cp_{max}. The blue line indicated the Cp_{max} tracking for below-rated control. The Cp_{max} tracking is to achieve the optimum power in below-rated region that ranges from 4 m/s to approximately 11 m/s. In the below-rated region, the rotor speed is varied with the wind speeds following the $k\Omega^2$ equation where k is the coefficient referring to the torque. The rotor speed, Ω starts to vary from approximately 0.72 rad/s to 12.4 rad/s to track the Cp_{max}. The controller is switched to above above-rated control after $11m/s$. At above-rated region, the gain-schedule technique applies. At the above-rated control, the C_p and the rotor speed, Ω are kept constant and the power generated from the wind turbine is maintained at 5MW as the wind speeds change within the above-rated range.

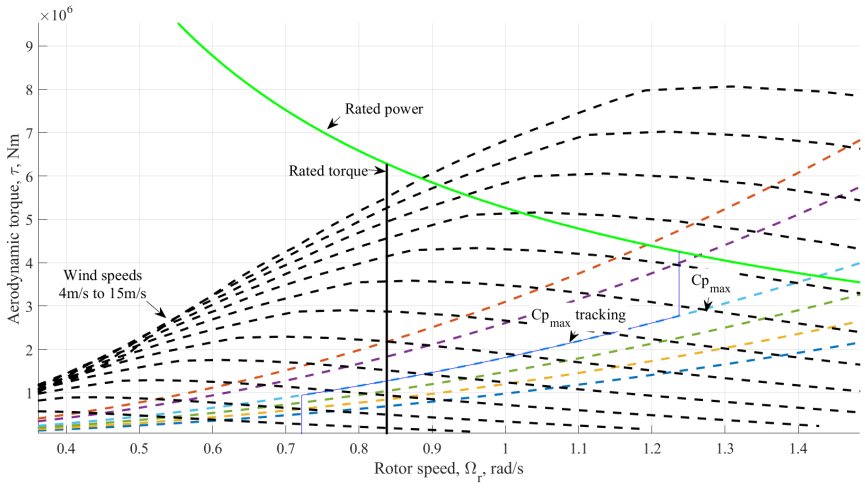

Figure 6.6: Control strategy for Model 3 with Controller 1

Model 3 is developed and examined in GL Bladed, where the new power coefficient, C_p with regards to the new blade design structure is exported to the 5MW Simulink model.

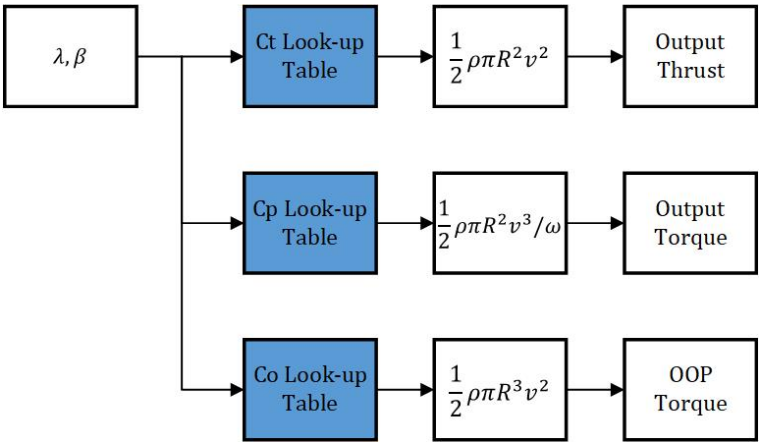

Figure 6.7: New parameters update in Simulink configuration

Figure 6.7 shows the simplified block diagram based on the Simulink model blocks. The input parameters, tip speed ratio, λ and pitch angle, β refer to the aerodynamic input that gives impact to the 3 main coefficients which are the thrust coefficient, C_t, the power coefficient, S_p, and the torque coefficient, C_o. The coefficients are tabulated in a look-up table where the inputs will determine the outputs based on the data in the look-up table. The outputs from look-up tables are multiplied by the coefficients to achieve the outputs as shown in the figure. With the update of the new power coefficient value, C_p also affected the torque coefficient value, C_t and these values need to be updated in the Simulink wind turbine model. The updated values are updated for the aerodynamic block in the Simulink model as shown in the figure of Appendix B.1. The aerodynamics of the Simulink wind turbine model is determined by the values of the power coefficient, C_p and torque coefficient, C_t. These values are selected using the lookup table function in Simulink where the table will select the dedicated power coefficient, C_p value with respect to the selected wind speed and pitch angle, β.

6.3 MPC Simulation Set-up for ATB Wind Turbine

The power coefficient, C_p for Model 3 has a maximum value almost similar to Model 0. As such, Model 3 is tested with the gain-scheduling baseline controller (Controller 1). The results for Model 3 with Controller 1 are compared to Model 0 with Controller 1 as presented in Section 6.1. Based on the results, Figure 6.8 shows the magnified image of Figure 6.3. It can be seen that Model 3 starts to pitch at a slightly higher wind speed and the pitch angle is slightly smaller for Model 3 as compared to Model 0. After 12 m/s, the pitch angle for Model 3 is higher than Model 0 and the difference is wider towards 17 m/s.

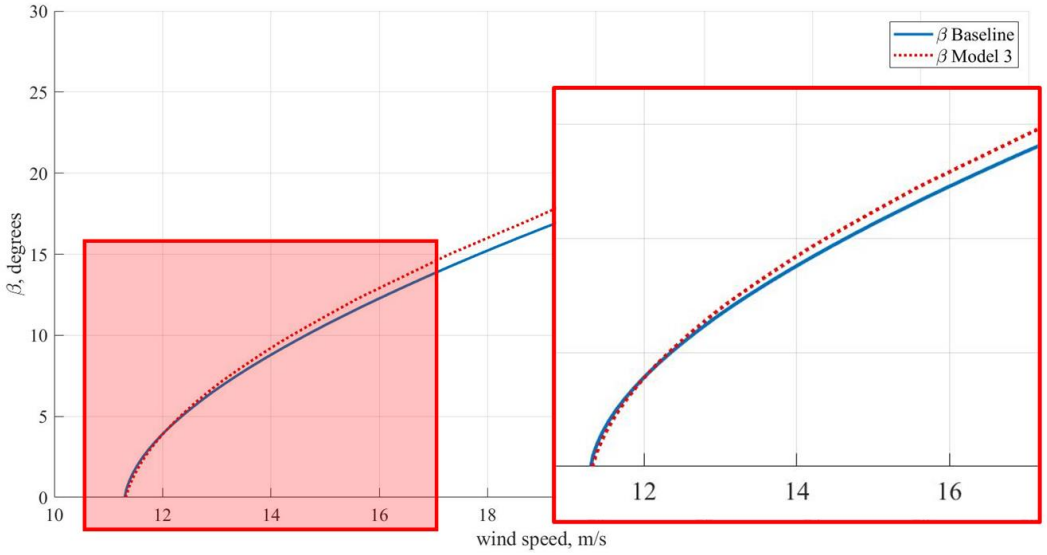

Figure 6.8: Magnified steady pitch comparison

The similarity between Model 0 and Model 3 suggests the same control tuning parameters to control the performance. The performance is evaluated and presented in Figure 6.10 and Figure 6.11. Apart from the gain-scheduling baseline controller (Controller 1), MPC is selected as an alternative controller for the wind turbine model. MPC is discussed in Chapter 5 for Model 2 and the approach is extended to Model 3. The MPC for the ATB wind turbine model for the new blade material in this chapter applies a similar approach as in Chapter 5. This model has a modified power coefficient,

C_p value due to the blade structure and the materials used in the blade.

The steps of applying MPC to the ATB wind turbine with composite materials blade are similar to Section 5.5. The details were presented in Section 5.5 and this chapter will present the results only. The Simulink model with updated power coefficient, C_p, and torque coefficient, C_T is linearised in Matlab as a single input single output (SISO) system. The input is the pitch angle and the output is the generator speed. A standard MPC is applied to the linearised Model 3 and is tuned until it achieves the expected results.

6.3.1 MPC parameter tuning

The control tuning parameters for MPC for Model 3 are given as Table 6.1. The control tuning parameter is similar to the MPC controller for Model 2. The objective function for MPC is to minimise the cost function by penalising the input with weights. The constraints are also crucial in determining the performance of the wind turbine model. The constraint for the ATB wind turbine model is the pitch angle. This is relevant to the selected wind speed of 16 m/s representing the above-rated wind speed. The constraints are limited to -0.3 rad and 0.3 rad and -0.01 rad and 0.01 rad. The prediction horizon is 20 and the control horizon is 2 with a sampling time of 0.2 s. The time taken for the prediction horizon and control horizon is 4 s and 0.4 s respectively. The weighting is 1.1 for the input of the system model.

Table 6.1: MPC tuning parameters for Model 3

MPC parameters	**Values**
Sampling time	0.2 s
Prediction horizon	20
Control horizon	2
Constraints	-0.3 rad $\leq \beta \leq 0.3$ rad -0.01 rad $\leq \dot{\beta} \leq 0.01$ rad
Weightings	1.1

In Chapter 5, Model 2 responds well to the MPC parameters and a similar approach is applied to Model 3. The model is initially linearised to obtain the state space equation

to test with MPC. The output response of Model 3 is feasible and the nonlinear model of Model 3 is evaluated using the same MPC configuration with adjusted parameter tuning.

The state space equation of Model 3 has 13 states that resemble Model 0 except Model 3 has the embedded ATB characteristic in the system. The states' names and descriptions are shown in Table 6.2.

Table 6.2: States and descriptions for Model 3

States	Description	Symbol
x_1	rotor displacement	θ_R
x_2	rotor speed	$\dot{\theta}_R$
x_3	hub speed	Ω_H
x_4	tower displacement ss	θ_T
x_5	tower speed ss	$\dot{\theta}_T$
x_6	rotor displacement oop	ϕ_R
x_7	rotor speed oop	$\dot{\phi}_R$
x_8	tower displacement oop	ϕ_T
x_9	tower speed oop	$\dot{\phi}_T$
x_{12}	equivalent LSS and HSS displacement	θ_s
x_{13}	generator speed	Ω_g

6.3.2 Adaptive MPC for 5MW ATB wind turbine with composite materials blade

The adaptive MPC structure for Model 3 is the same as ATB Model 2 where the input and output from the linearised model are discretised and estimated as a polynomial model using a recursive polynomial model estimator in Simulink. The input of the block requires the polynomial data from the nonlinear plant. The polynomial output from the model estimator is the estimated model which then is updated in the model update block. The model update receives the estimated model and updates the model based on the estimated states. The updated model with the number of states is directed to adaptive MPC. Adaptive MPC is reliable and gives the results as expected even though the inputs are changing by adapting and adjusting accordingly.

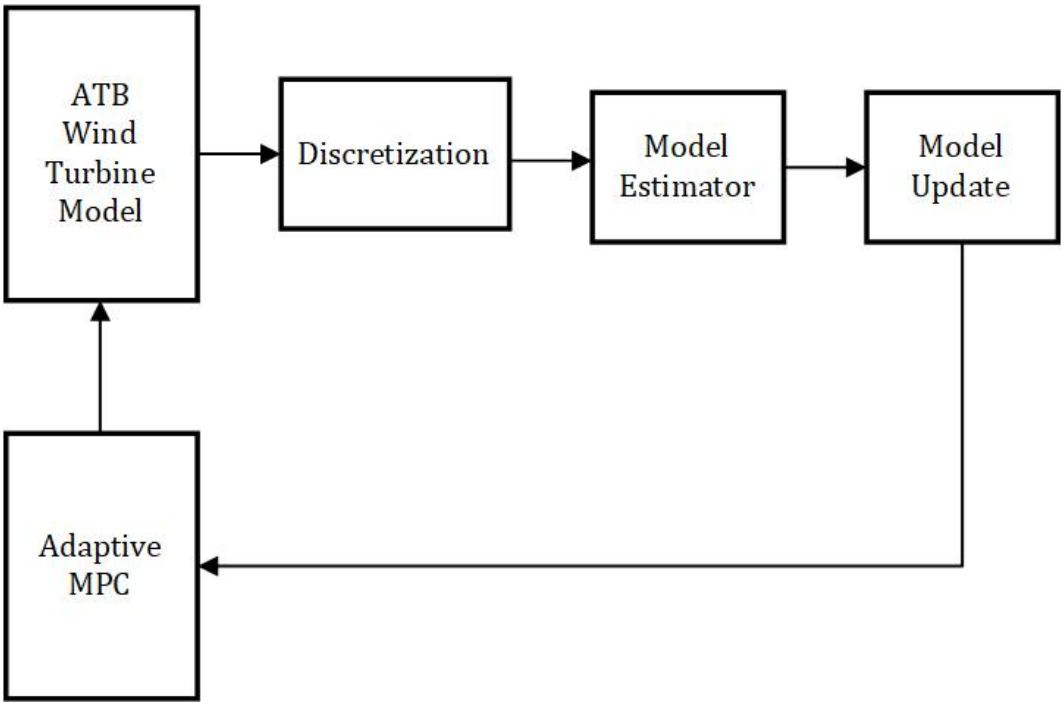

Figure 6.9: Adaptive MPC configuration for Model 3

In particular, the configuration in Figure 6.9 refers to the pitch angle and the generator speed as the input and the output. The selection of input and output for Model 3 is consistent with Model 0 and Model 2 input and output selection in order to compare the performance of the models.

Since Model 3 is very similar to Model 0 based on the power coefficients comparison, the performance of Model 3 with MPC (Controller 2) and the performance of Model 3 with gain-scheduling baseline controller (Controller 1) can be evaluated significantly. The performance of Model 0 and Controller 1 is taken as the benchmark for the evaluation of all models. Basically, Model 0 and Controller 1 are compared to Model 3 and Controller 1 and Model 3 and Controller 2. Also, to conclude the work, the models are compared to Model 2 and Controller 2. This is to highlight the importance of Model 2 as a low fidelity alternative to Model 3, the high fidelity model. Then to explore the feasibility of Controller 2 as an alternative to the established Controller 1.

6.4 Results and Discussions

The outputs show consistency as shown on the power coefficient, C_p output in Figure 6.1 where the difference between Model 0 and Model 3 is very small. The power generation for Model 0 and Model 3 with Controller 1 is compared to observe the similarities and dissimilarities between the 2 models. The power generation also compares Model 3 with MPC (Controller 2) and Model 2 with Controller 2 to analyse the significance of Model 2 as the low fidelity model and Model 3 as high fidelity model performance with MPC.

6.4.1 Model 3 performance evaluation and analysis

The results for Model 0 and Model 3 with Controller 1, and Model 3 with MPC are shown in Figure 6.10 and Figure 6.11. Figure 6.10 shows the power generated performance of Model 0 and Model 3 with a gain-scheduling baseline controller (Controller 1). The purpose of observing the performance of both models is to observe and analyse the performance of Model 3 with the existing controller, Controller 1 before applying MPC as the alternative controller to the model. Based on the figure, the results show a very small difference between Model 0 and Model 3. It satisfies the expected results where the power coefficients between the 2 models are basically almost the same.

Figure 6.10 provides evidence of the close correspondence observed in the results obtained from Model 0 and Model 3 with the utilization of Controller 1. The minor deviations in power coefficients for both models explain the similarity in the outcomes, signifying that the improvement in the wind turbine blades does not compromise the power generated by the system. The comparisons are also presented in Figure 6.11 and Figure 6.12. Although Figure 6.10 shows very limited differences, Figure 6.11 shows a better pitch output response for analysis purposes. From the figure, Model 3 has a higher pitch angle as compared to Model 0. It also shows Model 3 has fewer oscillations at the beginning of the transient response compared to Model 0. The pitch angle for Model 3 is slightly higher than Model 0 due to the blade structure for Model 3 being heavier compared to Model 0. This is consistent with the findings by Capuzzi et al.

(2014*a*).

Figure 6.12 illustrates a clearer difference between Model 0 and Model 3 with controller 1. The tower acceleration in the fore-aft for Model 3 is reduced by approximately more than 50%.

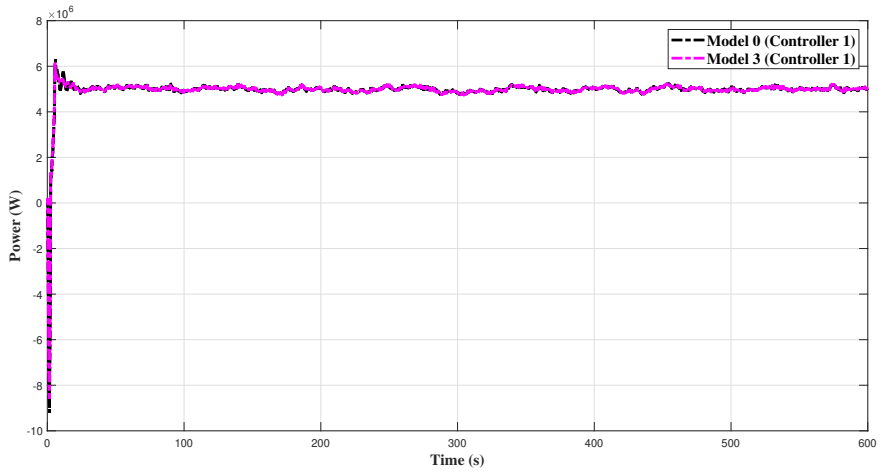

Figure 6.10: Controller 1 for Model 0 and Model 3 power generation comparison

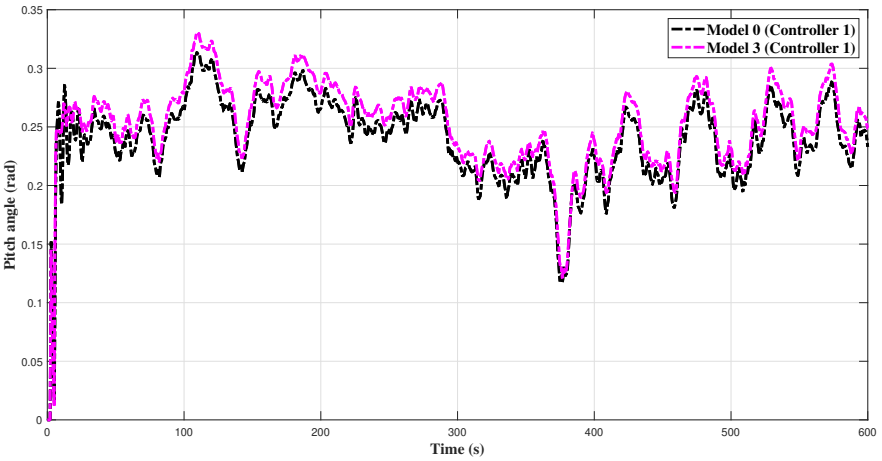

Figure 6.11: Controller 1 for Model 0 and Model 3 pitch angle comparison

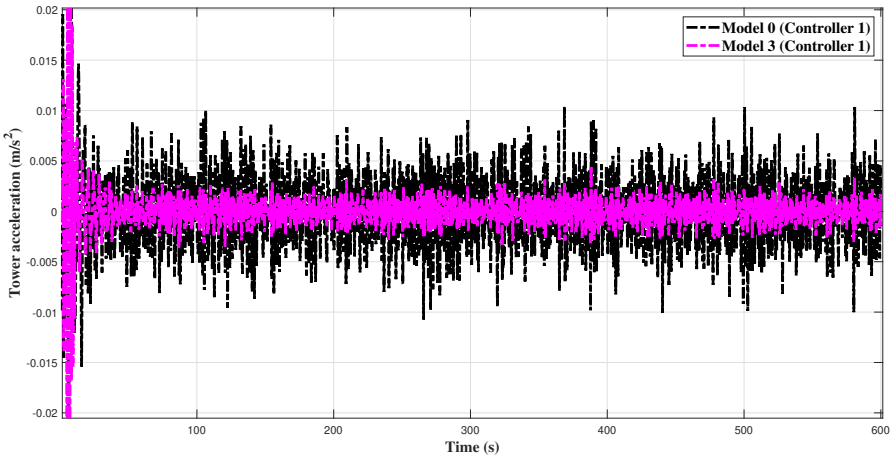

Figure 6.12: Controller 1 for Model 0 and Model 3 tower acceleration comparison

Figure 6.13 presented Model 3 and Model 2 performance with MPC. The 2 models are also compared to Model 3 and Controller 1 as the benchmark. It shows the average power production for MPC Model 2 and Model 3 is approximately 4MW. Although it is less than the rated power, the results are promising for an analytical ATB wind turbine model. Model 3 with Controller 1 obviously outperforms Model 3 with MPC in which Controller 1 is a well established PI controller for wind turbine systems. MPC is suggested as an alternative controller to the existing controller. Although MPC does not perform as good as Controller 1, it is indeed a promising option for controllers in the wind turbine area.

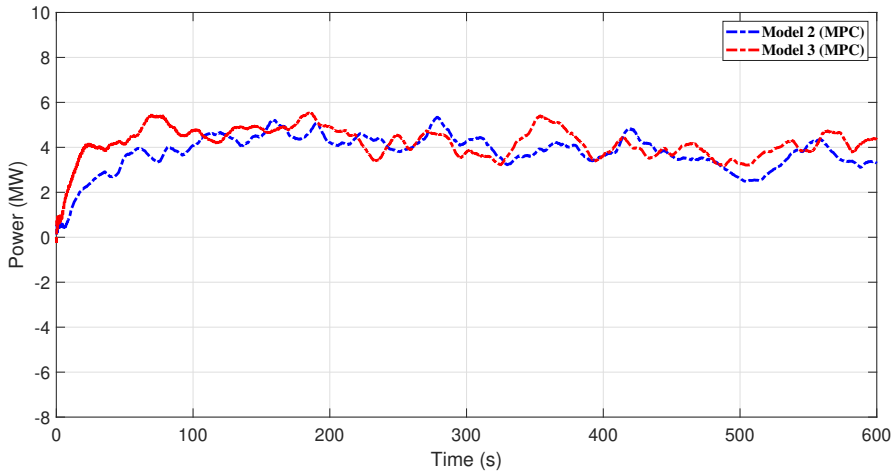

Figure 6.13: MPC for Model 2 and Model 3 power generation comparison

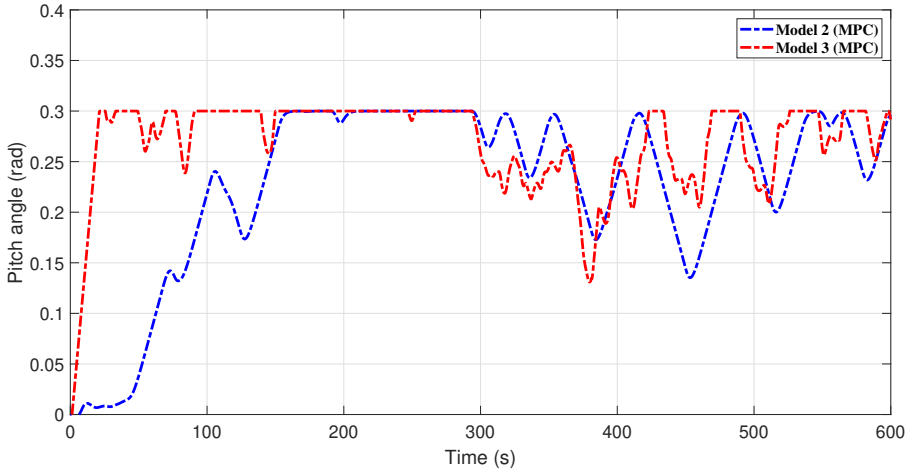

Figure 6.14: MPC for Model 2 and Model 3 pitch angle comparison

The results in Figure 6.14 show the comparison between Model 2 and Model 3 with MPC and Model 3 with Controller 1. Figure 6.14 is translating the MPC constraints where it shows the pitch angle did not violate the constraints. The transient of MPC Model 2 is slower as compared to MPC Model 3. This response has an impact on the output performance of the system such as the power production and the generator speed.

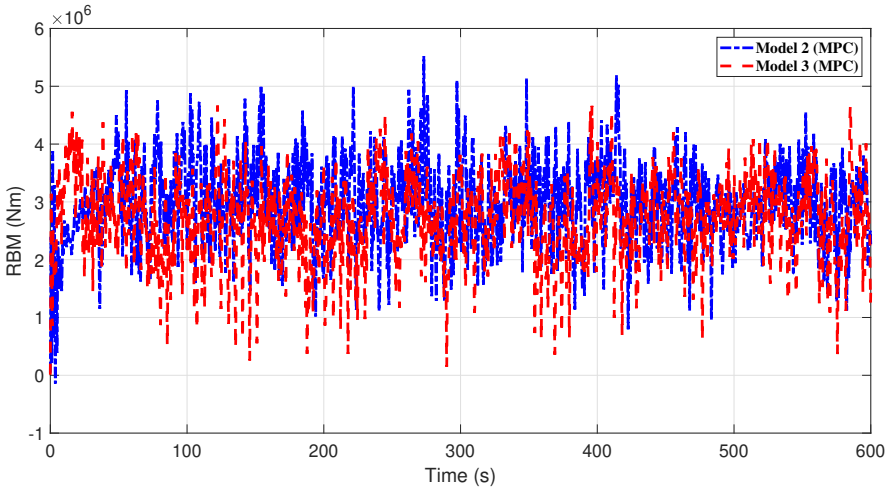

Figure 6.15: MPC for Model 2 and Model 3 RBM comparison

Figure 6.15 is the root bending moment comparison between Model 2 and Model 3 with MPC and Model 3 with Controller 1. The results show Model 2 and Model 3 have a smaller moment as compared to the baseline model.

Figure 6.16 is the comparison of tower acceleration for Model 2 and Model 3 with MPC and Model 3 with Controller 1. The results show the variation for Model 3 is smaller than Model 2 and the baseline model. As compared to all 3 models, Model 2 and Model 3 are smaller than the baseline model.

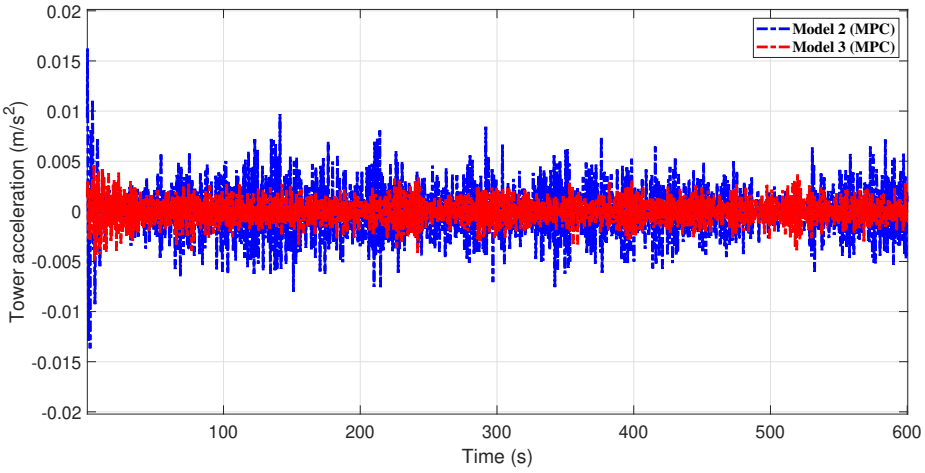

Figure 6.16: MPC for Model 2 and Model 3 tower acceleration comparison

6.4.2 Performance analysis with PSD and CPSD for 16 m/s wind speed

PSD and CPSD for 16 m/s are presented and analysed for 4 outputs which are the power generation, generation speed, root bending moment and tower acceleration. The outputs are depicted from Figure 6.17 to Figure 6.24 respectively to compare Model 2 with MPC and Model 3 with MPC.

As previously discussed in Chapter 5, PSD and CPSD plots are valuable tools for visualising the wind turbine's output responses in the frequency domain, offering insights into the distribution of cumulated energy across different frequencies. The presence of a peak at the natural frequency of 1 rad/s is evident in both Figure 6.17 and Figure 6.19, as previously noted. The analysis in relation to this peak at 1 rad/s remains consistent with the discussions in Chapter 5, where this frequency component is considered significant in the evaluation of the wind turbine's performance, structural dynamics, and response to varying wind conditions.

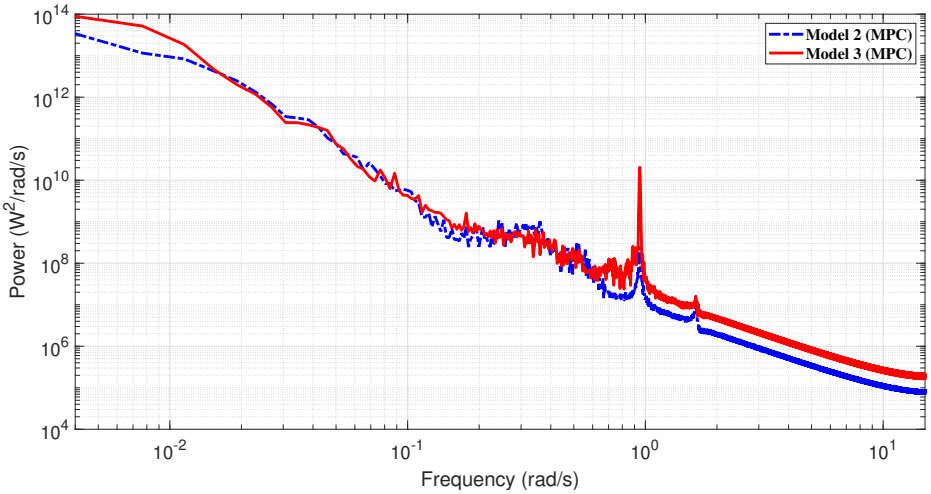

Figure 6.17: PSD for power generation

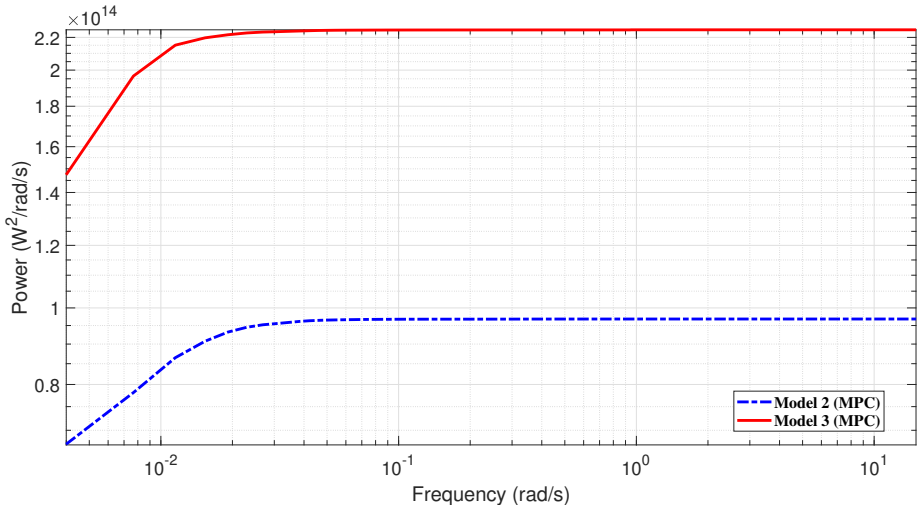

Figure 6.18: CPSD for power generation

The results in the above figures are the power generation output comparison between Model 2 and Model 3 in PSD and CPSD points of view. The results suggest that MPC can be applied to Model 2 and Model 3. However, further fine-tuning is required to achieve better results.

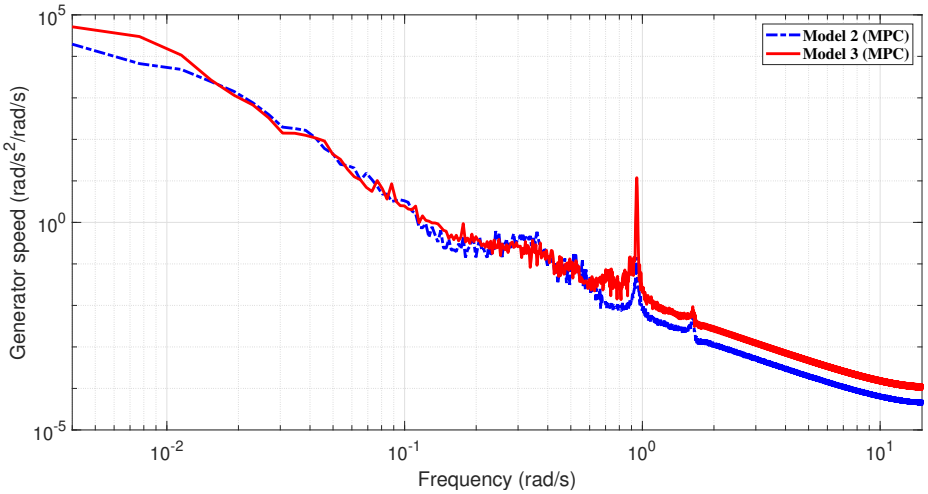

Figure 6.19: PSD for generator speed

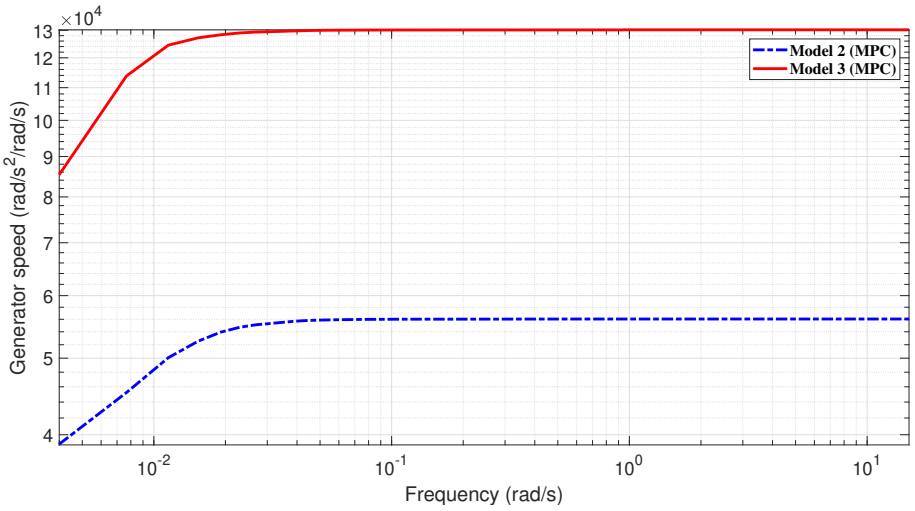

Figure 6.20: CPSD for generator speed

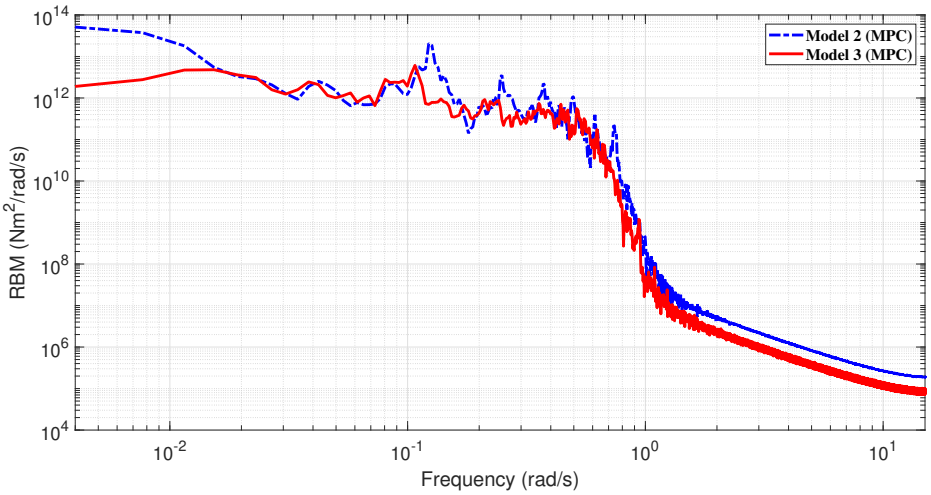

Figure 6.21: PSD for RBM

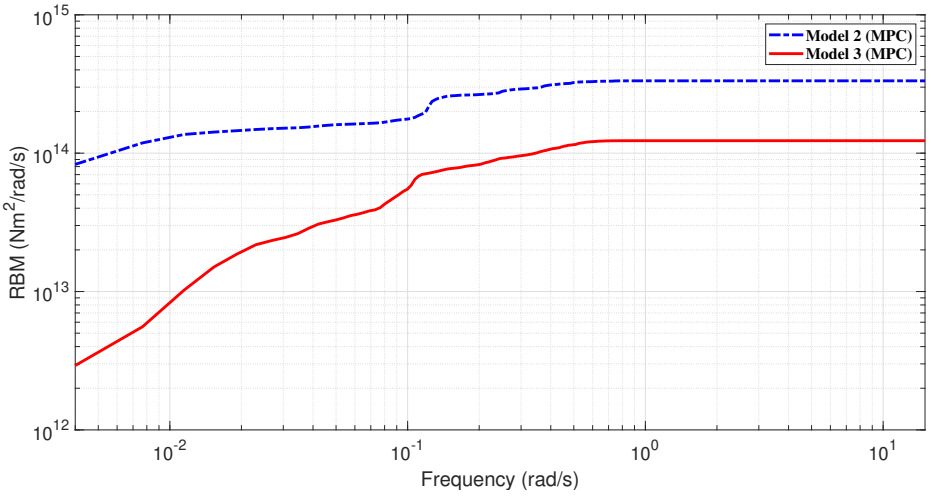

Figure 6.22: CPSD for RBM

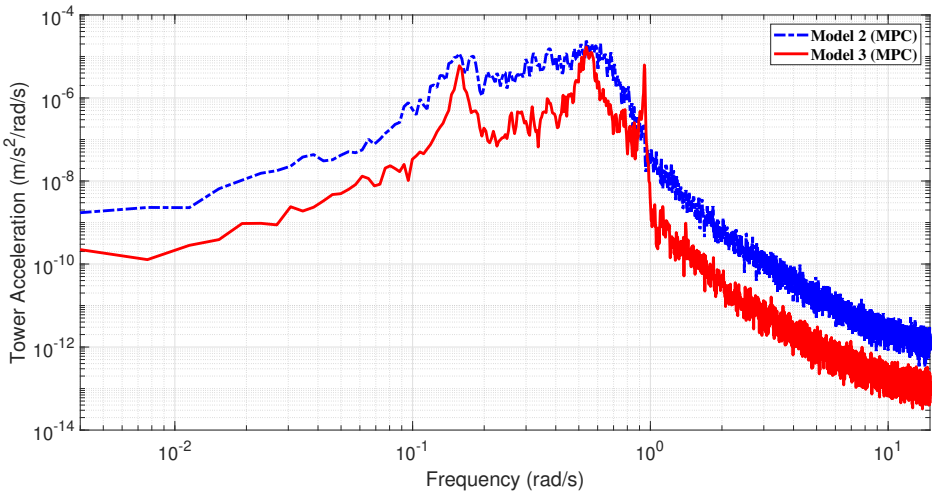

Figure 6.23: PSD for tower acceleration

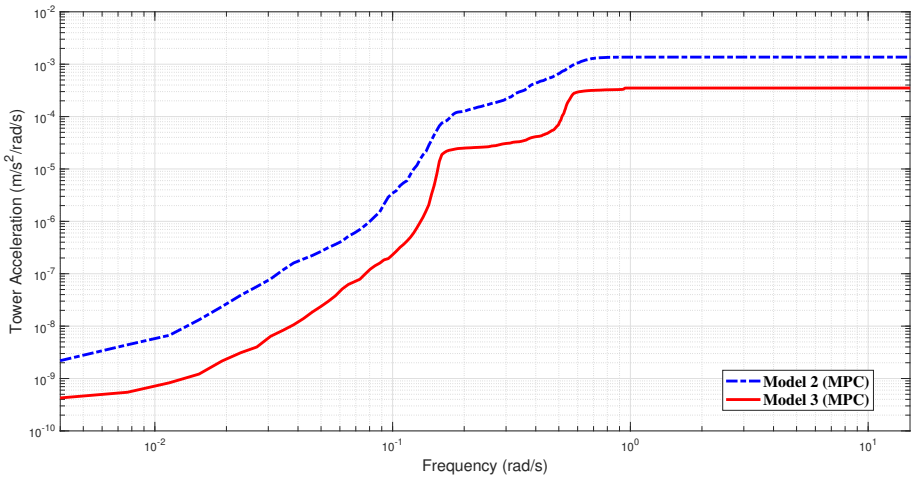

Figure 6.24: CPSD for tower acceleration

Based on the CPSD figures in Figure 6.18, and 6.20, the y-axis values for Model 2 with MPC are lower than Model 3 with MPC. However, Figure 6.22, and 6.24, show otherwise.

6.4.3 Statistical analysis of 4 wind turbine models

The results for pitch angle and power generation are analysed using the box and whisker plot diagram which indicates important information such as the median, the lower median, the upper median, the minimum, and maximum values of the data, and the outliers. Another important value in statistical analysis is the mean and standard deviation where the mean is the average value of the data and the standard deviation is the spread of the data from the mean value. Table 6.3 to Table 6.6 present the data for 3 wind turbine models, Model 2 with MPC, Model 3 with MPC, and Model 3 with Controller 1. However, Figure 6.26 to Figure 6.28 shows the box and whisker data for all 3 models including one additional model, Model 0 with Controller 1 for comparison in visual.

Table 6.3 to Table 6.6 summarise the results into the median, minimum and maximum values for the power generation distribution, pitch angle distribution, root bending moment and the tower acceleration distribution. The power generation results have a

median of 3.95 MW for Model 2 with MPC, 4.28 MW for Model 3 with MPC and 4.98 for Model 3 with Controller 1. The value for Model 2 is low compared to the other 2 models and also lower than the expected 5 MW output. The results for Model 2 are related to the low pitch angle as shown in Table 6.4. The results for power generated are tabulated in Table 6.3. Figure 6.25 illustrates the power generation range for fair understanding.

Table 6.4 shows the median pitch angle is less than 0.3 rad, which are 0.15 rad for Model 2 with MPC, 0.30 for Model 3 with MPC, 0.26 for Model 3 with gain-scheduling baseline controller or Controller 1 and Model 0 of baseline wind turbine model with Controller 1. The *Upper whisker* values for Model 2 and Model 3 with MPC are 0.3 rad due to the system responding to the MPC constraints. The MPC constraint is limited to a maximum of 0.3 rad pitch angle.

The results for RBM and tower acceleration are shown in Table 6.5 and Table 6.6 The median for Model 2 is significantly higher when compared to Model 3 with MPC and Model 3 with controller 1. The median for tower acceleration does not show so much difference as compared to RBM.

Table 6.3: Power data comparison ($\times 10^6$)

Model	Model 2 (MPC)	Model 3 (MPC)	Model 3 (Controller 1)
Minimum	2.47	3.18	4.69
Lower Whisker	2.47	3.18	4.69
First Quartile (Q1)	3.52	3.82	4.98
Median (Q2)	3.95	4.28	4.98
Third Quartile (Q3)	4.36	4.71	5.07
Upper Whisker	5.35	5.56	5.31
Maximum	5.35	5.56	5.31
Numbers of Outliers	0	0	0

Table 6.4: Pitch angle data comparison

Model	Model 2 (MPC)	Model 3 (MPC)	Model 3 (Controller 1)
Minimum	0.10	0.13	0.12
Lower Whisker	0.10	0.17	0.15
First Quartile (Q1)	0.13	0.25	0.23
Median (Q2)	0.15	0.30	0.26
Third Quartile (Q3)	0.18	0.30	0.28
Upper Whisker	0.19	0.30	0.33
Maximum	0.19	0.30	0.33
Numbers of Outliers	0	473	367

Table 6.5: RBM data comparison ($\times 10^6$)

Model	Model 2 (MPC)	Model 3 (MPC)	Model 3 (Controller 1)
Minimum	15.25	0.93	2.29
Lower Whisker	15.25	2.23	2.35
First Quartile (Q1)	23.07	5.10	5.15
Median (Q2)	25.74	6.04	6.12
Third Quartile (Q3)	28.57	7.02	7.02
Upper Whisker	36.82	9.88	9.83
Maximum	40.69	10.37	11.09
Numbers of Outliers	160	91	119

Table 6.6: Tower acceleration data comparison ($\times 10^{-3}$)

Model	Model 2 (MPC)	Model 3 (MPC)	Model 3 (Controller 1)
Minimum	-8	-4	-3
Lower Whisker	-6	-3	-0.7
First Quartile (Q1)	-1.5	-0.6	-0.7
Median (Q2)	0.02	-0.005	-0.01
Third Quartile (Q3)	1.5	0.7	0.7
Upper Whisker	6	2.9	2.9
Maximum	9.9	4	4.5
Numbers of Outliers	283	176	140

Figure 6.25 shows the boxplot diagram and the normal distribution for power generation distributions of 4 wind turbine models. The box for Model 3 and Model 0 with Controller 1 is much thinner compared to Model 2 and Model 3 with MPC. This

indicates the power generation variations for Model 3 and Model 0 with Controller 1 are smaller and can be interpreted as more stable compared to Model 2 and Model 3 with MPC. The median for Model 2 and Model 3 is less than 5 MW and most of the variations appear in the range between 3.5 MW to 4.4 MW. The median for Model 3 with MPC is slightly higher than Model 2 and the variations range between 3.3 MW and 4.7 MW. Although the box or the range for Model 2 and Model 3 with MPC is much larger than Model 3 and Model 0 with Controller 1, the analytical model (Model 2) is comparable to Model 3 which is developed from the laboratory experiments and simulations.

Figure 6.26 shows the pitch angle distribution results for Model 2 with MPC, Model 3 with MPC, Model 3 with Controller 1 and Model 0 with Controller 1. Model 0 with Controller 1 is taken as the standard for comparison. The figure consists of information such as the median, the minimum and maximum values of the pitch angle for different models, and the number of outliers. Outliers refer to the data that does not belong to the box and whiskers which indicate the pitch angle values less than 0.08 rad for Model 2 is too low compared to the 3 other models. Model 3 with MPC and Controller 1 has 473 and 367 outliers which are considered roughly close to each other. However, the median for Model 3 with MPC is very close to the maximum value. The maximum value for Model 2 and Model 3 with MPC is capped at 0.3 rad and it also indicates that upper box values are very close to the maximum values. This is because MPC determines the upper constraints are bound at 0.3 rad.

Figure 6.27 presents the comparisons of root bending moment (RBM) for 4 wind turbine models. From the figure, it is clearly seen Model 3 with MPC and Model 3 with Controller 1 has almost similar box and whisker plot. The medians for all 4 models spread differently and the box for Model 3 (MPC) and Model 3 (Controller 1) is very thin compared to Model 2 and Model 0. The outliers for Model 2 with MPC are all on the upper whisker side whereas Model 2 has more outliers than Model 3 with MPC. Model 3 with MPC and Controller 1, and Model 0 with Controller 1 have outliers on both the upper whisker and lower whisker only Model 3 with Controller 1 has fewer outliers compared to Model 0 with Controller 1. Regardless of the data spreads of all

the wind turbine models, it shows that RBM for Model 2 and Model 3 is reduced as compared to Model 0.

Figure 6.28 presents the comparisons of tower acceleration for 4 wind turbine models. All models have their own sets of outliers where Model 3 with MPC and Controller 1 has the least numbers of outliers compared to Model 2 and Mode 0. Figure 6.28 also shows that Model 2 and Model 3 have the tower accelerations reduced as compared to Model 0.

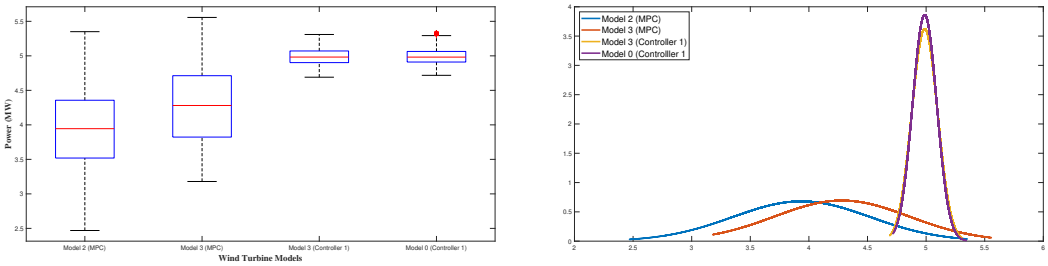

(a) Boxplot (b) Normal distribution

Figure 6.25: Power generation comparison for 4 wind turbine models

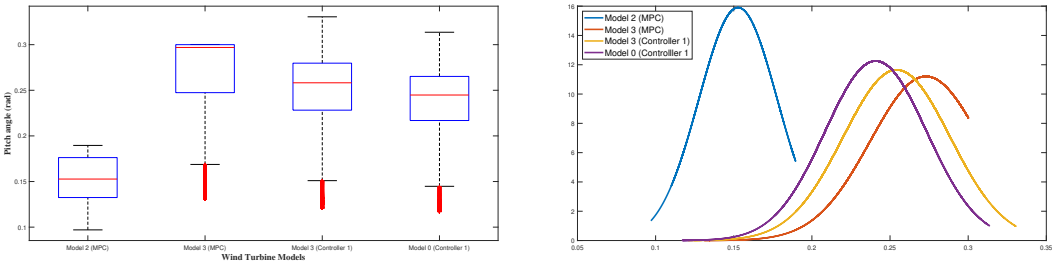

(a) Boxplot (b) Normal distribution

Figure 6.26: Pitch angle comparison for 4 wind turbine models

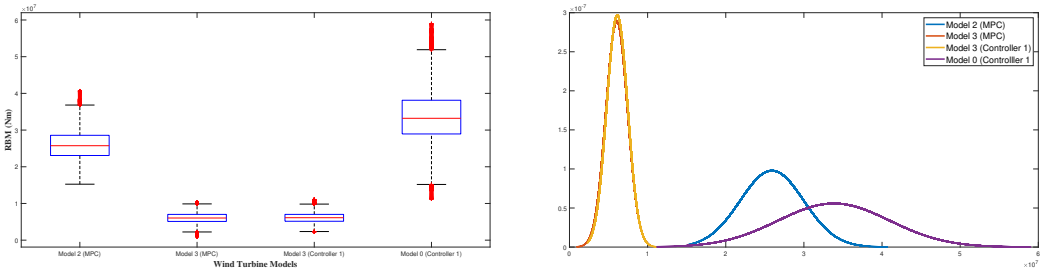

(a) Boxplot (b) Normal distribution

Figure 6.27: RBM comparison for 4 wind turbine models

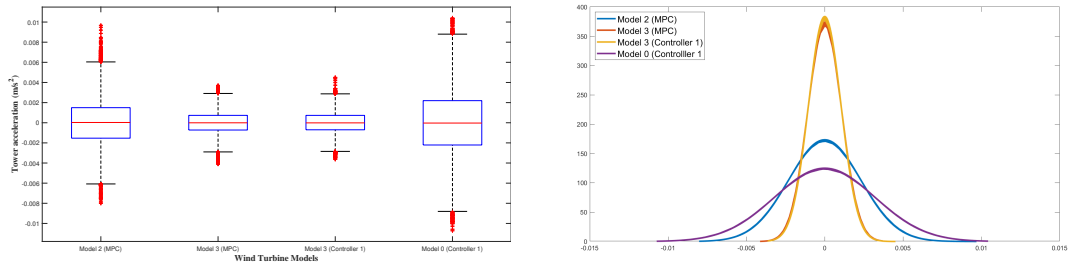

(a) Boxplot (b) Normal distribution

Figure 6.28: Tower acceleration comparison for 4 wind turbine models

6.5 Summary

This chapter presents the analysis of a 5MW wind turbine model with a blade made up of composite materials and aeroelastically tailored performances. The blade is physically tested in a laboratory and the data is shared to be simulated in GL Bladed. The model is referred to as Model 3. As mentioned earlier, GL Bladed is a software that can simulate the wind turbine model with high similarity to the actual wind turbine response. An adaptive MPC is applied to the model (Model 3) and the performance is compared to the ATB wind turbine with a spring damper model (Model 2).

These 2 models are developed using different approaches and both are compared with the same controller, MPC. The results show the comparison of ATB wind turbine Model 2 and Model 3 performance with MPC and Model 3 with gain-scheduling controller (Controller 1). Model 3 is developed physically and the data is simulated to the real world application and is validated by researchers from the University of Bristol. The data of the developed ATB blade model (Model 3) is applied and examined with Controller 1 for control analysis purposes.

Controller 1 is an established wind turbine PI controller and MPC is an alternative controller that has the potential to broaden wind turbine controller options. The results for Model 3 with Controller 1 are comparable to Model 0 with Controller 1 which suggests that Model 3 is feasible for the study. The main difference captured from Model 3 is the power coefficient, C_p is slightly different from the power coefficient, C_p for Model 0. At a glance, it shows very limited contrast between the 2 models. However, looking into its aerodynamic effects on the blade itself, even though the difference is too small, the impact on the wind turbine system performance is big. For instance, Model 3 with Controller 1 pitches around 12 m/s which is later than Model 0 with Controller 1 which pitches around 11 m/s. This scenario causes the loading effect on the wind turbine system to be reduced. Also, note that the blade for Model 3 is not only different in the use of composite materials but also the blade design structure such as the planform design and the pre-twist angle design of the blade.

After Model 3 is validated for its feasibility, an alternative controller which is MPC

is applied to the model. The purpose of examining MPC to Model 3 is to investigate its performance with an alternative controller and compare it to Model 3 with Controller 1 performance. The first attempt is by using the same MPC tuning parameters and observing the performance.

The performance of Model 2 and Model 3 is compared with MPC and also compared with Model 3 and Controller 1 at specifically 16 m/s. The selection of wind speed at 16 m/s is mainly to evaluate the performance of the wind turbine blade at the above-rated region for its pitching activities. Apart from 16 m/s, the ATB wind turbine models are also evaluated at 12 m/s, 14 m/s, 18 m/s, and 20 m/s. Taking into account that MPC is designed specifically at 1 selected wind speed, the output response at all other wind speeds is as expected.

In summary, Model 3 demonstrates effective performance when coupled with MPC and could benefit from enhancements through the integration of MPC with a traditional PI controller like Controller 1. Additionally, Model 2, introduced in Chapter 4, shows comparable performance to Model 3.

Chapter 7

Conclusions and Future Work

7.1 Introduction

The thesis presented research findings of the main aspects concerning the modelling and control of ATB wind turbines. The first phase focused on the reliable implementation of aeroelastic characteristics and structural dynamics in a simulation model. An investigation was conducted into the relationship between the structural dynamics of the wind turbine and the aerodynamics of ATB blades. To achieve this, the study focused on identifying the design factors that have an impact on the behaviour of the system. Furthermore, assumptions were made about the material selection, considering the importance of the aeroelastic characteristics and the effects on the performance of the wind turbine. A simulation model that represents the relationship between aeroelasticity and structural dynamics, providing a foundation for future controller design and analysis was developed.

The following phase in this study focused on comprehending the performance characteristics and challenges encountered during the operation of ATB wind turbines at above-rated region. This involved further exploration of the wind turbines' behaviour under varying wind conditions, specifically when operating in the above-rated region. The study focused on evaluating the effectiveness of the baseline controller when working with the ATB wind turbines. The baseline controller, designed for a full envelope operating range, was evaluated for its adaptability and robustness when the wind tur-

bine operated in the above-rated region. The analysis took into account a range of operational scenarios, exploring the wind turbine response to specific wind speeds, turbulence, and the surroundings. By examining these performance characteristics and challenges, the research aimed to provide an understanding of the limitations of the baseline controller.

The focus of the next phase was to delve into the adaptation of MPC to harness the specific advantages offered by ATB wind turbines. The objective was to predict improvements in comparison to the baseline controller, implying a targeted enhancement in the control strategy. The study aimed to improve performance through the targeted application of MPC. This included developing a control framework that made use of predictive models to forecast future system behaviour and change control inputs accordingly. The study included assumptions about the potential of implementing MPC, such as the availability of data for reliable forecasts, sufficient computer resources to execute complex predictive algorithms, and model integrity to ensure prediction reliability. By exploring these assumptions and adapting MPC to the specific advantages of ATB wind turbines, the study demonstrated the potential of advanced control strategies in optimising wind turbines under a specific operational condition.

The final phase highlighted investigating the comparative responses of the advanced controller when applied to an alternative ATB wind turbine model. It aimed to understand the variations in design parameters that affect the effectiveness of the advanced controller for different wind turbine models. This study considered changes in important design parameters, identifying the impact on the turbine's structural and aerodynamic properties. Furthermore, assumptions were made regarding the structural similarities between the alternative wind turbine models and the developed ATB wind turbine model, allowing for a systematic exploration of the advanced controller's robustness to different wind turbine configurations. By examining these variations and assumptions, the research aimed to provide insights into the controller's performance under diverse conditions and designs. The synthesis of findings from the research questions in phases contributed to a comprehensive understanding of modelling, controlling, and comparing ATB wind turbines. This collective knowledge offered valuable insights

that can advance the field of wind energy research and technology, contributing to the development of more efficient and adaptable wind turbine systems.

7.2 Thesis Contributions

The thesis made substantial contributions to both the modelling and control aspects of ATB wind turbines, aiming to enhance the understanding and performance of these systems. The first contribution involved the development of an industrial-scale static ATB wind turbine model (Model 1). This model was developed to represent the static features, taking into account aeroelastic characteristics, structural dynamics, and important elements such as blade shape and aerodynamics data. Model 1 offered valuable insights into the static characteristics of ATB turbines, providing a foundational framework for subsequent dynamic studies and control system design.

The second contribution extended the modelling efforts with the development of a dynamic ATB wind turbine model using an analytical method (Model 2). This dynamic model attempted to capture the aeroelastic behaviours and reactions of ATB wind turbines. Analytical approaches were employed to simulate the dynamic interactions between the wind, blades, and wind turbine structure. Model 2 was a combination of Model 1 with a spring-damper model. It enriched the understanding of ATB wind turbine dynamic characteristics, providing a more comprehensive representation of the behaviour under varying dynamic conditions.

The third contribution was the development of a composite materials model of ATB wind turbines (Model 3). This advanced model addressed the complexity of material properties associated with ATB construction, incorporating different properties of multiple materials used in ATBs. It offered a more realistic representation compared to simpler models.

The contributions in controller development further enhance the thesis. The development of a baseline controller for ATB wind turbines (Controller 1) established a fundamental control strategy for a full range of wind speeds like pitch control and generator torque. Controller 1 aimed to ensure consistent and efficient performance under varying wind conditions. The subsequent development of MPC for ATB wind turbines

(Controller 2) represented an advanced step in control strategies. By integrating predictive models to optimise control inputs over a specified time horizon, Controller 2 improved its adaptability, load mitigation, and energy capture efficiency compared to the baseline controller. This marked a significant advancement toward more sophisticated and adaptive control approaches, ensuring optimal performance of ATB wind turbines across diverse wind conditions.

In essence, the contributions made in this thesis significantly advance the understanding, modelling, and control strategies for ATB wind turbines, contributing to the broader field of wind energy research and technology.

7.3 Research Impact and Future Works

The study conducted for this thesis has a significant impact on the development of wind energy technology and its incorporation into sustainable energy solutions. The developed static and dynamic models for ATB wind turbines offer a sophisticated understanding of the behaviour, serving as crucial tools for further analysis and design refinement. The implications extend to the broader wind energy community, providing valuable insights for optimising the performance of ATB turbines in real-world scenarios. The developed controllers, which include the baseline and MPC, help establish fundamental and advanced control techniques, providing the method for enhanced and responsive turbine operation. Looking ahead, the future works indicated offer an opportunity for further developments, such as the incorporation of experimental validation, the research of more sophisticated control strategies, and considerations for the integration of ATB turbines into larger energy systems. This comprehensive approach not only promotes academic knowledge but also serves the research as an encouragement for practical implementation and cooperation with industry partners. As the wind energy market grows, the research impact and future activities presented in this thesis highlight its potential to determine the trajectory of ATB wind turbine technology, thereby contributing significantly to the sector.

Bibliography

(n.d.).

Ahlström, A. (2005), Aerolastic simulation of wind turbine dynamics, PhD thesis.

Anand, A., Loew, S. & Bottasso, C. L. (2022), Economic nonlinear model predictive control of fatigue for a hybrid wind-battery generation system, *in* 'Journal of Physics: Conference Series', Vol. 2265, IOP Publishing, p. 032106.
URL: *https://doi.org/10.1088/1742-6596/2265/3/032106*

Asareh, M. A., Schonberg, W. & Volz, J. (2016), 'Fragility analysis of a 5-mw nrel wind turbine considering aero-elastic and seismic interaction using finite element method', *Finite Elements in Analysis and Design* **120**, 57–67.
URL: *https://doi.org/10.1016/j.finel.2016.06.006*

Barbarino, S., Gandhi, F. & Webster, S. D. (2010), Design of extendable chord sections for morphing helicopter rotor blades, *in* 'Smart Materials, Adaptive Structures and Intelligent Systems', Vol. 44168, pp. 323–336.
URL: *https://doi.org/10.1115/SMASIS2010-3668*

Baumgart, A. (2002), 'A mathematical model for wind turbine blades', *Journal of sound and vibration* **251**(1), 1–12.
URL: *https://doi.org/10.1006/jsvi.2001.3806*

Beardsell, A., Collier, W. & Han, T. (2016), 'Effect of linear and non-linear blade modelling techniques on simulated fatigue and extreme loads using bladed', *Journal of Physics: Conference Series* **753**(4), 042002.
URL: *https://doi.org/10.1088/1742-6596/753/4/042002*

Bhattacharya, S. & Adhikari, S. (2011), 'Experimental validation of soil–structure interaction of offshore wind turbines', *Soil Dynamics and Earthquake Engineering* **31**(5-6), 805–816.
URL: *https://doi.org/10.1016/j.soildyn.2011.01.004*

Bichiou, Y., Abdelkefi, A. & Hajj, M. (2014), 'Nonlinear aeroelastic characterization of wind turbine blades', *J. Vib. Contr.* **22**, 621–631.
URL: *https://doi.org/10.1177/1077546314529986*

Bossanyi, E. (2003), 'Wind turbine control for load reduction', *Wind Energy: An International Journal for Progress and Applications in Wind Power Conversion Technology* **6**(3), 229–244.
URL: *https://doi.org/10.1002/we.95*

Bossanyi, E. (2009), 'Gh bladed user manual', *Garrad Hassan Bladed* .

Branner, K., Blasques, J. P. A. A., Kim, T., Fedorov, V., Berring, P., Bitsche, R. & Berggreen, C. (2012), Anisotropic beam model for analysis and design of passive controlled wind turbine blades, Technical report, DTU Wind Energy.
URL: *http://orbit-dtu-dk.cvt.dk/services/downloadRegister/7582390/DTU$_W ind_E nergy_{E0}001_E N.p$*

Buijs, J., Ludlage, J., Van Brempt, W. & De Moor, B. (2002), 'Quadratic programming in model predictive control for large scale systems', *IFAC Proceedings Volumes* **35**(1), 301–306.
URL: *https://doi.org/10.3182/20020721-6-ES-1901.00300*

Burton, T., Sharpe, D., Jenkins, N. & Bossanyo, E. (2001), *Wind Energy Handbook*, John Wiley and Sons.
URL: *http://202.62.79.41:8080/jspui/bitstream/123456789/416/1/170.pdf*

Busarello, T. D. C. & Simões, M. G. (2019), A tutorial on implementing kalman filters with commonly used blocks, *in* 'IECON 2019-45th Annual Conference of the IEEE Industrial Electronics Society', Vol. 1, IEEE, pp. 60–67.

Capuzzi, M., Pirrera, A. & Weaver, P. (2014*a*), 'A novel adaptive blade concept for large-scale wind turbines. part i: Aeroelastic behaviour', *Energy* **73**, 15–24.
URL: *https://doi.org/10.1016/j.energy.2014.06.044*

Capuzzi, M., Pirrera, A. & Weaver, P. (2014*b*), 'A novel adaptive blade concept for large-scale wind turbines. part ii: Structural design and power performance', *Energy* **73**, 25–32.
URL: *https://doi.org/10.1016/j.energy.2014.04.073*

Capuzzi, M., Pirrera, A. & Weaver, P. M. (2015), 'Structural design of a novel aeroelastically tailored wind turbine blade', *Thin-Walled Structures* **95**, 7–15.
URL: *https://doi.org/10.1016/j.tws.2015.06.006*

Chatzopoulos, A.-P. (2011), 'Full envelope wind turbine controller design for power regulation and tower load reduction'.

Collier, W. & Sanz, J. M. (2016), 'Comparison of linear and non-linear blade model predictions in bladed to measurement data from ge 6mw wind turbine', *Journal of Physics: Conference Series* **753**(8), 082004.
URL: *https://doi.org/10.1088/1742-6596/753/8/082004*

Cornette, D., Kerdreux, B., Michon, G. & Gourinat, Y. (2015), 'Aeroelastic tailoring of helicopter blades', *J. Comput. Nonl. Dynamics* **10**, 061001.
URL: *https://doi.org/10.1115/1.4027717*

Diaconu, C. G., Weaver, P. M. & Mattioni, F. (2008), 'Concepts for morphing airfoil sections using bi-stable laminated composite structures', *Thin-Walled Structures* **46**, 689–701.
URL: *https://doi.org/10.1016/j.tws.2007.11.002*

Ding, F., Kareem, A. & Wan, J. (2019), 'Aerodynamic tailoring of structures using computational fluid dynamics', *Structural Engineering International* **29**(1), 26–39.

Dittmer, A., Sharan, B. & Werner, H. (2021), A velocity quasilpv-mpc algorithm for wind turbine control, *in* '2021 European Control Conference (ECC)', IEEE, pp. 1550–

1555.
URL: *https://doi.org/10.23919/ECC54610.2021.9654878*

Dwyer, S. & Teske, S. (2018), Renewables 2017 global status report, Technical report.

Dyrska, R., Mitze, R. & Mönnigmann, M. (2021), Regional control laws as fallback strategy for nonlinear mpc: Application to wind turbine control, *in* '2021 European Control Conference (ECC)', IEEE, pp. 1531–1536.
URL: *https://doi.org/10.23919/ECC54610.2021.9655046*

Fedorov, V., Berggreen, C., Krenk, S. & Branner, K. (2012), 'Bend-twist coupling effects in wind turbine blades', *Dis-473 sertation, Technical University of Denmark* **474**.
URL: *https://core.ac.uk/download/pdf/13803642.pdf*

Gala Santos, M. L. (2018), 'Aerodynamics and wind-field models for wind turbine control'.
URL: *https://doi.org/10.48730/94sz-1f50*

Ganeriwala, S. N., Kanakasabai, V. & Richardson, M. (2011), Modes indicate cracks in wind turbine blades, *in* 'Rotating Machinery, Structural Health Monitoring, Shock and Vibration, Volume 5', Springer, pp. 509–513.

Gros, S. & Schild, A. (2017), 'Real-time economic nonlinear model predictive control for wind turbine control', *International Journal of Control* **90**(12), 2799–2812.
URL: *https://doi.org/10.1080/00207179.2016.1266514*

Hassena, M. B., Najar, F., Aydi, B., Choura, S. & Ghorbel, F. (2013), 'A new dynamical model of flexible cracked wind turbines for health monitoring', *Journal of Dynamic Systems, Measurement, and Control* **135**(3), 031013.
URL: *https://doi.org/10.1115/1.4023210*

Hayat, K., de Lecea, A. G. M., Moriones, C. D. & Ha, S. K. (2016), 'Flutter performance of bend twist coupled large scale wind turbine blades', *Journal of Sound and*

Vibration **370**, 149–162.
URL: *https://doi.org/10.1016/j.jsv.2016.01.032*

Hodges, D. H. & Pierce, G. A. (2011), *Introduction to structural dynamics and aeroelasticity*, Vol. 15, cambridge university press.

Holierhoek, J. G. (2013b), 'An overview of possible aeroelastic instabilities for wind turbine blades', *Wind Eng.* **37**, 421–440.
URL: *https://doi.org/10.1260/0309-524X.37.4.421*

Horner, M., Pakzad, S. N. & Gulgec, N. S. (2019), 'Parameter estimation of autoregressive-exogenous and autoregressive models subject to missing data using expectation maximization', *Frontiers in Built Environment* p. 109.
URL: *https://doi.org/10.3389/fbuil.2019.00109*

Hughes, T. J. (2012), *The finite element method: linear static and dynamic finite element analysis*, Courier Corporation.
URL: *https://www.academia.edu/7872259/The$_f$inite$_e$lement$_m$ethod$_l$inear$_s$tatic$_a$nd$_d$ynamic$_f$inite*

Ivan Komusanac, Guy Brindley, D. F. L. R. R. O. et al. (2022), 'Wind energy in europe: 2021 statistics and the outlook for 2022–2026', *Wind Europe Report: Brussels, Belgium* .

Jain, A., Schildbach, G., Fagiano, L. & Morari, M. (2015), 'On the design and tuning of linear model predictive control for wind turbines', *Renewable Energy* **80**, 664–673.
URL: *https://doi.org/10.1016/j.renene.2015.02.057*

Jamieson, P., Leithead, W. & Gala Santos, M. (2011), 'The aerodynamic basis of a torque separability property', *Proceedings of EWEA* .

Jawad, R., Ahmed, M., Salih, H. M. & Mahmood, Y. A. (2022), 'Variable speed controller of wind generation system using model predictive control and narma controller'.
URL: *https://doi.org/10.37917/ijeee.18.2.6*

Koerber, A. & King, R. (2013), 'Combined feedback-feedforward control of wind turbines using state-constrained model predictive control', *IEEE Transactions on Control Systems Technology* **21**(4), 1117–1128.
URL: *https://doi.org/10.1109/TCST.2013.2260749*

Kong, C., Bang, J. & Sugiyama, Y. (2005), 'Structural investigation of composite wind turbine blade considering various load cases and fatigue life', *Energy* **30**(11-12), 2101–2114.
URL: *https://doi.org/10.1016/j.energy.2004.08.016*

Kumar, Y., Ringenberg, J., Depuru, S. S., Devabhaktuni, V. K., Lee, J. W., Nikolaidis, E., Andersen, B. & Afjeh, A. (2016), 'Wind energy: Trends and enabling technologies', *Renewable and Sustainable Energy Reviews* **53**, 209–224.
URL: *https://doi.org/10.1016/j.rser.2015.07.200*

Lachenal, X., Daynes, S. & Weaver, P. M. (2013), 'Review of morphing concepts and materials for wind turbine blade applications', *Wind Energy* **16**, 283–307.
URL: *https://doi.org/10.1002/we.531*

Lago, L. I., Ponta, F. L. & Otero, A. D. (2013), 'Analysis of alternative adaptive geometrical configurations for the nrel-5 mw wind turbine blade', *Renewable Energy* **59**, 13–22.
URL: *https://doi.org/10.1016/j.renene.2013.03.007*

Leith, D. & Leithead, W. (1997), 'Implementation of wind turbine controllers', *International Journal of Control* **66**(3), 349–380.

Leithead, W. & Connor, B. (2000), 'Control of variable speed wind turbines: Design task', *International Journal of Control* **73**(13), 1189–1212.
URL: *https://doi.org/10.1080/002071700417849*

Leithead, W., De La Salle, S., Reardon, D. & Grimble, M. (1991), Wind turbine modelling and control, *in* 'International Conference on Control 1991. Control'91', IET, pp. 1–6.

Leithead, W. E. & Rogers, M. (1996a), 'Drive-train characteristics of constant speed hawt's: Part i - representation by simple dynamic models', *Wind Eng.* **20**, 149–174.

Leithead, W. E. & Rogers, M. (1996b), 'Drive-train characteristics of constant speed hawt's: Part ii - representation by simple dynamic models', *Wind Eng.* **20**, 175–201.

Leithead, W., Rogers, M. & Agius, R. (1992), 'Dynamic analysis of the compliant tip', *Report prepared for the Department of Energy (ETSU), University of Strathclyde, UK Government* .

Leithead, W., Rogers, M., Leith, D. & Connor, B. (1995), Design of wind turbine controllers, *in* 'Proceedings of EURACO Workshop 'Recent Results in Robust & Adaptive Control', Florence'.

Leu, T.-S., Yo, J.-M., Tsai, Y.-T., Miau, J.-J., Wang, T.-C. & Tseng, C.-C. (2014), Assessment of iec 61400-1 normal turbulence model for wind conditions in taiwan west coast areas, *in* 'International Journal of Modern Physics: Conference Series', Vol. 34, World Scientific, p. 1460382.

Li, C., Hu, J., Yu, J., Xue, J., Yang, R., Fu, Y. & Sun, B. (2021), 'A review on the application of the mpc technology in wind power control of wind farms', *Journal of Energy and Power Technology* **3**(3), 1–1.
URL: *http://dx.doi.org/10.21926/jept.2103033*

Li, D., Gong, C., Da Ronch, A., Chen, G. & Li, Y. (2019), 'An efficient implementation of aeroelastic tailoring based on efficient computational fluid dynamics-based reduced order model', *Journal of Fluids and Structures* **84**, 182–198.

Li, L., Li, Y., Liu, Q. & Lv, H. (2014), 'A mathematical model for horizontal axis wind turbine blades', *Applied Mathematical Modelling* **38**(11-12), 2695–2715.
URL: *https://doi.org/10.1016/j.apm.2013.10.068*

Liberzon, D. & Morse, A. S. (1999), 'Basic problems in stability and design of switched systems', *IEEE control systems magazine* **19**(5), 59–70.
URL: *https://doi.org/10.1109/37.793443*

Librescu, L. & Marzocca, P. (2005), 'Advances in the linear/nonlinear control of aeroelastic structural systems', *Acta Mech.* **178**, 147–186.
URL: *https://doi.org/10.1007/s00707-005-0222-6*

Lim, J. W. & Chopra, I. (1990), 'Response and hub loads sensitivity analysis of a helicopter rotor', *AIAA Journal* **28**(1), 75–82.
URL: *https://doi.org/10.2514/3.10355*

Liu, X., Lu, C., Liang, S., Godbole, A. & Chen, Y. (2015), 'Influence of the vibration of large-scale wind turbine blade on the aerodynamic load', *Energy procedia* **75**, 873–879.
URL: *https://doi.org/10.1016/j.egypro.2015.07.196*

Liu, X., Lu, C., Liang, S., Godbole, A. & Chen, Y. (2017), 'Vibration-induced aerodynamic loads on large horizontal axis wind turbine blades', *Applied Energy* **185**, 1109–1119.
URL: *https://doi.org/10.1016/j.apenergy.2015.11.080*

Loew, S., Obradovic, D. & Bottasso, C. L. (2022), 'Economic nonlinear model predictive control of fatigue—formulation and application to wind turbine control', *Optimal Control Applications and Methods* .
URL: *https://doi.org/10.1002/oca.2870*

Marten, D., Wendler, J., Pechlivanoglou, G., Nayeri, C. & Paschereit, C. (2013), 'Qblade: An open source tool for design and simulation of horizontal and vertical axis wins turbines', *International Journal of Emerging Technology and Advanced Engineering* **3**(3), 264–269.
URL: *https://www.academia.edu/download/41461813/QBlade*$_a$*n*$_O$*pen*$_S$*ource*$_T$*ool*$_f$*or*$_D$*esign*$_a$*n*2016
$0224731 - 15rj8uv.pdf$

Mirzaei, M., Poulsen, N. K. & Niemann, H. H. (2012), Robust model predictive control of a wind turbine, *in* '2012 American Control Conference (ACC)', IEEE, pp. 4393–4398.
URL: *https://doi.org/10.1109/ACC.2012.6314887*

Munters, W. & Meyers, J. (2018), 'Dynamic strategies for yaw and induction control of wind farms based on large-eddy simulation and optimization', *Energies* **11**(1), 177.
URL: *https://doi.org/10.3390/en11010177*

Murdock, H. E., Gibb, D., André, T., Sawin, J. L., Brown, A., Ranalder, L., Collier, U., Dent, C., Epp, B., Hareesh Kumar, C. et al. (2021), 'Renewables 2021-global status report'.

Nezamolmolki, D. & Shooshtari, A. (2016), 'Investigation of nonlinear dynamic behavior of lattice structure wind turbines', *Renewable Energy* **97**, 33–46.
URL: *https://doi.org/10.1016/j.renene.2016.05.070*

Palejiya, D. & Chen, D. (2015), 'Performance improvements of switching control for wind turbines', *IEEE Transactions on Sustainable Energy* **7**(2), 526–534.
URL: *https://doi.org/10.1109/TSTE.2015.2502262*

Pamososuryo, A., Liu, Y., Hovgaard, T., Ferrari, R. & van Wingerden, J. (2022), Individual pitch control by convex economic model predictive control for wind turbine side-side tower load alleviation, *in* 'Journal of Physics: Conference Series', Vol. 2265, IOP Publishing, p. 032071.
URL: *https://doi.org/10.1088/1742-6596/2265/3/032071*

Petrović, V., Jelavić, M. & Baotić, M. (2021), 'Mpc framework for constrained wind turbine individual pitch control', *Wind Energy* **24**(1), 54–68.
URL: *https://doi.org/10.1002/we.2558*

Pirrera, A., Capuzzi, M., Buckney, N. & Weaver, P. (2012), Optimization of wind turbine blade spars, *in* '53rd AIAA/ASME/ASCE/AHS/ASC Structures, Structural Dynamics and Materials Conference 20th AIAA/ASME/AHS Adaptive Structures Conference 14th AIAA', p. 1500.
URL: *https://doi.org/10.2514/6.2012-1500*

Politakis, G., Haans, W. & van Bussel, G. (2008), 'Suppression of classical flutter using a'smart blade", p. 1301.
URL: *https://doi.org/10.2514/6.2008-1301*

Pustina, L., Biral, F. & Serafini, J. (2022), A novel nonlinear model predictive controller for power maximization on floating offshore wind turbines, *in* 'Journal of Physics: Conference Series', Vol. 2265, IOP Publishing, p. 042002.
URL: *https://doi.org/10.1088/1742-6596/2265/4/042002*

R. Stäblein, A. (2016), Analysis and design of bend-twist coupled wind turbine blades, *in* 'MARE-WINT', Springer, pp. 67–80.

R. Stäblein, A., Hansen, M. & Verelst, D. (2016), 'Modal properties and stability of bend-twist coupled wind turbine blades', pp. 1–27.
URL: *https://doi.org/10.5194/wes-2-343-2017*

Recalde-Camacho, L., Stock, A., Giles, A. D. & Leithead, W. (2020), 'Control of aeroelastically-tailored wind turbines'.
URL: *https://strathprints.strath.ac.uk/77283/*

Reddy, J. N. (2004), *An Introduction to Nonlinear Finite Element Analysis: with applications to heat transfer, fluid mechanics, and solid mechanics*, OUP Oxford.
URL: *https://doi.org/10.1093/acprof:oso/9780199641758.001.0001*

Rezaei, M. M., Behzad, M., Haddadpour, H. & Moradi, H. (2015), 'Development of a reduced order model for nonlinear analysis of the wind turbine blade dynamics', *Renewable energy* **76**, 264–282.
URL: *https://doi.org/10.1016/j.renene.2014.11.021*

Riziotis, V. A. & Voutsinas, S. G. (2006), Advanced aeroelastic modelling of complete wind turbine configurations in view of assessing stability characteristics, *in* 'Proceedings of the EWEC', Vol. 6.

Sanchez, H., Escobet, T., Puig, V. & Odgaard, P. F. (2015), 'Health-aware model predictive control of wind turbines using fatigue prognosis', *IFAC-PapersOnLine* **48**(21), 1363–1368.
URL: *https://doi.org/10.1016/j.ifacol.2015.09.715*

Sarkar, S. & Fitzgerald, B. (2020), 'Vibration control of spar-type floating offshore wind turbine towers using a tuned mass-damper-inerter', *Structural Control and Health Monitoring* **27**(1), e2471.
URL: *https://doi.org/10.1002/stc.2471*

Schlipf, D., Pao, L. Y. & Cheng, P. W. (2012), Comparison of feedforward and model predictive control of wind turbines using lidar, *in* '2012 IEEE 51st IEEE Conference on Decision and Control (CDC)', IEEE, pp. 3050–3055.
URL: *https://doi.org/10.1109/CDC.2012.6426063*

Scott, S., Greaves, P., Weaver, P. M., Pirrera, A. & Macquart, T. (2020), Efficient structural optimisation of a 20 mw wind turbine blade, *in* 'Journal of Physics: Conference Series', Vol. 1618, IOP Publishing, p. 042025.
URL: *https://doi.org/10.1088/1742-6596/1618/4/042025*

Service, G. D. (2022), 'Policy paper british energy security strategy'. [Updated 7 April 2022].
URL: *https://www.gov.uk/government/publications/british-energy-security-strategy/british-energy-security-strategy*

Shams, S. & Esbati Lavasani, R. (2019), 'Aeroelastic stability analysis of a wind turbine blade section with trailing edge flap using a flexible unsteady blade elements momentum theory', *Journal of the Brazilian Society of Mechanical Sciences and Engineering* **41**, 1–16.

Shan, M., Guo, J. & Gill, E. (2020), 'An analysis of the flexibility modeling of a net for space debris removal', *Advances in Space Research* **65**(3), 1083–1094.
URL: *https://doi.org/10.1016/j.asr.2019.10.041*

Shirzadeh, R., Devriendt, C., Bidakhvidi, M. A. & Guillaume, P. (2013), 'Experimental and computational damping estimation of an offshore wind turbine on a monopile foundation', *Journal of Wind Engineering and Industrial Aerodynamics* **120**, 96–106.
URL: *https://doi.org/10.1016/j.jweia.2013.07.004*

Sinner, M., Petrović, V., Langidis, A., Neuhaus, L., Hölling, M., Kühn, M. & Pao, L. Y. (2021), 'Experimental testing of a preview-enabled model predictive controller for blade pitch control of wind turbines', *IEEE Transactions on Control Systems Technology* **30**(2), 583–597.
URL: *https://doi.org/10.1109/TCST.2021.3070342*

Stäblein, A. R. (2016), *Analysis and design of bend-twist coupled wind turbine blades*, Springer, Cham, pp. 67–80.

Sun, L. & Chen, L. (2017), 'Residual mode correction in calibrating nonlinear damper for vibration control of flexible structures', *Journal of Sound and Vibration* **406**, 197–207.
URL: *https://doi.org/10.1016/j.jsv.2017.06.015*

Tingrui, L. & Yongsheng, R. (2008), Aeroelastic stability of wind turbine blades based on beddoes-leishman model, *in* '2008 IEEE International Symposium on Knowledge Acquisition and Modeling Workshop', IEEE, pp. 605–608.
URL: *https://doi.org/10.1109/KAMW.2008.4810561*

Veers, P., Lobitz, D. & Bir, G. (1998), 'Aeroelastic tailoring in wind-turbine blade applications'.

Veers, P. S., Ashwill, T. D., Sutherland, H. J., Laird, D. L., Lobitz, D. W., Griffin, D. A., Mandell, J. F., Musial, W. D., Jackson, K., Zuteck, M. et al. (2003), 'Trends in the design, manufacture and evaluation of wind turbine blades', *Wind Energy: An International Journal for Progress and Applications in Wind Power Conversion Technology* **6**(3), 245–259.
URL: *https://doi.org/10.1002/we.90*

Vesel Jr, R. W. & McNamara, J. J. (2014), 'Performance enhancement and load reduction of a 5 mw wind turbine blade', *Renewable energy* **66**, 391–401.
URL: *https://doi.org/10.1016/j.renene.2013.12.019*

Wang, L., Liu, X. & Kolios, A. (2016), 'State of the art in the aeroelasticity of wind turbine blades: Aeroelastic modelling', *Renewable and Sustainable Energy Reviews*

64, 195–210.
URL: *https://doi.org/10.1016/j.rser.2016.06.007*

Wang, L., Liu, X., Renevier, N., Stables, M. & Hall, G. M. (2014), 'Nonlinear aeroelastic modelling for wind turbine blades based on blade element momentum theory and geometrically exact beam theory', *Energy* **76**, 487–501.
URL: *https://doi.org/10.1016/j.energy.2014.08.046*

Wright, A. & Fingersh, L. (2008), Advanced control design for wind turbines part i: Control design, implementation, and initial tests, Technical report, National Renewable Energy Lab.(NREL)/TP-500-42437, Golden, Colorado.
URL: *https://doi.org/10.2172/927269*

Xie, F. & Aly, A.-M. (2020), 'Structural control and vibration issues in wind turbines: A review', *Engineering Structures* **210**, 110087.
URL: *https://doi.org/10.1016/j.engstruct.2019.110087*

Xing, W. & Singh, S. N. (2000), 'Adaptive output feedback control of a nonlinear aeroelastic structure', *Journal of guidance, control, and dynamics* **23**(6), 1109–1116.
URL: *http://dx.doi.org/10.2514/2.4662*

Xing, X., Meng, H., Xie, L., Yue, L. & Lin, Z. (2018), 'Switching performance improvement based on model-predictive control for wind turbine covering the whole wind speed range', *IEEE Transactions on Sustainable Energy* **10**(1), 290–300.
URL: *https://doi.org/10.1109/TSTE.2018.2833634*

Zhang, J., Cheng, M., Chen, Z. & Fu, X. (2008), Pitch angle control for variable speed wind turbines, *in* '2008 Third International Conference on Electric Utility Deregulation and Restructuring and Power Technologies', IEEE, pp. 2691–2696.
URL: *https://doi.org/10.1109/DRPT.2008.4523867*

Zhang, M., Tan, B. & Xu, J. (2016), 'Smart fatigue load control on the large-scale wind turbine blades using different sensing signals', *Renewable energy* **87**, 111–119.
URL: *https://doi.org/10.1016/j.renene.2015.10.011*

Appendix A

Wind turbine model summary

Aerodynamics:

$$\begin{aligned} J\ddot{\theta}_R = &-(K_E + J\dot{\theta}_R^2)[(\theta_R - cos\beta) - (\phi_R - \phi_T)sin\beta]cos\beta \\ &-(K_F + J\dot{\theta}_R^2)[(\theta_R - \theta_H)sin\beta + (\phi_R - \phi_T)cos\beta]sin\beta + F_1 \end{aligned} \tag{A.1}$$

Rotor dynamics

$$\begin{aligned} \frac{1 - \frac{J_C^2}{JJ_T}}{1 + \frac{J_C}{J_T}} J\ddot{\phi}_R = &(K_E + J\dot{\theta}_R^2)[(\theta_R - \theta_H)cos\beta - (\phi_R - \phi_T)sin\beta]sin\beta \\ &-(K_F + J\dot{\theta_R^2})[(\theta_R - \theta_H)sin\beta + (\phi_R - \phi_T)cos\beta]cos\beta \\ &+[F_2 + \frac{J_C}{J_T}B_T\dot{\phi_T} + \frac{J_C}{J_T}K_T\phi_T]/(1 + \frac{J_C}{J_T}) \end{aligned} \tag{A.2}$$

Tower dynamics:

$$\begin{aligned} \frac{1 - J_C^2/JJ_T}{1 + J_C/J_T} J\ddot{\phi}_T = &-(K_E + J\dot{\theta}_R^2)[(\theta_R - \theta_H)cos\beta - (\phi_R - \phi_T)sin\beta]sin\beta \\ &+J\dot{\theta}_R^2[(\theta_R - \theta_H)sin\beta + (\phi_R - \phi_T)cos\beta]cos\beta \\ &-[B_T\dot{\phi}_T + K_T\phi_T + \frac{J_C}{J}F_2]/(1 + \frac{J_C}{J}) \end{aligned} \tag{A.3}$$

Appendix B

MPC

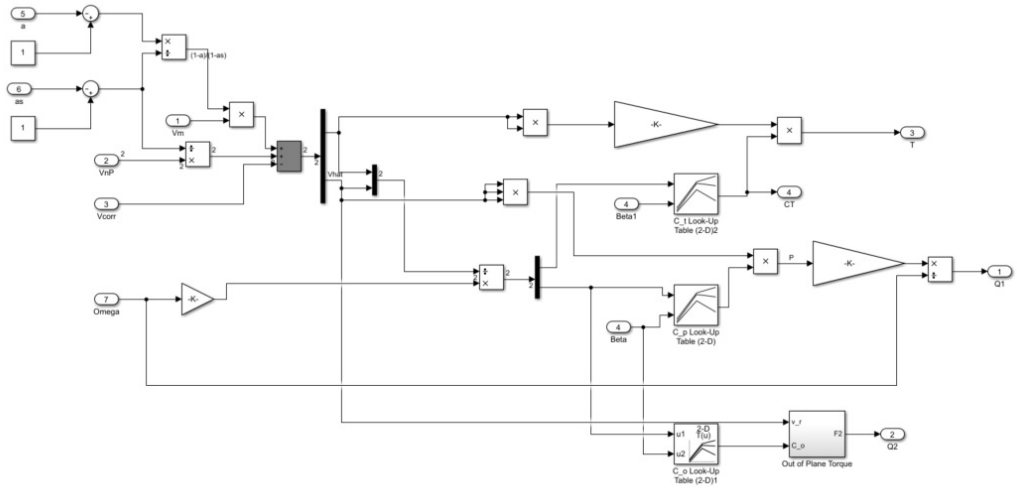

Figure B.1: Simulink aerodynamic model

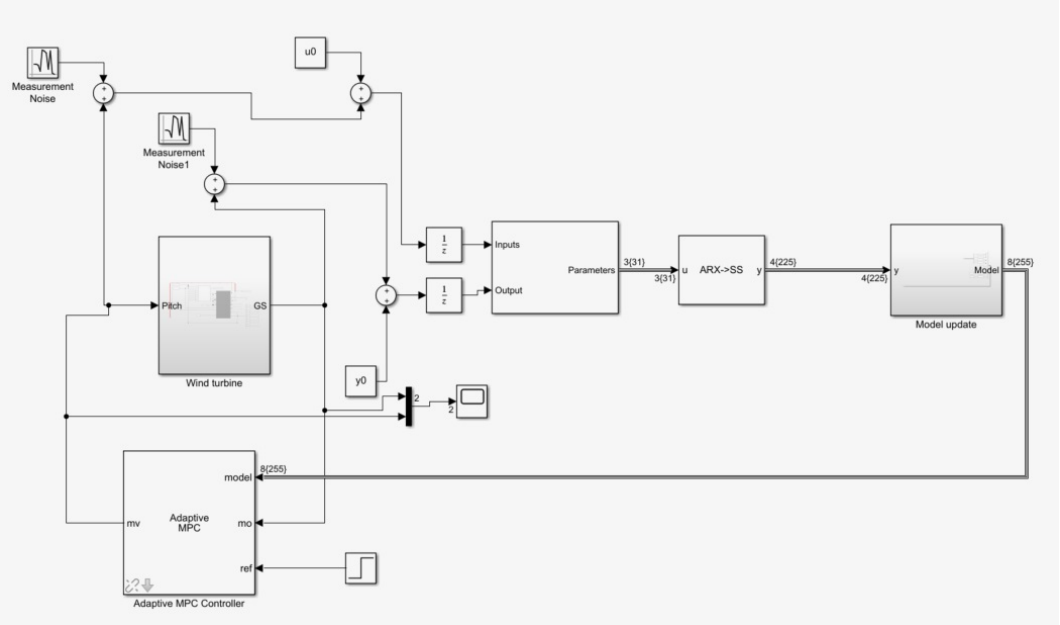

Figure B.2: Adaptive MPC for ATB wind turbine model with combined materials blade

B.1 Recursive parameter estimation

A linear time invariant (LTI) system can be written as,

$$\begin{aligned} y(k) = &- a_1 y(k-1) - ... - a_m y(k-m) \\ &+ b_1 u(k-d-1) + ... + b_m u(k-d-m) \\ &+ v(k) + d_1 v(k-1) + ... + d_m v(k-m) \end{aligned} \tag{B.1}$$

where $k = t/T0 = 0, 1, 2, ...$ is the discrete time, T_0 is the sample time, d is the discrete dead time and,

$$\begin{aligned} y(k) &= Y(k) - Y_0 \\ u(k) &= U(k) - U_0 \end{aligned} \tag{B.2}$$

are the deviation of the measured output $Y(k)$ and the input $U(k)$ from Y_0 and U_0

The noise signal is independant given by,

$$Ev(k) = 0 \tag{B.3}$$

$$y(z) = \underbrace{\frac{B(z^{-1})}{A(z^{-1})}z^{-d}u(z)}_{G_p(z^{-1})} + \underbrace{\frac{D(z^{-1})}{A(z^{-1})}v(z)}_{G_v(z^{-1})} \tag{B.4}$$

where $G_p(z^{-1})$ is the system model, $G_v(z^{-1})$ is the noise model, The noise filter denominator is equal to the system model denominator which can simplify the closed loop parameter estimation and the controller design.

Eq B.1 can be simplified to

$$y(k) = \psi^T(k)\theta + v(k) \tag{B.5}$$

with the data vector

$$\psi^T(k) = [-y(k-1), ..., -y(k-m)]|u(k-d-1), ..., u(k-d-m)|v(k-1), ..., v(k-m)] \tag{B.6}$$

and the parameter vector

$$\theta = [a_1, ..., a_m|b_1, ..., b_m|d_1, ..., d_m]^T \tag{B.7}$$

For estimation of the unknown parameters, the folowing model is assumed,

$$y(z) = \underbrace{\frac{\hat{B}(z^{-1})}{\hat{A}(z^{-1})}z^{-d}u(z)}_{G_p(z^{-1})} + \underbrace{\frac{\hat{D}(z^{-1})}{\hat{A}(z^{-1})}e(z)}_{G_v(z^{-1})} \tag{B.8}$$

where $\hat{A}, \hat{B}$ and $\hat{D}$ are the estimates matrices.

The least square (LS) method is based on the minimisation of the loss function,

$$V = \sum_k e^2(k) \tag{B.9}$$

due to the unknown parameter $\hat{\theta}$

$$e(k+1) = y(k+1) - \psi^T(k+1)\hat{\theta}(k) \tag{B.10}$$

B.2 Recursive finite history estimation

Finite history estimation algorithm aims to minimise the error between the observed and predicted outputs for a finite number of past time steps. The methods find parameter estimates $\theta(t)$ by minimising,

$$\sum_{k=t-N+1}^{t} (y(k) - \hat{y}(k|\theta))^2 \tag{B.11}$$

where $y(k)$ is the observed output at time k, $\hat{y}(k|]theta)$ is the predicted output at time k. Finite history estimation methods minimise prediction errors for the last N time steps. In Simulink ARX structure, the output $\hat{y}(k|\theta)$ is given by,

$$\hat{y}(k|\theta) = \Psi(k)\theta(k-1) \tag{B.12}$$

where Psi is the buffer of regressors and $y(k) = t-N+1, t-N+2, ..., t-2, t-1, 1$.

B.3 Autoregressive-Exogenous (ARX)

Autoregressive-eXogenous(ARX) is used to simulate datasets. It is fit to the existing model data. ARX model assumes the current output of the system is a function of the previous system. It can be applied to multi-input-multi-output (MIMO) system. The simulation model has single-input-single-output (SISO) system. ARX has the disadvantage of missing observations of the regression model Horner et al. (2019).

The $ARX(n, m)$ is defined as,

$$\begin{aligned} y(k) = a_1 y(k-1) + a_2 y(k-2) + ... + a_n y(k-n) + \\ b_1 u(k-1) + b_2 u(k-2) + ... + b_m u(k-m) + \\ v(k) \end{aligned} \tag{B.13}$$

where n is the number of outputs, m is the number of inputs, y is the model output, u is the model input, a_i is the ith autoregressive (AR) parameter, b_i is the ith exogenous (X) parameter and v is the noise.

B.4 Derivation of quadratic programming problem

For current time step k, the cost function depends on the tracking error, $\mathbf{e}^k = \mathbf{y}_D^k - \mathbf{r}^k$.

The evolution of the error over the prediction horizon starting from current time step, k as,

$$\mathbf{e}^k = C_d\mathbf{x}_D^k + D_d\mathbf{u}_D^k - \mathbf{r}^k \tag{B.14}$$

$$\mathbf{e}^{k+1} = C_d\mathbf{x}_D^{k+1} + D_d\mathbf{u}_D^{k+1} - \mathbf{r}^{k+1} = C_dA_d\mathbf{x}_D^k + C_dD_d\mathbf{u}_D^k + C_d\mathbb{K} + D_d\mathbf{u}_D^{k+1} - \mathbf{r}^{k+1} \tag{B.15}$$

$$\mathbf{e}^{k+2} = C_d\mathbf{x}_D^{k+2} + D_d\mathbf{u}_D^{k+2} - \mathbf{r}^{k+2} = C_dA_d^2\mathbf{x}_D^k + C_dA_dD_d\mathbf{u}_D^k + C_dB_d\mathbf{u}_D^{k+1} + C_dA_d\mathbb{K} + C_d\mathbb{K} + D_d\mathbf{u}_D^{k+2} - \mathbf{r}^{k+2} \tag{B.16}$$

Appendix C

Wind turbine models performance comparison for 12 m/s, 14 m/s, 18 m/s and 20 m/s

The focus of this thesis is to develop an MPC for 16 m/s wind speed. Besides 16 m/s, the results are also presented for a wider range of wind speeds. The selected wind speeds are 12 m/s, 14 m/s, 18 m/s, and 20 m/s. All the selected wind speeds are tested with MPC with 1 set of parameter tuning as shown in Table 5.1 and illustrated in power spectral density (PSD) and cumulative PSD (CPSD) plots. The results in Figure C.1 to C.32 are PSD results and the CPSD for power generation, generator speed, root bending moment, and tower acceleration measurements for 5 selected wind speeds as listed above. PSD shows the strength of energy variation in frequency function while cumulative PSD is obtained from the PSD through the noise-reducing process of integration.

C.1 12 m/s wind speed

PSD and CPSD for 12 m/s are presented in Figure C.1 and C.2 for power generation, Figure C.3 and C.4 for generator speed, Figure C.5 and C.6 for root bending moment, and Figure C.7 and C.8 for tower acceleration. The PSD for power generation for 3

models shows that Model 2 with MPC has the lowest peak compared to Model 3 with MPC and Model 3 with Controller 1. Referring to Model 3 with Controller 1, the peaks are visible at 0.2 radians/s, 0.4 radians/s, and 0.8 radians/s, and Model 2 with MPC has the highest peak at 1 radian. Another peak at 1 radian is the peak of Model 3 with MPC which is the highest peak compared to the other 2 models. The peak is also visible in the generator speed diagram. The RBM plots for PSD show that Model 3 with MPC and Controller 1 have approximately similar magnitude as compared to Model 2 with MPC. It is consistent with the CPSD plots where Model 2 with MPC has the lowest magnitude compared to Model 3 with MPC and MPC with Controller 1. The tower acceleration PSD plot shows a similar response at lower frequencies and begins to show differences at higher frequencies. CPSD for tower acceleration also shows a low magnitude for Model 2 with MPC compared to the other 2 models.

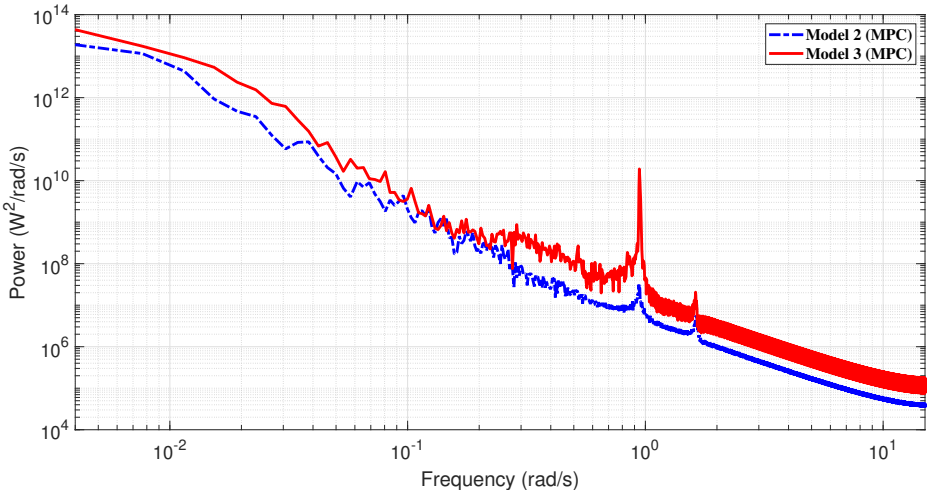

Figure C.1: Power generation PSD for 12 m/s

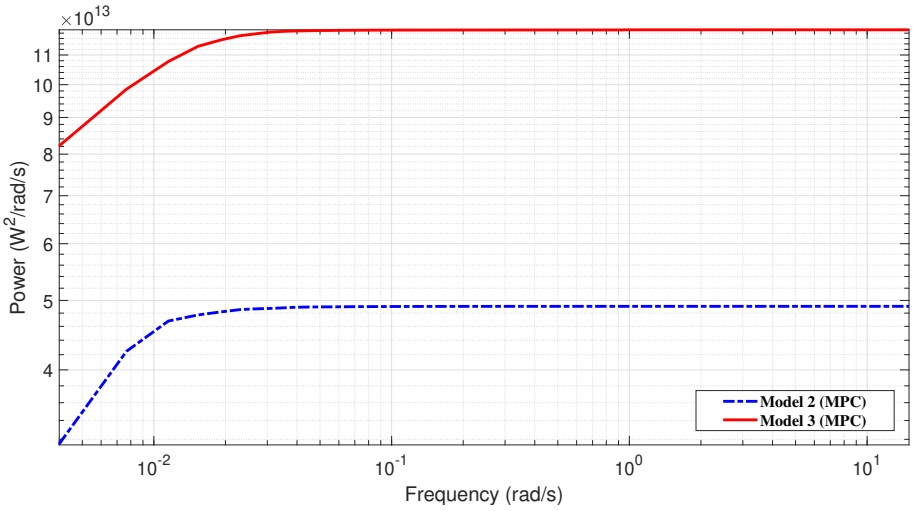

Figure C.2: Power generation CPSD for 12 m/s

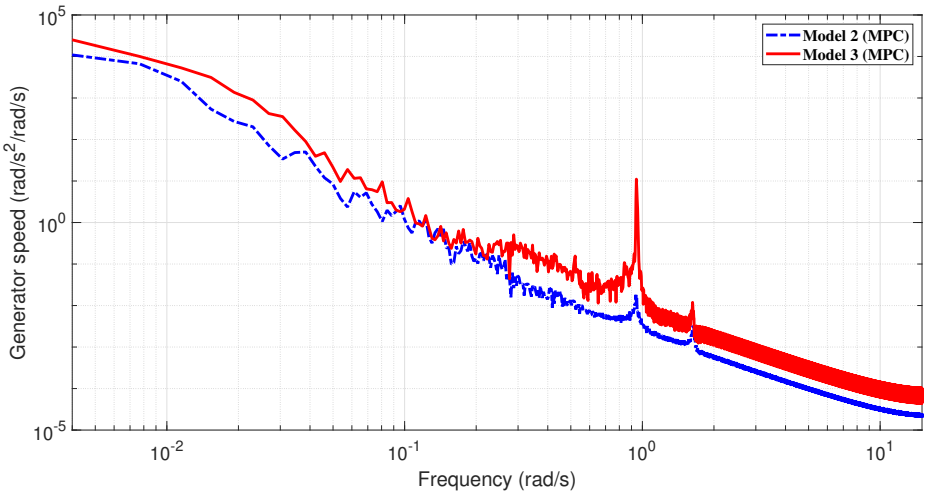

Figure C.3: Generator speed PSD for 12 m/s

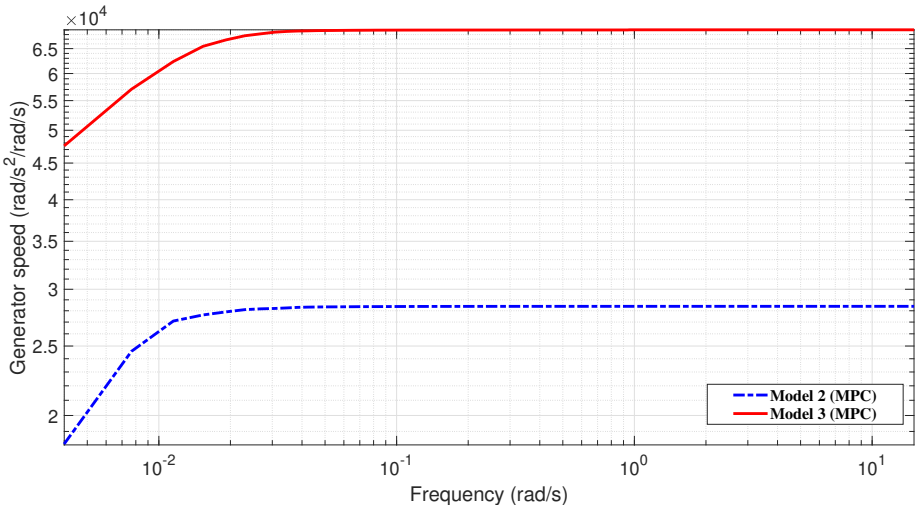

Figure C.4: Generator speed CPSD for 12 m/s

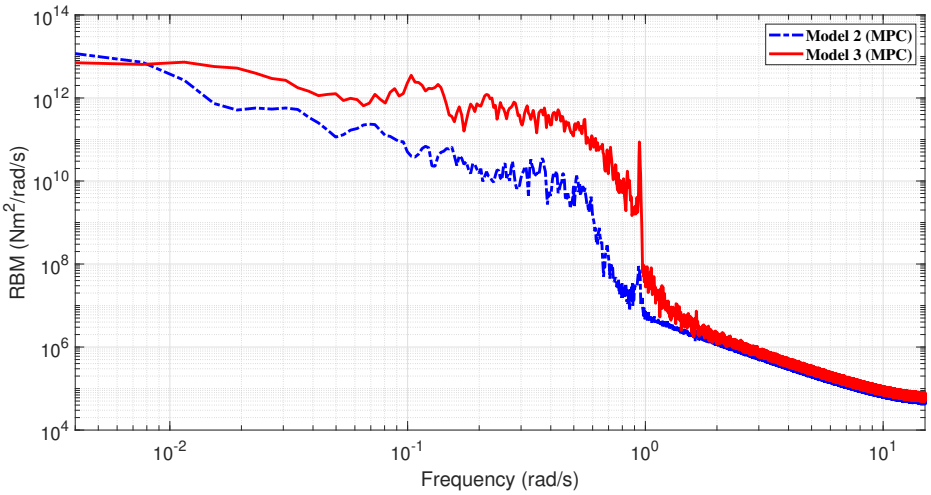

Figure C.5: RBM PSD for 12 m/s

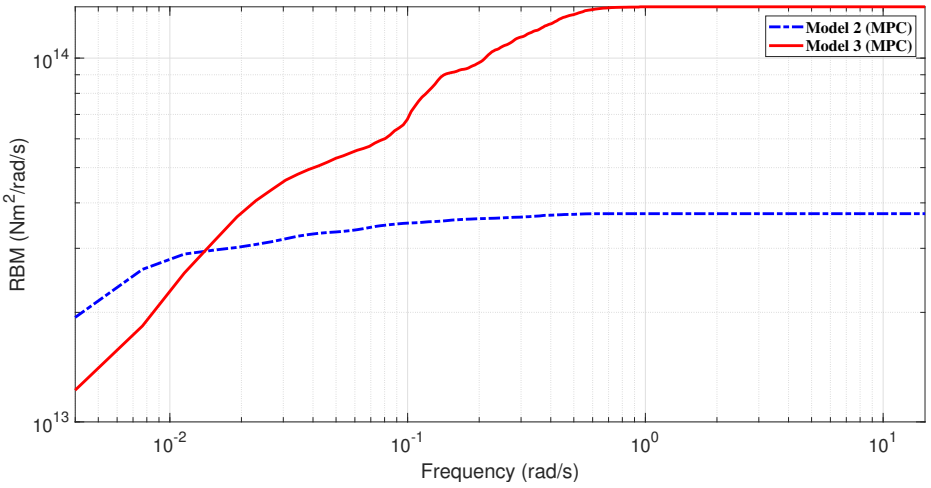

Figure C.6: RBM CPSD for 12 m/s

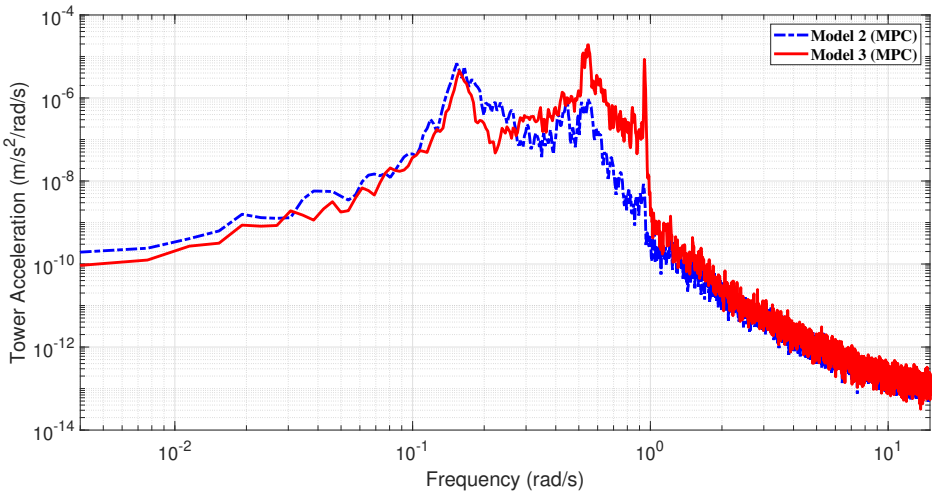

Figure C.7: Tower acceleration PSD for 12 m/s

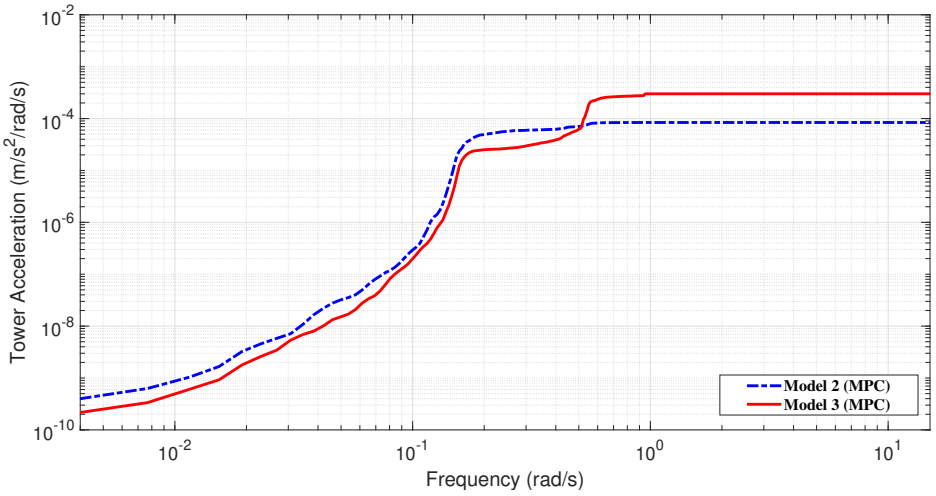

Figure C.8: Tower acceleration CPSD for 12 m/s

C.2 14 m/s wind speed

PSD and CPSD for 14 m/s are presented in Figure C.9 and C.10 for power generation, Figure C.11 and C.12 for generator speed, Figure C.13 and C.14 for root bending moment, and Figure C.15 and C.16 for tower acceleration. For 14 m/s wind speeds, the PSD for power generation shows results similar to the 12 m/s power generation which the peaks are visible at the same frequencies and Model 3 with MPC again shows the highest peak at 1 radian compared to Model 2 with MPC and Model 3 with Controller 1. Model 3 with Controller 1 of CPSD for generator speed is lower than Model 2 and Model 3 with MPC. The PSD and CPSD for RBM also show that Model 2 with MPC has higher magnitudes for 14 m/s compared to 12 m/s. The tower acceleration for 14 m/s shows Model 2 with MPC has higher magnitude than Model 3 with MPC and Model 3 with Controller 1. It also shows that Model 3 with MPC has high peak at 1 radian/s.

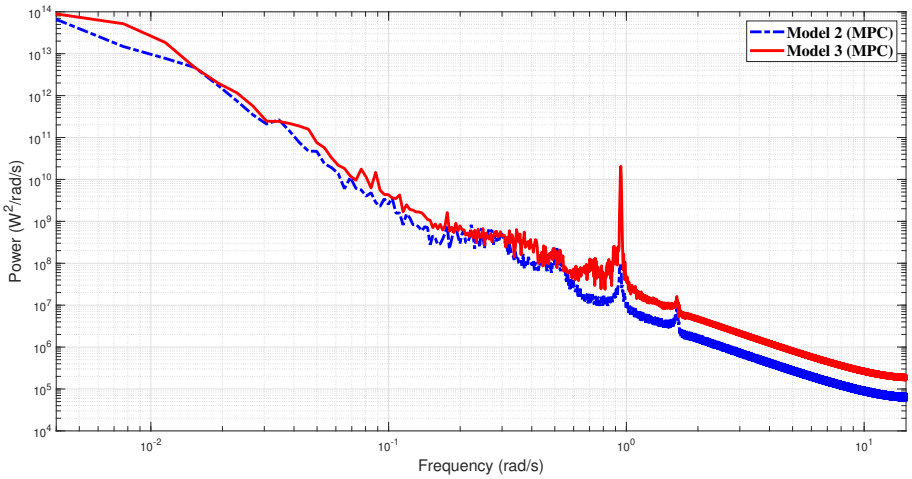

Figure C.9: Power generation PSD for 14 m/s

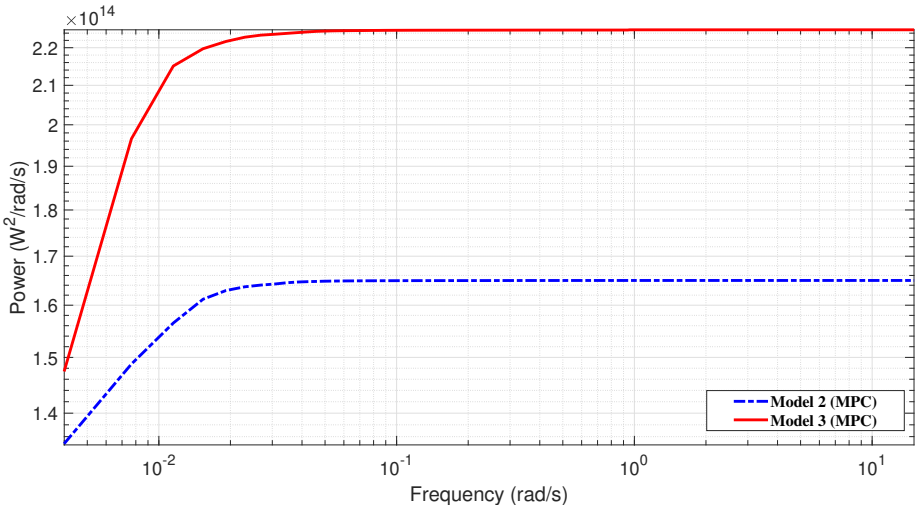

Figure C.10: Power generation CPSD for 14 m/s

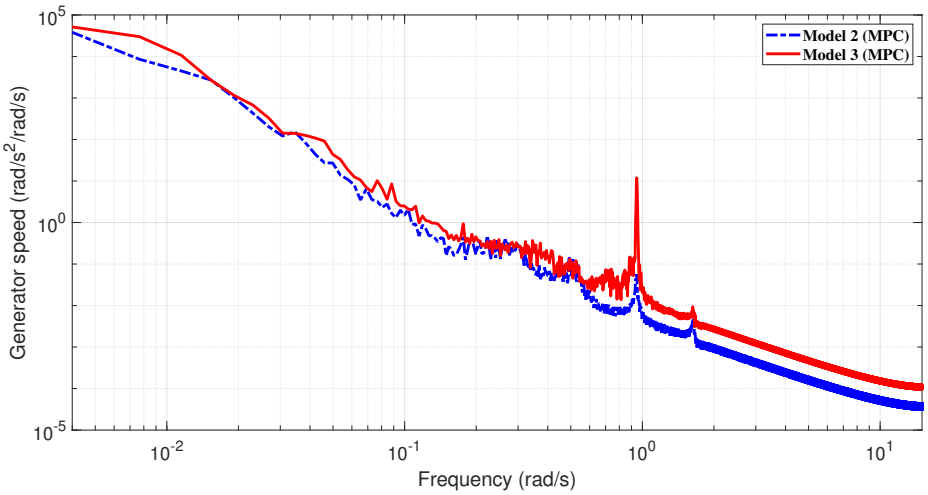

Figure C.11: Generator speed PSD for 14 m/s

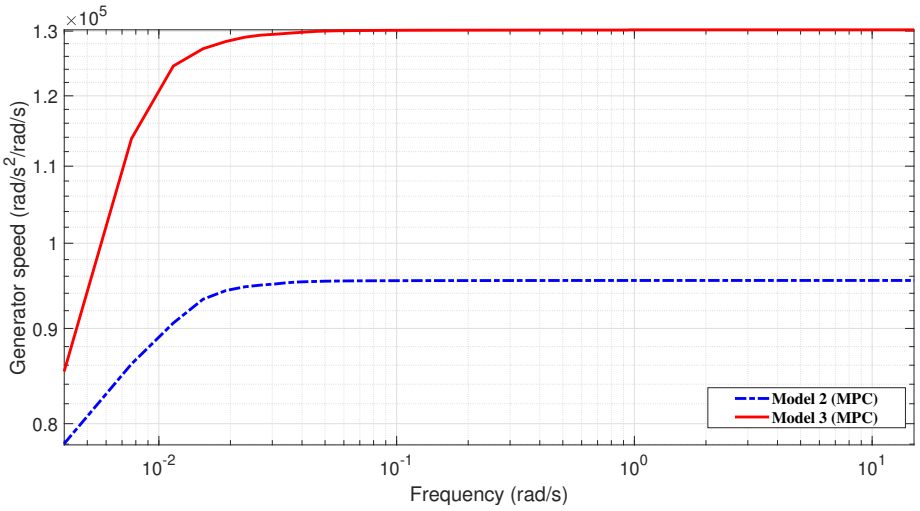

Figure C.12: Generator speed CPSD for 14 m/s

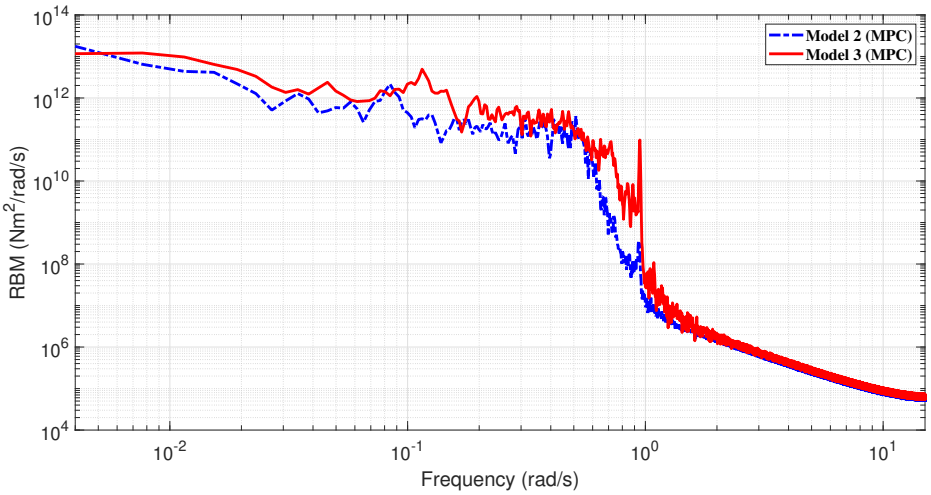

Figure C.13: RBM PSD for 14 m/s

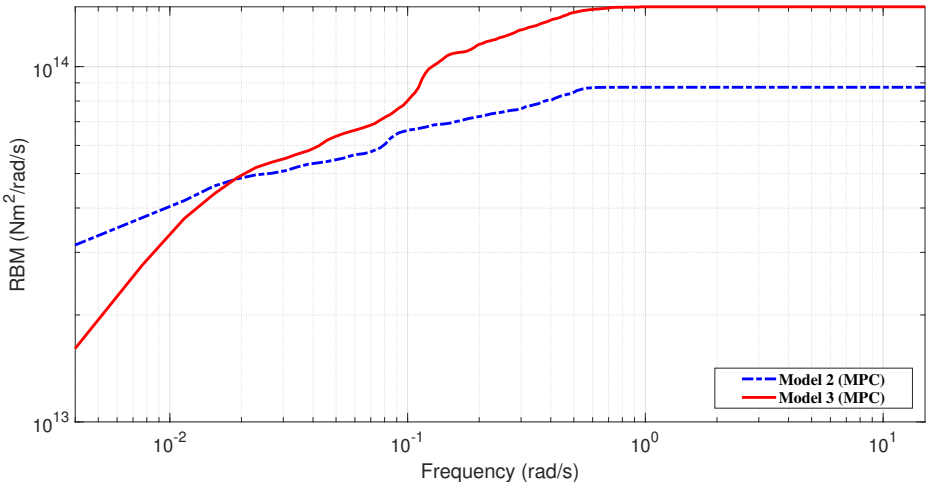

Figure C.14: RBM CPSD for 14 m/s

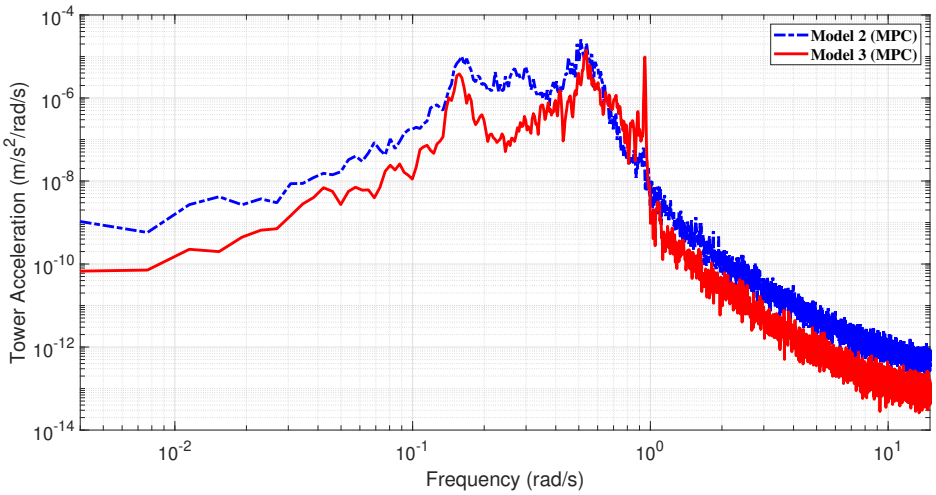

Figure C.15: Tower acceleration PSD for 14 m/s

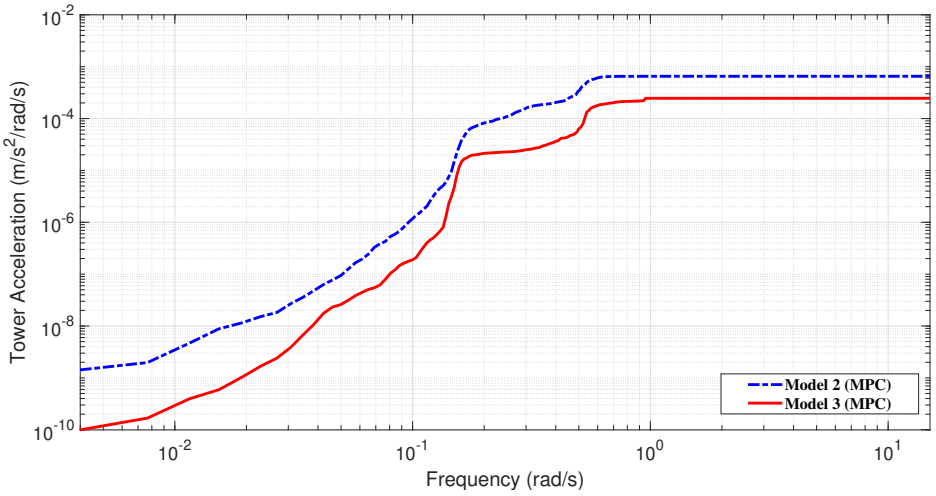

Figure C.16: Tower acceleration CPSD for 14 m/s

C.3 18 m/s wind speed

PSD and CPSD for 18 m/s are presented in Figure C.17 and C.18 for power generation, Figure C.19 and C.20 for generator speed, Figure C.21 and C.22 for root bending moment, and Figure C.23 and C.24 for tower acceleration. The PSD for power generation at 18 m/s shows Model 2 with MPC is slightly higher than Model 3 compared to 16 m/s. The peaks for the 3 models are visible at the same frequencies. The CPSD does not show much difference compared to 16 m/s. The PSD and CPSD for generator speed also show similar variations as the power generation. The PSD for RBM shows the peak for Model 2 with MPC is higher than the peak for Model 3 with Controller 1 after 0.1 radians/s and the CPSD shows Model 3 with Controller 1 is higher than Model 2 and Model 3 with MPC compared to 16 m/s. The tower acceleration PSD and CPSD show similar output compared to 16 m/s.

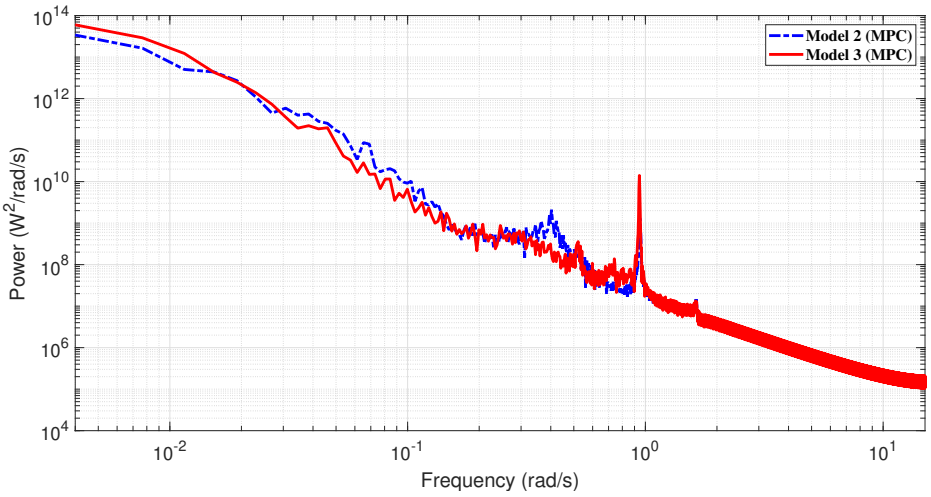

Figure C.17: Power generation PSD for 18 m/s

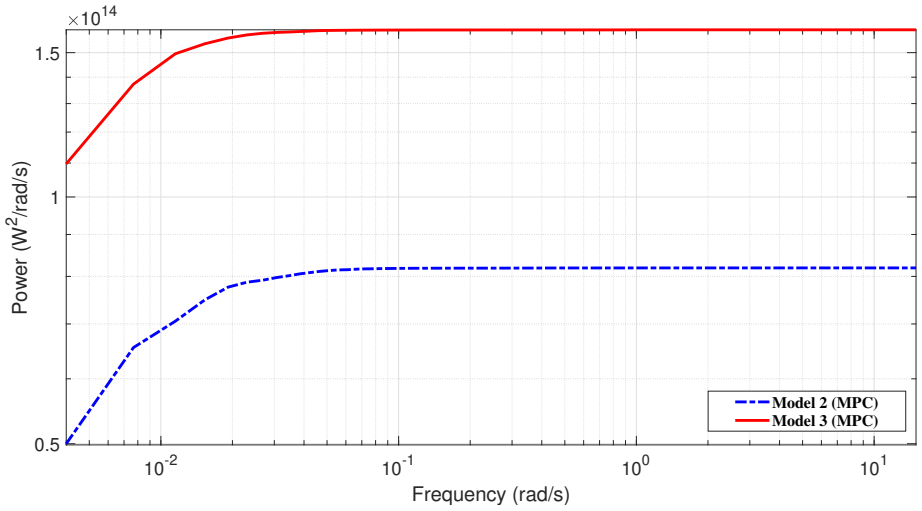

Figure C.18: Power generation CPSD for 18 m/s

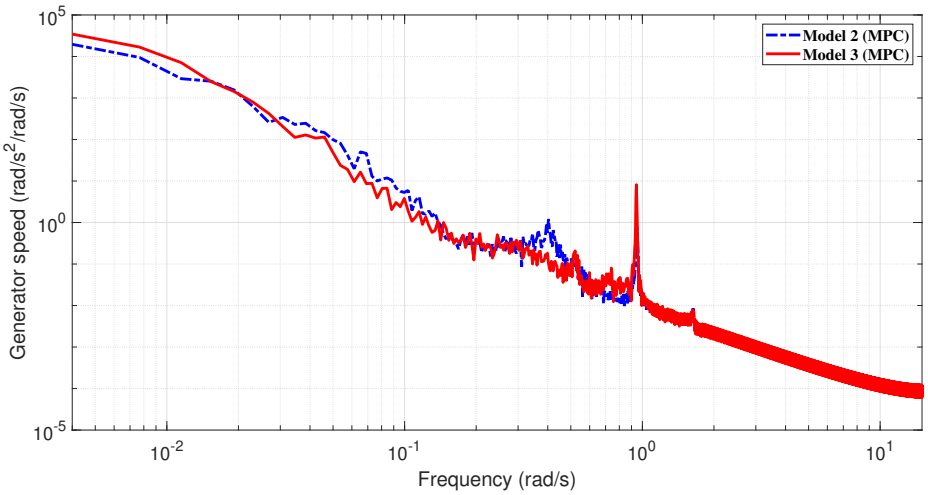

Figure C.19: Generator speed PSD for 18 m/s

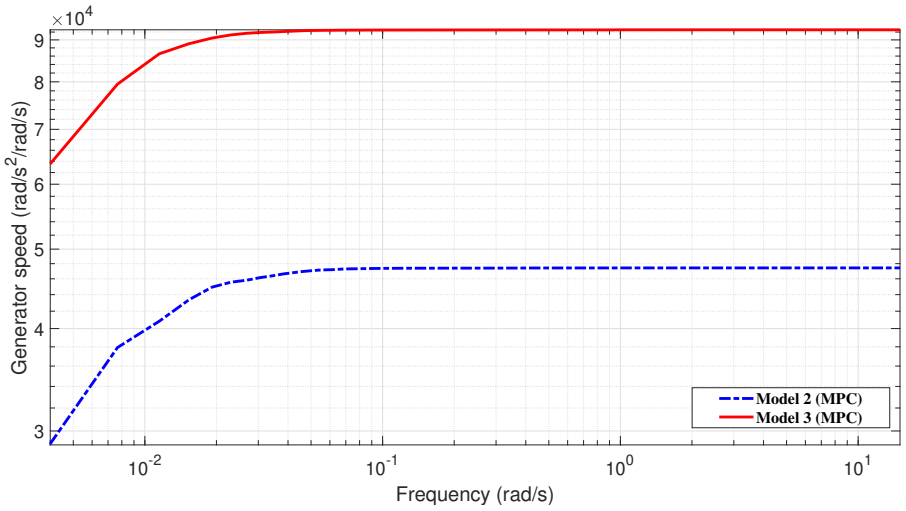

Figure C.20: Generator speed CPSD for 18 m/s

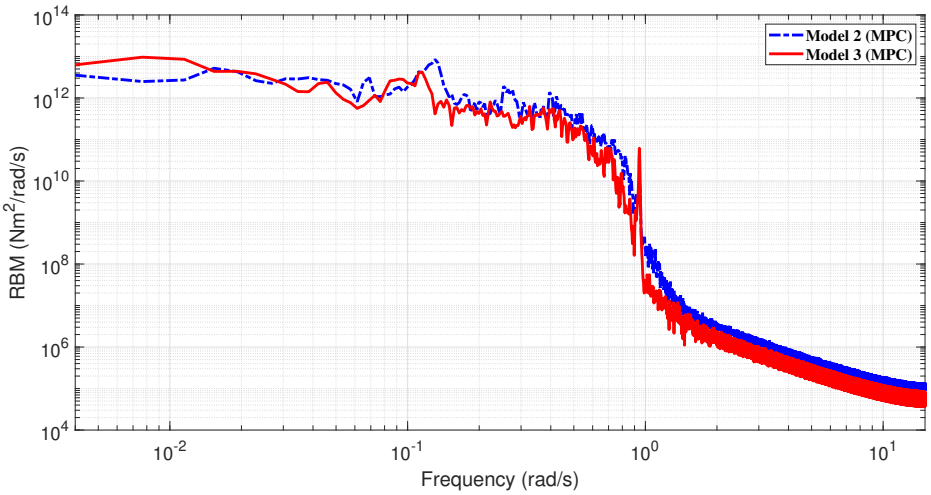

Figure C.21: RBM PSD for 18 m/s

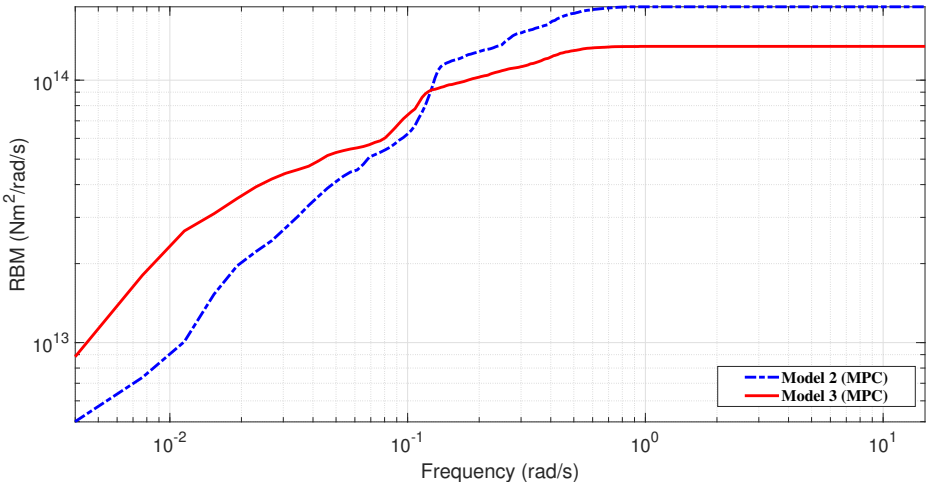

Figure C.22: RBM CPSD for 18 m/s

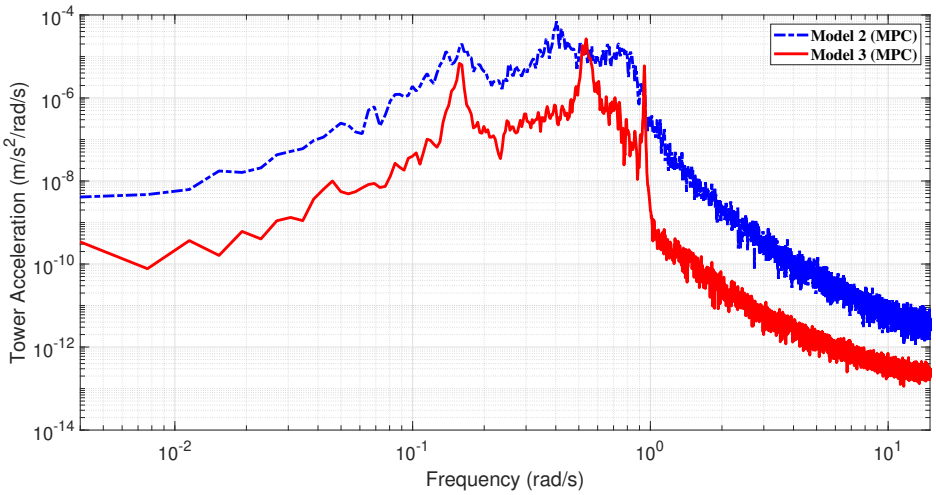

Figure C.23: Tower acceleration PSD for 18 m/s

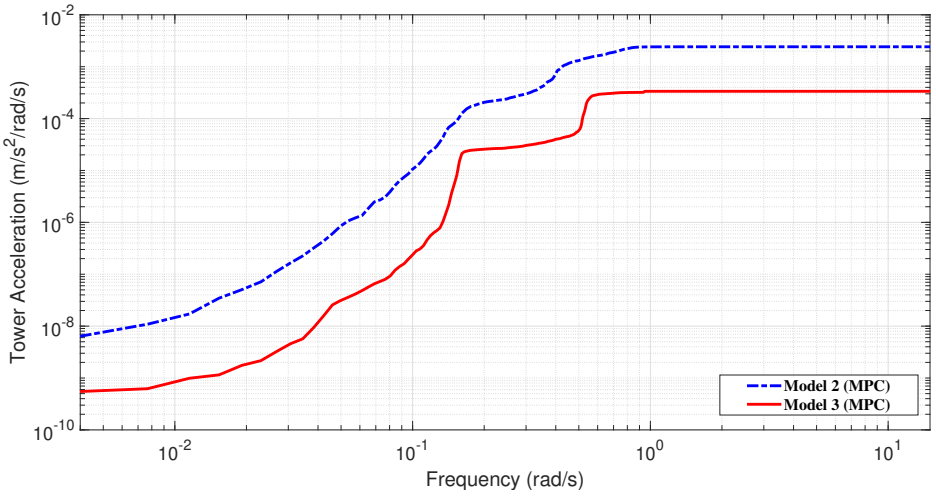

Figure C.24: Tower acceleration CPSD for 18 m/s

C.4 20 m/s wind speed

PSD and CPSD for 20 m/s are presented in Figure C.25 and C.26 for power generation, Figure C.27 and C.28 for generator speed, Figure C.29 and C.14 for root bending moment, and Figure C.31 and C.32 for tower acceleration. The PSD and CPSD for power generation for 20 m/s show that the variations of the 3 models are clearly visible compared to 16 m/s and 18 m/s. The CPSD for power generation shows Model 2 and Model 3 with MPC have the highest magnitude compared to Model 3 with Controller 1. The PSD and CPSD for generator speed also show a similar response. The PSD and CPSD for RBM does not show much difference compared to 18 m/s. Finally, the PSD and CPSD for tower acceleration show a significant peak for Model 3 with Controller 1 compared to 18 m/s. The output response for Model 2 and Model 3 with MPC show similar response compared to 18 m/s.

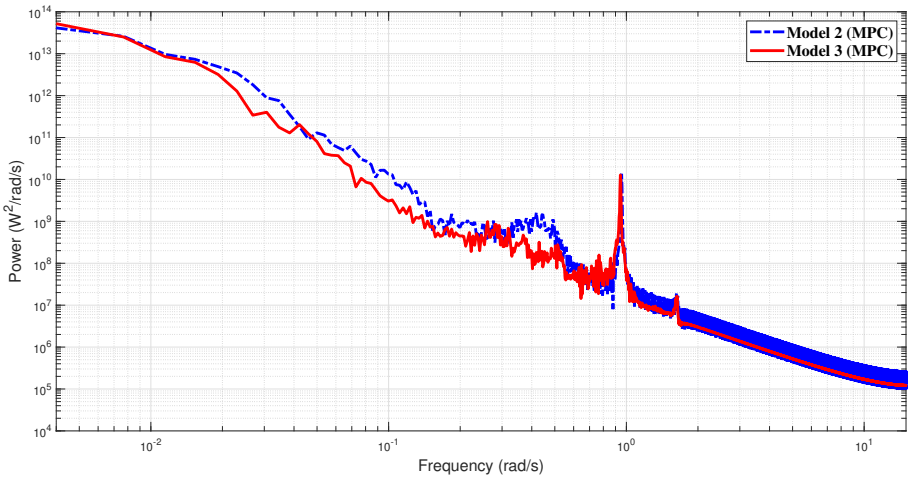

Figure C.25: Power generation PSD for 20 m/s

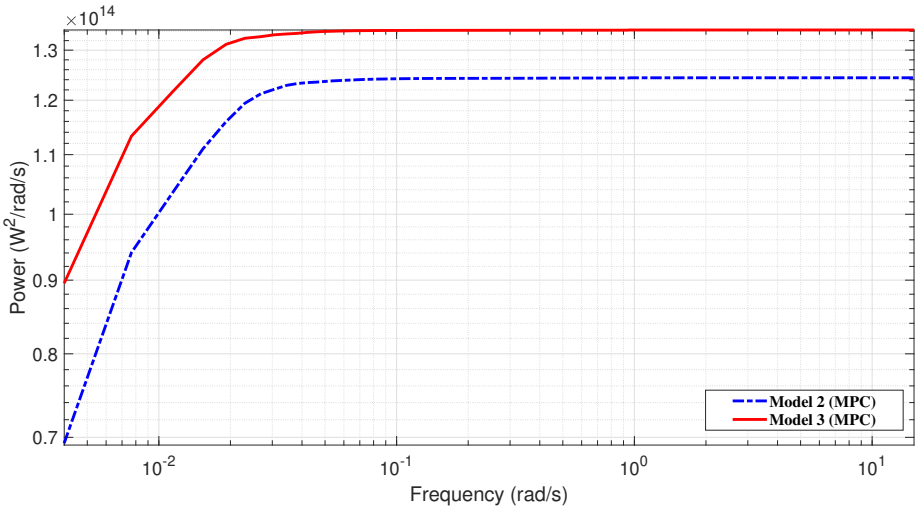

Figure C.26: Power generation CPSD for 20 m/s

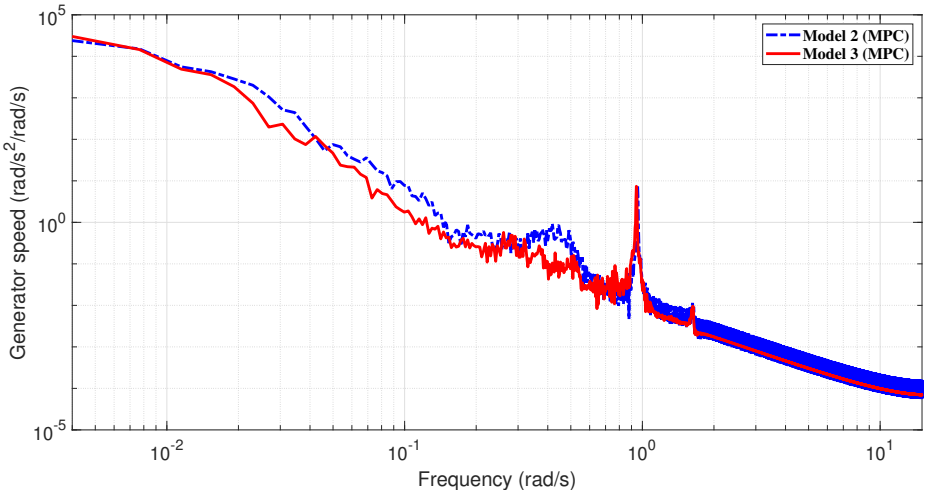

Figure C.27: Generator speed PSD for 20 m/s

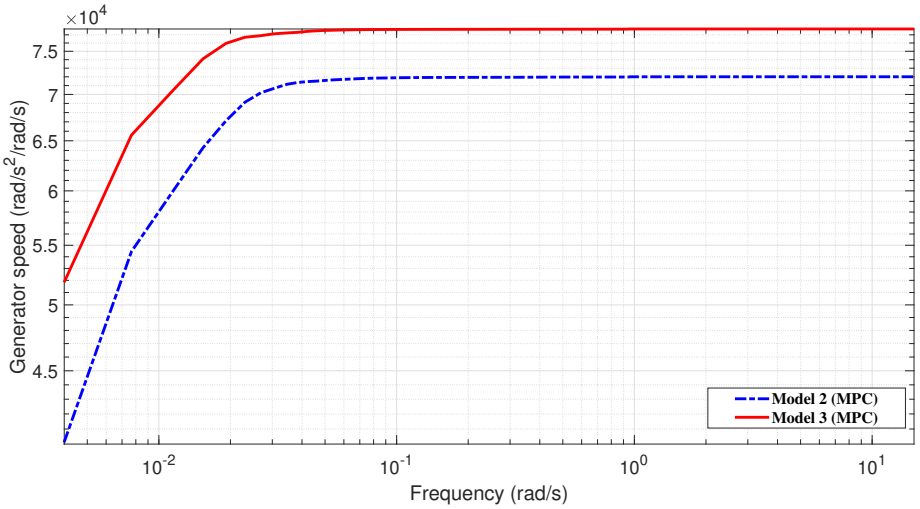

Figure C.28: Generator speed CPSD for 20 m/s

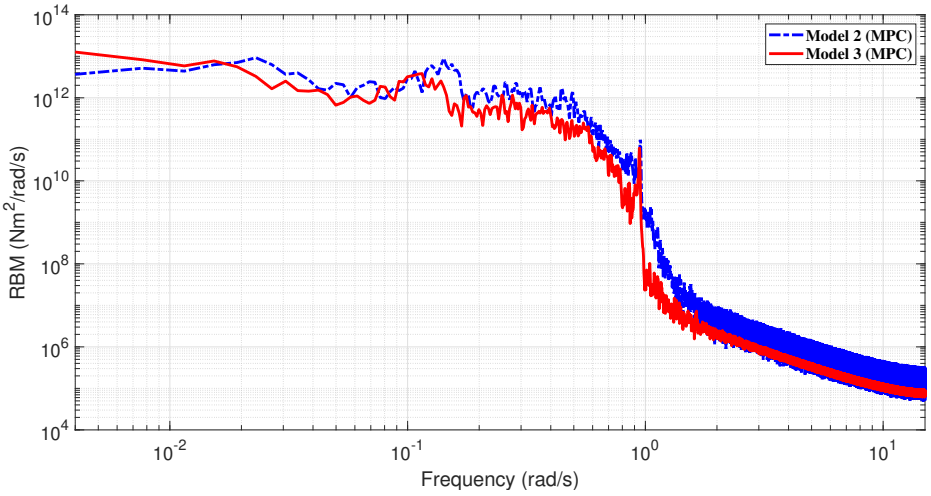

Figure C.29: RBM PSD for 20 m/s

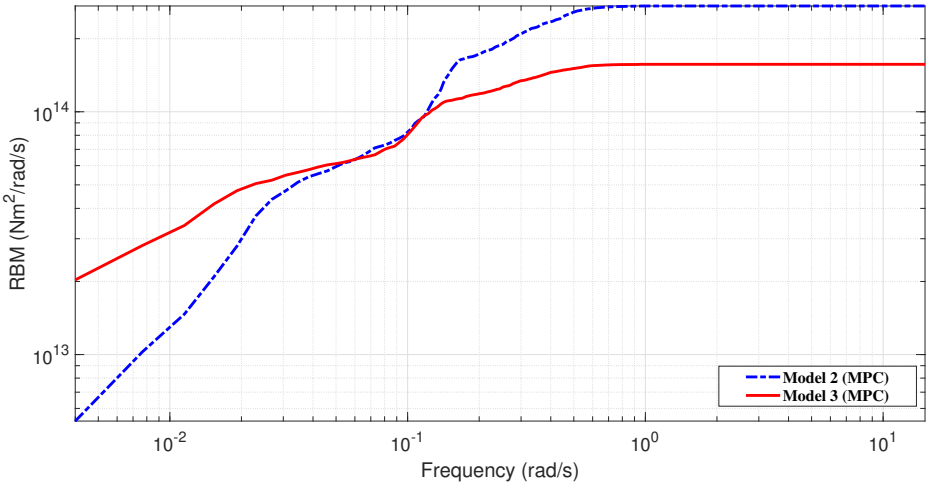

Figure C.30: RBM CPSD for 20 m/s

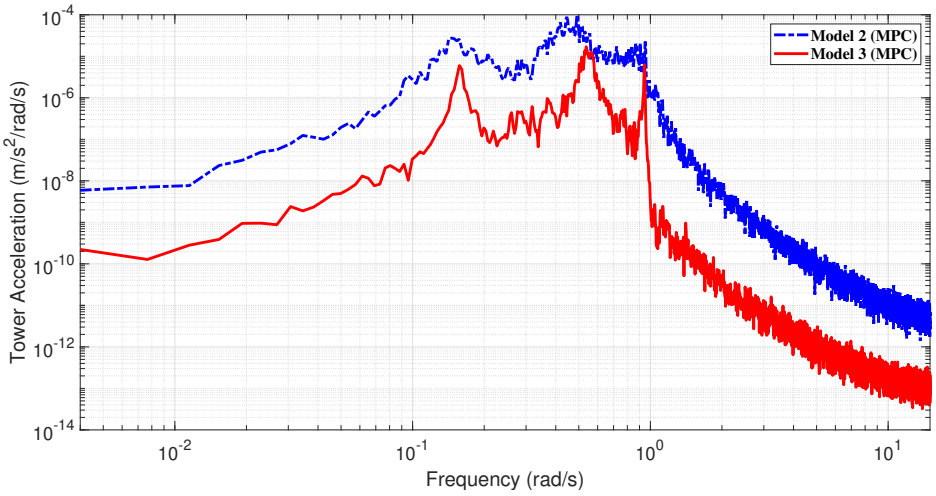

Figure C.31: Tower acceleration PSD for 20 m/s

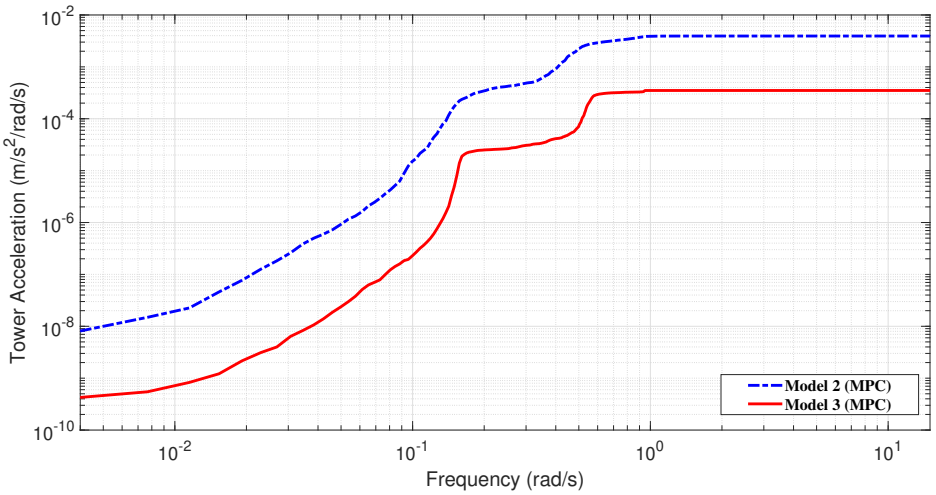

Figure C.32: Tower acceleration CPSD for 20 m/s

Appendix D

IEC 61400-1

Design situation	DLC	Wind condition	Other conditions	Type of analysis	Partial safety factors
1) Power production	1.1	NTM $V_{in} < V_{hub} < V_{out}$	For extrapolation of extreme events	U	N
	1.2	NTM $V_{in} < V_{hub} < V_{out}$		F	*
	1.3	ETM $V_{in} < V_{hub} < V_{out}$		U	N
	1.4	ECD $V_{hub} = V_r - 2$ m/s, V_r, $V_r + 2$ m/s		U	N
	1.5	EWS $V_{in} < V_{hub} < V_{out}$		U	N
2) Power production plus occurrence of fault	2.1	NTM $V_{in} < V_{hub} < V_{out}$	Control system fault or loss of electrical network	U	N
	2.2	NTM $V_{in} < V_{hub} < V_{out}$	Protection system or preceding internal electrical fault	U	A
	2.3	EOG $V_{hub} = V_r \pm 2$ m/s and V_{out}	External or internal electrical fault including loss of electrical network	U	A
	2.4	NTM $V_{in} < V_{hub} < V_{out}$	Control, protection, or electrical system faults including loss of electrical network	F	*
3) Start up	3.1	NWP $V_{in} < V_{hub} < V_{out}$		F	*
	3.2	EOG $V_{hub} = V_{in}$, $V_r \pm 2$ m/s and V_{out}		U	N
	3.3	EDC $V_{hub} = V_{in}$, $V_r \pm 2$ m/s and V_{out}		U	N
4) Normal shut down	4.1	NWP $V_{in} < V_{hub} < V_{out}$		F	*
	4.2	EOG $V_{hub} = V_r \pm 2$ m/s and V_{out}		U	N
5) Emergency shut down	5.1	NTM $V_{hub} = V_r \pm 2$ m/s and V_{out}		U	N
6) Parked (standing still or idling)	6.1	EWM 50-year recurrence period		U	N
	6.2	EWM 50-year recurrence period	Loss of electrical network connection	U	A
	6.3	EWM 1-year recurrence period	Extreme yaw misalignment	U	N
	6.4	NTM $V_{hub} < 0{,}7\ V_{ref}$		F	*
7) Parked and fault conditions	7.1	EWM 1-year recurrence period		U	A
8) Transport, assembly, maintenance and repair	8.1	NTM V_{maint} to be stated by the manufacturer		U	T
	8.2	EWM 1-year recurrence period		U	A

IEC 61400-1 ed.3.0 Copyright © 2005 IEC Geneva, Switzerland.www.iec.ch

Figure D.1: IEC 61400-1